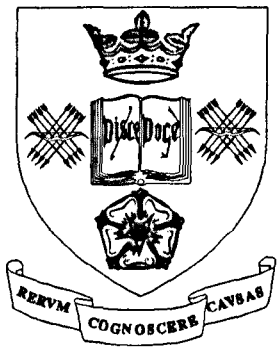

Dynamic Modelling and Control of a Flexible Manipulator

Zaharuddin Mohamed

A thesis submitted to the University of Sheffield for the degree of
Doctor of Philosophy

Department of Automatic Control and Systems Engineering
Faculty of Engineering
The University of Sheffield

April 2003

Abstract

This thesis presents investigations into dynamic modelling and control of a flexible manipulator system. The work on dynamic modelling involves finite element and symbolic manipulation techniques. The control strategies investigated include feedforward control using command shaping techniques and combined feedforward and feedback control schemes. A constrained planar single-link flexible manipulator is used as test and verification platform throughout this work.

Dynamic model of a single-link flexible manipulator incorporating structural damping, hub inertia and payload is developed using the finite element method. Experiments are performed on a laboratory-scale single-link flexible manipulator with and without payload for verification of the developed dynamic model. Simulated and experimental system responses to a single-switch bang-bang torque input are presented in the time and frequency domains. Resonance frequencies of the system for the first three modes are identified. The performance and accuracy of the simulation algorithm are studied in comparison to the experimental results in both domains. The effects of damping and payload on the dynamic behaviour of the manipulator are addressed. Moreover, the impact of using higher number of elements is studied.

The application of a symbolic manipulation approach for modelling and performance analysis of a flexible manipulator system is investigated. System transfer function can be retained in symbolic form using this approach and good approximation of the system transfer function can be obtained. Relationships between system characteristics and parameters such as payload and hub inertia are accordingly explored. Simulation and experimental exercises are presented to demonstrate the effectiveness of the symbolic approach in modelling and simulation of the flexible manipulator system.

Simulation and experimental investigations into the development of feedforward control strategies based on command shaping techniques for vibration control of flexible manipulators are presented. The command shaping techniques using input shaping, low-pass and band-stop filters are considered. The command shaping techniques are designed based on the parameters of the system obtained using the unshaped bang-bang torque input.

Performances of the techniques are evaluated in terms of level of vibration reduction, time response specifications, robustness to error in natural frequencies and processing times. The effect of using higher number of impulses and filter orders on the system performance is also investigated. Moreover, the effectiveness of the command shaping techniques in reducing vibrations due to inclusion of payload into the system is examined. A comparative assessment of the performance of the command shaping techniques in vibration reduction of the system is presented.

The development of hybrid control schemes for input tracking and vibration suppression of flexible manipulators is presented. The hybrid control schemes based on collocated feedback controllers for rigid body motion control with non-collocated PID control and feedforward control for vibration suppression of the system are examined. The non-collocated PID control is designed utilising the end-point deflection (elastic deformation) feedback whereas feedforward control is designed using the input shaping technique. The developed hybrid schemes are tested within the simulation environment of the flexible manipulator with and without payload. The performances of the control schemes are evaluated in terms of input tracking capability and vibration suppression of the flexible manipulator. Initially, a collocated PD utilising the hub-angle and hub-velocity feedback signals is used as a feedback controller. Subsequently, to achieve uniform performance in the presence of a payload, a collocated adaptive control is designed based on pole-assignment self-tuning control scheme. Lastly, a comparative assessment of the performance of the hybrid control schemes is presented.

Acknowledgements

I would like to express my deepest gratitude to my supervisor Dr. M. Osman Tokhi for his supervision, guidance and encouragement throughout this work.

Many thanks also go to my research colleagues, staff of the department and my friend for their help, suggestion and discussion in this work. The financial support of the Islamic Development Bank and Universiti Teknologi Malaysia are gratefully acknowledged.

Finally, I would like to thank my mother Dasimah Ibrahim, my wife Sharifah Saleha Syed Mansor and my children Muhammad Mujahid, Mawaddah and Mursyidah for their continuous support and understanding over the years.

Contents

List of Tables

Notation

a_1, a_2, b_0	Coefficients of identified model
a_{ij}	Elements of matrix
$b_1, b_2, c_1, c_2, c_3, g$	Constants
d	Filter order
f_1, f_2	Natural frequency
h_1, h_2, h_3, h_4, h_5	Functions
j	Unit imaginary number
k	Local variable
l	Length of an element
m	Coefficient determining size of a matrix
m_{ij}	Elements of elemental mass matrix
m_p	Payload
n	Number of elements
p	Pole
q	Number of impulses
r	Reference hub angle
r_α	Reference end-point deflection
s	Laplace variable
t	Time
t_i	Time location of impulse i
u	Input matrix
$u(t)$	Input torque as function of time
v	System states
w	Elastic deflection
w_α	End-point deflection

x	Distance from the hub
y	Total displacement
$y_\delta(t)$	Impulse response
z	z-transform variable
A, B, C	Matrices
D	Damping matrix
D_{ww}	Element of damping matrix
E	Young Modulus
E_K	Kinetic energy
E_P	Potential energy
$F(t)$	Force
$G(s)$	System transfer function
$G_1(s), G_{1a}(s), G_{1b}(s)$	Transfer functions from torque input to end-point displacement
$G_2(s), G_{2a}(s), G_{2b}(s)$	Transfer functions from torque input to hub-angle
H	Constant
$H(j\omega)$	Frequency response
I	Area moment of inertia
I_D	Identity matrix
I_h	Hub inertia
J_i, J_j	Magnitudes of impulses
K	Stiffness matrix
K_d, K_i, K_p	Derivative, Integral, Proportional gains of PID controller
K_n	Elemental stiffness matrix
K_v	Derivative gain of PD control
K_{ww}	Element of stiffness matrix
L	Length
M	Mass matrix
M_{ij}	Elements of mass matrix
M_n	Elemental mass matrix

$N(x), N_a(x)$	Shape function vector
$Q(t), Q_a(t)$	Nodal displacement vector
S	Cross sectional area
$R(s)$	Input torque in frequency domain
$U(s)$	Control signal
V , V_1, V_2	Amplitude of residual vibration
W	Impulse response magnitude
Y	Vector of total displacement
Z	Compensator zero
α	Weight of the manipulator
β	Flexural rigidity of the manipulator
χ	A function
δ_1, δ_2	Filter attenuation
ε	Band edge value
$\phi_1, \phi_2, \phi_3, \phi_4$	Elements of shape function vector
Φ	Constant
φ	A function of a matrix
γ_1, γ_2	Coefficients of a damping equation
η	Zero
λ_i	A function of impulse response magnitude
Λ	Langragian
θ	Hub-angle
$\theta(s)$	Hub-angle in frequency domain
θ_α	End-point rotation
$\dot{\theta}$	Hub-velocity
ρ	Mass density per unit volume
σ_i	A function of damped frequency and time
τ	Torque
τ_s	Sampling time

ω	Radian frequency
ω_c	Filter cut-off frequency
ω_d	Damped frequency in radian/sec
ω_n	Natural frequency in radian/sec
ω_p	Pass-band edge frequency
ω_s	Stop-band edge frequency
ψ	Polynomial
ψ_1, ψ_2	Coefficients of polynomial
ζ, ζ_1, ζ_2	Damping ratio

Abbreviations

A/D	Analogue to digital
BS	Band-stop filter (sixth-order)
D/A	Digital to analogue
FD	Finite difference
FE	Finite element
IIR	Infinite impulse response
I/O	Input output
IS	Input shaping (four-impulse sequence)
lhp	Left half of s-plane
LP	Low-pass filter (sixth-order)
MRAC	Model reference adaptive control
NN	Neural networks
PD	Proportional-Derivative
PDE	Partial differential equation
PDIS	Hybrid PD with input shaping
PDPID	Hybrid PD with PID
PID	Proportional-Integral-Derivative
PSD	Power spectral density
RLS	Recursive least squares
RH	Routh-Hurtwiz
rhp	Right half of s-plane
VSC	Variable structure control

Chapter 1

Introduction

1.1. Background

Robot manipulators are finding an increasing number of applications especially in automation and manufacturing industries. Robots that were once used to pick and place work-pieces are now being used in more complex tasks such as assembling and working at unmanned places. Most existing robotic manipulators are designed with maximum stiffness, in an attempt to minimise system vibration and achieve good positional accuracy. High stiffness is achieved by using heavy material. As a consequence, such robots are usually heavy with respect to the operating payload. This, in turn, limits the speed of operation of the robot manipulation, increases the size of actuator, boosts energy consumption and increases the overall cost. Moreover, the payload to robot weight ratio, under such situations, is low. In order to solve these problems, robotic systems are designed to be lightweight and thus possess some level of flexibility. Conversely, flexible robot manipulators exhibit many advantages over their rigid counterparts: they require less material, are lighter in weight, higher manipulation speed, lower energy consumption, require smaller actuators, are more manoeuvrable and transportable, have less overall cost and higher payload to robot weight ratio (Azad, 1994; Book and Majette, 1983). Due to such advantages flexible manipulators are being used in various applications including space exploration and hazardous environments. In space exploration, space robots must be very lightweight to reduce their launching costs to space (Yamano et al., 2000). In hazardous plants where access to underground storage tanks is limited, flexible-link robots are used in handling hazardous waste material (Jamshidi et al., 1998).

The control of flexible robot manipulators to maintain accurate positioning is a challenging problem. Due to the flexible nature and distributed characteristics of the system, the dynamics are highly non-linear and complex. Problems arise due to precise positioning requirement, vibration due to system flexibility, the difficulty in obtaining accurate model

and non-minimum phase characteristics of the system (Piedboeuf et al., 1993; Yurkovich, 1992). Therefore, to attain end-point positional accuracy, a control mechanism that accounts for both the rigid body and flexural motions of the system is required. The complexity of this problem increases dramatically when a flexible manipulator carries a payload. Practically, a robot is required to perform a single or a set of tasks in sequence such as to pick up a payload, move to a specified location or along a pre-planned trajectory and place the payload. However, the dynamic behaviour of the manipulator is significantly affected by payload variations (Menq and Chen, 1988; Poerwanto, 1998). If the advantages associated with lightness are not to be sacrificed, accurate models and efficient control strategies for flexible robot manipulators have to be developed.

1.2. Literature Review

A significant amount of research has been carried out to devise methodologies for modelling and control of flexible robot manipulator systems. Various experimental investigations have accordingly been carried out for verification of the proposed modelling and control approaches (Hu, 1993). Most of the experimental work is restricted to either vertical or horizontal planes. Moreover, these are limited to single-link and two-link flexible manipulators due to the complexity of multi-link manipulator systems. This section presents a review of modelling and control of flexible robot manipulators.

1.2.1. Modelling

The main goal in modelling of a flexible manipulator system is to achieve an accurate representation of an actual system. It is important to recognise the flexible nature and dynamic behaviour of the system and construct a mathematical model that accounts for several effects including damping, inertia and payload. By obtaining such a model, a satisfactory and good control algorithm can be designed. The dynamic behaviour of a flexible manipulator is obtained based on a fourth order partial differential equation (PDE) of Bernoulli-Euler beam equation which represents an infinite dimensional model of the system (Book, 1990). In order to approximate the true infinite dimensional model, finite dimensional models are required. Various approaches have previously been utilised for this purpose. The modelling approaches can mainly be divided into three main categories as:

- Assumed mode method.
- Singular perturbation technique and frequency domain analysis.

- Numerical analysis approach.

1.2.1.1. Assumed Mode Method

Assumed mode method is the most widely used approach in modelling of flexible manipulators. This approach looks at obtaining approximate modes by solving the PDE characterising the dynamic behaviour of the system. In this approach, the Lagrange equation is used to derive the dynamic model of a structure. An ordinary differential equation can be obtained by representing the deflection of the manipulator as a summation of modes. Each mode is assumed as a product of two functions, one as a function of the distance along the length of the manipulator and the other, as a generalised co-ordinate dependent upon time. The model contains an infinite number of modes but for practical purposes, a finite number of modes is required. It has been reported that the first two modes are sufficient to identify the dynamics of flexible manipulators (Hasting and Book, 1986).

Previous studies utilising the assumed mode method for modelling a single-link flexible manipulator have been reported (Book, 1984; Cannon and Schmitz, 1984; Hastings and Book, 1987; Wang and Vidyasagar, 1991). Following this, a linear state space representation of the system is developed. It has been shown that a good agreement between theory and experiments is obtained utilising this approach. The model eigen values agree well with experimentally determined frequencies of the vibrational model. However, using this approach, the model does not always represent the fine details of the system (Hughes, 1987). This modelling approach has also been utilised in modelling of two-link flexible manipulator systems (Book, 1984; De Luca and Siciliano, 1991). These investigations have assumed two modes of vibration for each link.

1.2.1.2. Singular Perturbation and Frequency-domain Techniques

In the singular perturbation technique, the characteristic modes of the system are separated into two distinct groups: a set of low frequency or slow modes and a set of high frequency or fast modes. In the case of flexible manipulators, the rigid body modes are the slow modes and the flexible modes are the fast modes. The dynamics of the system can then be divided into two sub-systems. The slow sub-system is of the same order as that of the equivalent rigid manipulator. The slow variables are considered as constant parameters for the fast sub-system (Khorrami and Ozguner, 1988).

An alternative to modelling of the manipulator in the time domain is to use a method based on frequency domain analysis (Book and Majette, 1983). This method develops a

concise transfer matrix model using the Bernoulli-Euler beam equation for a uniform beam. The weakness of this method is that it makes no allowance for interaction between the gross motion and the flexible dynamics of the manipulator, nor can these effects be easily included in the model. As a result, the model can only be regarded as approximate.

1.2.1.3. Numerical Analysis Techniques

Numerical analysis techniques based on finite difference (FD) and finite element (FE) methods are commonly used for modelling of flexible manipulator systems. Previous simulation studies with FD method have shown that the method is simple in mathematical terms and is more appropriate in applications involving uniform structures such as flexible manipulator systems. Furthermore, these studies have shown the relative simplicity of the method (Kormoulis, 1990). The method involves discretising the system into several sections and developing a linear relation for the deflection of each section using FD approximations.

The FD approach has previously been utilised in obtaining the dynamic characterisation of single-link flexible manipulator systems incorporating damping, hub inertia and payload (Tokhi and Azad, 1995; Tokhi, et al., 1995; Tzes, et al., 1989). Experiments have also been conducted to verify and validate the theoretical and simulation results. It has been demonstrated that a satisfactory agreement between simulation and experimental results is obtained. However, this modelling approach has not been utilised for modelling of multi-link flexible manipulator systems.

The FE method has been successfully used in solving many materials and structural problems. The method involves discretising the actual system into a number of elements with associated elastic and inertia properties of the system. This gives approximate static and dynamic characterisation of the actual system. The performance of the FE technique in modelling of flexible manipulators has previously been investigated (Aoustin et al., 1994; Menq and Chen, 1988; Tokhi et al., 1997; Usoro et al., 1986). These investigations have shown that the method can be used to obtain a good representation of the system. It has been reported that in using FE methods, a single element is sufficient to describe the dynamic behaviour of a flexible manipulator reasonably well. Using a single element, the first two modes of vibration are well-described (Aoustin et al., 1994). Moreover, the FE method exhibits several advantages over the FD method in terms of accuracy and computational requirements (Tokhi et al., 1997). However, in modelling of the manipulator using FE methods, the effects of structural damping and payload have not been adequately addressed. The study of the effect of payload on the manipulator is important for modelling and control

purposes, as successful implementation of a flexible manipulator control is contingent upon achieving acceptable uniform performance in the presence of payload variations. The damping in the real system is expected to make the residual motion to converge to zero as the energy is dissipated, and not to change the resonance modes of the system (Poerwanto, 1998).

1.2.2. Control

The control strategies for flexible robot manipulator systems can be classified as feedforward and feedback control techniques. Feedforward techniques are mainly developed for vibration suppression and involve altering the input command or reference so that system vibrations are reduced whereas feedback control techniques use measurement and estimate of the system states for rigid body motion control and vibration suppression of the system. This section discusses and reviews both feedforward and feedback control techniques for control of flexible robot manipulators.

1.2.2.1. Feedforward Control

Feedforward control techniques for vibration suppression of flexible robot manipulators consists of developing the control input through consideration of the physical and vibrational properties of the system, so that vibrations at response modes are reduced. This method does not require any additional sensors or actuators and does not account for changes in the system once the input is developed.

A number of techniques have been proposed as feedforward control strategies for flexible manipulators. Aspinwall (1980) has used a Fourier expansion for the forcing function through which the controller parameters are chosen to reduce the peaks of the frequency spectrum at discrete points. This only eliminates a few of the peaks and leaves some modes excited. Swigert (1980) has derived a shaped torque that minimises residual vibration and the effect of parameter variations that affect the modal frequencies. However, the forcing function is not time-optimal. Several researchers have presented and studied the application of computed torque techniques for control of flexible manipulators (Alberts et al., 1990; Bayo, 1988; Moulin and Bayo, 1991). In this approach, a detailed model of the system is first obtained, and by inverting the desired output trajectory, the required input needed to generate that trajectory is computed. For linear systems, this might involve dividing the frequency spectrum of the trajectory by the transfer function of the system, thus obtaining the frequency spectrum of the input. For non-linear systems, this technique involves inverting the equations describing the model. However, this technique suffers from several problems (Singer and

Seering, 1990). These are due to inaccuracy of a model, selection of poor trajectory to guarantee that the system can follow it, sensitivity to variations in system parameters and response time penalties for a causal input.

Bang-bang control involves the utilisation of single and multiple-switch bang-bang control functions (Onsay and Akay, 1991) which require accurate selection of switching time, depending on the representative dynamic model of the system. Minor modelling errors could cause switching errors, and result in a substantial increase in the residual vibrations (Sangveraphunsiri, 1984). Although, utilisation of minimum energy inputs has been shown to eliminate the problem of switching times that arise in the bang-bang input (Jayasuriya and Choura, 1991), the total response time, becomes longer (Meckl and Seering, 1990; Onsay and Akay, 1991). Meckl and Seering (1985, 1988) have examined the construction of input functions from either ramped sinusoids or versine functions. This approach involves adding up harmonics of one of these template functions. If all harmonics were included, the input would be a time optimal rectangular input function. The harmonics that have significant spectral energy at the natural frequencies of the system are eliminated. The resulting input which is given to the system approaches the rectangular shape, but does not significantly excite the resonance. The method has subsequently been tested on a cartesian robot, achieving considerable reduction in the residual vibrations (Meckl and Seering, 1990).

Another technique for feedforward control of flexible robot manipulators is the command shaping technique. Within this technique, a significant amount of work on shaped command inputs based on filtering techniques has been reported. In this approach, a shaped torque input is developed on the basis of extracting the input energy around the natural frequencies of the system, so that the vibration of the manipulator during and after the movement is reduced. The process of extracting the energy is based on filtering techniques. The filters are used for pre-processing the input to the plant, so that lower energy is fed into the system near its resonance. Various filtering techniques have been employed. These include low-pass filters, band-stop filters, notch filters and Gaussian shaped inputs (Singhose et al., 1995; Tokhi and Azad, 1996; Tokhi and Poerwanto, 1996). It has been shown that better performance in the reduction of level of vibration of the system is achieved using the low-pass filter. This is due to indiscriminate spectral attenuation in a low-pass filtered torque at all resonance modes of the system. Utilisation of the band-stop filter, however, is important as spectral attenuation in the input at the selected resonance modes of the system can be achieved. On the other hand, a Gaussian shaped torque input provides smooth energy

propagation into the system. In this sense, it comfortably excites the flexible manipulator without resulting excessive vibration at the resonance modes.

An approach in command shaping techniques known as input shaping has been proposed by Singer and co-workers which is currently receiving considerable attention in vibration control (Singer and Seering, 1990). The method involves convolving a desired command with a sequence of impulses known as input shaper. The shaped command that results from the convolution is then used to drive the system. Design objectives are to determine the amplitude and time locations of the impulses, so that the shaped command reduces the detrimental effects of system flexibility. These parameters are obtained from the system natural frequencies and damping ratio. Using this method, a response with less vibration can be achieved, however, with a slight time delay approximately equal to the length of the impulse sequence. The method has been shown to be effective in reducing vibration in flexible plants (Murphy and Watanabe, 1992). With more impulses, the system becomes more robust to flexible mode parameter changes, but this will result in longer delay in the system response. Previous investigations have shown that the input shaper can be designed to account for modelling errors in natural frequencies and damping ratio (Pao and Lau, 1999; Singhose et al., 1996).

By designing additional impulse sequences for other vibration modes, and then convolving the impulse sequences together, a combined impulse sequence that attenuates vibration at other modes of the system can be derived. Previous investigations have shown that conventionally designed filters are less effective for command shaping than input shaping (Singhose et al., 1995). The vibration reduction achieved with input shaping methods is considerably greater than that achieved with filters. Moreover, input shaping is far less sensitive to modelling errors as they are designed explicitly to deal with modelling errors in mechanical systems. Several researchers have presented alternative approaches to design input shapers. These include designs both in the time-domain (Singer and Seering, 1990) and the frequency-domain (Singh and Vidali, 1994), input shaper based on the pole-placement technique (Tuttle and Seering, 1994), for multiple modes (Hyde and Seering, 1991; Rappole et al., 1994) and for multi-input systems (Pao, 1996; Cutforth and Pao, 1999).

The major drawback of the command shaping techniques is their limitation in coping with parameter changes and disturbances to the system (Khorrami et al., 1994). Moreover, this technique requires relatively precise knowledge of the dynamics of the flexible manipulator. Modifications to provide some degree of robustness with respect to modelling errors, in respect of natural frequencies and damping ratio, however, decreases the speed of

the transient response. The issues of robustness of these methods to unmodelled dynamics have not been adequately addressed. In attempting to solve these problems, a number of researchers have examined closed-loop input shaping methods. Tzes and Yurkovich (1993) have developed an adaptive input shaping control scheme for end-point tracking and vibration control of a flexible manipulator to handle payload variations and disturbances. It has been shown that robustness of the controller can be improved and the length of the impulse sequence can be kept to minimum. Wang and co-workers have developed closed-loop input shaping based on PD control for a single-link flexible manipulator and a five-bar linkage manipulator (Drapeau and Wang, 1993; Zuo and Wang, 1992). A closed-loop input shaping technique using rigid body based controllers and time-delay control has also been proposed (Kapila et al., 2000; Khorrami et al., 1994).

1.2.2.2. Closed-loop Control

In general, control of a flexible robot manipulator can be made easier by locating every sensor exactly at the location of the actuator, as collocation of sensors and actuators guarantees stable servo control (Cannon and Schmitz, 1984; Gevartar, 1970). Therefore, most robots (rigid) are controlled by employing only sensors that are collocated with actuators. For end-point position control, the desired location is converted through real-time kinematics computation into the equivalent angle. Assuming that the robot is stiff enough, the end-point will thus be in the desired location. However, this method of controlling robots has two severe limitations: (a) The inherent flexibility of robot structure makes it difficult to achieve highly accurate manipulation. (b) Member and drive trains of the robot have to be made very stiff, and must therefore be very heavy in order to achieve some degree of precision. In the case of flexible manipulator systems, the end-point position is controlled by obtaining the parameters at the hub and end-point of the manipulator and using the measurement as a basis for applying control torque at the hub. Thus, the feedback control scheme can be divided into collocated and non-collocated control. By applying control torque based on non-collocated sensors, the problem of non-minimum phase and of achieving stability is of concern. Several approaches utilising closed-loop control strategies have been reported for flexible robot manipulators. These approaches can mainly be classified as linear state feedback control, adaptive control, robust control and intelligent control.

Linear State Feedback Control

Linear state feedback control schemes are among the earliest techniques that have been utilised for control of flexible manipulator systems. Cannon and Schmitz (1984) have reported one of the earliest results in this area and their paper is one of the most often cited in the literature. An analytical model utilising Bernoulli-Euler model, Lagrangian formulation and assumed mode method was derived from a single-link apparatus assuming a pinned-free configuration. Important parameters were determined experimentally. Then a control scheme utilising Linear Quadratic Gaussian approach was developed where an estimator was used to estimate all the system states. A good agreement between theoretical and experimental results was obtained. It has been shown that the system response is ultimately limited by the inherent wave propagation in the structure.

Utilising the same technique, Sakawa et al. (1985) proposed a linear quadratic control technique to dampen the flexible modes while tracking the hub reference angle. Stable factorisation (Wang and Vidyasagar, 1987) and optimal control techniques (Hasting and Book, 1987) have also been investigated. However, the proposed control schemes based on linear state feedback control are sensitive to payload variations and disturbances, and therefore, the system performance will deteriorate when a payload and/or a typical parameter of the manipulator vary with time (Menq and Chen, 1988).

Adaptive Control

The importance of an adaptive control technique for control of flexible robot manipulators becomes obvious when realising that successful employment of flexible manipulators is contingent upon achieving uniform performance with regard to payload variations. These control schemes are mostly designed utilising model reference adaptive control (MRAC) or a two-stage process in which a system identification stage is followed by the adaptation of the controller, namely self-tuning control.

A considerable number of schemes of design of adaptive controllers for flexible manipulator systems have been reported. Meldrum and Balas (1986) have utilised the MRAC scheme for control of a flexible manipulator, and have found that with non-collocated output feedback, odd numbered flexural modes tend to be unstable, therefore, small feedback gains are suggested. Harishima and Ueshiba (1986) have used an adaptive controller design based on an auto regressive model with a dead time to avoid unstable pole-zero cancellation. The experimental results have indicated that the algorithm is capable of adapting to payload variations. However, the algorithm has proved to be unstable on the Stanford flexible

manipulator (Rovner, 1987). Yuan et al. (1989) have proposed an MRAC scheme where the system is optimally controlled. The load adaptation for two different loading conditions has been demonstrated but the effect of payload changes on the controller has not been discussed.

Rovner and Cannon (1987) have used a recursive least squares (RLS) algorithm with the hub torque as the input and end-point position as the output information to identify the system transfer function with unknown payload at the end-point. Subsequently, the identified parameters were used on-line for the controller design. Experimental study on payload adaptation has been successfully performed. Nelson and Mitra (1986) have proposed a load adaptive control algorithm to control a flexible manipulator with unknown fixed payload. A steepest decent (gradient) algorithm was used to identify the mass and an optimal controller was designed to control the flexible manipulator. The parameter-updating algorithm proposed in this method might tend to diverge with certain inputs and unmodelled dynamics making it difficult to obtain the controller parameters for different systems (Menq and Chen, 1988). Moreover, the manipulator model used does not fully characterise a real flexible manipulator system. For example, if the payload mass is zero the dominant system frequency in that case would be infinite, but for a real flexible beam the dominant system frequency is always finite. Nemir et al. (1988) has experimentally controlled a flexible manipulator using a self-tuning controller. Their work, however, has been limited to the case of a constant payload. Rovner and Franklin (1988) have implemented an adaptive controller for a flexible manipulator that can handle payloads. However, problems due to transient behaviour during payload release have not been addressed. A technique to identify unknown payload, attached at the end-point, has been proposed using a payload adaptation algorithm (Menq and Chen, 1988). Simulation results have shown that the proposed algorithm is able to identify unknown payload and resulted in a good controller.

Feliu et al. (1993) have proposed an adaptive controller for a single-link flexible manipulator in the presence of joint friction and load changes. The proposed controller was developed with an inner loop to control a motor position and outer loop to control the end-point position. A simple control law with minimal computing effort has been achieved. However, the effectiveness of this controller with load variation, which is a common situation occurring in the practical application of robotics, has not been demonstrated. A situation where an unknown payload attached at one position and released at another position has also been investigated (Yang et al., 1992). The controller was designed based on an adaptive pole-assignment technique. However, experimental results have shown that an undesirable transient occurs during payload release. Poerwanto (1998) proposed an adaptive joint based

collocated control scheme utilising a pole-assignment technique for end-point position control and vibration suppression of a single-link flexible manipulator in the presence of payload variations. It has been demonstrated that the proposed controller is able to handle various payloads and has no difficulty in positioning the system to different locations.

Robust Control Techniques

Obtaining an accurate model of a flexible manipulator system is a challenging task. Certain parameters including damping coefficients, mode shape and natural frequencies, friction and payload cannot be exactly measured. Due to poor knowledge of these parameters, the system behaviour is subjected to significant uncertainty. An approach that can be employed to overcome the problems of uncertainty and unmodelled dynamics is robust control. Robust control schemes include the H-infinity control (Grimble and Johnson, 1991) and variable structure control (VSC) (Hung and Hung, 1993).

A noticeable amount of work on H-infinity control techniques for control of flexible robot manipulators has been reported. Balas (1990) presented an initial and significant work utilising this technique. Accordingly, various investigations on single and multi-link flexible manipulators have been carried out (Banavar and Dominic, 1995; Moser, 1993; Trautman and Wang, 1995; Yazdanpanah et al., 1998). Simulation and experimental results have demonstrated that the controller provides robustness in stability against unmodelled dynamics and overcomes many of the difficulties of structural control including problems due to spillover and non-minimum phase plant behaviour. Moreover, this control technique allows non-collocation of sensors and actuator which is a difficult problem in control of flexible manipulators (Moser, 1993). A hybrid control scheme utilising H-infinity and other control techniques to obtain both good system performance and robust stability has also been proposed. The considered controllers were based on inverse dynamic (Rijanto et al., 1996) and gain scheduling technique (Apkarian and Adams, 1998). Comparisons of linear and non-linear H-infinity control techniques have also been addressed in the context of control of flexible manipulators (Yazdanpanah et al., 1998)

The most distinguished feature of VSC is its ability to result in a very robust control system. In many cases, systems that are completely insensitive to parametric uncertainty and external disturbances are obtained. There are considerable numbers of VSC designs for flexible robot manipulators. Young (1978) has reported an initial investigation of VSC to a flexible robot manipulator. Simulation results have revealed the presence of chattering, a problem that has been studied in greater detail (Morgan and Ozguner, 1985). Ingole et al.

(1994) proposed a VSC for a single-link manipulator and a two-link manipulator with the last link flexible. It has been shown that the proposed control technique with sliding mode can provide an effective control for flexible robot manipulators. Qian and Ma (1992) developed a new technique in designing VSC scheme for the system. This method has the advantage of obtaining the required switching gain directly using a simple Lyapunov function without complicated matrix manipulations. The performance of VSC in comparison to classical PID controllers, non-linear control structures and singular perturbation for control of a single-link flexible manipulator has been addressed by Aoustin et al. (1994). It has been demonstrated through experiments that the VSC scheme can eventually be improved for the tracking purpose by including a constraint on the derivative of hub-angle in the sliding surface definition. Fung and Cheung (1995) developed a VSC for the trajectory tracking of a flexible manipulator by decomposing the end-point position into the rigid and flexible parts, thus resulting in two switching surfaces. The controller was successfully implemented on an experimental single-link manipulator. Yang et al. (1998) studied the application of VSC for a flexible manipulator under gravity. The system dynamics were expressed in new state variables that enable to consider the control design and vibration suppression separately. Simulation results have shown that the proposed controller can provide good joint angle regulation and can effectively damp out vibration in flexible manipulators. A control strategy based on the concept of sliding surfaces for a class of structurally flexible robot manipulators has also been reported (Moallem et al., 1998). In this work, outputs to points near the end-point position were redefined to achieve minimum phase characteristics. The performance of the proposed controller was demonstrated by simulation on a two-link manipulator with considerable parametric uncertainty.

Intelligent Control

An approach that looks promising for the control of flexible robot manipulator systems is intelligent control based on neural networks (NN), fuzzy logic and genetic algorithms. Intelligent control schemes have been widely developed for various control applications. Previous investigations have shown that, for certain systems, intelligent control schemes give better results as compared to other control techniques.

A considerable amount of work has been carried out to develop and implement NN-based controllers for flexible manipulators. Chen and Wen (1993) proposed a neuro-controller and observer to drive a flexible manipulator to a desired trajectory using hub position and velocity measurement. However, this work is restricted only to linear models

(Talebi et al., 1998). Control of a single-link flexible manipulator whose dynamics are partially known has been considered by Donne and Ozguner (1994). In this work, a model-based predictive control scheme has been adopted for the known dynamics and unsupervised NN-based control scheme is utilised to control the unknown system dynamics. Identification and control are implemented as a two-stage process where identification of the unknown part of the system is done using NN in supervised learning mode. Implementation of an NN tracking controller for a single flexible link has been developed by Gutierrez et al. (1998). In this work, the practical implementation of a multi-loop non-linear NN tracking controller for a single flexible link has been tested and its performance compared to that of the standard PD and PID controllers. The advantages of this controller over PD and PID controllers have also been demonstrated. Talebi et al. (1998) have considered an inverse dynamic control of flexible-link manipulators using NN, where a modified output redefined approach is utilised to overcome the problem caused by the non-minimum phase characteristics of the system. Furthermore other NN learning techniques have also been utilised for tracking control of flexible manipulators such as feedback error learning technique (Newton and Xu, 1993), back propagation technique (Mahmood and Walcott, 1993) and a discrete time multi-layered perceptron (Song and Koivo, 1998). Moreover, neuro-controllers have also been utilised based on a singular perturbation technique (Ge et al., 1997; Sun et al., 1996) and VSC (Sundareshan and Askew, 1994).

Similarly, fuzzy logic control schemes have been implemented for control of flexible robot manipulators. Kubica and Wang (1993) have utilised this control technique for a fast moving single-link flexible manipulator focusing on smooth and rigid body motions control. A self-tuning fuzzy controller that attempts to decrease the effects of plant uncertainty by identifying the system on-line has been proposed by Tzes and Kyriakides (1993). Garcia et al. (1991) proposed a two-level hierarchical control strategy to achieve accurate end-point position of a planar two-link flexible manipulator. In this work, a fuzzy-controller is combined with input shaping and end-point acceleration feedback control schemes. Lee et al. (1994) developed a fuzzy-controller, which does not use a mathematical model of the system. It has been demonstrated with simulation results that, without knowledge of mathematical model of the system, a controller, which is capable of controlling a flexible manipulator well, can be constructed, even with a heavy payload. A rule-based control strategy has also been investigated for a flexible manipulator (Moudgal, et al., 1994). In this work, two general forms of knowledge, namely experience gained from mathematical model and conventional control and an intuitive understanding of the dynamics of a two-link flexible manipulator

have been utilised. It has been shown that the rule-based supervisory control is effective for end-point vibration suppression of the system.

Genetic algorithms have also been used for control of flexible manipulator systems. These algorithms have been utilised to tune controllers such as NN (Jain et al., 1994) and a Lyapunov-based controller (Ge et al., 1996). These investigations have shown that genetic algorithms can be used to guarantee closed-loop stability and optimise performance of the flexible manipulator. An approach based on utilising relevant features and advantages of NN, fuzzy logic and genetic algorithms within an integrated framework has been reported for modelling and control of flexible manipulators (Sharma, 2000). It has been demonstrated that the approach has a great deal of potential for a large number of control applications.

1.3. Aims of the Research

This research focuses on the issues of modelling and control of flexible manipulators. The work comprises several components, each of which has been carried out with associated motivations and objectives. The main aims of this research are as follows:

a) Dynamic modelling of a flexible manipulator system incorporating structural damping, hub inertia and payload using the FE method, with the view to obtain an accurate model representing the actual system.
b) Assessment of the performance of the FE method in characterising the behaviour of the manipulator in terms of accuracy and computational requirements. This is accomplished by validating the simulation results with experiments.
c) Investigations into the development of a symbolic manipulation approach for modelling and analysis of flexible manipulators.
d) Development and performance evaluation of command shaping techniques based on input shaping and filtering techniques for vibration suppression of a flexible manipulator.
e) Development of hybrid control schemes consisting of feedback and feedforward controllers for input tracking and vibration suppression of a flexible manipulator.

1.4. Contributions of the Research

From the foregoing discussion it is evidenced that there are significant outstanding issues related to the modelling, analysis and control of flexible manipulator systems that need to be further investigated. By embarking on these, the thesis makes several contributions to the

modelling and control of flexible manipulators. These are also reflected in several journal and conference papers arising from this work as detailed in Section 1.6.1.

The FE method has previously been used for modelling of a single-link flexible manipulator system (Tokhi et al, 1997). In this work, the FE algorithm is extended to incorporate structural damping, hub inertia and payload into the dynamic model of the system. Inclusion of these parameters in the mathematical model is essential for a closer representation of the actual system. The performance of the FE method in characterising the behaviour of the manipulator in terms of accuracy and computational requirements is studied. Moreover, the performance of the developed dynamic model is verified with experimental exercises. These contributions are explained in more detail in Sections 3.3 – 3.6. These provide important performance indications that can be utilised in the development of an acceptable FE model of the system. Moreover, experimental investigations form an important step in assessing the performance of the FE model.

Modelling of a system using the FE method is numerical-based. With such an approach, dynamic characteristics of the manipulator including stability, time response and vibration frequencies are interpreted on the basis of a single particular case, with no provision for any generality. Moreover, numerical systems must operate using numeric approximations, whose precision is limited by the computer hardware. In an attempt to address such issues, modelling and performance analysis of the system using a symbolic algebraic manipulation approach is presented in this thesis. Using such an approach, exact quantities can be obtained by retaining the computations in a symbolic form, resulting in good approximation of system transfer functions. Moreover, relations between system parameters including payload and hub inertia and the system characteristic can be studied. These are discussed in Sections 4.3 and 4.4. The performance of the symbolic approach is assessed within simulation and experimental exercises.

Command shaping techniques based on low-pass and band-stop filters have previously been developed for control of flexible manipulator systems (Tokhi and Poerwanto, 1996). In this thesis the application of a command shaping technique based on input shaping for vibration suppression of flexible manipulator systems is investigated. This is emphasised, as a properly designed feedforward controller can reduce the complexity of the required feedback controller. The real-time implementation of the command shaping techniques is investigated. A comparative assessment of the performance of the techniques in terms of level of vibration reduction, time response specifications, robustness to error in natural frequencies and processing time are discussed. These are explained in Sections 5.4, 5.5 and

5.6. The work extends this by the development of hybrid control schemes for input tracking and vibration suppression of flexible manipulators. A collocated PD and non-collocated PID control has previously been developed for control of a flexible manipulator (Tokhi and Azad, 1996). In this thesis, a collocated PD control with input shaping is developed and the performances of the hybrid schemes are assessed in terms of input tracking and vibration suppression (Section 6.2). A hybrid control scheme consisting of input shaping and a collocated adaptive control for input tracking and vibration suppression of a flexible manipulator with various payloads is examined and reported in Section 6.3.

1.5. Outline of the Thesis

The organisation of the thesis reflects the sequence of steps involved in the development of modelling and control schemes for flexible manipulators. A brief outline of the contents of the thesis is as follows:

Chapter 1 presents background, literature review of modelling and control of flexible manipulator systems, contributions of the research and publications arising from this research.

Chapter 2 describes the flexible manipulator system considered in this study. Several assumptions adopted in the dynamic modelling of the system are discussed. A brief description of the experimental single-link flexible manipulator rig used for verification of modelling and control approaches in this research is also presented.

Chapter 3 extends the previous development of a dynamic model of the flexible manipulator system using the FE approach by incorporating structural damping, hub inertia and payload into the dynamic model. Experimental results are presented for verification and assessment of the developed FE model. The performance of the FE method in characterising the behaviour of the manipulator in terms of accuracy and computational requirement is discussed. The simulation environment, thus developed is used for test and verification of control strategies proposed in this work.

Chapter 4 focuses on the application of a symbolic manipulation approach for modelling and performance analysis of the flexible manipulator. System transfer functions are obtained in symbolic form and used to assess the dynamic characteristics of the system. Moreover, relations between system parameters and system characteristics are studied. Simulation and experimental exercises are performed to demonstrate the effectiveness of the symbolic approach.

Chapter 5 describes the development of a command shaping technique based on input shaping for vibration suppression of the flexible manipulator. Performance of the technique is compared with the previously developed low-pass and band-stop filtering techniques in terms of level of vibration reduction, robustness, time response specifications and processing times. The effects of number of impulses and filter orders on the performance of the system are also studied. Lastly, a comparative assessment of the performance of the techniques is presented.

Chapter 6 presents the development of hybrid control schemes for input tracking and vibration suppression of a flexible manipulator. A collocated PD controller with input shaping is designed and compared with the collocated PD controller and the non-collocated PID controller reported previously. A comparative assessment of the hybrid schemes is presented. Subsequently, a collocated adaptive control is combined with input shaping for input tracking and vibration suppression of the system to obtain uniform system performance in the presence of payload.

Chapter 7 concludes the thesis with notable remarks and achievements. Possible future research directions are also outlined in this chapter.

1.6. Publications

Publications arising from this research that are either published or accepted for publication (in press) are listed below.

1.6.1. Journal Papers

a) Tokhi, M. O., Mohamed, Z. and Shaheed, M. H. (2000). Dynamic modelling of a flexible manipulator system incorporating payload: theory and experiments, *Journal of Low Frequency Noise, Vibration and Active Control*, **19**(4), pp. 209-229.

b) Tokhi, M. O., Mohamed, Z. and Shaheed, M. H. (2001). Dynamic characterisation of a flexible manipulator system, *Robotica*, **19**(5), pp. 571-580.

c) Mohamed, Z. and Tokhi, M. O. (2002). A symbolic manipulation approach for modelling and performance analysis of flexible manipulator systems, *International Journal of Acoustics and Vibration*, **7**(1), pp. 27-37.

d) Mohamed, Z. and Tokhi, M. O. (2002). Vibration control of a single-link flexible manipulator using command shaping techniques, *Proceedings of IMechE-I: Journal of Systems and Control Engineering*, **216**(2), pp. 191-210.

e) Mohamed, Z. and Tokhi, M. O. (2003). Hybrid control schemes for input tracking and vibration suppression of a flexible manipulator, *Proceedings of IMechE-I: Journal of Systems and Control Engineering*, **217**(1), pp. 23-34.

f) Mohamed, Z. and Tokhi, M. O. (2003). Command shaping techniques for vibration control of a flexible robot manipulator, *Mechatronics* (in press).

g) Martins, J. M., Mohamed, Z., Tokhi, M. O., Sa da Costa, J. and Botto, M. A. (2003). Approaches for dynamic modelling of flexible manipulator systems, *Proceedings of IEE – Control Theory and Applications* (in press).

1.6.2. Conference Papers

a) Tokhi, M. O., Mohamed, Z. and Hashim, A. W. I. (2000). The effects of payload on the dynamic characteristics of a flexible robot manipulator, *CONTROL-2000: UKACC International Conference on Control*, Cambridge (UK), 4-7 September 2000.

b) Tokhi, M. O., Mohamed, Z., Shamsudin, H. M. Amin and Mamat, R. (2000). Dynamic characterisation of a flexible manipulator: theory and experiments, *Proceedings of TENCON-2000: IEEE International Conference on Intelligent Systems and Technologies*, Kuala Lumpur (Malaysia), 25-28 September 2000, pp. 166-171.

c) Mohamed, Z. and Tokhi, M. O. (2001). Simulation and experimental study of dynamic characterisation of a flexible robot manipulator, *Proceedings of ICSV8: International Congress on Sound and Vibration*, Hong Kong, 2-6 July 2001, pp. 1115-1122.

d) Mohamed, Z. and Tokhi, M. O. (2001). An input shaping technique for vibration control of a flexible robot manipulator, *Inter-Active 2001: IEE On-line Conference on Active Control of Sound and Vibration*, 1-13 November 2001.

e) Mohamed, Z. and Tokhi, M. O. (2002). Command shaping techniques for vibration control of a single-link flexible manipulator, *Proceedings of ICSV9: International Conference on Sound and Vibration*, Orlando (USA), 8-11 July 2002, Paper Ref. 344.

f) Mohamed, Z. and Tokhi, M. O. (2002). Experimental study of command shaping techniques for vibration control of a flexible manipulator with payload, *Proceedings of ACTIVE2002: International Symposium on Active Control of Sound and Vibration*, Southampton (UK), 15-17 July 2002, pp. 1155-1163.

g) Mohamed, Z. and Tokhi, M. O. (2002). Experimental evaluation of command shaping techniques for vibration control of a flexible manipulator, *Proceedings of Fourth Asian Control Conference*, Singapore, 25-27 September 2002, pp. 948-953.

h) Tokhi, M. O. and Mohamed, Z. (2003). Input shaping and feedback control of a single-link flexible manipulator, *Active Noise and Vibration Control Methods*, Cracow (Poland), 7-9 May 2003 (accepted).

i) Tokhi, M. O. and Mohamed, Z. (2003). Combined input shaping and feedback control of a flexible manipulator, *ICSV10: International Congress on Sound and Vibration*, Stockholm (Sweden), 7-10 July 2003 (accepted).

1.6.3. Research Reports

a) Mohamed, Z. and Tokhi, M. O. (2001). *Modelling and performance analysis of flexible manipulator systems using symbolic manipulation*, Research Report 797, Department of Automatic Control and System Engineering, The University of Sheffield, UK.

b) Tokhi, M. O. and Mohamed, Z. (2001). *Dynamic characterisation of a flexible manipulator system*, Research Report 798, Department of Automatic Control and System Engineering, The University of Sheffield, UK.

1.7. Summary

An introduction and review of modelling and control of flexible robot manipulator systems has been presented. Various modelling and control approaches have been discussed and thus, research direction has been identified. The aims and contributions of the thesis have been described. Lastly, publications arising from this research have been indicated.

Chapter 2

The Flexible Manipulator System

2.1. Introduction

This chapter describes the flexible manipulator system considered in this research. The operating characteristics of the system are described and several assumptions adopted in the process of obtaining the dynamic equations of motion of the system are briefly discussed. A description of the corresponding experimental single-link flexible manipulator rig used in this work for verification of modelling and control approaches is presented.

2.2. Description of the Flexible Manipulator

A mechanical model of the single-link flexible manipulator system considered in this work is shown in Figure 2.1, where X_oOY_o and XOY represent the stationary and moving co-ordinate frames respectively. The axis OX coincides with the neutral line of the link in its underformed configuration, and is tangent to it at the clamped end in a deformed configuration. τ represents the applied torque at the hub. E, I, ρ, S, I_h and m_p represent the Young modulus, area moment of inertia, mass density per unit volume, cross sectional area, hub inertia and payload of the manipulator respectively. $\theta(t)$ denotes an angular displacement (hub-angle) of the manipulator and $w(x,t)$ denotes an elastic deflection (deformation) of a point along the manipulator at a distance x from the hub of the manipulator. In this work, the motion of the manipulator is confined to the X_oOY_o plane. Since the manipulator is long and slender, the shear deformation and rotary inertia effects are neglected. This allows the use of the Bernoulli-Euler beam theory to model the elastic behaviour of the manipulator. The manipulator is assumed to be stiff in vertical bending and torsion, allowing it to vibrate dominantly in the horizontal direction and thus, the gravity effects are neglected. Moreover, the manipulator is considered to have constant cross section and uniform material properties throughout.

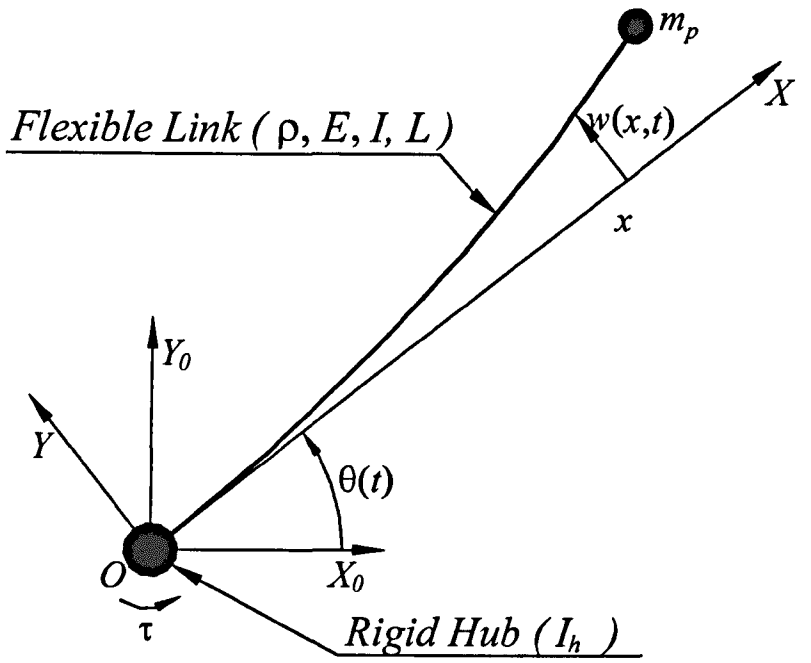

Figure 2.1: Mechanical model of the flexible manipulator system.

2.3. The Experimental Rig

The experimental manipulator rig used in this study is shown in Figure 2.2. The manipulator was designed for experimental verification of modelling and control approaches involving flexible manipulator systems (Tokhi and Azad, 1997). The main parts of the rig include the flexible arm, the driving motor with amplifier, measuring devices and a digital processor with interfacing system. A schematic diagram of the rig is shown in Figure 2.3.

2.3.1. The Flexible Arm

The flexible arm is the main part of the system. The size and weight of this arm as designed depends on the specific application. The arm of the manipulator considered in this investigation is constructed using a piece of thin aluminium alloy with parameters given in Table 2.1.

2.3.2. The Driving Motor with Amplifier

The experimental rig is equipped with a U9M4AT type printed circuit motor driving the flexible manipulator. This type of motor gives significant performance advantages for motion control applications, which can be listed as follows (Azad, 1994; PMI Motor Technologies, 1988):

Table 2.1: Parameters of the flexible arm.

Parameter	Value
Length	900.0 mm
Width	19.008 mm
Thickness	3.2004 mm
Young modulus	71×10^{9} Nm^{-2}
Area moment of inertia	5.1924×10^{-11} m^{4}
Mass density per unit volume	2710 kgm^{-3}
Hub inertia	5.8598×10^{-4} kgm^{2}

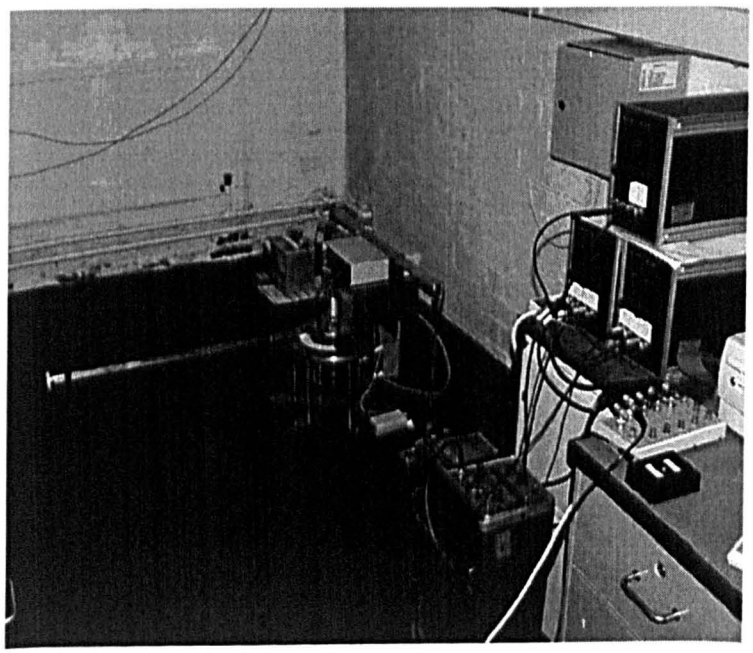

Figure 2.2: The laboratory-scale flexible manipulator.

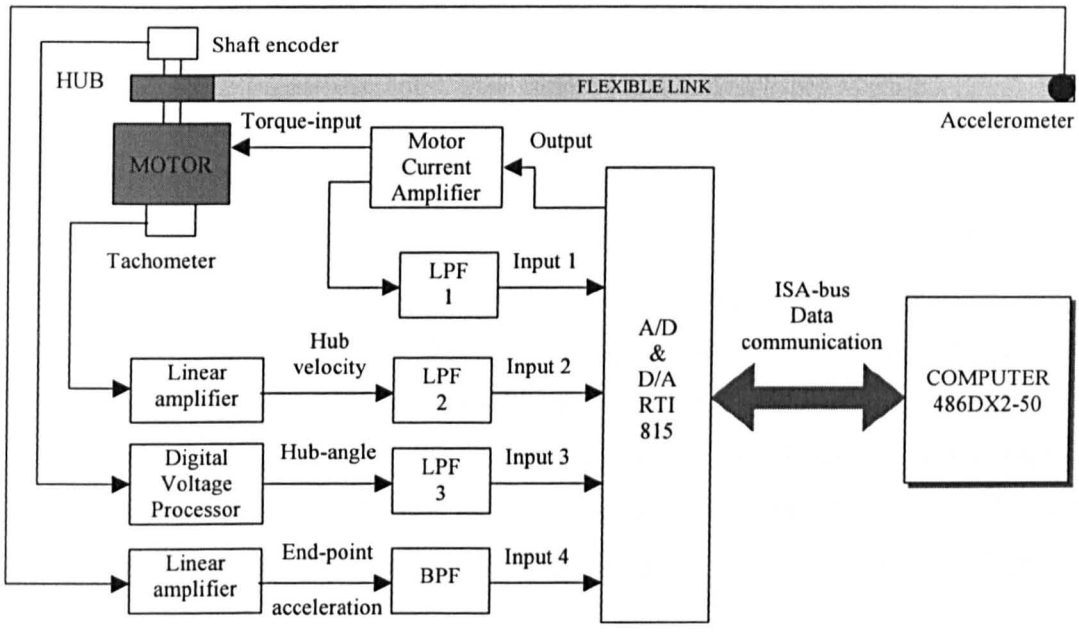

Figure 2.3: Schematic diagram of the experimental rig.

- It gives high acceleration since it is able to produce high torque combined with low armature inertia. This means shorter cycle times, more displacement per second and higher throughput.
- It has a very low inductance, which leads to a negligible electrical time constant and a short mechanical time constant (less than one millisecond). This implies almost instantaneous application of full torque which provides fast motion and accurate tracking.
- It does not have armature associated torque loss due to its construction and as a result delivers more torque over its entire speed range. Moreover, the torque is almost constant throughout its speed range.
- Due to the absence of any iron in the rotor and a large number of commutator bars and slots, extremely smooth torque is achieved.
- There is no stored energy in the armature to be dissipated during commutation, as the inductance is nearly zero. This eliminates arcing, which is the major cause of brush wear. This increases the reliability in operation and life expectancy.

The motor drive amplifier used is the LA5600 manufactured by Electro-Craft Corporation (Electrocraft Corporation, 1985). It is a bi-directional drive amplifier, as the motor needs to be driven in both directions to control the manipulator vibration. This motor

drive amplifier (current amplifier) delivers a current proportional to the input voltage. It serves as a velocity/position controller as well as a motor driver.

2.3.3. Measuring Devices

The measuring devices used to record the various responses of the manipulator are shaft encoder, tachometer and accelerometer along the arm. The shaft encoder is used for measuring the hub-angle of the manipulator. The hub-angle measurement is utilised to control rigid body motion of the system. Following a process of studying various available shaft encoders, a shaft encoder with a resolution of 2048 pulses/revolution, manufactured by Heidenhain, has been selected for this purpose (Azad, 1994). A precision interface circuit consisting of a TCHT2000 incremental encoder interface chip and MP7636A double buffered 16 bit multiplexing digital to analogue (D/A) converter is used to convert the shaft encoder output to an analogue signal.

The tachometer is used for measurement of the hub angular velocity of the manipulator. As an initial trial, a conventional type tachometer which is mounted on the same shaft of the driving motor was used. This device, however, was found to produce a considerable amount of ripple due to its commutation effect. To overcome this problem, a velocity transducer, was purpose designed for this application using the existing tachometer principle (Azad, 1994). On the other hand, the accelerometer is located at the end-point of the flexible arm measuring the end-point acceleration. Due to weight and size constraints, a miniature ICP (integrated circuit piezoelectric) accelerometer 303A03 is utilised. The characteristics of this accelerometer cover the range of frequencies involved in these investigations with voltage sensitivity of 1.02 mV/ms^{-2}. Moreover, it has low impedance output that allows the use of long cables without an appreciable signal loss or distortion. The accelerometer is mounted at the end-point of the manipulator using epoxy adhesive.

2.3.4. Digital Processor and Interfacing System

The processor used in this study is an IBM-PC compatible based on 486DX2-50MHz CPU. Data acquisition and control are accomplished through the utilisation of an RTI-815 I/O board. This board can provide a direct interface between the processor, the actuator and sensors. The RTI-815 board contains a single 12 bit A/D converter and two independent voltage output channels, each with its own 12 bit D/A converter, which can produce an output of 0 to +10 V or $\pm$10 V. The interface board is used with a conversion speed of 25

μsec for A/D conversion and settling time of 20 μsec for D/A conversion, which are adequate for the system under consideration. In this work, the experimental set-up requires one analogue output to the motor driver amplifier and four analogue inputs from the hub-angle, hub-velocity, end-point acceleration and motor current sensors.

2.4. Summary

Description of the flexible robot manipulator considered for this research has been presented in this chapter. Further, assumptions utilised for dynamic modelling of the system have been indicated. A description of the experimental single-link flexible manipulator rig used in this study has also been presented.

Chapter 3

Dynamic Modelling of a Flexible Manipulator

3.1. Introduction

This chapter focuses on the development of an FE simulation algorithm characterising the dynamic behaviour of the flexible robot manipulator system. Firstly, the FE method is briefly discussed. Then formulations to obtain the mass, stiffness and damping matrices and the dynamic equations of motion of the manipulator utilising the Lagrange equation are presented. The procedure is further extended to incorporate structural damping, hub inertia and payload into the dynamic model. The equations of motion are then expressed in a state-space form, so as to be solved using control system approaches. Performance of the algorithm in characterising the dynamic behaviour of the system is assessed in comparison to the experimental test-rig, described in Chapter 2. Experimental results are presented for validation of the developed FE model in the time and frequency domains.

3.2. The Finite Element Method

Since its introduction in the 1950s, the FE method has been continually developed and improved (Rao, 1989). The method involves decomposing a structure into several simple pieces or elements. The elements are assumed to be interconnected at certain points, known as nodes. For each element, an equation describing the behaviour of the element is obtained through an approximation technique. The elemental equations are then assembled to form the system equation. It is found that by reducing the element size of the structure, that is, increasing the number of elements, the overall solution of the system equation can be made to converge to the exact solution.

The main steps in an FE analysis can be listed as follows:

a) Discretisation of the structure into elements.

b) Selection of an approximating function to interpolate the result.

c) Derivation of the basic element equation.

d) Calculation of the system equation.

e) Incorporation of the boundary conditions.

f) Solving the system equation with the inclusion of the boundary conditions.

In this manner, the flexible manipulator is treated as an assemblage of n elements and the development of the algorithm can be divided into three main parts: the FE analysis, state-space representation and obtaining and analysing the system response.

3.3. Simulation Algorithm

The total displacement $y(x,t)$ of a point along the manipulator at a distance x from the hub can be described as a function of both the rigid body motion $\theta(t)$ and elastic deflection $w(x,t)$ measured from the line OX as

$$y(x,t) = x\theta(t) + w(x,t) \tag{3.1}$$

Using the standard FE method to solve dynamic problems, leads to the well-known equation

$$w(x,t) = N_a(x)Q_a(t) \tag{3.2}$$

where $N_a(x)$ and $Q_a(t)$ represent the shape function and nodal displacement respectively. The manipulator is approximated by partitioning it into n elements. As a consequence of using the Bernoulli-Euler beam theory, the FE method requires each node to possess two degrees of freedom, a transverse deflection and rotation. These necessitate the use of Hermite cubic basis functions as the element shape function (Ross, 1996). Hence, for an elemental length l, the shape function can be obtained as

$$N_a(x) = [\phi_1(x) \quad \phi_2(x) \quad \phi_3(x) \quad \phi_4(x)]$$

where

$$\phi_1(x) = 1 - \frac{3x^2}{l^2} + \frac{2x^3}{l^3} \; ; \; \phi_2(x) = x - \frac{2x^2}{l} + \frac{x^3}{l^2} \; ;$$

$$\phi_3(x) = \frac{3x^2}{l^2} - \frac{2x^3}{l^3} \; ; \; \phi_4(x) = -\frac{x^2}{l} + \frac{x^3}{l^2} .$$

For element n the nodal displacement vector is given as

$$Q_a(t) = [w_{n-1}(t) \quad \theta_{n-1}(t) \quad w_n(t) \quad \theta_n(t)]$$

where $w_{n-1}(t)$ and $w_n(t)$ are the elastic deflections of the element and $\theta_{n-1}(t)$ and $\theta_n(t)$ are the corresponding rotations. Substituting for $w(x,t)$ from equation (3.2) into equation (3.1) and simplifying yields

$$y(x,t) = N(x)\, Q_b(t) \tag{3.3}$$

where

$$N(x) = [x \quad N_a(x)] \text{ and } Q_b(t) = [\theta(t) \quad Q_a(t)]^T$$

The new shape function $N(x)$ and nodal displacement vector $Q_b(t)$ in equation (3.3) incorporate local and global variables. Among these, the angle $\theta(t)$ and the distance x are global variables while $N_a(x)$ and $Q_a(t)$ are local variables. Defining $k = x - \sum_{i=1}^{n-1} l_i$ as a local variable of the nth element, where l_i is the length of the ith element, the kinetic energy of an element n can be expressed as

$$E_K^n = \frac{1}{2}\int_0^l \rho S\left[\frac{\partial y(k,t)}{\partial t}\right]^2 dk = \frac{1}{2}\int_0^l \rho S \dot{Y}^T \dot{Y} dk = \frac{1}{2}\dot{Q}_b{}^T\left[\int_0^l \rho S (N^T N)\, dk\right]\dot{Q}_b \tag{3.4}$$

and the potential energy of the element can be obtained as

$$E_P^n = \frac{1}{2}\int_0^l EI\left[\frac{\partial^2 y(k,t)}{\partial k^2}\right]^2 dk = \frac{1}{2}\int_0^l EI(\Phi Q_b)^T(\Phi Q_b)\, dk = \frac{1}{2}Q_b{}^T\left[\int_0^l EI(\Phi^T\Phi)\, dk\right]Q_b \tag{3.5}$$

where $\Phi = \dfrac{d^2 N}{dk^2}$.

Defining M_n and K_n as

$$M_n = \int_0^l \rho S(N^T N)\, dk = \text{element mass matrix} \tag{3.6}$$

$$K_n = \int_0^l EI\,(\Phi^T \Phi)\, dk = \text{element stiffness matrix} \tag{3.7}$$

and solving equations (3.6) and (3.7) for the n elements, the element mass and stiffness matrices can be obtained as

$$M_n = \frac{\rho S l}{420}\begin{bmatrix} m_{11} & m_{12} & m_{13} & m_{14} & m_{15} \\ m_{21} & 156 & 22l & 54 & -13l \\ m_{31} & 22l & 4l^2 & 13l & -3l^2 \\ m_{41} & 54 & 13l & 156 & -22l \\ m_{51} & -13l & -3l^2 & -22l & 4l^2 \end{bmatrix}$$

$$K_n = \frac{EI}{l^3}\begin{bmatrix} 0 & 0 & 0 & 0 & 0 \\ 0 & 12 & 6l & -12 & 6l \\ 0 & 6l & 4l^2 & -6l & 2l^2 \\ 0 & -12 & -6l & 12 & -6l \\ 0 & 6l & 2l^2 & -6l & 4l^2 \end{bmatrix}$$

where

$$\begin{aligned} m_{11} &= 140l^2(3n^2 - 3n + 1) \\ m_{12} &= m_{21} = 21l(10n - 7) \\ m_{13} &= m_{31} = 7l^2(5n - 3) \\ m_{14} &= m_{41} = 21l(10n - 3) \\ m_{15} &= m_{51} = -7l^2(5n - 2) \end{aligned}$$

Assembling the element mass and stiffness matrices, the total kinetic and potential energies from equations (3.4) and (3.5) can be written as

$$E_K = \frac{1}{2}\dot{Q}^T M \dot{Q}$$

$$E_P = \frac{1}{2} Q^T K Q$$

where $Q(t) = [\theta \quad w_0 \quad \theta_0 \quad . \quad . \quad . \quad w_\alpha \quad \theta_\alpha]^T$, M and K are global mass and stiffness matrices of the manipulator respectively. w_α and θ_α are deflection and rotation at the end-point of the manipulator respectively.

The dynamic equations of motion of the flexible manipulator can be derived utilising the Lagrange equation as

$$\frac{d}{dt}\left\{\frac{\partial \Lambda}{\partial \dot{Q}}\right\} - \left\{\frac{\partial \Lambda}{\partial Q}\right\} = F$$

where $\Lambda = E_K - E_P$ is the Lagrangian and F is a vector of external forces. Considering the damping, the desired dynamic equations of motion of the system can accordingly be obtained as

$$M\ddot{Q}(t) + D\dot{Q}(t) + KQ(t) = F(t) \tag{3.8}$$

where D is a global damping matrix, normally determined through experimentation.

For the flexible manipulator under consideration, the global mass matrix can be represented as

$$M = \begin{bmatrix} M_{\theta\theta} & M_{\theta w} \\ M_{\theta w} & M_{ww} \end{bmatrix}$$

where M_{ww} is associated with the elastic degrees of freedom (elastic motion), $M_{\theta w}$ represents the coupling between these elastic degrees of freedom and the hub-angle θ and $M_{\theta\theta}$ is associated with the inertia of the system about the motor axis. Similarly, the global stiffness matrix can be written as

$$K = \begin{bmatrix} 0 & 0 \\ 0 & K_{ww} \end{bmatrix}$$

where K_{ww} is associated with the elastic degrees of freedom (elastic motion). It can be shown that the elastic degrees of freedom do not couple with the hub-angle through the stiffness matrix.

The global damping matrix D in equation (3.8) can be represented as

$$D=\begin{bmatrix}0 & 0\\ 0 & D_{ww}\end{bmatrix}$$

where D_{ww} denotes the sub-matrix associated with the structural damping. The matrix is obtained by assuming that the manipulator exhibits the characteristics of Rayleigh damping. This proportional damping model has been assumed because it allows experimentally determined damping ratios of individual modes to be used directly in forming the global matrix. It also allows assignment of individual damping ratios to individual modes, such that the total manipulator damping is constituted with the sum of the dampings associated with the modes. Using this assumption, the damping related to the first two modes, which are dominant modes, can be obtained as (Chapnik et al., 1991)

$$D_{ww}=\gamma_1 M_{ww}+\gamma_2 K_{ww} \tag{3.9}$$

where

$$\gamma_1=\frac{2 f_1 f_2(\zeta_1 f_2-\zeta_2 f_1)}{f_2^{\,2}-f_1^{\,2}} \quad \text{and} \quad \gamma_2=\frac{2(\zeta_2 f_2-\zeta_1 f_1)}{f_2^{\,2}-f_1^{\,2}}$$

with ζ_1, ζ_2, f_1 and f_2 representing the damping ratios and natural frequencies of the first and second modes respectively.

3.3.1. Incorporation of Hub Inertia and Payload

By incorporating the hub inertia and payload of the flexible manipulator, the kinetic energy of the system can be obtained as (Azad, 1994)

$$E_K=\frac{1}{2}\int_0^L \rho S\left[\frac{\partial y(k,t)}{\partial t}\right]^2 dk+\frac{1}{2}I_h\dot{\theta}^2+\frac{1}{2}m_p\left(\frac{\partial y(x,t)}{\partial t}\right)^2\Bigg|_{x=L}$$

Hence

$$E_K = \frac{1}{2}\int_0^L \rho S\left[\frac{\partial y(k,t)}{\partial t}\right]^2 dk + \frac{1}{2} I_h \dot{\theta}^2 + \frac{1}{2} m_p (L\dot{\theta}(t) + \dot{w}(L,t))^2$$

or

$$E_K = \frac{1}{2}\int_0^L \rho S\left[\frac{\partial y(k,t)}{\partial t}\right]^2 dk + \frac{1}{2}(I_h + m_p L^2)\dot{\theta}^2 + \frac{1}{2} m_p \dot{w}_a{}^2 + m_p L \dot{\theta} \dot{w}_a \qquad (3.10)$$

In equation (3.10) the second term on the right hand side demonstrates the contribution of hub inertia and payload to the rotary inertia of the system about the motor axis and contributes to the 1×1 sub-matrix $M_{\theta\theta}$. The third term shows the effect of payload on the end-point deflection of the manipulator and contributes to M_{ww} whilst the last term contributes to the coupling matrix $M_{\theta w}$. Utilising equation (3.10) and the FE formulation (Meirovitch, 1975), a new global mass matrix can be obtained.

3.3.2. State-space Representation

The M, D and K matrices in equation (3.8) are of size $m \times m$ and $F(t)$ is of size $m \times 1$, where $m = 2n+1$. For the manipulator, considered as a clamped-free arm with the applied torque τ at the hub, the flexural and rotational displacement, velocity and acceleration are all zero at the hub at $t = 0$ and the external force is $F(t) = [\tau \quad 0 \quad \cdots \quad 0]^T$. Moreover, in this work, it is assumed that $Q(0) = 0$.

The matrix differential equation in equation (3.8) can be represented in a state-space form as

$$\dot{v} = Av + Bu$$
$$y = Cv$$

where

$$A = \left[\begin{array}{c|c} 0_m & I_{Dm} \\ \hline -M^{-1}K & -M^{-1}D \end{array}\right], \quad B = \left[\begin{array}{c} 0_{m\times1} \\ \hline M^{-1} \end{array}\right],$$

$$C = [0_m \mid I_{Dm}]$$

0_m is an $m \times m$ null matrix, I_{Dm} is an $m \times m$ identity matrix, $0_{m\times 1}$ is an $m \times 1$ null vector, $u = [\tau \quad 0 \quad \cdots \quad 0]^T$ and $v = [\theta \quad w_1 \quad \theta_1 \quad \cdots \quad w_\alpha \quad \theta_\alpha \quad \dot{\theta} \quad \dot{w}_1 \quad \dot{\theta}_1 \quad \cdots \quad \dot{w}_\alpha \quad \dot{\theta}_\alpha]^T$. Solving the state-space matrices gives the vector of states v, that is, the angular, nodal flexural and rotational displacements and velocities.

3.4. Simulation Results

In this section, simulation results of the dynamic behaviour of the flexible manipulator system are presented in the time and frequency domains. The system is considered with and without payload. A single-switch bang-bang signal of amplitude ±0.3 Nm, shown in Figure 3.1(a), is used as an input torque, applied at the hub of the manipulator. Figure 3.1(b) shows the corresponding power spectral density (PSD) of the input torque. A bang-bang torque has a positive (acceleration) and negative (deceleration) period allowing the manipulator to, initially, accelerate and then decelerate and eventually stop at a target location. System responses are monitored for a duration of 3 sec, and the results are recorded with a sampling time of 2 msec.

The developed FE model was implemented within the Matlab environment on a Pentium III 650 MHz processor. To demonstrate the effect of damping on the system response, investigations with and without damping were carried out. Previous experimental investigations with the flexible manipulator have shown that the damping ratio of the system ranges from 0.024 to 0.1 (Azad, 1994). The damping ratios were deduced through a trial and error analysis process as 0.026, 0.038 and 0.04 for the first, second and third vibration modes respectively. Using the first two resonance frequencies, obtained from experiments, as 12 Hz and 35 Hz (Azad, 1994), γ_1 and γ_2 in equation (3.9) can be obtained as 0.3528 and 0.0019 respectively. To investigate the accuracy of the FE simulation algorithm in characterising the behaviour of the flexible manipulator, the algorithm was implemented on the basis of varying the number of elements from 1 to 20. Four system responses namely the hub-angle, hub-velocity, end-point deflection and end-point acceleration with the corresponding PSDs are obtained and evaluated.

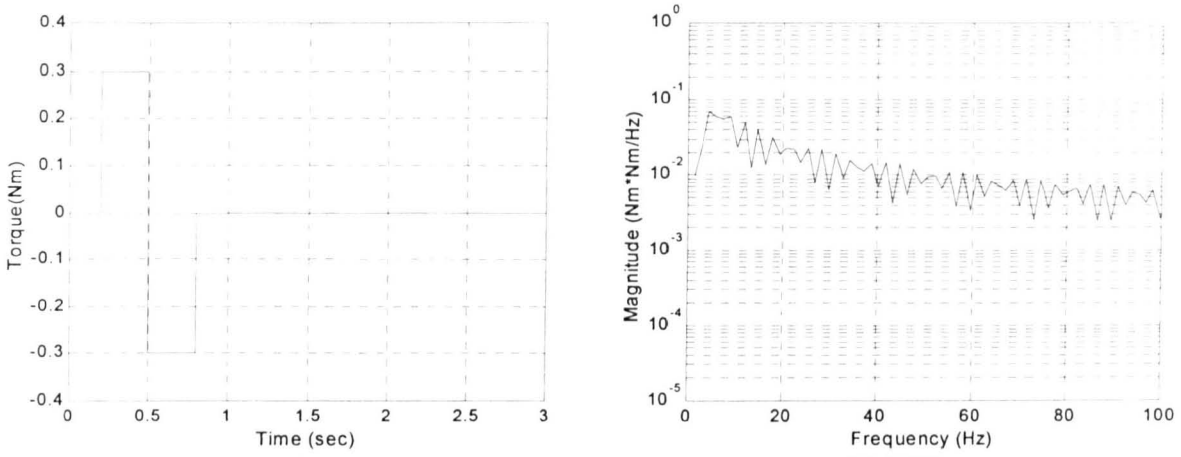

(a) Time domain. (b) PSD.

Figure 3.1: The bang-bang input torque.

3.4.1. System without Payload

Figures 3.2 – 3.9 show the response of the system with the corresponding PSDs without the presence of damping using one and ten elements respectively. It is noted that a steady-state hub-angle level of 38 degrees was achieved within 0.9 sec using one or more elements. These proved that a satisfactory dynamic behaviour of a flexible manipulator, up to the second mode, could be achieved with one or more elements. Further modes of the system are obtained with increasing the number of elements as shown in Figures 3.6 – 3.9. As expected, without the damping effect, the system response exhibits persistent oscillation. Using one element, the poles of the system transfer function from torque input to end-point displacement output were obtained as 0, 0, $\pm j90.82$ and $\pm j300.07$. The corresponding zeros were obtained as ± 58.59 and ± 229.14 respectively. Since there are two system zeros on the right-hand of s-plane, the system response characterises a non-minimum phase behaviour. This agrees with previously developed models (Cannon and Schmitz, 1984).

The flexible motion of the system is found to be characterised by the first three modes of vibration. Resonance frequencies of the system were obtained by transforming the time-domain representation of the system into the frequency domain. As shown in Figures 3.2 – 3.9, with one element, the resonance frequencies of the system were obtained as 14.49 Hz and 47.70 Hz whereas with ten elements these were 11.99 Hz, 35.22 Hz and 65.2 Hz. It is noted that by increasing the number of elements, the system resonance frequencies converge to more accurate values, but at the expense of higher execution times. This is mainly due to an increase in the size of the mass, damping, stiffness and state-space matrices. The inter-relation between the number of elements, execution time and resonance frequencies of the

system is summarised in Table 3.1. With the resolution used in these investigations, it is noted that there are no significant changes in the vibration frequencies of mode 2 between 3 and 5 elements and between 10 and 20 elements.

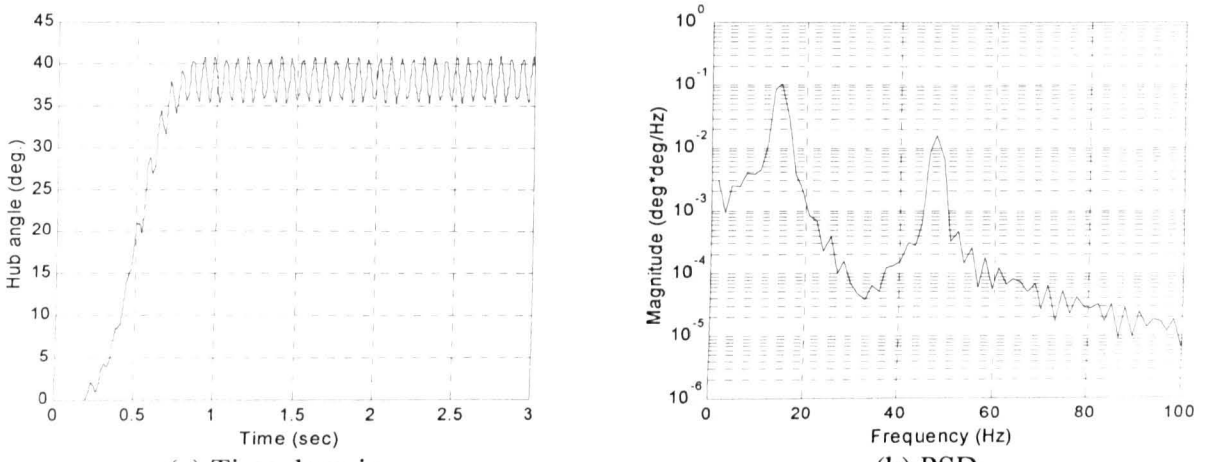

(a) Time domain. (b) PSD.

Figure 3.2: Simulated hub-angle response of the flexible manipulator (without damping and payload, number of element = 1).

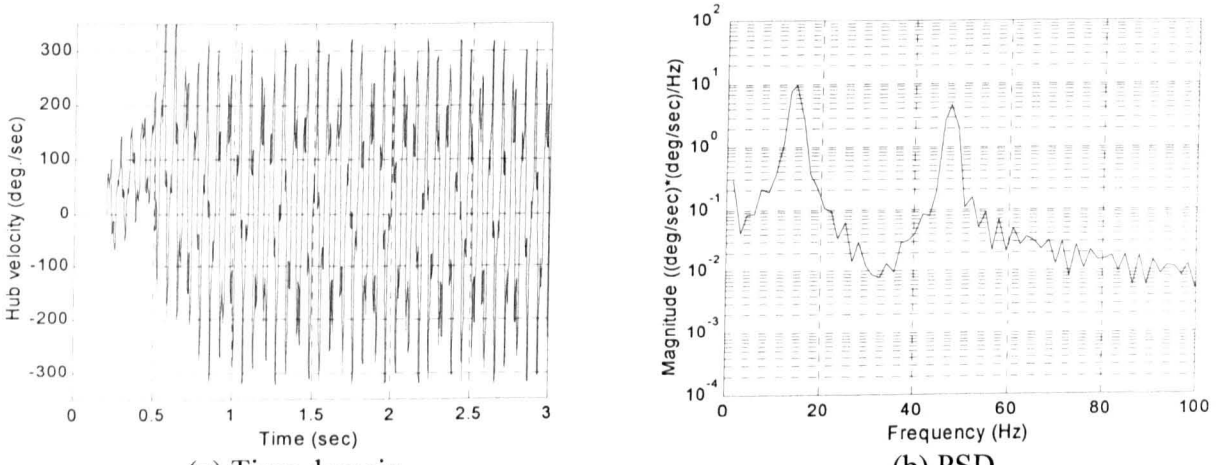

(a) Time domain. (b) PSD.

Figure 3.3: Simulated hub-velocity response of the flexible manipulator (without damping and payload, number of element = 1).

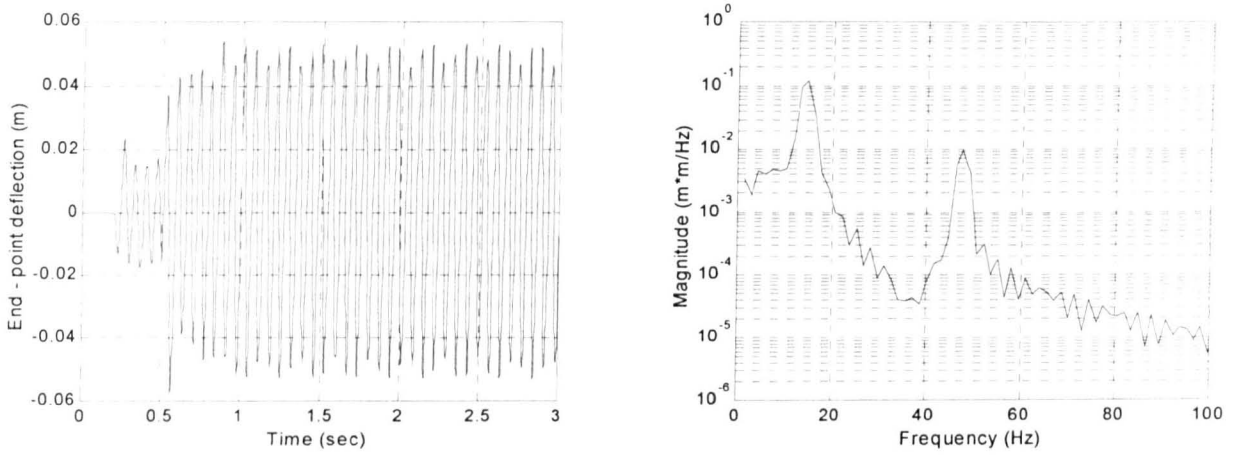

(a) Time domain. (b) PSD.

Figure 3.4: Simulated end-point deflection response of the flexible manipulator (without damping and payload, number of element = 1).

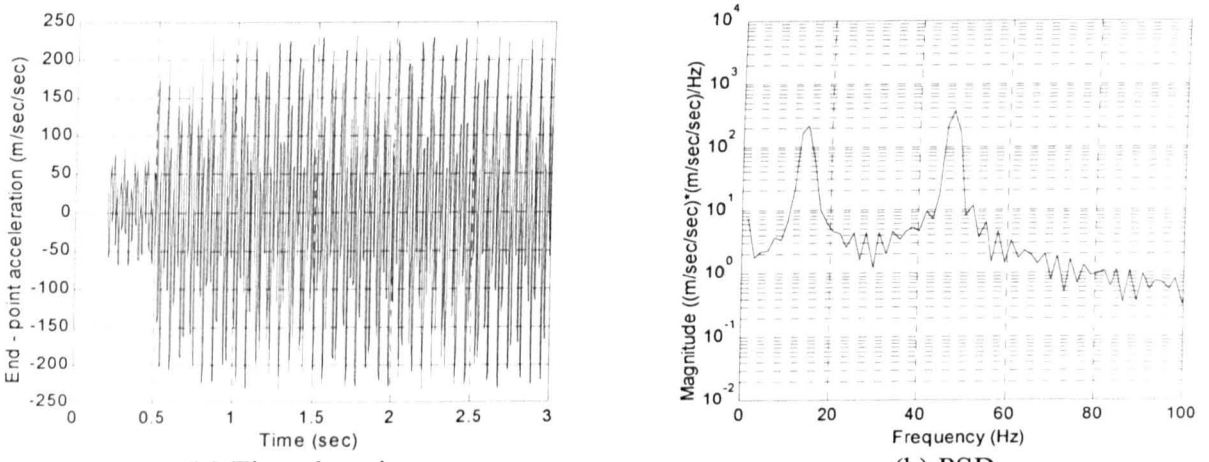

(a) Time domain. (b) PSD.

Figure 3.5: Simulated end-point acceleration response of the flexible manipulator (without damping and payload, number of elements = 1).

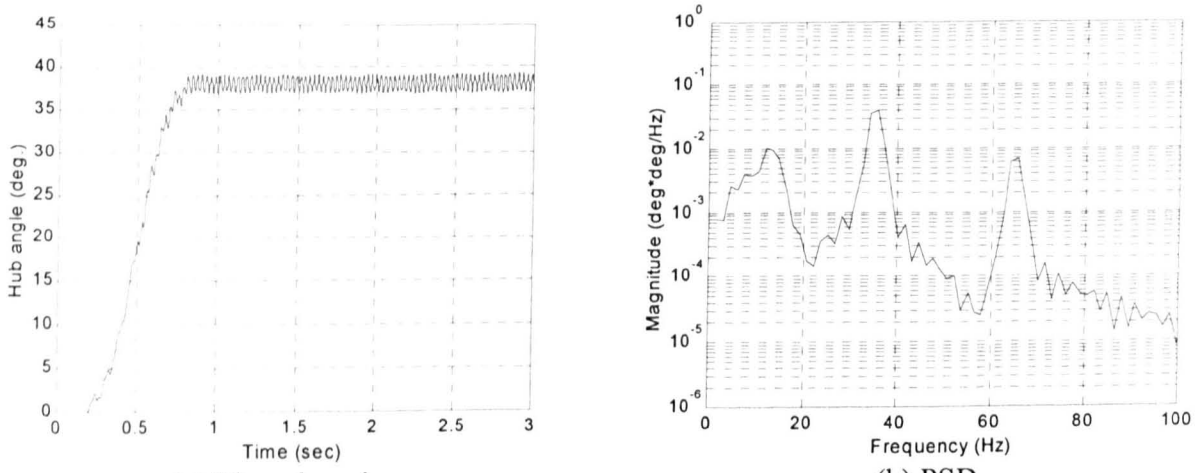

(a) Time domain. (b) PSD.

Figure 3.6: Simulated hub-angle response of the flexible manipulator (without damping and payload, number of element = 10).

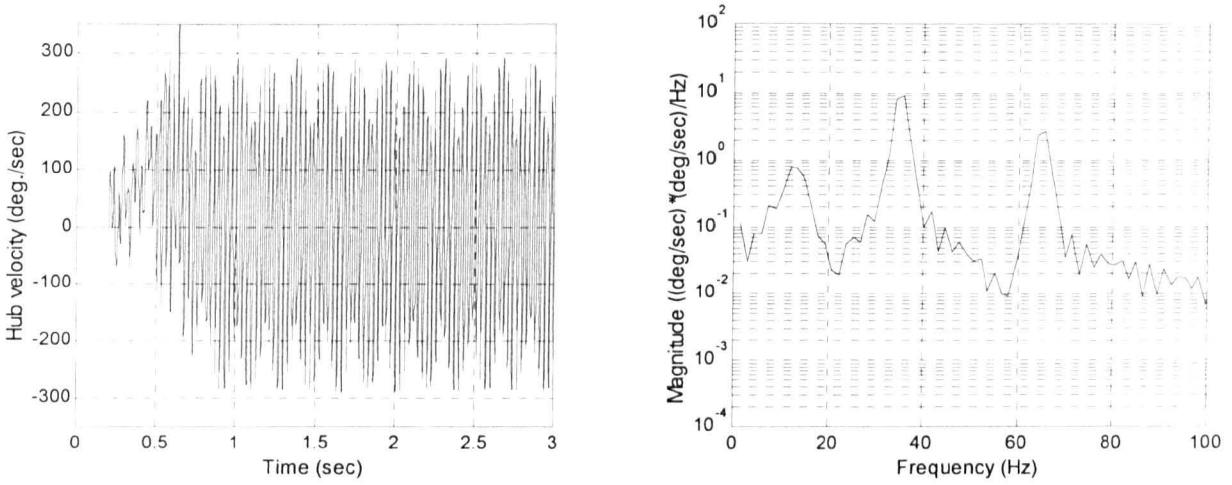

(a) Time domain. (b) PSD.

Figure 3.7: Simulated hub-velocity response of the flexible manipulator (without damping and payload, number of element = 10).

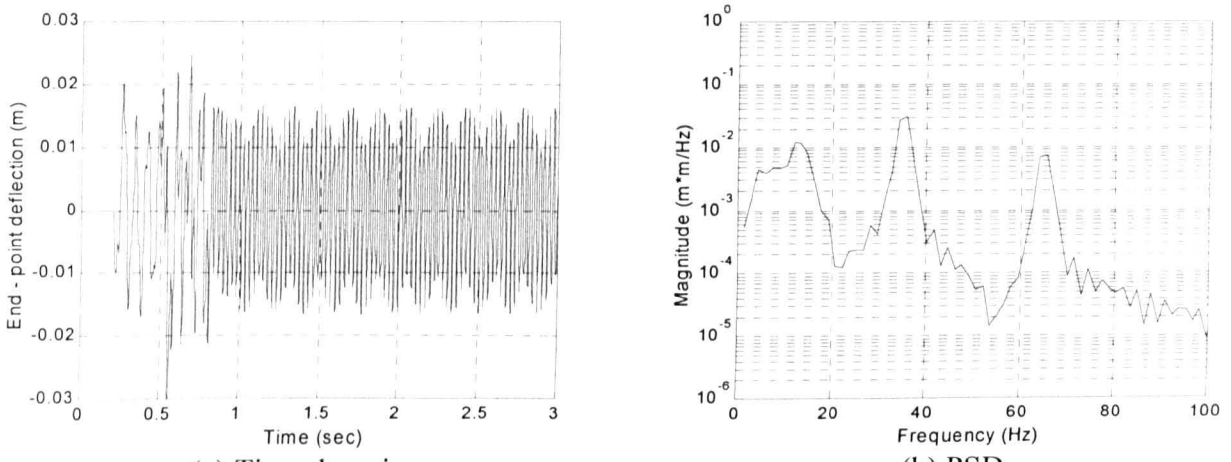

(a) Time domain. (b) PSD.

Figure 3.8: Simulated end-point deflection response of the flexible manipulator (without damping and payload, number of element = 10).

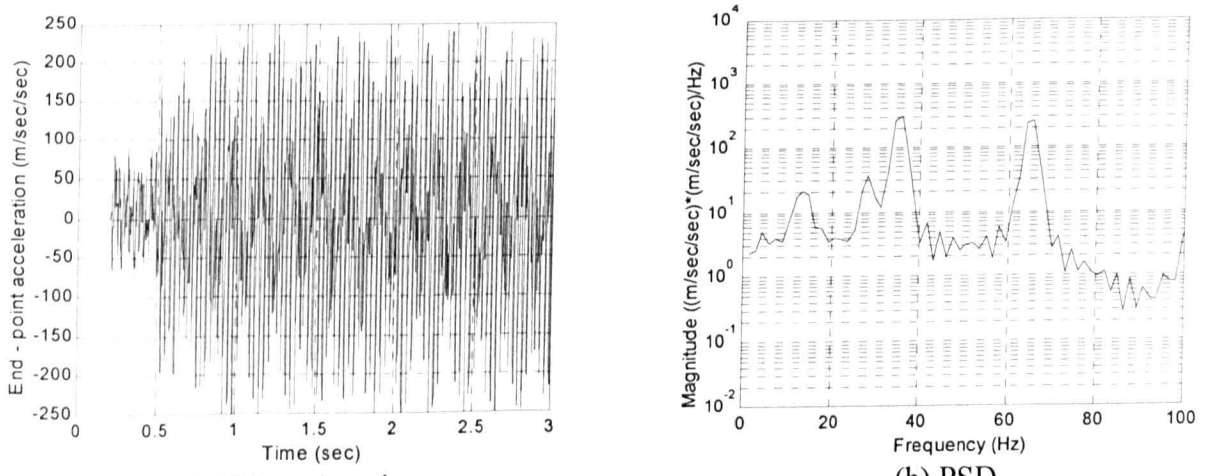

(a) Time domain. (b) PSD.

Figure 3.9: Simulated end-point acceleration response of the flexible manipulator (without damping and payload, number of element = 10).

Table 3.1: Relation between number of elements, execution times and resonance frequencies of the flexible manipulator.

Number of Elements	Execution time (sec)	Resonance frequencies (Hz)		
		Mode 1	Mode 2	Mode 3
1	0.38	14.49	47.7	-
2	0.44	11.99	35.71	77.17
3	0.55	11.99	35.46	65.68
5	0.67	11.99	35.46	65.43
10	0.98	11.99	35.22	65.2
20	2.72	11.99	35.22	65.2

Figures 3.10 – 3.13 show the dynamic behaviour of the system in the presence of damping with ten elements. The damping has considerably dampened system response oscillations. Note that vibrations occur at the hub and end-point during movement of the manipulator. Analysing the system time response, it is noted that a steady-state hub-angle level of 38 degrees was achieved. Moreover, the hub-velocity, end-point deflection and end-point acceleration of the system converged to zero within 1.8 sec. The end-point deflection and acceleration responses were found to oscillate dominantly between 15 mm to -10 mm and –150 to 150 m/sec^2 respectively with maximum deflection of 29 mm. It is noted with damping that the level of vibration reduces.

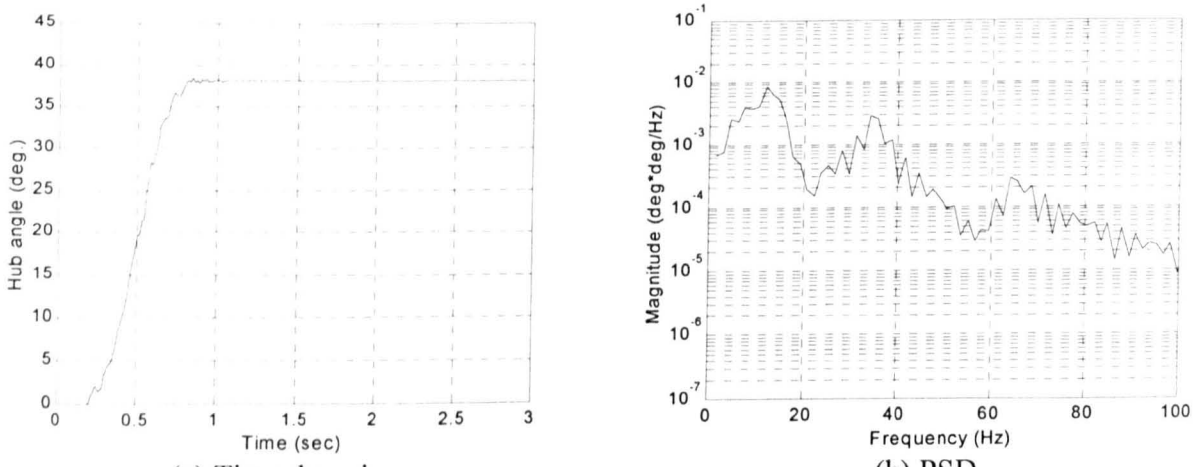

(a) Time domain. (b) PSD.

Figure 3.10: Simulated hub-angle response of the flexible manipulator (with damping, without payload, number of element = 10).

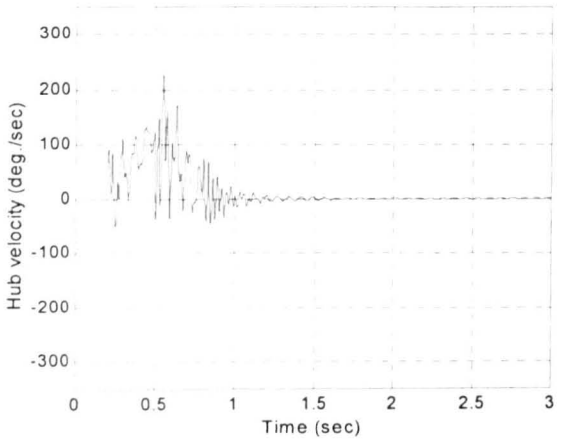

(a) Time domain.

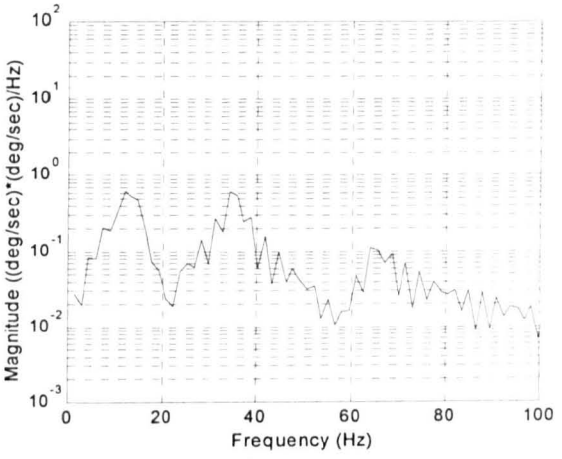

(b) PSD.

Figure 3.11: Simulated hub-velocity response of the flexible manipulator (with damping, without payload, number of element = 10).

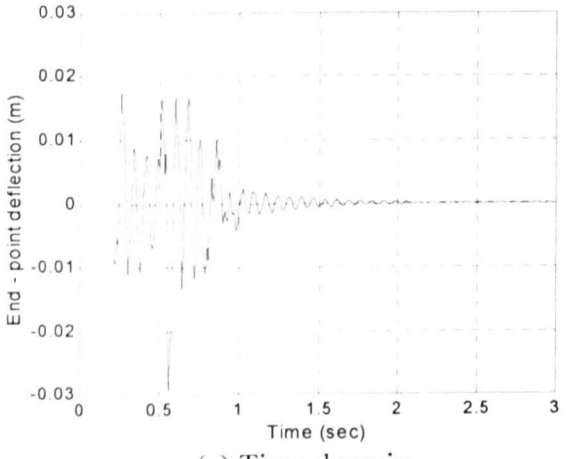

(a) Time domain.

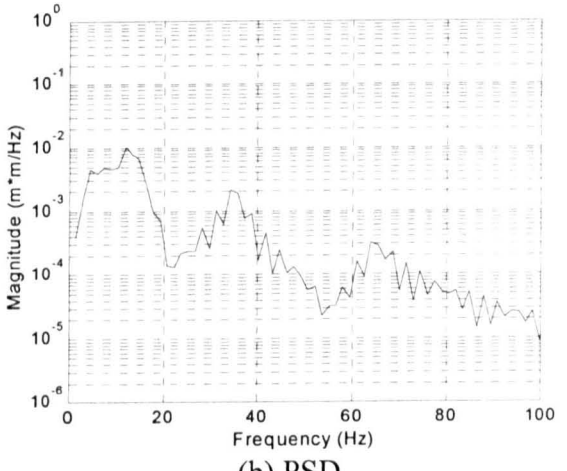

(b) PSD.

Figure 3.12: Simulated end-point deflection response of the flexible manipulator (with damping, without payload, number of element = 10).

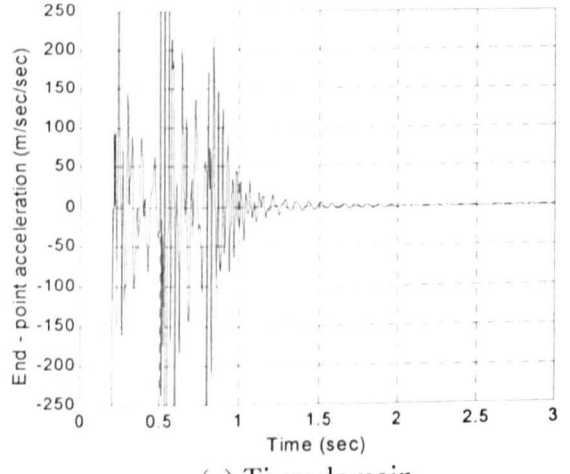

(a) Time domain

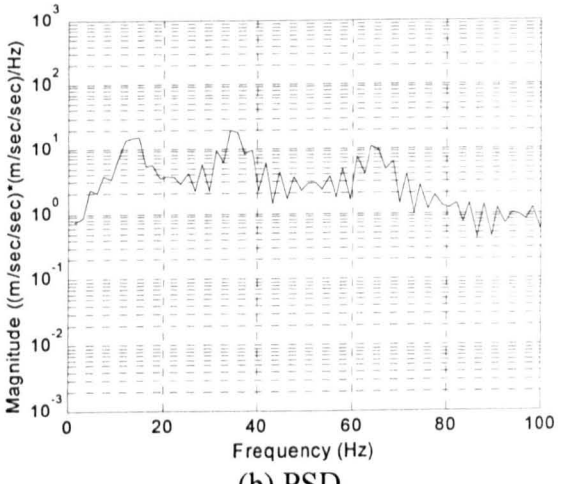

(b) PSD.

Figure 3.13: Simulated end-point acceleration response of the flexible manipulator (with damping, without payload, number of element = 10).

3.4.2. System with Payload

To demonstrate the effect of payload on the dynamic behaviour of the system, various payloads of up to 60 percent of the manipulator weight were simulated. Figures 3.14 – 3.17 show the system response with payloads of 20 grams and 40 grams. These results were obtained with damping using 10 elements. It is noted that the hub-angle decreases with increasing payloads. For payloads of 20 grams and 40 grams, the steady-state hub-angle levels settled at 27 degrees and 21 degrees respectively. With payload, it is also noted that the system response exhibits higher vibration and requires longer time to converge to zero as compared with the case without payload. It is also evidenced from the PSD of the system response, that the resonance modes of vibration of the system shift to lower frequencies with increasing payloads. This implies that the manipulator oscillates at lower frequency rates than those without payload. Table 3.2 summarises the relation between payload and the resonance frequencies of the system. Similarly, it is noted that there is no change in the vibration frequncies of mode 2 between 50 grams and 60 grams, with the resolution used.

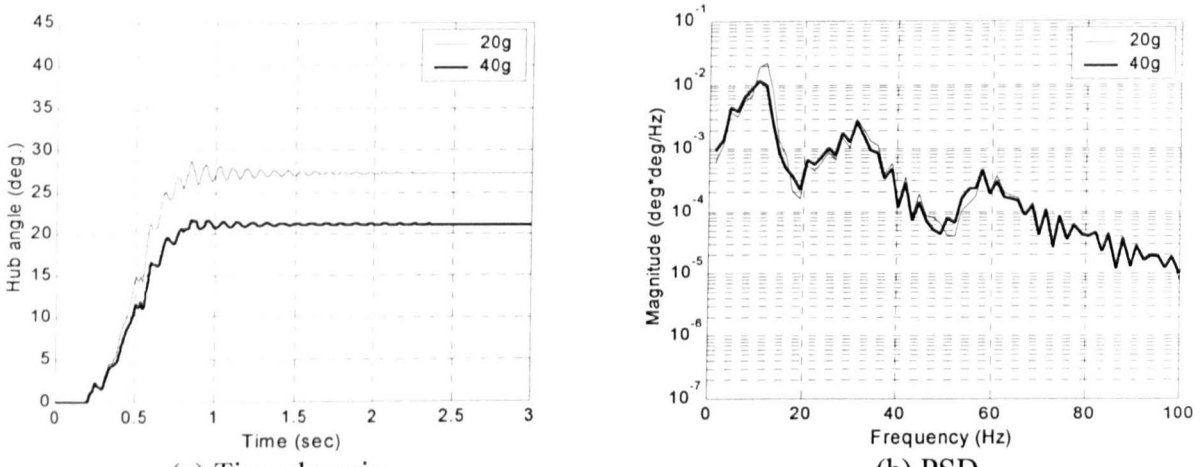

(a) Time domain. (b) PSD.

Figure 3.14: Simulated hub-angle response of the flexible manipulator (with payloads, number of element = 10).

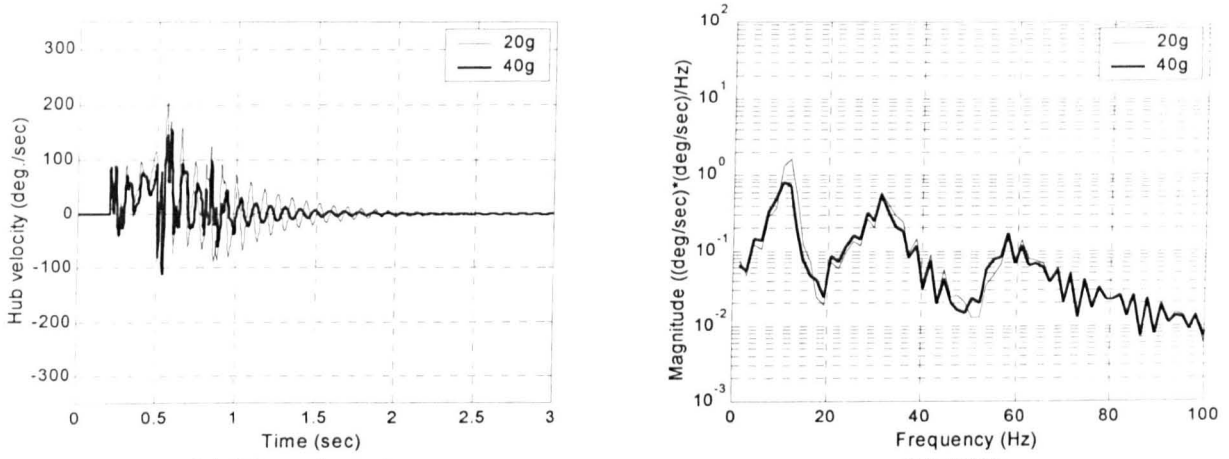

(a) Time domain. (b) PSD.

Figure 3.15: Simulated hub-velocity response of the flexible manipulator (with payloads, number of element = 10).

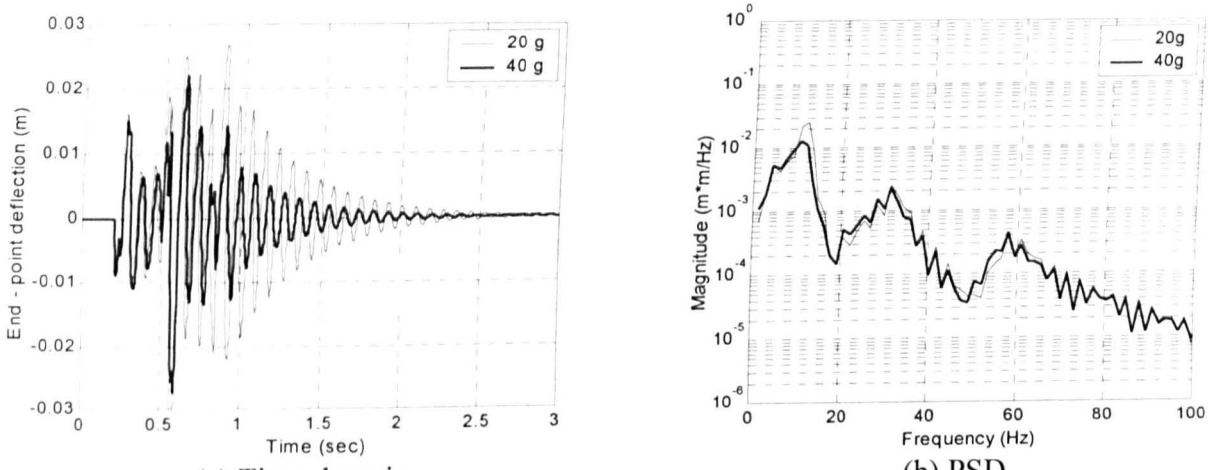

(a) Time domain. (b) PSD.

Figure 3.16: Simulated end-point deflection response of the flexible manipulator (with payloads, number of element = 10).

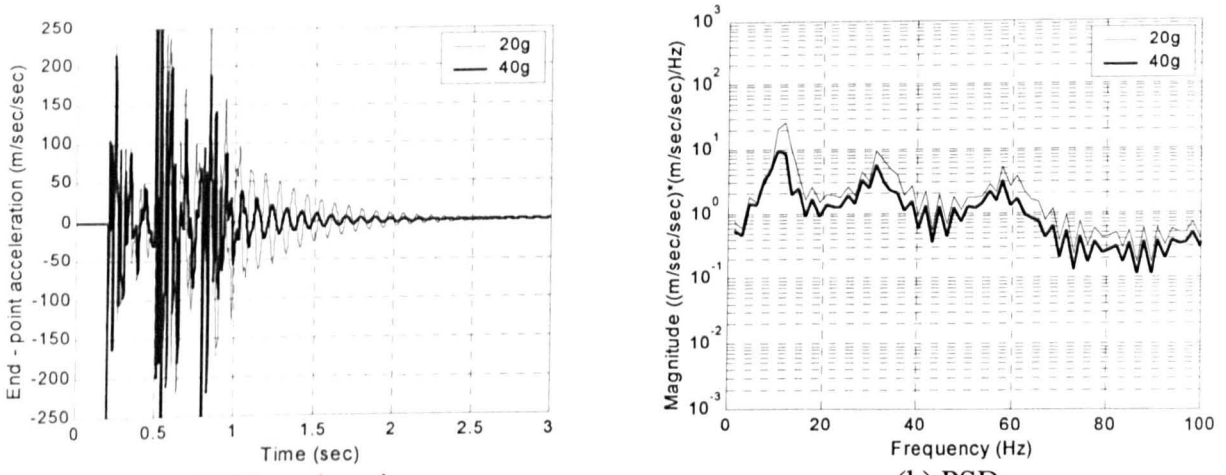

(a) Time domain. (b) PSD.

Figure 3.17: Simulated end-point acceleration response of the flexible manipulator (with payloads, number of element = 10).

Table 3.2: Relation between payload and resonance frequencies of the flexible manipulator. Number of elements = 10.

Payloads (grams)	Resonance frequencies (Hz)		
	Mode 1	Mode 2	Mode 3
0	11.99	35.22	65.20
10	11.65	33.22	61.19
20	11.49	32.22	59.44
30	10.99	31.72	58.69
40	10.74	31.22	58.19
50	10.49	30.97	57.69
60	10.24	30.97	57.44

3.5. Experiments

Experiments using the described experimental rig were conducted for verification of the developed FE model. In the experiments, a single-switch bang-bang input torque with the same parameters as in the simulation was used. The hub-angle, hub-velocity and end-point acceleration were measured and the corresponding PSDs were obtained. These were then compared with the simulation results. Figures 3.18 – 3.20 show the hub-angle, hub-velocity, and end-point acceleration, with their PSDs, of the flexible manipulator without payload. It is noted that for the hub-angle, the steady-state level of 38 degrees was achieved within 1.8 sec. Note that vibration occurs during movement of the manipulator as evidenced in the hub-angle, hub-velocity and end-point acceleration responses. The end-point acceleration response was found to oscillate dominantly between 100 to -100 m/sec^2 respectively. The first three modes of vibration were obtained as 11.72 Hz, 35.15 Hz and 65.60 Hz.

To investigate the effect of payload on the performance of the manipulator, experiments were performed using various payloads ranging from 10 grams to 60 grams. Figures 3.21 – 3.23 show the hub-angle, hub-velocity, end-point acceleration, with their PSDs with payloads of 20 grams and 40 grams. The system response demonstrates that levels of hub-angle decrease with increasing payloads. For payloads of 20 grams and 40 grams, the steady-state levels were obtained as 31 degrees and 26 degrees respectively. It is also noted that the settling time of the manipulator response was affected by variations in the payload. This shows that the manipulator response has higher settling times with increasing payloads. Analysing the PSDs, it is noted that the resonance frequencies of the system shift to lower frequencies with increasing payloads. The relation between payload and resonance frequencies of the system is summarised in Table 3.3.

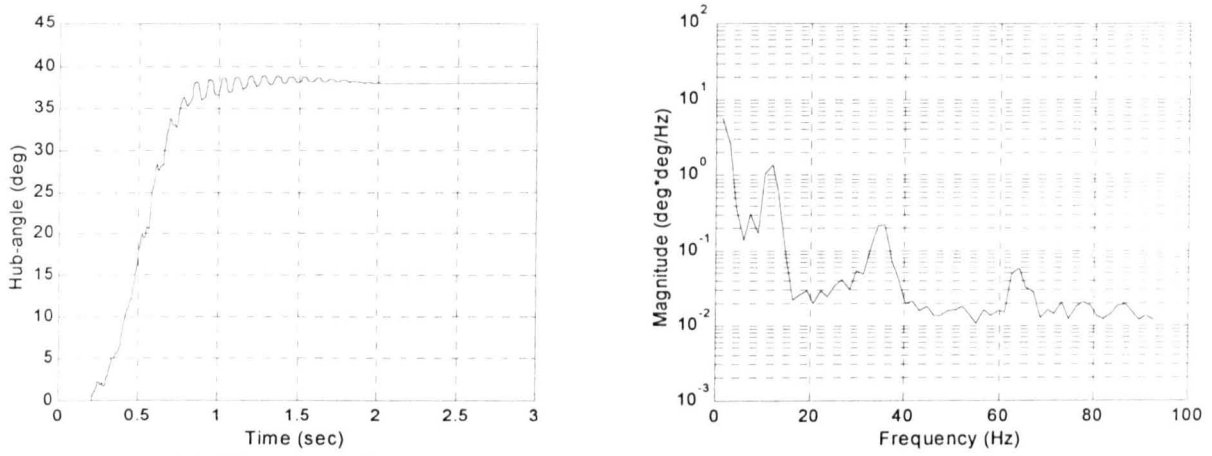

(a) Time domain. (b) PSD.

Figure 3.18: Hub-angle response of the flexible manipulator experimental rig without payload.

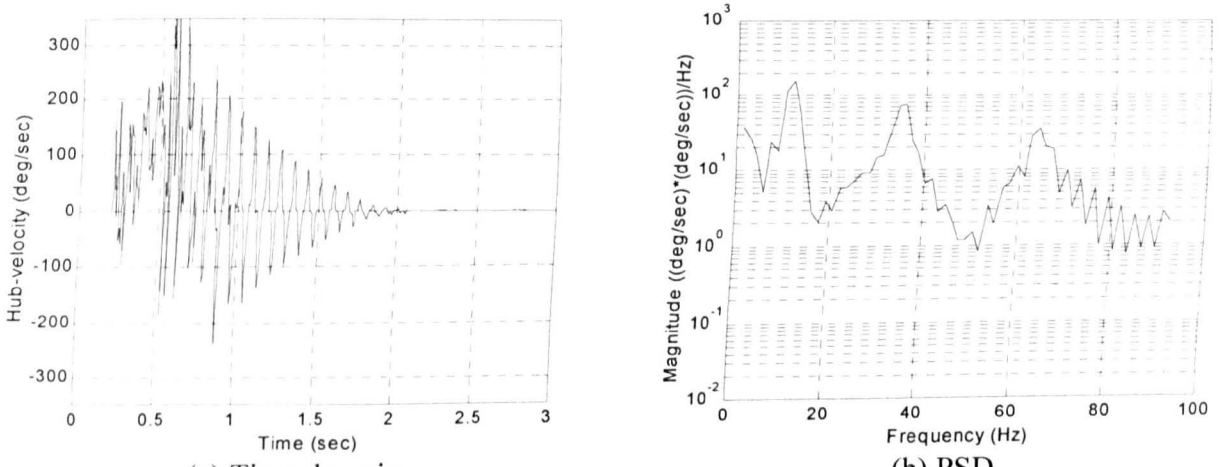

(a) Time domain. (b) PSD.

Figure 3.19: Hub-velocity response of the flexible manipulator experimental rig without payload.

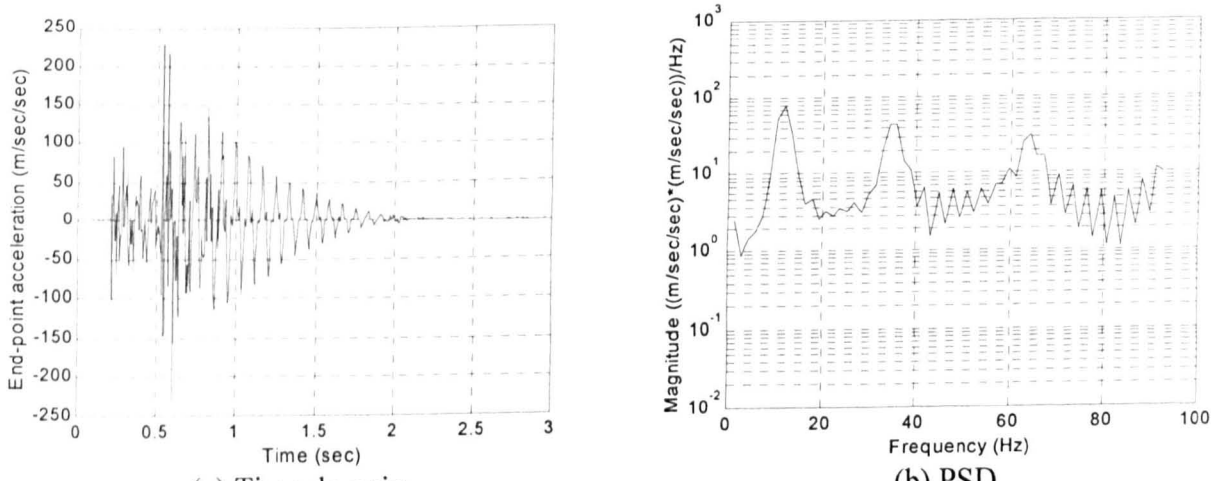

(a) Time domain. (b) PSD.

Figure 3.20: End-point acceleration response of the flexible manipulator experimental rig without payload.

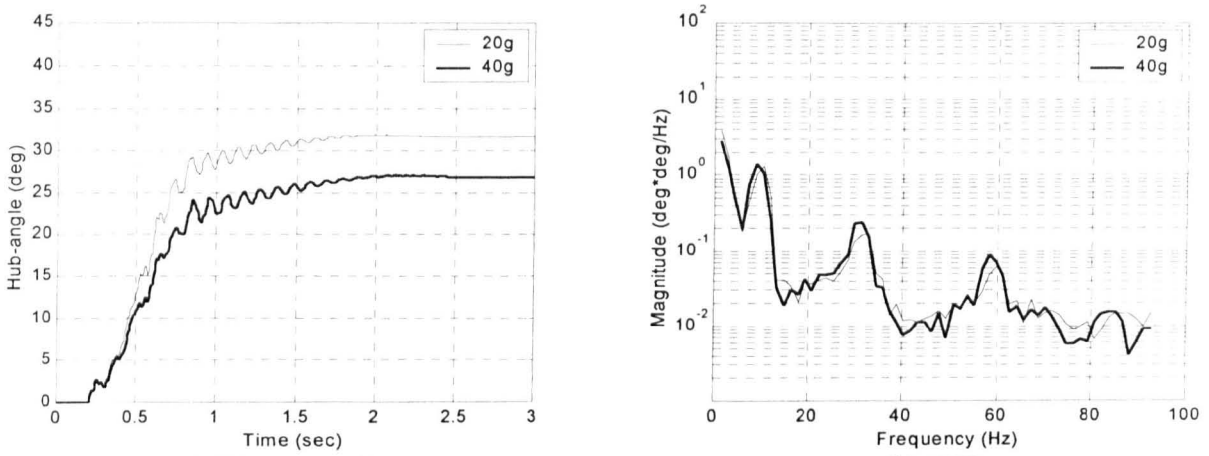

(a) Time domain. (b) PSD.

Figure 3.21: Hub-angle response of the flexible manipulator experimental rig with payloads.

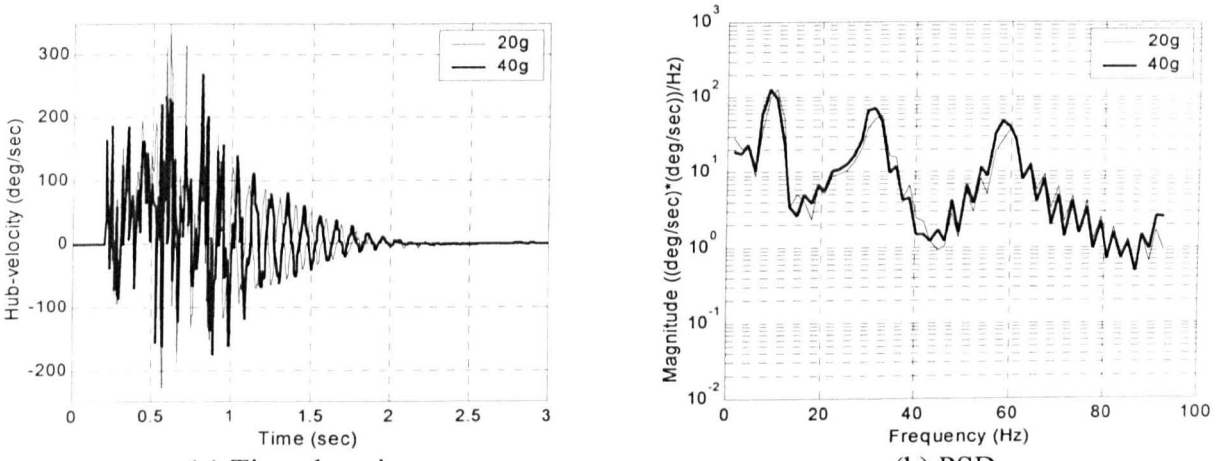

(a) Time domain. (b) PSD.

Figure 3.22: Hub-velocity response of the flexible manipulator experimental rig with payloads.

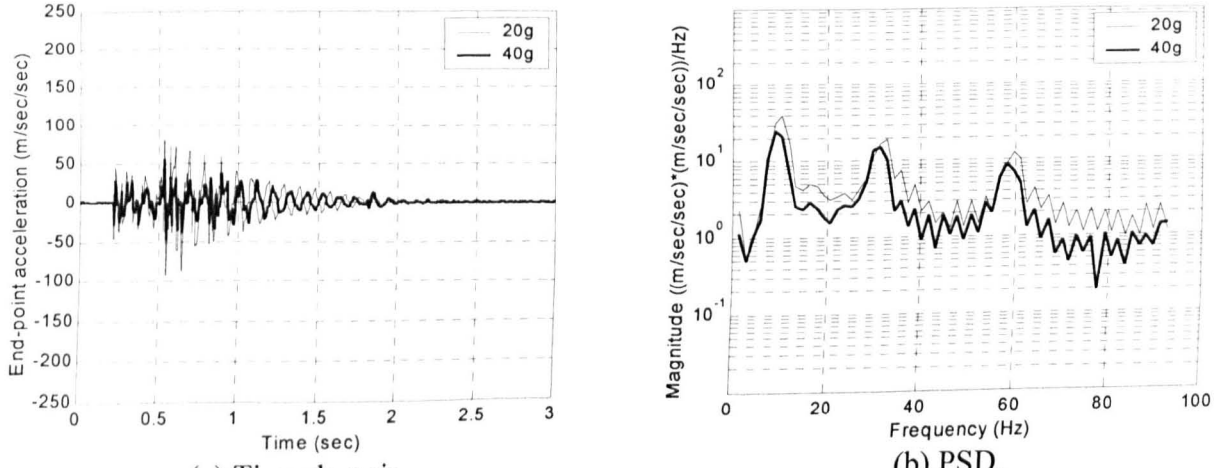

(a) Time domain. (b) PSD.

Figure 3.23: End-point acceleration response of the flexible manipulator experimental rig with payloads.

Table 3.3: Relation between payload and resonance frequencies of the flexible manipulator experimental rig.

Payloads (grams)	Resonance frequencies (Hz)		
	Mode 1	Mode 2	Mode 3
0	11.72	35.15	65.60
10	10.97	33.40	61.85
20	10.23	32.95	59.35
30	9.97	31.42	59.35
40	9.48	30.92	58.85
50	9.23	30.42	58.10
60	8.97	30.17	56.61

3.6. Model Validation

Validation of a dynamic model for use in simulation and control is an important step before the model can be employed with confidence. Typically, model validation can be considered in two parts: frequency-domain validation, which involves the resonance frequencies of the system, and time-domain validation, which focuses on the time response of various system states to an input command. Matching of natural frequencies is a good indication of accurately modelled mass and stiffness properties whereas time-domain results show the effects of assumptions concerning the non-linear terms in the equations of motion.

Validation of the developed FE model was carried out by comparing the simulation and experimental results in time and frequency domains. Comparisons of the responses of the manipulator without payload show that a close agreement between experimental and simulation results in the time responses and resonance frequencies was obtained. For the hub-angle, a steady-state level of 38 degrees was achieved in both cases. Similar characteristics are also noted in the transient response of the system. Furthermore, reasonably close agreement between the simulation and experimental results is noted with the end-point acceleration response. It is also noted in Table 3.1 that the first three modes of vibration of the system converged to 11.99 Hz, 35.22 Hz and 65.20 Hz with 10 elements or more. The experimental results, however, gave 11.72 Hz, 35.15 Hz and 65.60 Hz. The corresponding errors between the simulation and experimental results for modes 1, 2 and 3 are accordingly 2.3 %, 0.2 % and 0.6 %, which are considered negligibly small. Earlier work using the FD method for modelling of the single-link flexible manipulator has shown that with 10 sections, the vibration frequencies of the system were obtained as 12.4 Hz, 37.9 Hz and 77.0 Hz (Tokhi et al., 1997). The corresponding errors between the FD algorithm and experiments for

the first three modes are accordingly 5.8%, 7.8% and 17.4% which are higher than the errors with FE algorithm. It can thus be concluded that FE methods can successfully be used for modelling of a flexible manipulator. Moreover, these validate the assumptions used in this work.

For the manipulator with payload, it can be observed that simulation and experimental results were slightly different in the steady-state level and settling time of the hub-angle of the system. It is noted that the differences increase with increasing payloads. The differences are within 2 – 6 degrees. These could mainly be due to payload rotary inertia and the gravity effect, which are ignored in the simulation. Theoretically, gravity contributes to the potential energy and thus the mass matrix of the system. However, with increasing payloads, both cases show a decrease in the level of hub-angle responses. In the frequency-domain, comparisons of experimental and simulation results in Tables 3.2 and 3.3, show that reasonably close results were achieved for all payloads for mode 2 and mode 3, with the maximum error of 2.65%. For mode 1, with increasing payload, the errors between simulation and experiments increased from 6.19% to 14.15%. Although slight differences were noted in the time-response, the simulation algorithm provided a close characteristic behaviour of the experimental rig with increasing payloads. Such characteristic behaviour is important and essential for development of suitable control strategies for flexible manipulator systems.

3.7. Summary

Theoretical and experimental investigations into the dynamic modelling and characterisation of a single-link flexible manipulator system have been presented. A dynamic model of the manipulator incorporating structural damping, hub inertia and payload has been developed using FE methods. The performance and accuracy of the algorithm has been studied in comparison to an experimental rig. The effects of damping and payload on the system behaviour have been addressed. Experiments have been performed using the experimental rig and used for validation of the FE model. A very close agreement between simulation and experimental results has been achieved. Thus, confidence in the accuracy of the model for utilisation in subsequent investigations, at development of control strategies for flexible manipulator systems, has been established.

Chapter 4

Modelling and Performance Analysis Using a Symbolic Manipulation Approach

4.1. Introduction

This chapter presents the application of a symbolic manipulation approach for modelling and performance analysis of a flexible manipulator system using the FE method. The single-link flexible manipulator described in Chapter 2 is considered. The objective of this chapter is to provide an alternative approach to the analysis of the dynamics of the system. Several advantages of using the symbolic approach in analysis of the flexible manipulator are investigated, which can also be applied in other control systems. For purposes of simplicity, a single-link flexible manipulator without damping and with a single element is considered. A symbolic algorithm characterising the dynamic behaviour of the system is developed using a symbolic language. Using such an approach, a good approximation of the transfer function representing the actual flexible manipulator is obtained in symbolic form. Analyses and investigations in terms of system stability, time response to an input command and vibration frequencies are presented. The relations between the physical parameters and the poles, zeros, stability, vibration frequencies and time response of the system are also studied. Comparisons of the symbolic and experimental results are presented to demonstrate the performance of the symbolic algorithm for modelling and analysis of characteristic behaviour of a flexible manipulator. The analyses presented in this chapter can also be carried out using the FE approach described in Chapter 3. However, the approach using symbolic manipulation provides more transparent results.

4.2. A Symbolic Manipulation Approach

As highlighted in Chapter 1, various approaches have previously been devised for modelling of flexible manipulators. These include the assumed modes, singular perturbation, frequency-domain, FD and FE methods to solve the PDE characterising the dynamic behaviour of a flexible manipulator system. Investigations in Chapter 3 showed that the FE method can be utilised in obtaining a good representation of the system, and even a single element is sufficient to describe the dynamic behaviour of a flexible manipulator reasonably well. Moreover, the FE method exhibits several advantages over the FD method in terms of accuracy and computational requirements (Tokhi et al., 1997).

However, in most cases, investigations involving the FE method are numerical-based. Dynamic characteristics of the manipulator including stability, time response and vibration frequencies are interpreted on the basis of a single particular case, with no provision for any generality. Moreover, numerical systems must operate using numeric approximations, whose precision is limited by the computer hardware. Alternatively, exact quantities can be obtained by retaining the computations in a symbolic form. A distinguishing feature of symbolic-based methods is the mathematically comprehensive output they generate, so that the significance of individual terms, or group of terms, may be identified. This brings with it the opportunity to gain insights into the model that would otherwise not be available. A symbolic manipulation will open up the possibility of analysing a system in both new and interesting ways. It can be seen that the trend over time has been away from fully numeric methods of formulation towards those with a strong and total symbolic flavour to them. This is due to the overwhelmingly rapid improvements in computer hardware technology in general and in computer algebra software in particular (Larcombe and Brown, 1997).

Symbolic approaches for modelling and simulation of flexible manipulators have previously been investigated. Most of these investigations have developed automated symbolic derivations of dynamic equations of motion of rigid and flexible manipulators utilising Lagrangian formulation and assumed mode methods (Cetinkunt and Ittop, 1992; De Luca et al., 1988; Lin and Lewis, 1994), Hamilton's principle and non-linear integro-differential equations (Low and Vidyasagar, 1988) and FD approximations (Tzes et al., 1988). These have demonstrated that the approach has some advantages, such as allowing independent variation of flexure parameters. However, in utilising this manipulation approach, not much work has been done on modelling and analysis of a flexible manipulator using the FE method. Moreover, relations between system parameters including payload and

hub inertia and the system characteristics can be further investigated. The effect of payload on the manipulator is important for modelling and control purposes, as successful implementation of a flexible manipulator control is contingent upon achieving acceptable uniform performance in the presence of payload variations.

4.3. Development of the Symbolic Algorithm

This section focuses on the development of the symbolic algorithm in characterising the dynamic behaviour of the flexible manipulator system. In this work, structural damping is ignored. Formulations to obtain the dynamic equations of motion of the system incorporating the payload and hub inertia presented in the previous chapter are utilised. In this approach, all the manipulations are carried out symbolically using Macsyma, a symbolic algebraic manipulation language. Two transfer functions, namely, from torque input to end-point displacement and from torque input to hub-angle of the manipulator are considered.

4.3.1. Dynamic Equations of Motion

As demonstrated in equations (3.1), (3.2) and (3.3), the total displacement $y(x,t)$ of a point along the manipulator at a distance x from the hub can be obtained as

$$y(x,t) = x\theta(t) + w(x,t)$$

where $w(x,t) = N_a(x)Q_a(t)$.

Hence, the displacement can be obtained as

$$y(x,t) = N(x)\,Q_b(t) \tag{4.1}$$

where

$$N(x) = \begin{bmatrix} x & N_a(x) \end{bmatrix} \text{ and } Q_b(t) = \begin{bmatrix} \theta(t) & Q_a(t) \end{bmatrix}^T$$

The shape function $N(x)$ and nodal displacement vector $Q_b(t)$ in equation (4.1) incorporate local and global variables. Among these, the angle $\theta(t)$ and the distance x are global

variables while $N_a(x)$ and $Q_a(t)$ are local variables. Defining $k = x - \sum_{i=1}^{n-1} l_i$ as a local variable of the nth element, where l_i is the length of the ith element and utilising Macsyma, the shape function can be expressed in symbolic form as

$$N(k) = \left[k + l(n-1) \;\; 1 - \frac{3k^2}{l^2} + \frac{2k^3}{l^3} \;\; k - \frac{2k^2}{l} + \frac{k^3}{l^2} \;\; \frac{3k^2}{l^2} - \frac{2k^3}{l^3} \;\; -\frac{k^2}{l} + \frac{k^3}{l^2} \right]$$

Accordingly, by solving equations (3.6) and (3.7) with

$$\Phi = \frac{d^2 N(k)}{dk^2} = \left[0 \;\; \frac{12k}{l^3} - \frac{6}{l^2} \;\; \frac{6k}{l^2} - \frac{4}{l} \;\; \frac{6}{l^2} - \frac{12k}{l^3} \;\; \frac{6k}{l^2} - \frac{2}{l} \right],$$

the element mass and stiffness matrices can be obtained as

$$M_n = \frac{\rho S l}{420} \begin{bmatrix} 140l^2(3n^2 - 3n + 1) & 21l(10n-7) & 7l^2(5n-3) & 21l(10n-3) & -7l^2(5n-2) \\ 21l(10n-7) & 156 & 22l & 54 & -13l \\ 7l^2(5n-3) & 22l & 4l^2 & 13l & -3l^2 \\ 21l(10n-3) & 54 & 13l & 156 & -22l \\ -7l^2(5n-2) & -13l & -3l^2 & -22l & 4l^2 \end{bmatrix}$$

$$K_n = \frac{EI}{l^3} \begin{bmatrix} 0 & 0 & 0 & 0 & 0 \\ 0 & 12 & 6l & -12 & 6l \\ 0 & 6l & 4l^2 & -6l & 2l^2 \\ 0 & -12 & -6l & 12 & -6l \\ 0 & 6l & 2l^2 & -6l & 4l^2 \end{bmatrix}$$

The matrices from above are assembled to obtain mass and stiffness matrices of the system, M and K, and used in the Lagrange equation to obtain the dynamic equation of the flexible manipulator as

$$M\ddot{Q}(t) + KQ(t) = F(t) \tag{4.2}$$

where $F(t)$ is the vector of external forces and $Q(t) = [\theta \quad w_0 \quad \theta_0 \quad . \quad . \quad . \quad w_\alpha \quad \theta_\alpha]^T$. Using a single element, $n = 1$, the dynamic equation of motion of the flexible manipulator can be obtained as in equation (4.2) with

$$M = \frac{\rho S l}{420}\begin{bmatrix} 140l^2 & 63l & 14l^2 & 147l & -21l^2 \\ 63l & 156 & 22l & 54 & -13l \\ 14l^2 & 22l & 4l^2 & 13l & -3l^2 \\ 147l & 54 & 13l & 156 & -22l \\ -21l^2 & -13l & -3l^2 & -22l & 4l^2 \end{bmatrix},$$

$$K = \frac{EI}{l^3}\begin{bmatrix} 0 & 0 & 0 & 0 & 0 \\ 0 & 12 & 6l & -12 & 6l \\ 0 & 6l & 4l^2 & -6l & 2l^2 \\ 0 & -12 & -6l & 12 & -6l \\ 0 & 6l & 2l^2 & -6l & 4l^2 \end{bmatrix},$$

$$Q(t) = [\theta \quad w_0 \quad \theta_0 \quad w_\alpha \quad \theta_\alpha]^T \text{ and } F(t) = [\tau \quad 0 \quad 0 \quad 0 \quad 0]^T.$$

Using the same formulation as presented in Chapter 3, to incorporate the payload and hub inertia into the dynamic model of the system, for a single element, a new system mass matrix that incorporates the hub inertia and payload can be obtained as

$$M = \frac{\rho S l}{420}\begin{bmatrix} 140l^2 + l^2 m_p + I_h & 63l & 14l^2 & 147l + lm_p & -21l^2 \\ 63l & 156 & 22l & 54 & -13l \\ 14l^2 & 22l & 4l^2 & 13l & -3l^2 \\ 147l + lm_p & 54 & 13l & 156 + m_p & -22l \\ -21l^2 & -13l & -3l^2 & -22l & 4l^2 \end{bmatrix}$$

For the manipulator considered as a clamped-free arm, with the applied torque τ at the hub, the flexural and angular displacements, velocities and accelerations are all zero at the hub at $t = 0$. Moreover, in this work, it is assumed that $Q(0) = 0$. Incorporating the initial conditions, with flexural and angular displacements at the hub as zero, the second and third rows and columns in M, K, Q and F are thus ignored. This yields

$$M = \frac{\rho Sl}{420}\begin{bmatrix} 140l^2 + l^2 m_p + I_h & 147l + lm_p & -21l^2 \\ 147l + lm_p & 156 + m_p & -22l \\ -21l^2 & -22l & 4l^2 \end{bmatrix},\quad K = \frac{EI}{l^3}\begin{bmatrix} 0 & 0 & 0 \\ 0 & 12 & -6l \\ 0 & -6l & 4l^2 \end{bmatrix},$$

$$Q(t) = [\theta \quad w_a \quad \theta_a]^T \text{ and } F(t) = [\tau \quad 0 \quad 0]^T.$$

4.3.2. Transfer Functions

For control purposes, the matrix differential equation in equation (4.2) is represented in a state-space form as

$$\begin{aligned} \dot{v} &= Av + Bu \\ y &= Cv \end{aligned} \tag{4.3}$$

where

$$A = \left[\begin{array}{c|c} 0_3 & I_{D3} \\ \hline -M^{-1}K & 0_3 \end{array}\right],\quad B = \left[\begin{array}{c} 0_{3\times 1} \\ \hline M_1^{-1} \end{array}\right]$$

$u = [\tau]$ and the state, $v = [\theta \quad w_a \quad \theta_a \quad \dot{\theta} \quad \dot{w}_a \quad \dot{\theta}_a]^T$ that is the angular, nodal flexural and rotational displacements and velocities. 0_3 is a 3×3 null matrix, I_{D3} is a 3×3 identity matrix, $0_{3\times 1}$ is a 3×1 null vector and M_1^{-1} is the first column of M^{-1}. The output matrix C depends on desired transfer functions. For torque input to end-point displacement output, $C = [L \quad 1 \quad 0 \quad 0 \quad 0 \quad 0]$ whilst for torque input to hub-angle output, $C = [1 \quad 0 \quad 0 \quad 0 \quad 0 \quad 0]$.

Using a single element, the matrix A can be obtained as

$$A = \begin{bmatrix} 0_3 & I_{D3} \\ A_{21} & 0_3 \end{bmatrix}$$

With $\alpha = \rho Sl$ representing the weight and $\beta = EI$ representing the flexural rigidity of the manipulator, the sub-matrix A_{21} can be obtained as

$$A_{21} = \frac{\beta}{\varphi}\begin{bmatrix} 0 & a_{12} & a_{13} \\ 0 & a_{22} & a_{23} \\ 0 & a_{32} & a_{33} \end{bmatrix}$$

where

$$\varphi = (15\alpha l^2 + 3600 I_h) m_p + \alpha^2 l^2 + 300\alpha I_h$$

$$a_{12} = \frac{12(3600 l m_p + 270\alpha l)}{l^3} - \frac{6(900 m_p - 90\alpha)}{l^2}$$

$$a_{13} = \frac{4(900 m_p - 90\alpha)}{l} - \frac{6(3600 l m_p + 270\alpha l)}{l^2}$$

$$a_{22} = \frac{6(900 l^2 m_p - 15\alpha l^2 + 19800 I_h) - 12(3600 l^2 m_p + 255\alpha l^2 + 3600 I_h)}{l^3}$$

$$a_{23} = \frac{6(3600 l^2 m_p + 255\alpha l^2 + 3600 I_h) - 4(900 l^2 m_p - 15\alpha l^2 + 19800 I_h)}{l^2}$$

$$a_{32} = \frac{6(1800\alpha l^2 + 37800 I_h) m_p + 495\alpha^2 l^2 + 140400\alpha I_h}{\alpha l^4} - \frac{12(900 l^2 m_p - 15\alpha l^2 + 19800 I_h)}{l^4}$$

$$a_{33} = \frac{6(900 l^2 m_p - 15\alpha l^2 + 19800 I_h)}{l^3} - \frac{4(1800\alpha l^2 + 37800 I_h) m_p + 495\alpha^2 l^2 + 140400\alpha I_h}{\alpha l^3}$$

Similarly, the matrix B can be obtained as

$$B = \frac{1}{(15\alpha l^2 + 3600 I_h) m_p + \alpha^2 l^2 + 300\alpha I_h}\begin{bmatrix} 0 \\ 0 \\ 0 \\ 300\alpha + 3600 m_p \\ -270\alpha - 3600 m_p l \\ 90\alpha - 900 m_p \end{bmatrix}$$

Using equation (4.3), the transfer function of the system can be expressed as

$$G(s) = \frac{Y(s)}{U(s)} = C(sI_D - A)^{-1} B \tag{4.4}$$

where s is the Laplace variable and I_D is the identity matrix.

For the transfer function from torque input to end-point displacement, substituting for the matrices A, B and C from equation (4.3) into equation (4.4) and simplifying yields

$$G_1(s) = \frac{30\alpha^2 l^7 s^4 - 48600\alpha\beta l^4 s^2 + 4536000\beta^2 l}{s^2[((15\alpha^2 l^8 + 3600\alpha l^6 I_h)m_p + \alpha^3 l^8 + 300\alpha^2 l^6 I_h)s^4 + ((39600\alpha\beta l^5 + 1512000\beta l^3 I_h)m_p + 5220\alpha^2\beta l^5 + 367200\alpha\beta l^3 I_h)s^2 + (4536000\beta^2 l^2 m_p + 1512000\alpha\beta^2 l^2 + 4536000\beta^2 I_h)]} \quad (4.5)$$

Similarly, the transfer function from torque input to hub-angle output of the manipulator can be obtained as

$$G_2(s) = \frac{(3600\alpha l^6 m_p + 300\alpha^2 l^6)s^4 + (1512000\beta l^3 m_p + 367200\alpha\beta l^3)s^2 + 4536000\beta^2}{s^2[((15\alpha^2 l^8 + 3600\alpha l^6 I_h)m_p + \alpha^3 l^8 + 300\alpha^2 l^6 I_h)s^4 + ((39600\alpha\beta l^5 + 1512000\beta l^3 I_h)m_p + 5220\alpha^2\beta l^5 + 367200\alpha\beta l^3 I_h)s^2 + (4536000\beta^2 l^2 m_p + 1512000\alpha\beta^2 l^2 + 4536000\beta^2 I_h)]} \quad (4.6)$$

4.4. Analysis

In this section, the transfer functions obtained in the previous section are analysed and assessed in the dynamic characterisation of the flexible manipulator system. Firstly, a system without payload and hub inertia is considered. Then effects of payload and hub inertia on the dynamic behaviour of the system are examined. This involves obtaining and investigating the system characteristics including poles, zeros, stability, vibration frequency and time response to an input command. Relationships between the physical parameters and the system characteristics are then investigated. Note that in this work, the effect of damping is ignored. Therefore, the system is expected to be marginally stable, exhibiting a response of oscillatory nature.

4.4.1. System without Payload and Hub Inertia

For a flexible manipulator without payload and hub inertia, the system transfer functions can be obtained by solving equations (4.5) and (4.6) with $m_p = 0$ and $I_h = 0$. Thus, the transfer function from torque input to end-point displacement can be obtained as

$$G_{1a}(s)=\frac{30\alpha^2 l^7 s^4-48600\alpha\beta l^4 s^2+4536000\beta^2 l}{s^2(\alpha^3 l^8 s^4+5220\alpha^2\beta l^5 s^2+1512000\alpha\beta^2 l^2)} \tag{4.7}$$

and the transfer function from torque input to hub-angle output can be obtained as

$$G_{2a}(s)=\frac{300\alpha^2 l^6 s^4+367200\alpha\beta l^3 s^2+4536000\beta^2}{s^2(\alpha^3 l^8 s^4+5220\alpha^2\beta l^5 s^2+1512000\alpha\beta^2 l^2)} \tag{4.8}$$

Factoring the numerator and denominator polynomials of equation (4.7) yields system zeros as

$$\eta=\pm 38.9944\sqrt{\frac{\beta}{\alpha l^3}},\ \pm 9.9718\sqrt{\frac{\beta}{\alpha l^3}} \tag{4.9}$$

and system poles as

$$p=\pm j17.5444\sqrt{\frac{\beta}{\alpha l^3}},\ \pm j70.087\sqrt{\frac{\beta}{\alpha l^3}},0,0. \tag{4.10}$$

The poles on the imaginary axis give the system natural frequencies. These, in turn, determine vibration modes of the system. Evaluating equation (4.10) yields vibration frequencies at modes 1 and 2 as $\frac{17.5444}{2\pi}\sqrt{\frac{\beta}{\alpha l^3}}$ Hz and $\frac{70.087}{2\pi}\sqrt{\frac{\beta}{\alpha l^3}}$ Hz respectively. These demonstrate that the frequencies depend on α, β and l. Figure 4.1 shows the effect of flexural rigidity, β of a manipulator on the vibration frequencies of modes 1 and 2 with a constant weight of the manipulator, α. Practically, changing the value of β implies changing the manipulator material. In this case, $\alpha=0.15$ kg is used. Similarly, the inter-relation between α and the vibration frequencies of the system with a constant β can be investigated. The result with $\beta=3.69$ Nm^2 is shown in Figure 4.2. It is also important to investigate, for the same material, the effect of changing the manipulator length on vibration frequency. Figure 4.3 shows the result with two different materials, $\beta=1.2$ Nm^2 and 3.6 Nm^2 . It follows from these results that the system vibration frequencies can be increased by either (i)

increasing the flexural rigidity of the manipulator, or (ii) reducing the weight of the manipulator, or (iii) reducing the length of the manipulator. These are further evidenced in Figures 4.4 and 4.5, which demonstrate the relation of α and β with vibration frequencies at modes 1 and 2 respectively. These show that high system vibration frequency is obtained with small α and large β of a flexible manipulator.

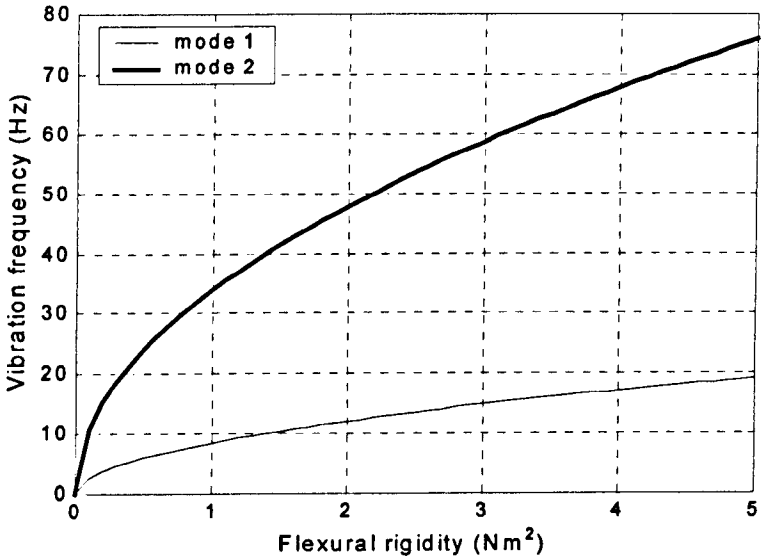

Figure 4.1: Effect of flexural rigidity on vibration frequency ($\alpha = 0.15$ kg).

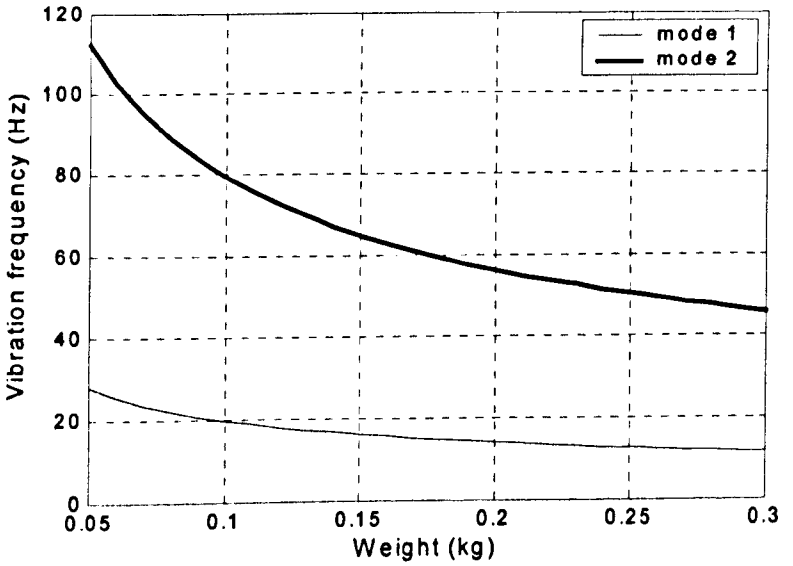

Figure 4.2: Effect of the weight of a manipulator on vibration frequency ($\beta = 3.69$ Nm^2).

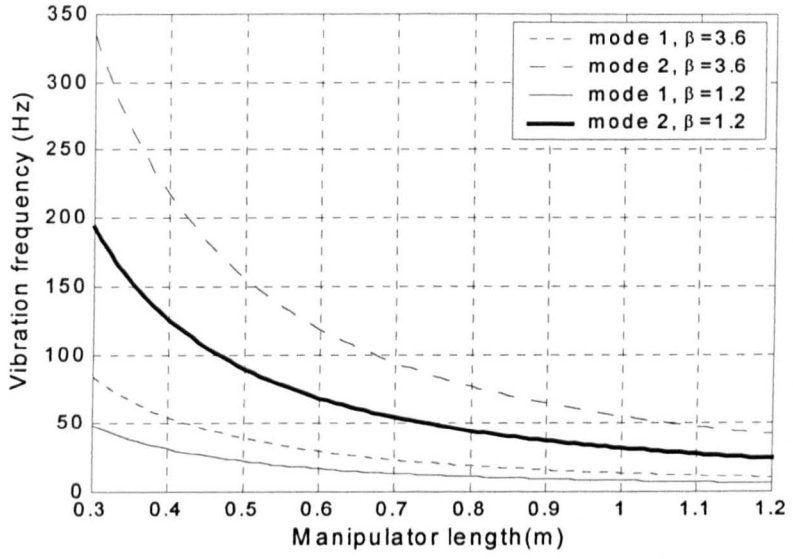

Figure 4.3: Effect of length of a manipulator on vibration frequency with two types of material.

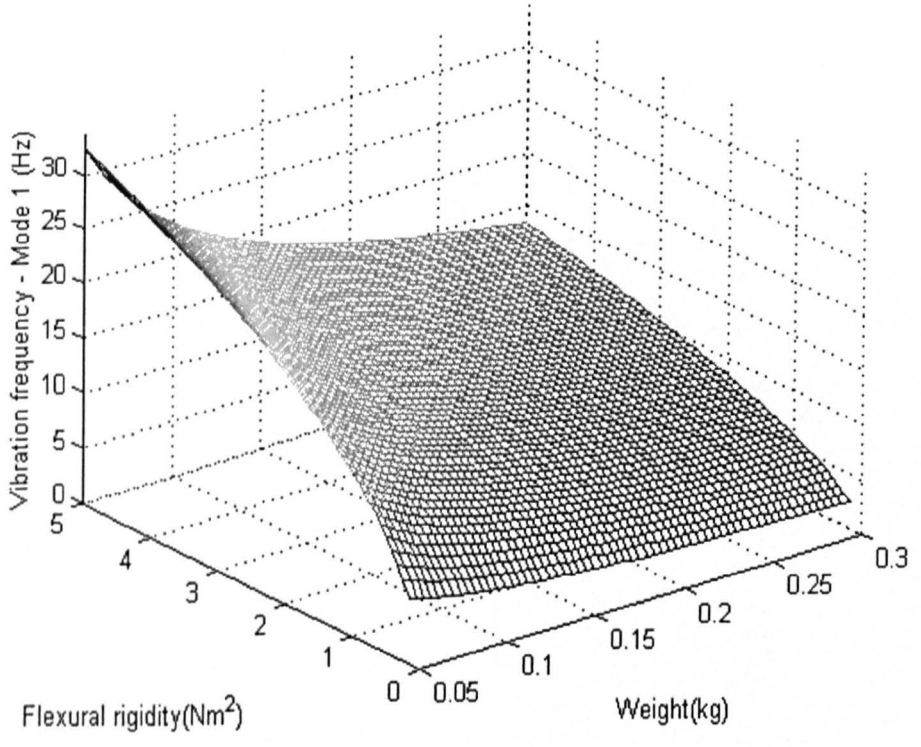

Figure 4.4: Relationship between flexural rigidity, weight and vibration frequency (mode 1).

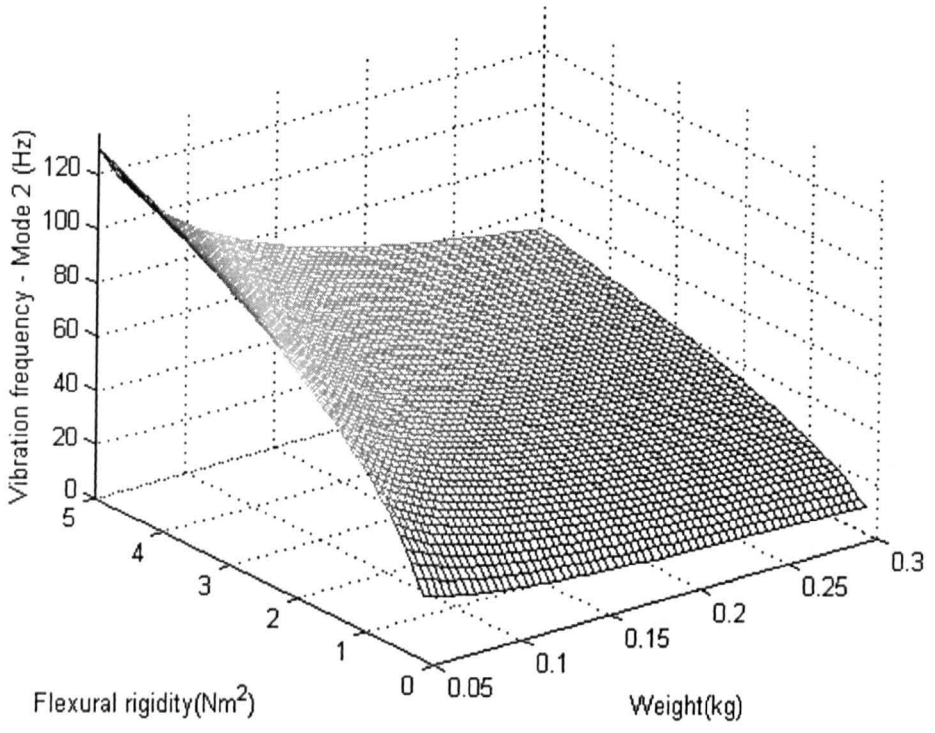

Figure 4.5: Relationship between flexural rigidity, weight and vibration frequency (mode 2).

4.4.2. System with Payload and Hub Inertia

It is noted from the transfer function $G_1(s)$ in equation (4.5) that the hub inertia and payload terms are not in the numerator of the transfer function. Therefore, they do not affect the system zeros. The zeros will determine whether the system exhibits minimum-phase or non-minimum phase behaviour and will determine the magnitude of response of the system. The system poles, on the other hand, are affected by the payload and the hub inertia, see equation (4.5). Conversely, for the transfer function $G_2(s)$ in equation (4.6), it is noted that the zeros are affected by the payload. Furthermore, it is noted that the flexible manipulator is a type two system, which implies that zero steady-state error can only be achieved using step and ramp command inputs to the system.

By equating the numerator of the transfer function $G_1(s)$ to zero and solving yields the zeros as

$$\eta = \pm 38.9944\sqrt{\frac{\beta}{\alpha l^3}}, \quad \pm 9.9718\sqrt{\frac{\beta}{\alpha l^3}}$$

It is noted that, with any α, β and l values, two zeros lie on the right half of s-plane (rhp) and the others on the left half of s-plane (lhp). Thus, the system is non-minimum phase and undershoot is expected at the start in the end-point displacement response. This agrees, with the result reported earlier in respect of a system incorporating non-collocated sensors and actuators (Book, 1984; Cannon and Schmitz, 1984; Hastings and Book, 1987, Tokhi et al., 1997).

To investigate the effects of payload and hub inertia on the dynamic behaviour of the system, the transfer functions $G_1(s)$ and $G_2(s)$ were solved for a system with physical parameters corresponding to the flexible manipulator experimental rig introduced in Chapter 2. Thus, the transfer function from the torque input to end-point displacement can be obtained as

$$G_{1b}(s) = \frac{0.32s^4 - 17669.9s^2 + 5.69\times10^7}{s^2[((283.92I_h + 0.14)m_p + 3.51I_h + 0.0014)s^4 + ((4116780I_h + 12960.4)m_p + 148368.8I_h + 253.53)s^2 + (5.13\times10^7 m_p + 61.65\times10^6 I_h + 2535290)]} \quad (4.11)$$

and the transfer function from torque input to hub-angle can be obtained as

$$G_{2b}(s) = \frac{(283.86m_p + 3.51)s^4 + (4116760m_p + 148339.8)s^2 + 6.33\times10^7}{s^2[((283.92I_h + 0.14)m_p + 3.51I_h + 0.0014)s^4 + ((4116780I_h + 12960.4)m_p + 148368.8I_h + 253.53)s^2 + (5.13\times10^7 m_p + 61.65\times10^6 + 2535290)]} \quad (4.12)$$

By factorising the denominator of the system transfer functions $G_{1b}(s)$ and $G_{2b}(s)$, the system poles in terms of payload and hub inertia can be obtained as

$$p_{1,2} = \pm 6.09\sqrt{\frac{6.47h_1}{h_2}}, \; p_{3,4} = \pm 6.09\sqrt{\frac{-6.47h_1}{h_2}}, \; p_5 = 0, \; p_6 = 0 \quad (4.13)$$

where

$$h_1 = \sqrt{\begin{aligned}&((2.12\times10^8 I_h^{\,2} + 605827.8I_h + 1733.88)m_p^{\,2} + (1.44\times10^7 I_h^{\,2}\\ &+ 28705.3I_h + 60.47)m_p + 263847.6I_h^{\,2} + 490.47I_h + 0.62)\\ &- (94119.5I_h m_p + 296.31m_p + 3392.06I_h + 5.8)\end{aligned}}$$

and $h_2 = 480.82I_h m_p + 0.24m_p + 5.95I_h + 0.0024$.

Further, with the hub inertia $I_h = 5.8598\times10^{-4}$ kgm^2, the denominator of the system transfer functions can be obtained as

$$(0.3m_p + 0.0035)s^6 + (15370.2m_p + 340.36)s^4 + (5.13\times10^7 m_p + 2571860)s^2 \quad (4.14)$$

Therefore, the poles in terms of payload can be obtained as

$$p_{1,2} = \pm 6.09\sqrt{\frac{6.47h_3 - (351.5m_p + 7.8)}{0.5m_p + 0.006}},$$

$$p_{3,4} = \pm 6.09\sqrt{\frac{-6.47h_3 - (351.5m_p + 7.8)}{0.5m_p + 0.006}},\ p_5 = 0,\ p_6 = 0 \quad (4.15)$$

where $h_3 = \sqrt{2161.6m_p^{\,2} + 82.2m_p + 1.0}$.

Note that for a single element, the system has six poles, two of which are at the origin. For $m_p \geq 0$, the terms under the square roots in equation (4.15) can be shown to be negative. Consider the square root,

$$\sqrt{\frac{6.47\sqrt{(2161m_p^{\,2} + 82.2m_p + 1.0)} - (351.5m_p + 7.8)}{0.5m_p + 0.006}}$$

Let $b_1 = 6.47\sqrt{2161m_p^{\,2} + 82.2m_p + 1.0}$ and $b_2 = 351.5m_p + 7.8$. The result is negative if $b_1 < b_2$ for $m_p \geq 0$. Further analysis shows that

$$b_1 = 6.47\sqrt{2161m_p^2 + 82.2m_p + 1.0}$$
$$= \sqrt{90486.5m_p^2 + 3440.9m_p + 41.860}$$
$$b_1^2 = 90486.5m_p^2 + 3440.9m_p + 41.860 \quad (4.16)$$

and

$$b_2^2 = 123552.25m_p^2 + 5483.4m_p + 60.84 \quad (4.17)$$

Since all terms on the right-hand side of equation (4.16) are smaller than equation (4.17), it can be proved that $b_1^2 < b_2^2$ and $b_1 < b_2$. Thus, the remaining poles are purely imaginary and lie on the imaginary axis of the s-plane. These result in, as expected for a system without damping, a marginally stable system.

The system poles give the system vibration frequencies. These, in turn, determine vibration modes of the system, and thus the effects of payload and hub inertia on the vibration frequency can be investigated by solving equations (4.13) and (4.15). Figure 4.6 demonstrates the relation between payload and system vibration frequencies for modes 1 and 2 with $I_h = 5.8598 \times 10^{-4}$ kgm^2. Similarly, Figure 4.7 demonstrates the effect of hub inertia on the system vibration frequencies for modes 1 and 2 with a payload of 30 grams. It is noted that with increasing payload and hub inertia, the vibration frequencies decrease significantly. These are further evidenced in Figures 4.8 and 4.9 that demonstrate the relation between payload, hub inertia and vibration frequencies for modes 1 and 2 respectively.

For the transfer function $G_2(s)$, factorising the numerator yields the zeros as

$$\eta_{1,2} = \frac{\pm 3.5}{l}\sqrt{\frac{3.4\beta h_4 - (210\beta m_p + 51\alpha\beta)}{12\alpha l m_p + \alpha^2 l}} \quad (4.18)$$

$$\eta_3 = \frac{-3.8}{l}\sqrt{\frac{12.9h_5 - (784.3m_p + 28.2672)}{1.6m_p + 0.02}}$$

$$\eta_4 = \frac{-3.8}{l}\sqrt{\frac{-12.9h_5 - (784.3m_p + 28.2672)}{1.6m_p + 0.02}}$$

where $h_4 = \sqrt{3675m_p^2 + 1680\alpha m_p + 208\alpha^2}$ and $h_5 = \sqrt{3675m_p^2 + 249.3\alpha m_p + 4.6\alpha^2}$.

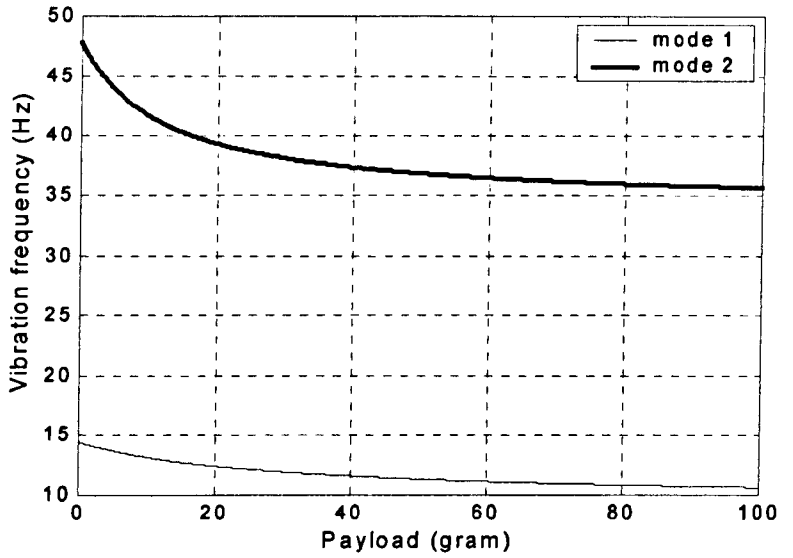

Figure 4.6: Effect of payload on the vibration frequency of the system using $I_h = 5.8598\times10^{-4}$ kgm^2.

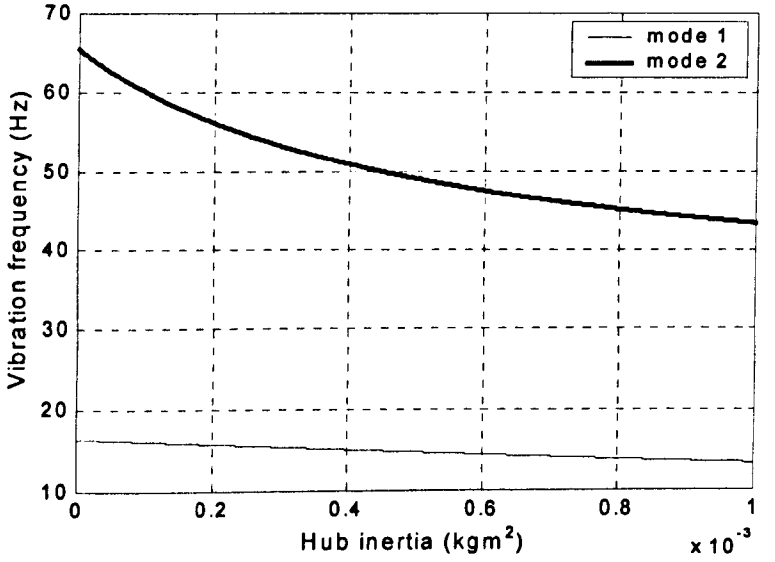

Figure 4.7: Effect of hub inertia on the vibration frequency of the system using $m_p = 30$ grams.

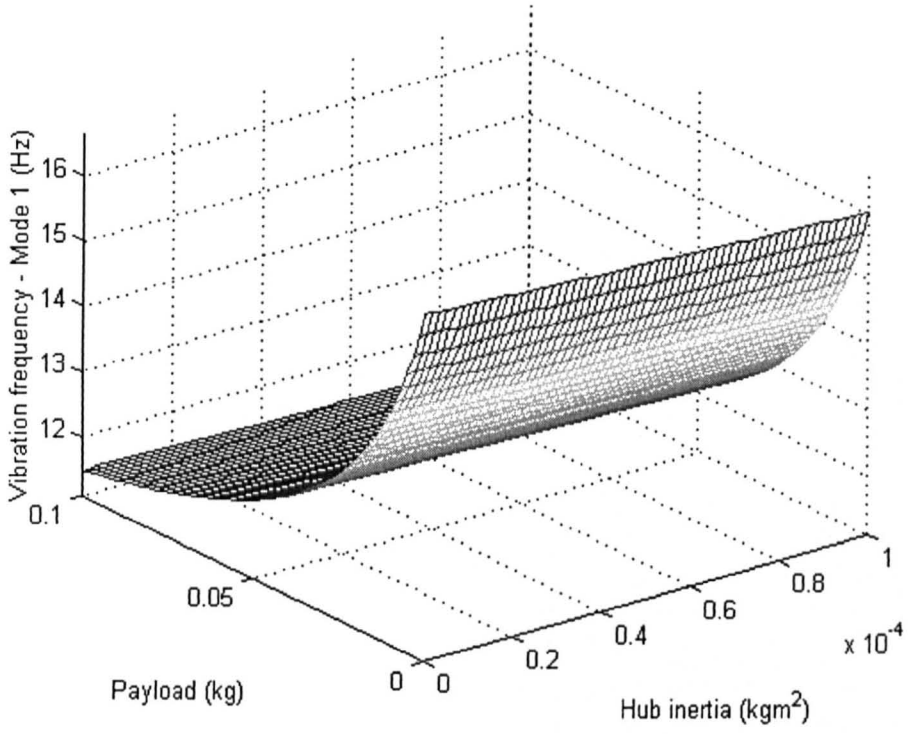

Figure 4.8: Relationship between hub inertia, payload and vibration frequency (mode 1).

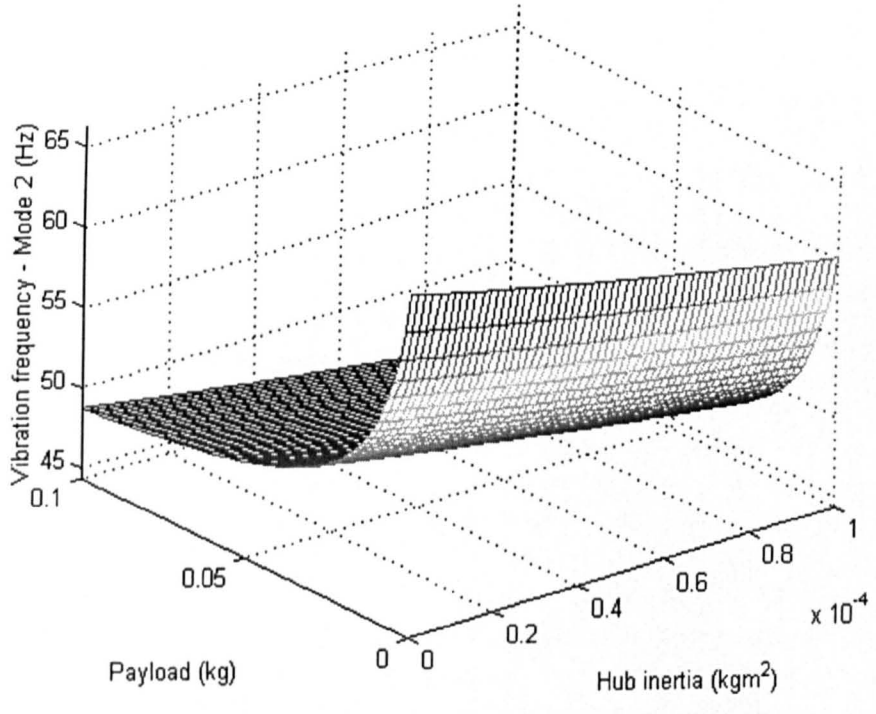

Figure 4.9: Relationship between hub inertia, payload and vibration frequency (mode 2).

Following the same procedure as for the poles of the system in equations (4.16) and (4,17), it can be shown that the terms under square roots in equation (4.18) are negative for $m_p \geq 0$, $0 < \alpha \leq 1$, and other parameters are positive,. Thus, all system zeros lie on the imaginary axis and as expected of a system with collocated sensors and actuator, the transfer function from torque input to hub-angle response exhibits a minimum phase behaviour. Figure 4.10 shows the relation between the payload and the system zeros. It is noted that the zeros move towards the origin of the s-plane with increasing payload.

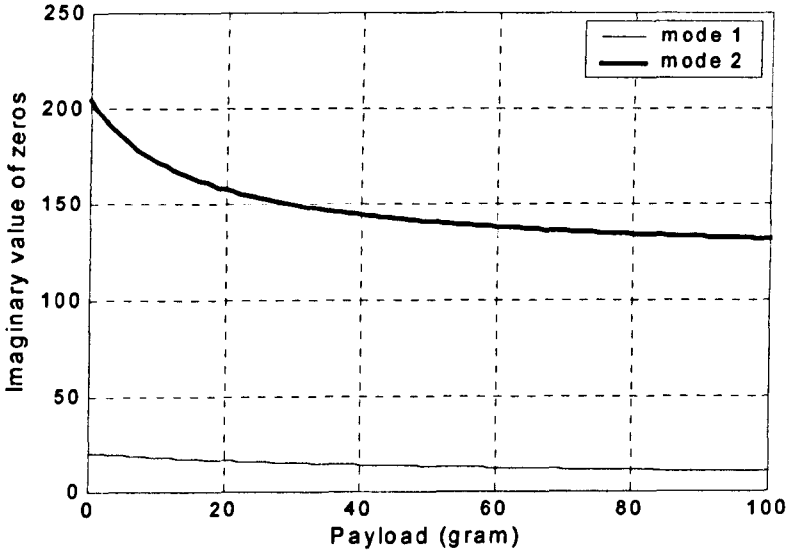

Figure 4.10: Effect of payload on the zeros of hub-angle response.

Since control of a non-minimum phase system is rather involved, this aspect is further analysed in this section. For the transfer function from the torque input to end-point displacement that exhibits a non-minimum phase characteristic, it is important to investigate whether the zeros can be relocated to the lhp by altering physical parameters of the system. If so, in designing a flexible manipulator, certain parameter values can be considered to make the system minimum phase. In this work, the analysis are carried out using the Routh-Hurtwiz (RH) criterion (Nise, 1995). Accordingly, if there is no sign change in the first column of RH table, then all roots of the polynomial will be on the lhp. Utilising the RH criterion, the first column of RH table for numerator of $G_1(s)$ is shown in Table 4.1. It is noted that there are two sign changes, that are from s^3 to s^2 and s^1 to s^0, indicating that two zeros exist on the

rhp. Moreover, the result shows that, since all terms are single, the zeros cannot be relocated by altering any physical parameter value.

Table 4.1: The first column of RH table for the numerator of $G_1(s)$.

s^4	$30\alpha^2 l^7$
s^3	$120\alpha^2 l^7$
s^2	$-24300\alpha\beta l^4$
s^1	$-74800\alpha\beta l^4$
s^0	$4536000\beta^2 l$

For the transfer function $G_2(s)$, the effect of payload on the location of zeros can be investigated. Table 4.2 shows the first column of RH table for the numerator of $G_2(s)$. Since the numerator is an even polynomial, a row of zeros exists at s^3. Thus, if there are no sign change, all zeros of the transfer function lie on the imaginary axis. It is noted, as all the physical parameters, including the payload are positive, no sign change occurs in the first column of the RH table. This implies that all the system zeros lie on the imaginary axis and the system is minimum phase.

Similarly, the effect of payload on the system poles and stability can be studied. Furthermore, a range of payloads that ensures system stability could be determined. Table 4.3 shows the first column of RH table for the denominator of the transfer function, equation (4.14). Again, as the denominator is an even polynomial, a row of zeros exists at s^5. It is noted that, no sign change occurs. This implies that all poles of the system lie on the imaginary axis and the system is marginally stable.

Table 4.2: The first column of RH table for the numerator of $G_2(s)$.

s^4	$30\alpha l^6(12m_p+\alpha)$
s^3	$120\alpha l^6(12m_p+\alpha)$
s^2	$10800\beta l^3(17\alpha+70m_p)$
s^1	$\frac{57600(\beta l^3(17\alpha+70m_p)}{17\alpha+70m_p}$
s^0	$4536000\beta^2$

Table 4.3: The first column of RH table for denominator of the system.

s^6	$0.3m_p+0.0035$
s^5	$1.9m_p+0.0208$
s^4	$5123.4m_p+113.5$
s^3	$\frac{7.6\times10^8 m_p^{\,2}+3.0\times10^7 m_p+356584.8}{15370.2m_p+340.4}$
s^2	$\frac{1.4\times10^{27} m_p^{\,3}+1.3\times10^{26} m_p^{\,2}+3.4\times10^{24} m_p+3.3\times10^{22}}{6.1\times10^{19} m_p^{\,2}+2.4\times10^{18} m_p+2.8\times10^{16}}$
s^1	$1.0\times10^8 m_p+5143720$
s^0	0

The effect of payload on the dynamic behaviour of the system is further analysed by obtaining the time responses of the end-point displacement and hub-angle of the manipulator.

Both transfer functions $G_1(s)$ and $G_2(s)$ are considered. In this work, a single-switch bang-bang torque input is applied at the hub of the manipulator. The input torque can be expressed in the time-domain as

$$u(t) = gu(t-c_1) - 2gu(t-c_2) + gu(t-c_3)$$

where c_1, c_2, c_3 and g are constants. In the frequency-domain, the input torque can be written as

$$U(s) = \frac{1}{s}(ge^{-c_1 s} - 2ge^{-c_2 s} + ge^{-c_3 s}) \tag{4.19}$$

Multiplying the system transfer functions in equations (4.5) and (4.6) with the input torque in equation (4.19) and utilising the inverse Laplace transform yield the time-domain expressions of the end-point displacement and hub-angle for the system responses.

To demonstrate the performance of the developed symbolic algorithm, simulated exercises with the flexible manipulator system with $I_h = 5.8598\times10^{-4}$ kgm^2 were carried out. In these exercises, a bang-bang input torque as shown in Figure 3.1 with amplitude of ±0.3 Nm, $c_1 = 0.2, c_2 = 0.5, c_3 = 0.8$ and $g = 0.3$ was used. The system responses at the end-point and hub-angle were obtained over a period of 3 sec. Figures 4.11 and 4.12 show the simulated responses of the end-point displacement and hub-angle of the manipulator with a payload of 20 grams respectively. It is noted that the responses of the system achieved steady-state values of 0.43 m and 27 degrees within 0.9 sec with persistent oscillations. The end-point response demonstrates that the system is non-minimum phase, as the response slightly undershoots at start up. This agrees with the symbolic results that were presented and discussed earlier.

To investigate the effect of payload on the system response, steady-state values of the system responses were monitored with various payloads. Based on the assumption that the manipulator achieves a steady-state value after 4 sec, the relations between payload and steady-state values of end-point displacement and hub-angle are shown in Figures 4.13 and 4.14 respectively. In both cases, the output levels decrease significantly with increasing

payload. The results demonstrate that controllers that are capable of adapting with changing system characteristics have to be developed.

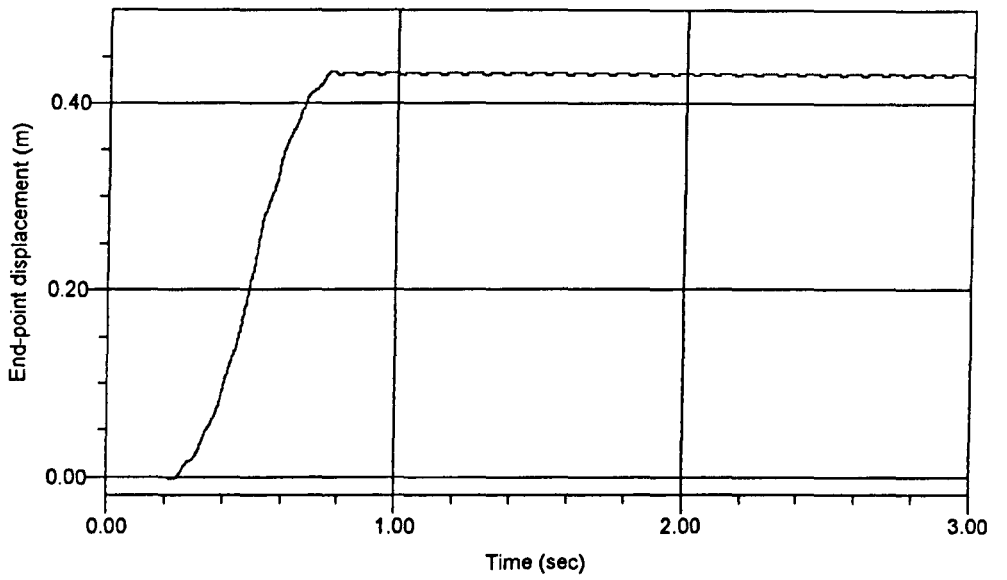

Figure 4.11: Simulated end-point displacement response of the flexible manipulator ($m_p = 20$ grams).

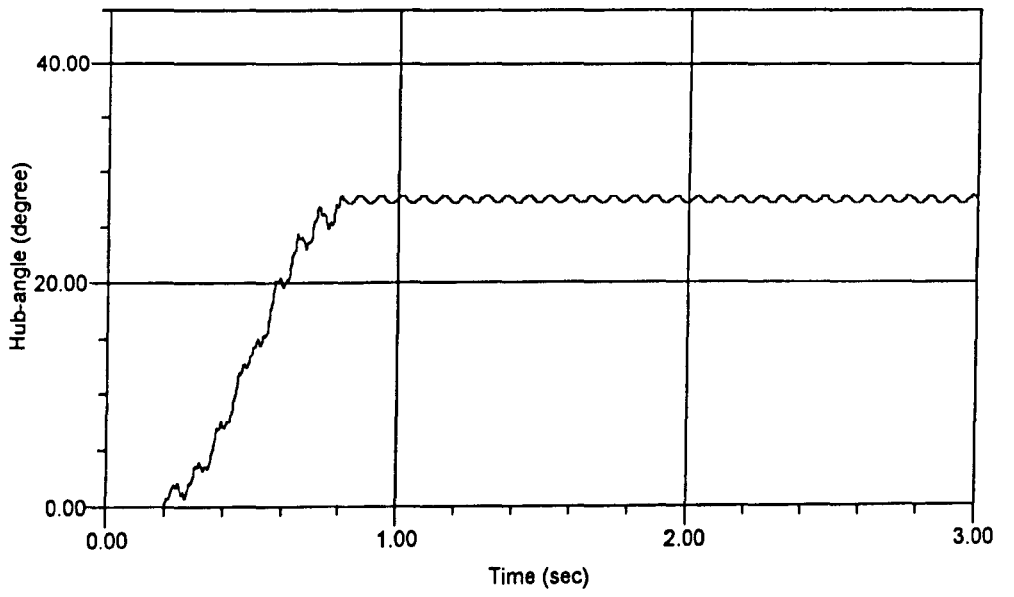

Figure 4.12: Simulated hub-angle response of the flexible manipulator ($m_p = 20$ grams).

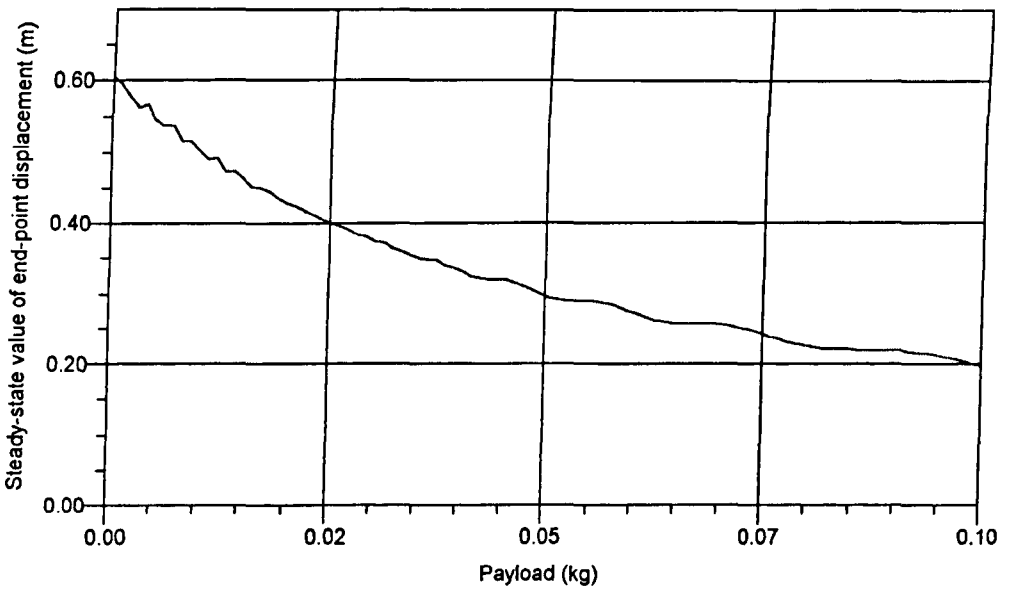

Figure 4.13: Effect of payload on the steady-state value of end-point displacement response (t = 4 sec).

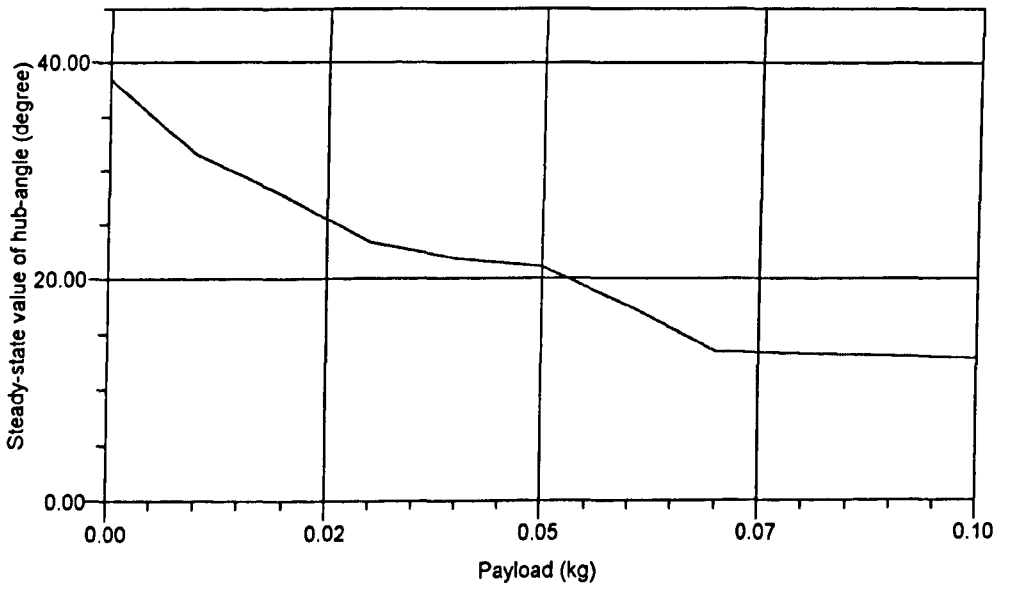

Figure 4.14: Effect of payload on the steady-state value of hub-angle response (t = 4 sec).

4.5. Validation and Performance Analysis

To validate the developed symbolic model of the flexible manipulator for use in simulation and control, the symbolic results are examined in comparison to the experimental results presented in the previous chapter. Performance of the symbolic manipulation approach is accordingly assessed.

Figures 3.18 – 3.20 show the experimental results of the hub-angle, hub-velocity and end-point acceleration, with their PSDs, of the flexible manipulator without payload. The steady-state level of the hub-angle of 38 degrees was achieved within 1.8 sec. The first three modes of vibration were obtained as 11.72 Hz, 35.15 Hz and 65.60 Hz. Furthermore, it is noted that the hub-angle response is minimum phase as proved in the analysis using symbolic manipulation. However, with a single element, the symbolic approach gave the first two modes of vibration frequencies as shown in Figure 4.6 as 14 Hz and 47.5 Hz. More accurate results can be obtained with increasing the number of elements (Tokhi et al., 1997).

To investigate the effect of payload on the performance of the manipulator, experiments were performed using various payloads ranging from 10 grams to 60 grams. Figures 3.21 – 3.23 show the experimental results of the hub-angle, hub-velocity and end-point acceleration, with their PSDs with payloads of 20 grams and 40 grams respectively. Comparisons of Figures 4.12 and 3.21, for the manipulator with a payload of 20 grams, show that a reasonably close agreement between symbolic and experimental results in the time response was obtained. It is noted from the experimental results that the steady-state level of hub-angle response decreases with increasing payloads. For the payloads of 20 grams and 40 grams, the steady-state level of hub-angle was obtained as 31 degrees and 26 degrees respectively. Analysing the PSDs, it is also noted that the resonance frequencies of the system decrease with increasing payloads. Using the symbolic approach, similar results are obtained as shown in Figures 4.6 and 4.14. This validates the symbolic model in characterising the dynamic behaviour of a flexible manipulator for development of suitable control strategies. However, as in the case of simulated steady-state value of the hub-angle presented in Chapter 3, a difference of 4 degrees was observed. The difference, which is considered negligibly small, could mainly be due to the gravity effect, which was ignored in the simulation, whereas a payload that might be affected by gravity was used in the experiments. Moreover, payload rotary inertia was also ignored in the simulation.

4.6. Summary

The application of a symbolic manipulation approach for modelling and analysis of a flexible manipulator system has been presented. It has been demonstrated that the approach provides several advantages in characterising the dynamic behaviour of the manipulator, and in assessing the stability, response and vibration frequency of the system. The system transfer functions have been obtained in symbolic form and thus inter-relations between payload, hub inertia and system characteristics have been investigated. Simulation and experimental results have been presented demonstrating the performance of the symbolic approach in modelling and simulation of the flexible manipulator system.

Chapter 5

Vibration Control Using Command Shaping Techniques

5.1. Introduction

This chapter presents simulation and experimental investigations into the development of feedforward control schemes for vibration control of a flexible manipulator system using command shaping techniques. The FE model developed in Chapter 3 and the laboratory scale single-link flexible manipulator are considered with and without payload. The command shaping techniques based on input shaping with two- and four-impulse sequences and third and sixth order low-pass and band-stop filters are examined. A comparative assessment of the performance of these techniques is provided. Experiments are performed on the flexible manipulator to investigate the application of the command shaping techniques in real-time. Moreover, experiments are used for verification of the simulation results. The input shapers and filters are designed based on the characteristic parameters and properties of the manipulator presented in Chapter 3 and used for pre-processing the input, so that low energy is fed into the system at resonance modes. Performances of the developed controllers are assessed in terms of level of vibration reduction at resonance modes, time response specifications, robustness to errors in the natural frequencies of the system and processing times to develop the inputs. Moreover, the effects of number of impulses and filter orders on the performance of the system are investigated. The performance of the shaping techniques is also assessed with the flexible manipulator incorporating a payload. Simulation and experimental results in time and frequency domains of the response of the flexible manipulator to the shaped and filtered inputs are presented. The robustness of the control schemes is assessed with up to 30% error tolerance in the natural frequencies. Finally, a comparative assessment of the performances of the feedforward control strategies in vibration suppression of the manipulator is discussed.

5.2. Feedforward Control Techniques

In this section, input shaping, low-pass and band-stop filtering techniques are introduced for vibration control of the flexible manipulator. Both filtering techniques have previously been used for control of flexible manipulators (Tokhi and Poerwanto, 1996).

5.2.1. Input Shaping

The input shaping method involves convolving a desired command with a sequence of impulses known as input shaper (Singer and Seering, 1990). The shaped command that results from the convolution is then used to drive the system. The design objectives are to determine the amplitude and time location of the impulses from the natural frequencies and damping ratios of the system, so that the shaped command reduces the system vibration. The method is briefly described in this section. A vibratory system can be modelled as a superposition of second order systems each with a transfer function

$$G(s) = \frac{\omega_n^{\,2}}{s^2 + 2\zeta\omega_n s + \omega_n^{\,2}} \tag{5.1}$$

where ω_n is the natural frequency and ζ is the damping ratio of the system. Thus, the impulse response of the system at time t is

$$y_\delta(t) = \frac{J\omega_n}{\sqrt{1-\zeta^2}} e^{-\zeta\omega_n(t-t_o)} \sin(\omega_n\sqrt{1-\zeta^2}(t-t_o)) \tag{5.2}$$

where J and t_0 are the magnitude and time of the impulse respectively. Further, the response to a sequence of impulses can be obtained using the superposition principle. Thus, for q impulses, with damped frequency, $\omega_d = \omega_n\sqrt{1-\zeta^2}$, the impulse response can be expressed as

$$y_\delta(t) = W\sin(\omega_d t + \chi) \tag{5.3}$$

where

$$W = \sqrt{(\sum_{i=1}^{q} \lambda_i \cos\sigma_i)^2 + (\sum_{i=1}^{q} \lambda_i \sin\sigma_i)^2}$$

$$\lambda_i = \frac{J_i \omega_n}{\sqrt{1-\zeta^2}} e^{-\zeta\omega(t-t_i)},\ \sigma_i = \omega_d t_i \text{ and } \chi = \tan^{-1}\left(\sum_{i=1}^{q} \frac{\lambda_i \cos\sigma_i}{\lambda_i \sin\sigma_i}\right).$$

J_i and t_i are the magnitudes and times at which the impulses occur.

The residual single mode vibration amplitude of the impulse response is obtained at the time of the last impulse, t_N as

$$V = \sqrt{V_1^2 + V_2^2} \tag{5.4}$$

where

$$V_1 = \sum_{i=1}^{q} \frac{J_i \omega_n}{\sqrt{1-\zeta^2}} e^{-\zeta\omega_n(t_N - t_i)} \cos(\sigma_i),\ V_2 = \sum_{i=1}^{q} \frac{J_i \omega_n}{\sqrt{1-\zeta^2}} e^{-\zeta\omega_n(t_N - t_i)} \sin(\sigma_i)$$

To achieve zero vibration after the last impulse, it is required that both V_1 and V_2 in equation (5.4) are independently zero. Furthermore, to ensure that the shaped command input produces the same rigid body motion as the unshaped command, it is required that the sum of amplitudes of the impulses is unity. To avoid response delay, the first impulse is selected at time $t_1 = 0$. Hence by setting V_1 and V_2 in equation (5.4) to zero, $\sum_{i=1}^{q} J_i = 1$ and solving yields a two-impulse sequence as shown in Figure 5.1 with parameters as

$$t_1 = 0,\quad t_2 = \frac{\pi}{\omega_d},$$

$$J_1 = \frac{1}{1+H},\quad J_2 = \frac{H}{1+H} \tag{5.5}$$

where

$$H = e^{-\frac{\zeta\pi}{\sqrt{1-\zeta^2}}}$$

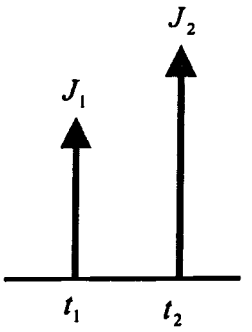

Figure 5.1: A two-impulse sequence input shaper.

The robustness of the input shaper to errors in natural frequencies of the system can be increased by setting $\frac{dV}{d\omega_n} = 0$. Setting the derivative to zero is equivalent of producing small changes in vibration corresponding to natural frequency changes. By obtaining the first derivatives of V_1 and V_2 in equation (5.4) and simplifying yields (Singer and Seering, 1990)

$$\frac{dV_1}{d\omega_n} = \sum_{i=1}^{q} J_i t_i e^{-\zeta\omega_n(t_N - t_i)} \sin(\sigma_i)$$

$$\frac{dV_2}{d\omega_n} = \sum_{i=1}^{q} J_i t_i e^{-\zeta\omega_n(t_N - t_i)} \cos(\sigma_i) \tag{5.6}$$

Hence by setting equations (5.4) and (5.6) to zero and solving yields a three-impulse sequence as shown in Figure 5.2 with parameters as

$$t_1 = 0, \quad t_2 = \frac{\pi}{\omega_d}, \quad t_3 = \frac{2\pi}{\omega_d},$$

$$J_1 = \frac{1}{1+2H+H^2}, \quad J_2 = \frac{2H}{1+2H+H^2}, \quad J_3 = \frac{H^2}{1+2H+H^2} \tag{5.7}$$

where H is as in equation (5.5). The robustness of the input shaper can further be increased by taking and solving the second derivative of the vibration in equation (5.4). Similarly, this yields a four-impulse sequence as shown in Figure 5.3 with parameters as

$$t_1 = 0, \quad t_2 = \frac{\pi}{\omega_d}, \quad t_3 = \frac{2\pi}{\omega_d}, \quad t_4 = \frac{3\pi}{\omega_d},$$

$$J_1 = \frac{1}{1+3H+3H^2+H^3}, \quad J_2 = \frac{3H}{1+3H+3H^2+H^3},$$
$$J_3 = \frac{3H^2}{1+3H+3H^2+H^3}, \quad J_4 = \frac{H^3}{1+3H+3H^2+H^3}. \tag{5.8}$$

where H is as in equation (5.5).

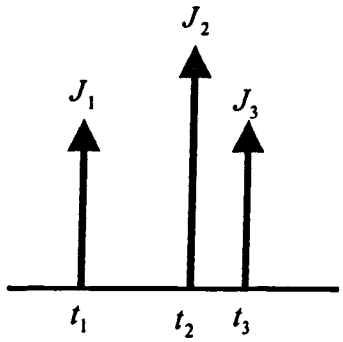

Figure 5.2: A three-impulse sequence input shaper.

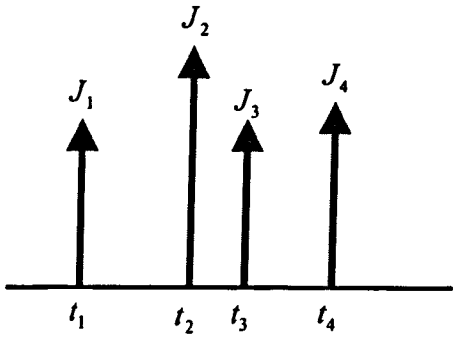

Figure 5.3: A four-impulse sequence input shaper.

To handle higher vibration modes, an impulse sequence for each vibration mode can be designed independently. Then the impulse sequences can be convoluted together to form a sequence of impulses that attenuate vibration at higher modes. In this manner, for a vibratory system, the vibration reduction can be accomplished by convolving a desired system input with the impulse sequence. This yields a shaped input that drives the system to a desired location with less vibration.

5.2.2. Filtering Techniques

Command shaping based on filtering techniques is developed on the basis of extracting the input energy around the natural frequencies of the system using filtering techniques. The filters are thus used for pre-processing the input signal so that low energy is fed into the system at the natural frequencies. In this manner, the flexural modes of the system are not excited, leading to a vibration-free motion. This can be realised by employing either low-pass or band-stop filters. In the former, the filter is designed with a cut-off frequency lower than the first natural frequency of the system. In the latter case, band-stop filters with centre frequencies at the natural frequencies of the system are designed. This will require one filter for each mode of the system. The band-stop filters thus designed are then implemented in cascade to pre-process the input signal. There are various filter types such as Butterworth, Chebyshev and Elliptic that can be designed and employed. In this investigation, infinite impulse response (IIR) Butterworth low-pass and band-stop filters are examined.

The magnitude of the frequency response of a low-pass Butterworth filter is given by (Jackson, 1989)

$$|H(j\omega)|^2 = \frac{1}{1+\left[\frac{\omega}{\omega_c}\right]^{2d}} = \frac{1}{1+\varepsilon^2\left[\frac{\omega}{\omega_p}\right]^{2d}} \tag{5.9}$$

where, d is a positive integer signifying the order of the filter, ω_c is the filter cut-off frequency, ω_p is the pass-band edge frequency and $(1+\varepsilon^2)^{-1}$ is the band edge value of $|H(j\omega)|^2$. Note that $|H(j\omega)|^2$ is monotomic in both the pass-band and stop-band. The order of the filter required to yield attenuation δ_2 at a specified frequency ω_s (stop-band edge frequency) is determined from equation (5.9) as

$$d = \frac{\log\left(\frac{1}{\delta_2^{\,2}}-1\right)}{2\log\left(\frac{\omega_s}{\omega_c}\right)} = \frac{\log\left(\frac{\delta_1}{\varepsilon}\right)}{\log\left(\frac{\omega_s}{\omega_p}\right)} \tag{5.10}$$

where, by definition, $\delta_2 = 1/\sqrt{(1+\delta_1^2)}$. Thus, the Butterworth filter is completely characterised by the parameters d, δ_2, ε and the ratio ω_s/ω_p.

Equation (5.10) can be employed with arbitrary δ_1, δ_2, ω_c and ω_s to yield the required filter order d from which the filter design is readily obtained. The Butterworth approximation results from the requirement that the magnitude response be maximally flat in both the pass-band and the stop-band. That is, the first $(2d-1)$ derivatives of $|H(j\omega)|^2$ are specified to be equal to zero at $\omega = 0$ and at $\omega = \infty$. The design relations for the low-pass filters given above can be utilised in normalised form to design the corresponding band-stop filters. This involves a transformation from low-pass to band-stop filter (Banks, 1990).

5.3. Implementation

The feedforward control techniques were designed on the basis of natural frequencies and damping ratios of the flexible manipulator system. In this investigation, the manipulator without payload and with a payload of 40 grams are considered. The system responses to the single-switch bang-bang torque input as shown in Figure 3.1 are utilised in obtaining the characteristic parameters of the manipulator. It is noted with the simulated responses of the manipulator without payload (Figures 3.10 – 3.13) that a steady-state hub-angle level of 38 degrees was achieved with a settling time of 0.788 sec. The natural frequencies of the first three resonance modes of the system were obtained as 11.99 Hz, 35.22 Hz and 65.2 Hz. The maximum deflection at the end-point of the manipulator was obtained as 29 mm. Moreover, the magnitudes of the PSDs of the end-point deflection and end-point acceleration at the resonance modes were obtained as 0.01 m^2/Hz, 0.002 m^2/Hz and 0.003 m^2/Hz and 15 m^2/sec^2/Hz, 20 m^2/sec^2/Hz and 10 m^2/sec^2/Hz respectively. Conversely, with a payload of 40 grams (Figures 3.14 – 3.17), the hub-angle reached 21 degrees with a settling time of 0.96 sec and the natural frequencies were obtained as 10.74 Hz, 31.22 Hz and 58.19 Hz. Figures 3.18 – 3.23 show the experimental responses of the manipulator to the bang-bang torque input and demonstrate that without payload, a steady-state hub-angle level of 38 degrees was achieved with settling time and overshoot of 1.55 sec and 2.6% respectively. The natural frequencies of the system were obtained as 11.72 Hz, 35.15 Hz and 65.6 Hz. The magnitudes of the PSDs of the end-point acceleration at the resonance modes were obtained as 80 m^2/sec^2/Hz, 50 m^2/sec^2/Hz and 30 m^2/sec^2/Hz respectively. With a payload, the hub-angle level reached 26 degrees with settling time and overshoot of 1.76 sec and 0.7%. Moreover, the natural

frequencies were obtained as 9.48 Hz, 30.92 Hz and 58.85 Hz. These simulation and experimental results were considered as the system response to the unshaped input and subsequently will be used to design and evaluate the performance of the command shaping techniques.

As indicated in Chapter 3, the damping ratios of the system were deduced as 0.026, 0.038 and 0.04 for the first, second and third modes respectively. In these simulation and experimental investigations, the input shapers and filters were designed with the natural frequencies for the first three modes as 12 Hz, 35 Hz and 65 Hz for the system without payload and 10 Hz, 31 Hz and 58 Hz for the system incorporating a payload. For evaluation of robustness, the control techniques were designed on the basis of 30% error tolerance in the natural frequencies. Accordingly, the system vibration frequencies were considered under this situation at 15.6 Hz, 45.5 Hz and 84.5 Hz for the system without payload and 13 Hz, 40 Hz and 75 Hz for the system with payload. The input shapers and filters thus designed were used for pre-processing the bang-bang torque input. The shaped and filtered torque inputs were then applied to the system in an open-loop configuration as shown in Figure 5.4. In this process, the shaped and filtered inputs were designed with a sampling frequency of 500 Hz.

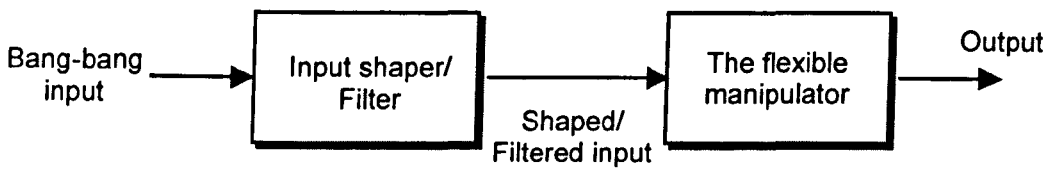

Figure 5.4: Block diagram of the feedforward control configuration.

Simulation and experimental results of the response of the flexible manipulator to the shaped and filtered inputs are presented in the time and frequency domains. To verify the performance of the control techniques, the results are examined in comparison to the unshaped bang-bang torque input for a similar input level in each case. The effects of number of impulses and filter orders on the performance of the system are investigated. Moreover, evaluations on the performance of the control schemes in vibration suppression of the flexible manipulator incorporating a payload of 40 grams are carried out. Four criteria are used to evaluate the performances of the control schemes:

(1) Level of vibration reduction at the natural frequencies. This is accomplished by comparing the responses to the shaped and filtered inputs with the response to the unshaped input. The results are presented in dB.

(2) Time response specifications. Parameters that are evaluated are settling time and overshoot of the hub-angle response. The settling time is calculated on the basis of ±2% of the steady-state value. Moreover, the magnitude of oscillation of the system response is observed.

(3) Robustness to parameter uncertainty. To examine the robustness of the techniques, the system performance is assessed with 30% error tolerance in natural frequencies. This is incorporated in the design of the input shapers and filters.

(4) Processing time. Processing times to develop the shaped and filtered inputs are calculated. This is an important aspect in real-time implementation of the controller.

5.3.1. Input Shaping

Using the natural frequencies and damping ratios of the system, input shapers with two- and four-impulse sequences for the first three modes of vibration were designed. The magnitude and time location of the impulses were obtained by solving equations (5.5) and (5.8) respectively. Similarly, for evaluation of robustness, input shapers with 30% error in the natural frequencies were also evaluated. As described, to avoid response delay, the first impulse is selected at time, $t = 0$. For the system without payload and with exact natural frequency, locations of the second impulse were obtained at 0.0417 sec, 0.0143 sec and 0.0077 sec for the three modes respectively. On the other hand, with erroneous natural frequencies, locations of the second impulse were obtained at 0.0321 sec, 0.0110 sec and 0.0059 sec. Magnitudes of the input shapers accordingly designed and used with both the exact and erroneous natural frequencies are shown in Table 5.1. For digital implementation of the input shapers, locations of the impulses were selected at the nearest sampling time. Figure 5.5 shows the shaped inputs and the corresponding PSDs using input shaping with two- and four-impulse sequences. It is noted that with higher number of impulses, the magnitudes of the PSDs at the natural frequencies reduce. Moreover, the range of frequency covered around the natural frequencies increases. Similarly, input shapers for the system incorporating payload were also designed.

Table 5.1: Magnitude of the input shapers.

Number of impulse sequences	Impulse	Magnitude		
		Mode 1	Mode 2	Mode 3
2	1	0.5205	0.5298	0.5315
	2	0.4795	0.4702	0.4685
4	1	0.1409	0.1487	0.1501
	2	0.3897	0.3960	0.3970
	3	0.3591	0.3514	0.3500
	4	0.1103	0.1039	0.1029

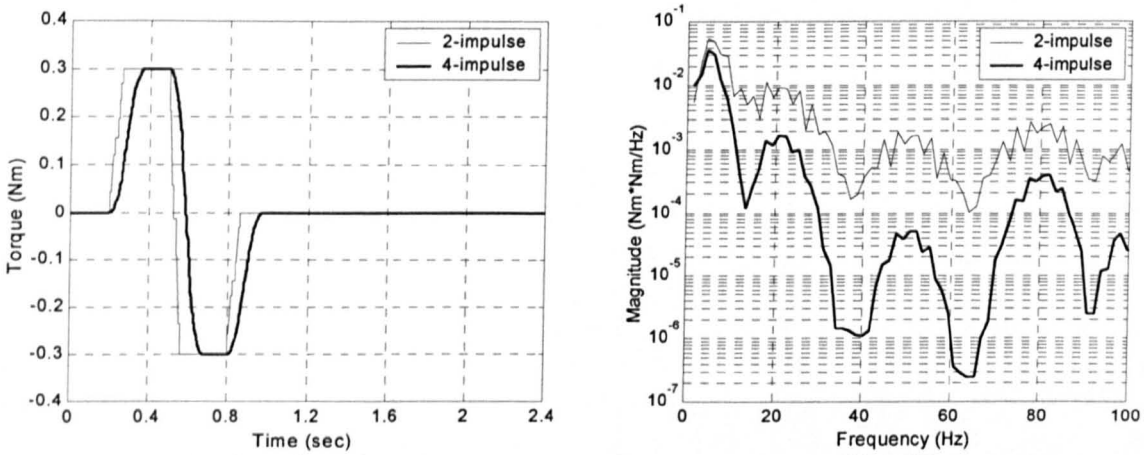

(a) Time domain. (b) PSD.

Figure 5.5: Shaped torque inputs using two- and four-impulse sequences.

5.3.2. Filtered Inputs

Using the low-pass filter, the input energy at all frequencies above the cut-off frequency can be attenuated. In this study, low-pass filters with cut-off frequency at 75% of the first vibration mode were designed. Thus, for the flexible manipulator without payload, the cut-off frequencies of the filters were selected at 9 Hz and 11.7 Hz for the two cases of exact and erroneous natural frequencies respectively. On the other hand, using the band-stop filter, the input energy at dominant modes of the system can be attenuated. In this study, band-stop filters with stop-bands of 5 Hz were designed for the first three modes. Similarly, the filters were designed with consideration of exact and 30% error in natural frequencies. Moreover, the filters were designed in each case with third and sixth orders. Thus, the effects of using

various orders of filters on the performance of the manipulator were studied. The filtered torque inputs and the corresponding PSDs with the low-pass and band-stop filters are shown in Figures 5.6 and 5.7 respectively. It is noted with the low-pass filter that the magnitudes of the PSDs at the natural frequencies reduced with higher filter orders. However, with the band-stop filter, the improvement achieved in the magnitudes of the PSDs with a higher filter order was not significant. Moreover, larger oscillation in the input signal was observed.

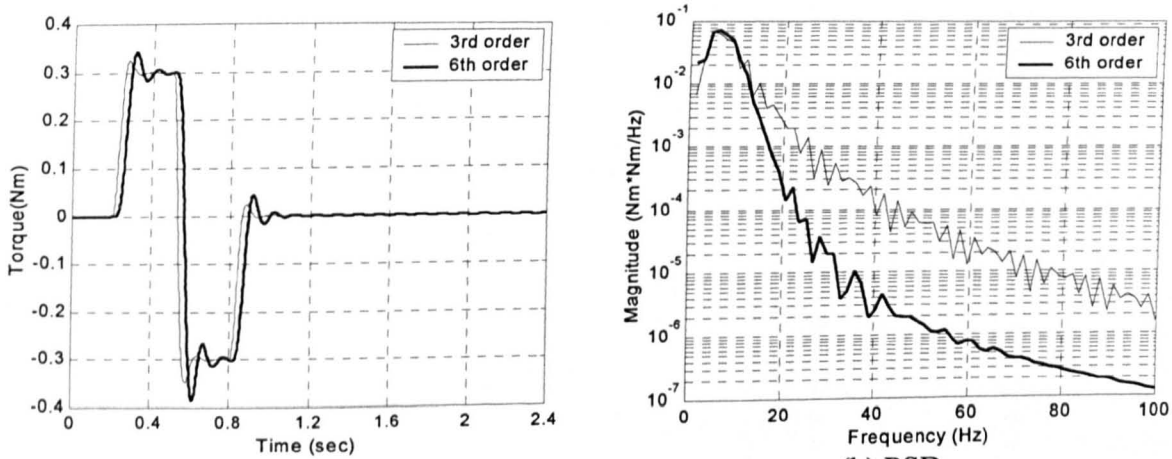

(a) Time domain. (b) PSD.

Figure 5.6: Filtered torque inputs using the Butterworth low-pass filters.

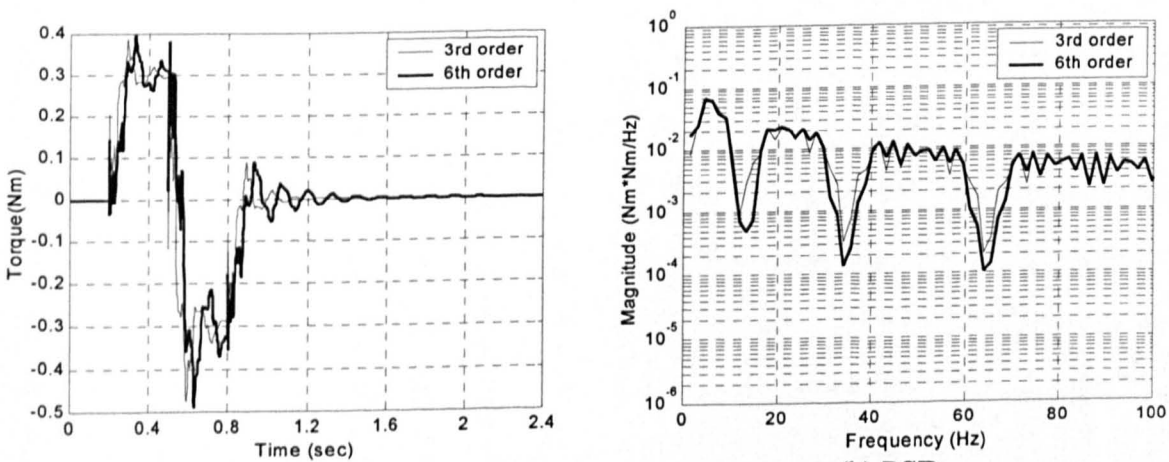

(a) Time domain. (b) PSD.

Figure 5.7: Filtered torque inputs using the Butterworth band-stop filters.

5.4. Simulation Results

In this section simulation results of the response of the flexible manipulator to the command shaping inputs are presented. System responses namely hub-angle, hub-velocity, end-point deflection and end-point acceleration with the corresponding PSDs are studied. For evaluation purposes, the system parameters are obtained in accordance with the criteria discussed in the previous section.

5.4.1. Input Shaping

Figures 5.8 – 5.11 show the simulated responses of the flexible manipulator without payload to the shaped input using two- and four-impulse sequences. It is noted in both cases that the magnitudes of vibration at the resonance modes of the system, with the hub-angle, hub-velocity, end-point deflection and end-point acceleration responses, have significantly been reduced. These can be observed by comparing the system responses to the unshaped input (Figures 3.10 – 3.13). With the four-impulse sequence, the oscillations in the system response were almost reduced to zero. Hence, a smoother response was achieved. The settling times of the hub-angle were obtained as 0.820 sec and 0.878 sec with the two- and four-impulse sequences respectively. These results show that the hub-angle response is slower than the response to the unshaped input. It is noted that the level of vibration reduction increases with an increase in the number of impulses, at the expense of increase in the delay (settling time) in the response of the system.

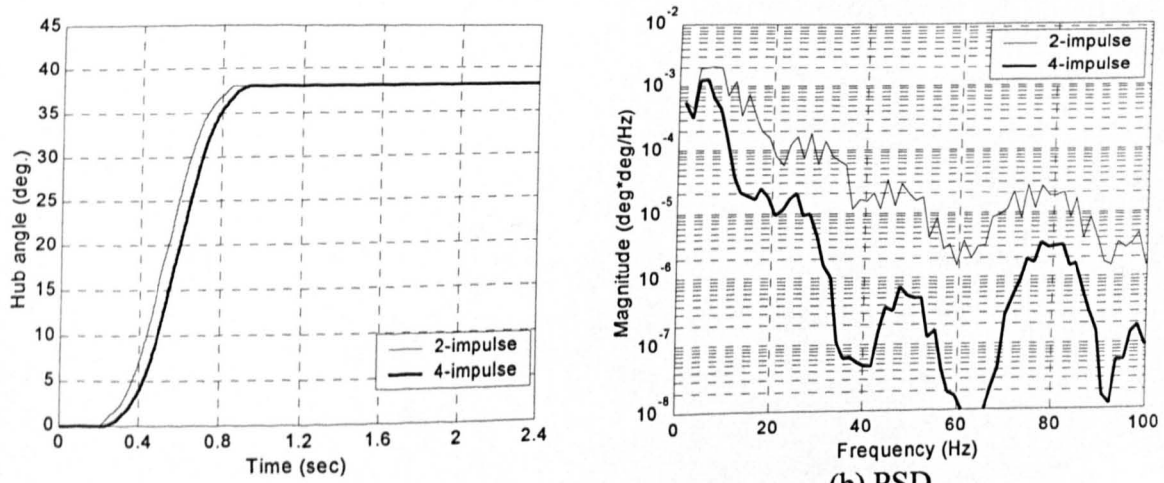

(a) Time domain. (b) PSD.

Figure 5.8: Simulated hub-angle response of the manipulator to the shaped inputs with exact frequencies.

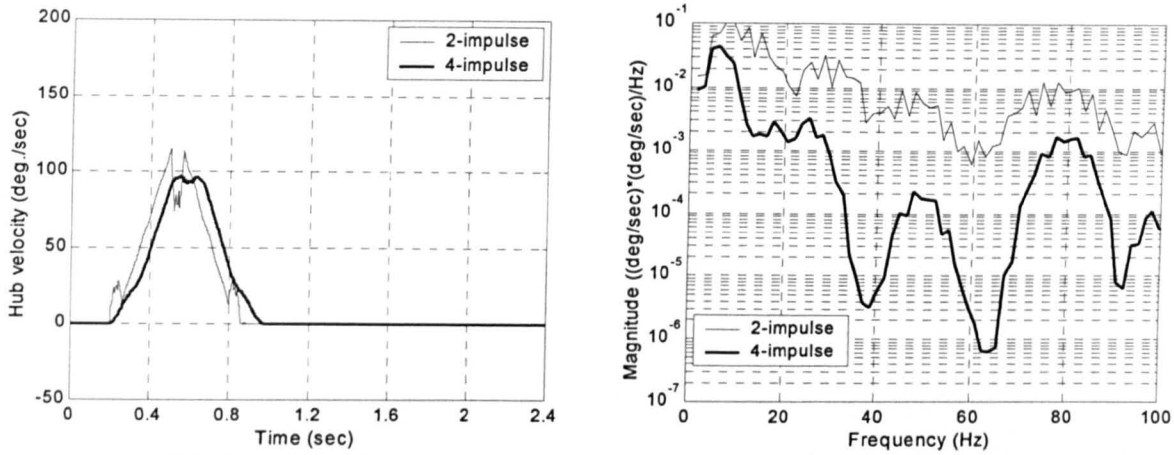

(a) Time domain. (b) PSD.

Figure 5.9: Simulated hub-velocity response of the manipulator to the shaped inputs with exact frequencies.

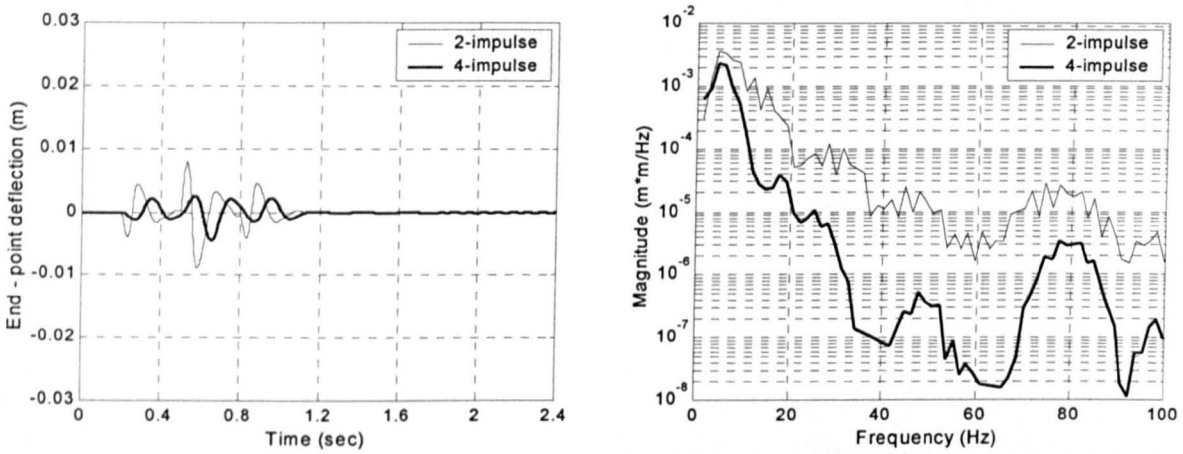

(a) Time domain. (b) PSD.

Figure 5.10: Simulated end-point deflection response of the manipulator to the shaped inputs with exact frequencies.

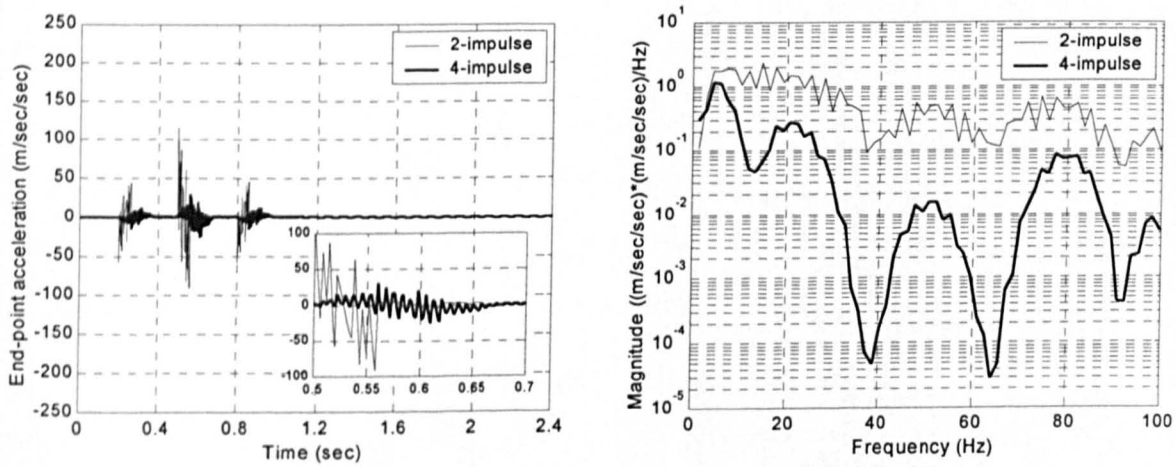

(a) Time domain. (b) PSD.

Figure 5.11: Simulated end-point acceleration response of the manipulator to the shaped inputs with exact frequencies.

Figures 5.12 – 5.15 show simulated responses of the manipulator to the shaped input using two- and four-impulse sequences with 30% error in the natural frequencies. This is used to examine the robustness of the technique. As noted with the system responses, the level of reduction in the vibration of the manipulator is slightly less than the case without error. Thus, higher levels of vibration were noted in the system responses. However, it is noted that significant vibration reduction was achieved as compared with response to the unshaped input, especially with a four-impulse sequence.

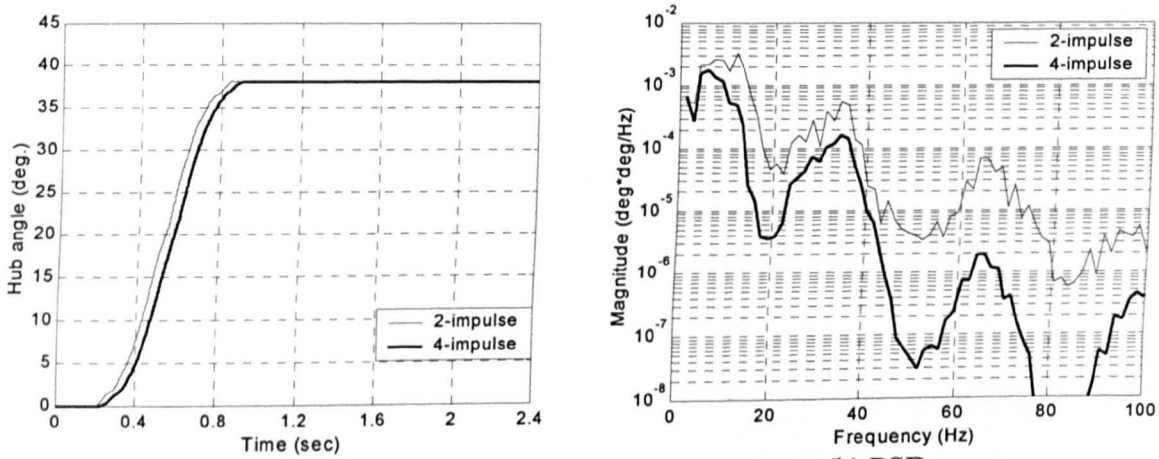

(a) Time domain. (b) PSD.

Figure 5.12: Simulated hub-angle response of the manipulator to the shaped inputs with erroneous natural frequencies.

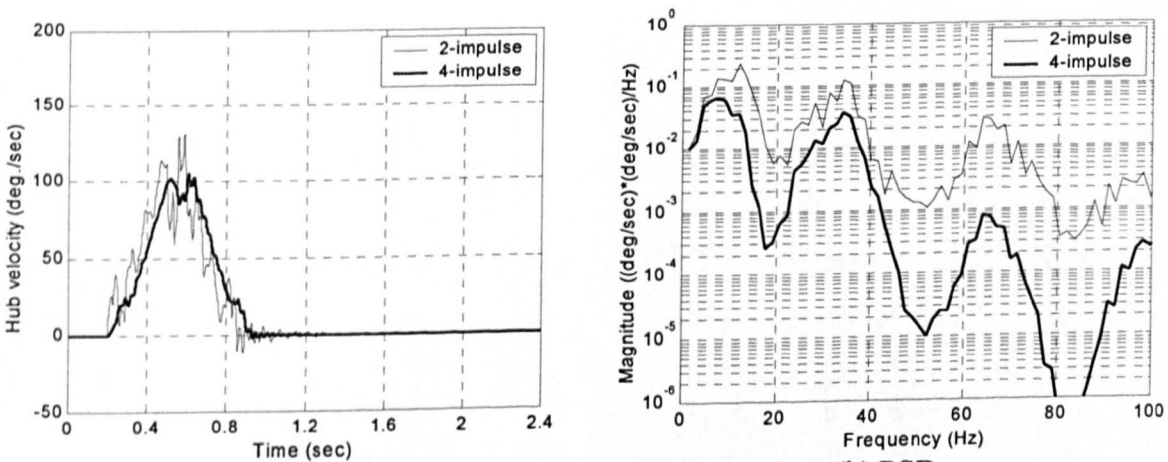

(a) Time domain. (b) PSD.

Figure 5.13: Simulated hub-velocity response of the manipulator to the shaped inputs with erroneous natural frequencies.

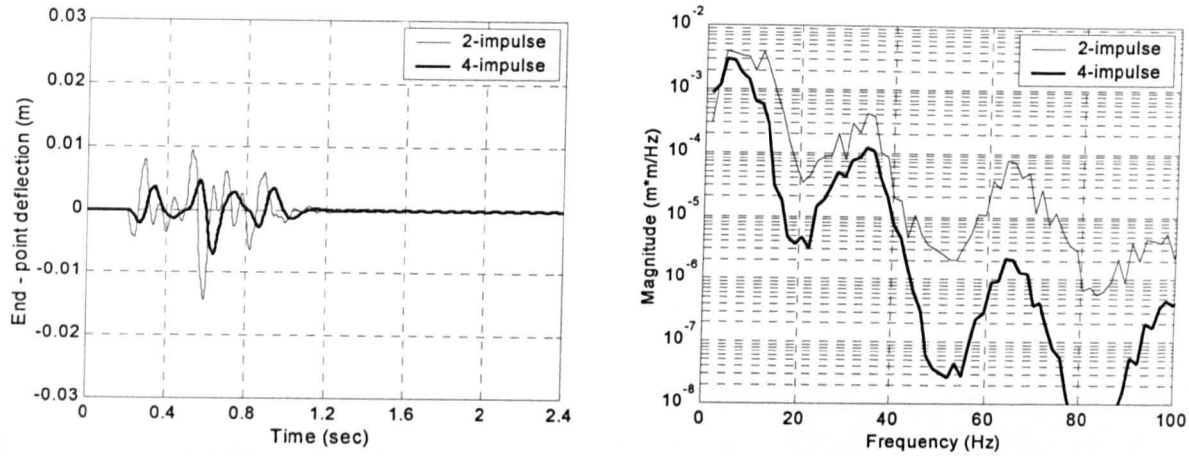

(a) Time domain. (b) PSD.

Figure 5.14: Simulated end-point deflection response of the manipulator to the shaped inputs with erroneous natural frequencies.

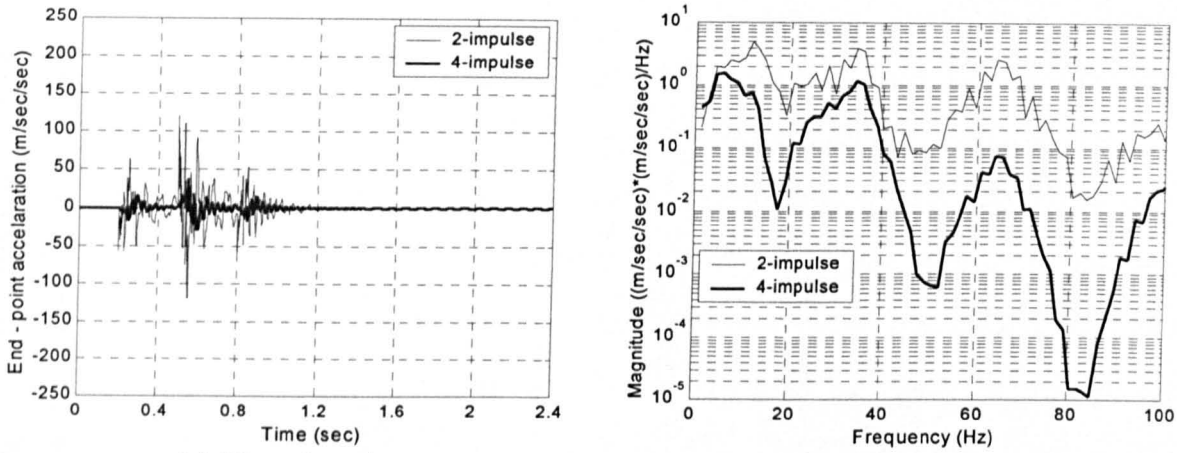

(a) Time domain. (b) PSD.

Figure 5.15: Simulated end-point acceleration response of the manipulator to the shaped inputs with erroneous natural frequencies.

The simulated responses of the system incorporating a payload of 40 grams to the shaped inputs using a four-impulse sequence with exact and erroneous natural frequencies are shown in Figures 5.16 – 5.19. It is noted that input shaping can handle vibrations resulting from inclusion of payload in the system. The magnitudes of vibration at the resonance modes of the system have significantly been reduced as compared with response to the unshaped input. Moreover, significant vibration reduction has been achieved using the shaped input with erroneous natural frequencies.

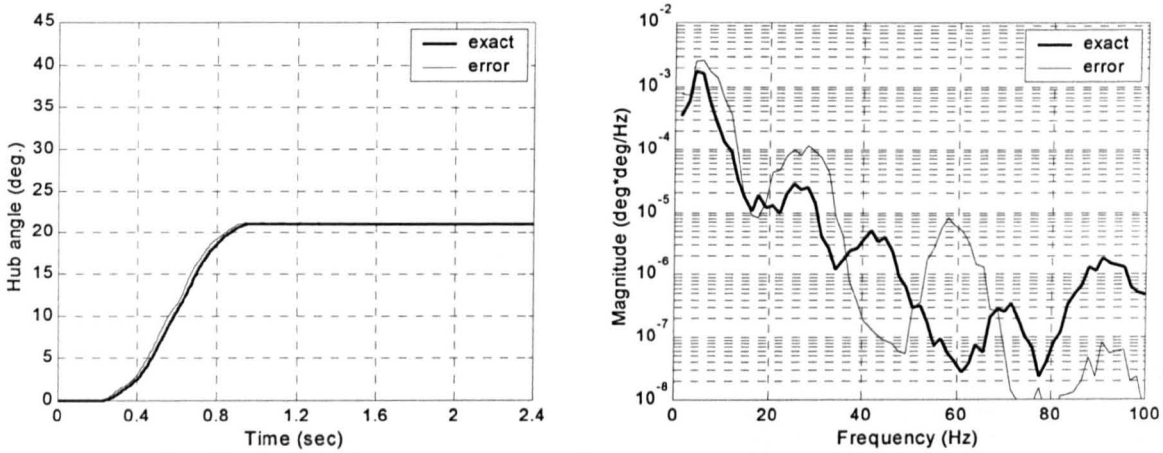

(a) Time domain. (b) PSD.

Figure 5.16: Simulated hub-angle response of the manipulator using the shaped inputs with exact and erroneous natural frequencies (with payload).

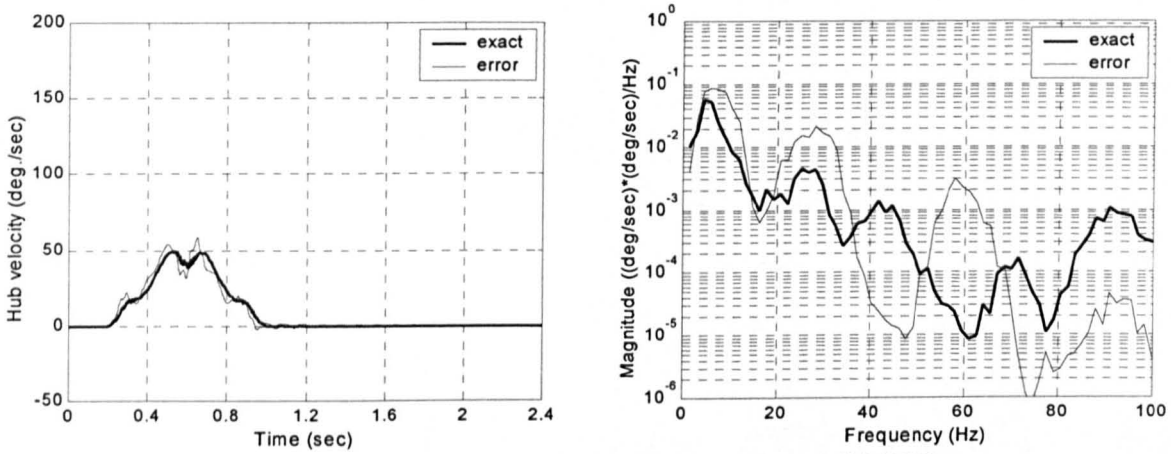

(a) Time domain. (b) PSD.

Figure 5.17: Simulated hub-velocity response of the manipulator using the shaped inputs with exact and erroneous natural frequencies (with payload).

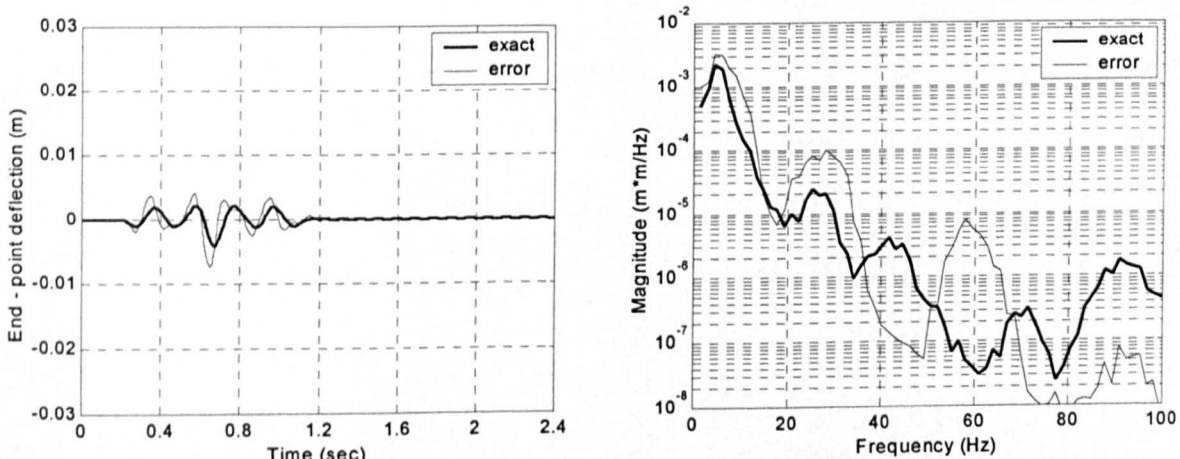

(a) Time domain. (b) PSD.

Figure 5.18: Simulated end-point deflection response of the manipulator using the shaped inputs with exact and erroneous natural frequencies (with payload).

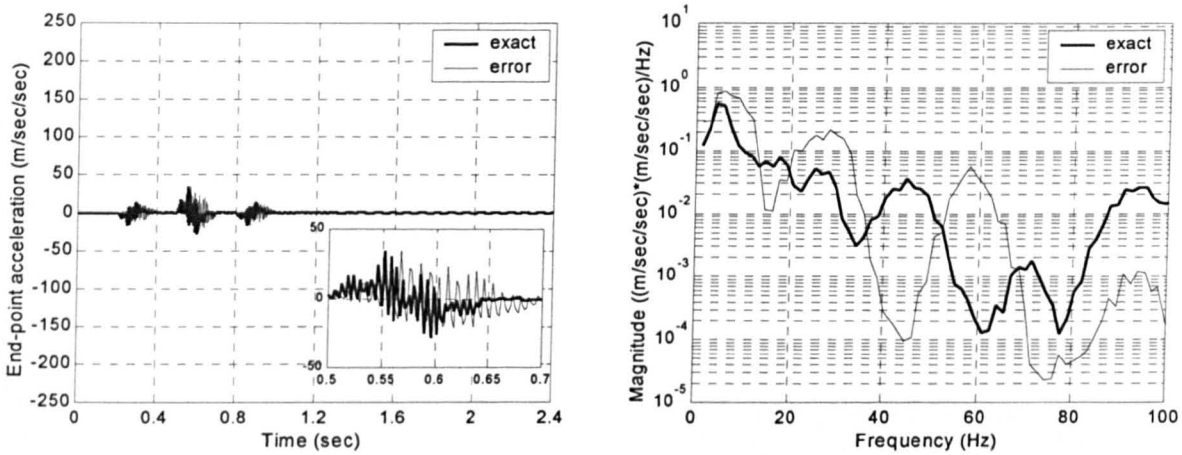

(a) Time domain. (b) PSD.

Figure 5.19: Simulated end-point acceleration response of the manipulator using the shaped inputs with exact and erroneous natural frequencies (with payload).

5.4.2. Low-pass Filtered Inputs

Figures 5.20 – 5.23 show responses of the flexible manipulator without payload to the filtered torque using third and sixth order Butterworth low-pass filters. It is noted that the system vibrations at resonance modes were considerably reduced in comparison to the unshaped bang-bang torque input. As demonstrated, the level of reduction increases with higher filter orders. Using this control technique, the settling times of the hub-angle response were obtained as 0.826 sec and 0.858 sec with third and sixth order filters respectively.

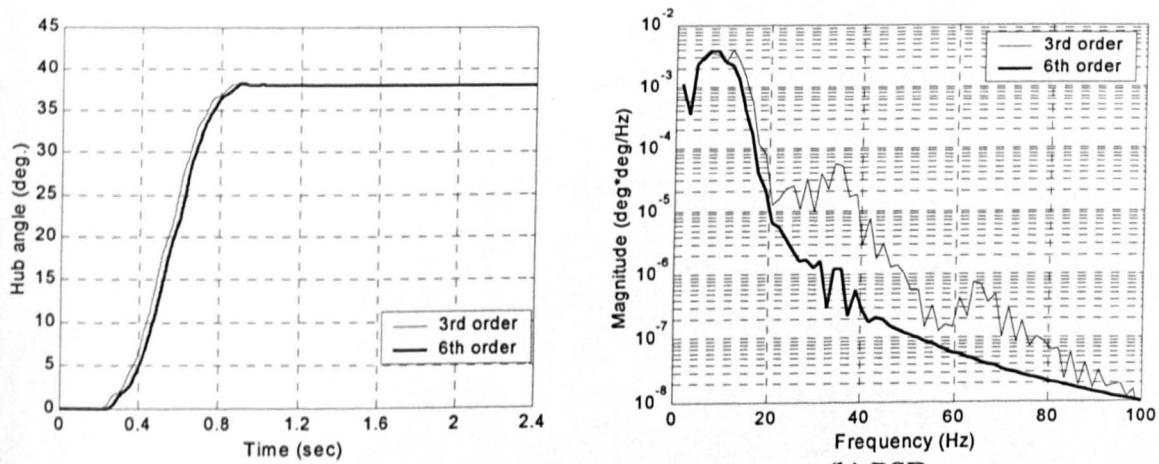

(a) Time domain. (b) PSD.

Figure 5.20: Simulated hub-angle response of the manipulator to the low-pass filtered inputs with exact natural frequencies.

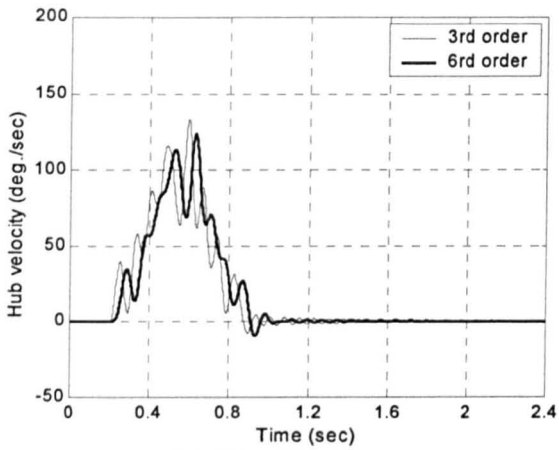

(a) Time domain.

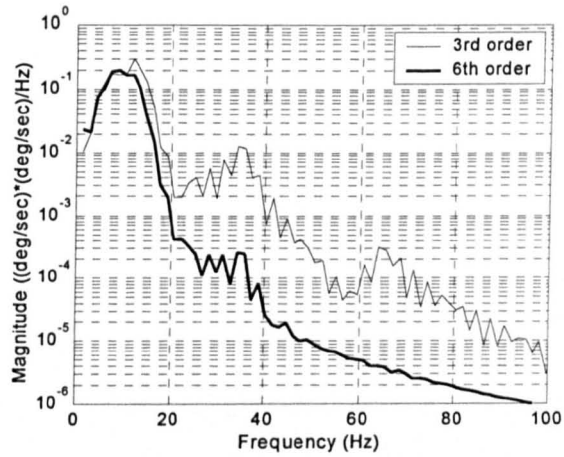

(b) PSD.

Figure 5.21: Simulated hub-velocity response of the manipulator to the low-pass filtered inputs with exact natural frequencies.

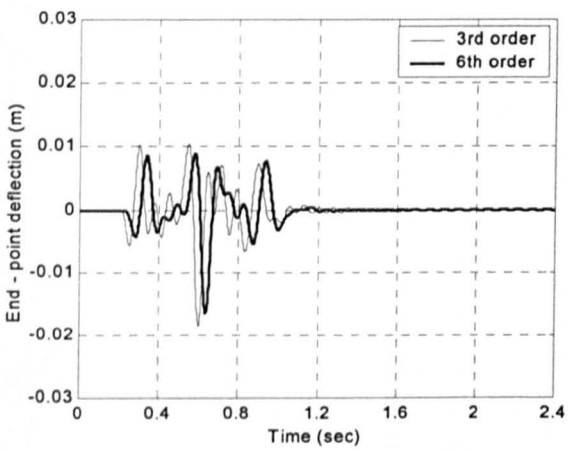

(a) Time domain.

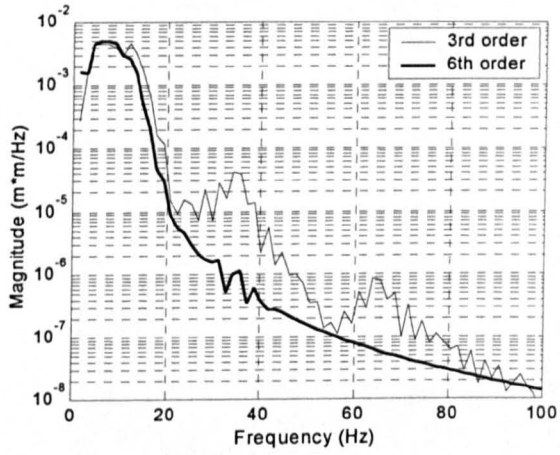

(b) PSD.

Figure 5.22: Simulated end-point deflection response of the manipulator to the low-pass filtered inputs with exact natural frequencies.

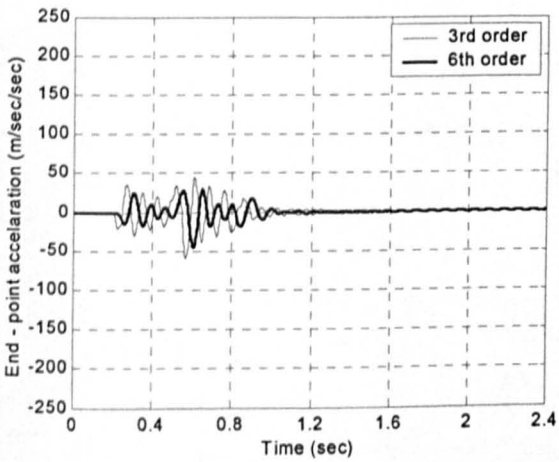

(a) Time domain.

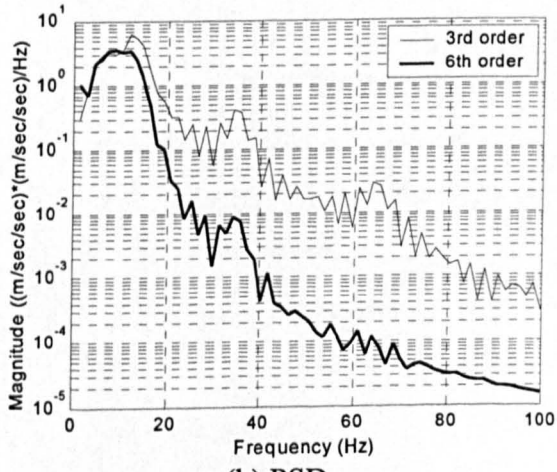

(b) PSD.

Figure 5.23: Simulated end-point acceleration response of the manipulator to the low-pass filtered inputs with exact natural frequencies.

The robustness of the technique is demonstrated in Figures 5.24 – 5.27, where the system response to the filtered torque with 30% error in the natural frequencies is shown. As evidenced in the magnitude of the time response, relatively small reduction in the system vibration was achieved.

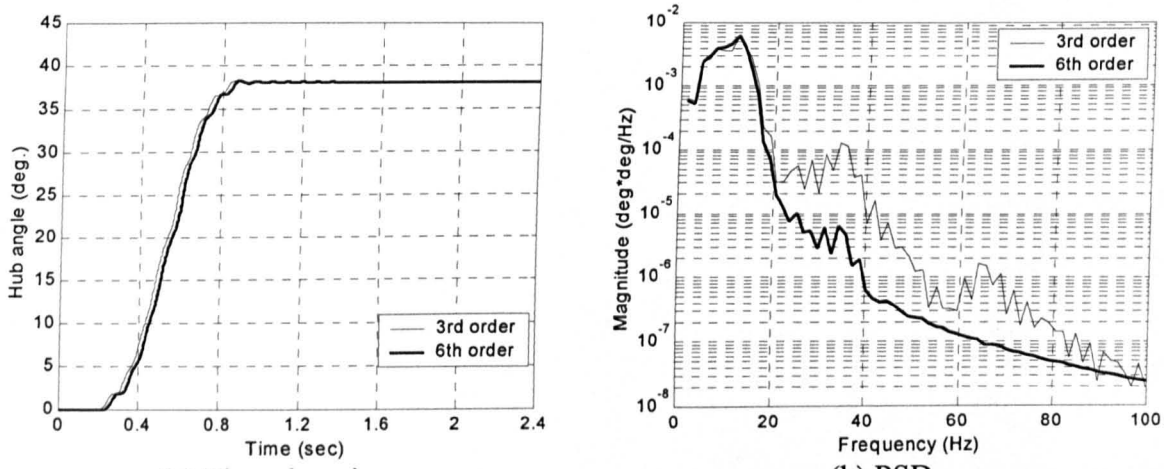

(a) Time domain. (b) PSD.

Figure 5.24: Simulated hub-angle response of the manipulator to the low-pass filtered inputs with erroneous natural frequencies.

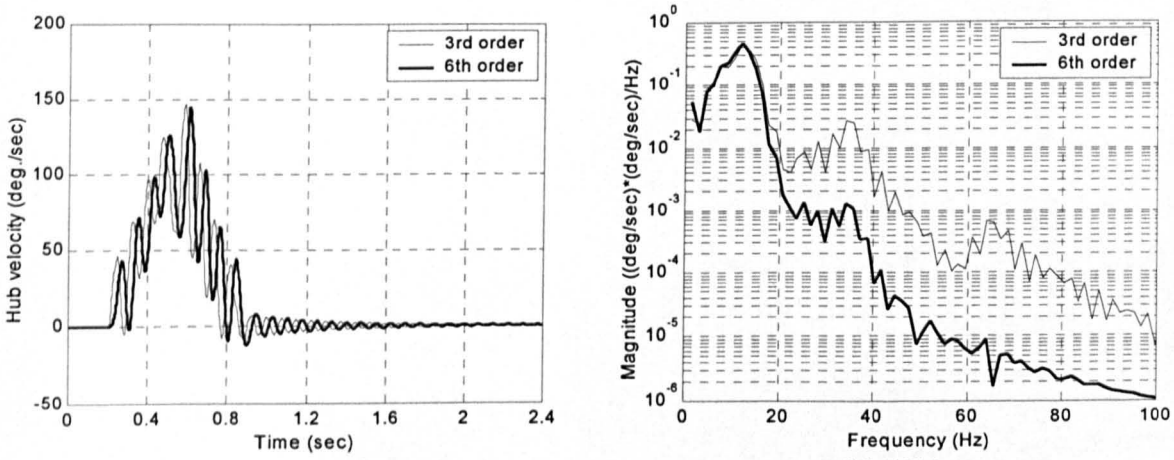

(a) Time domain. (b) PSD.

Figure 5.25: Simulated hub-velocity response of the manipulator to the low-pass filtered inputs with erroneous natural frequencies.

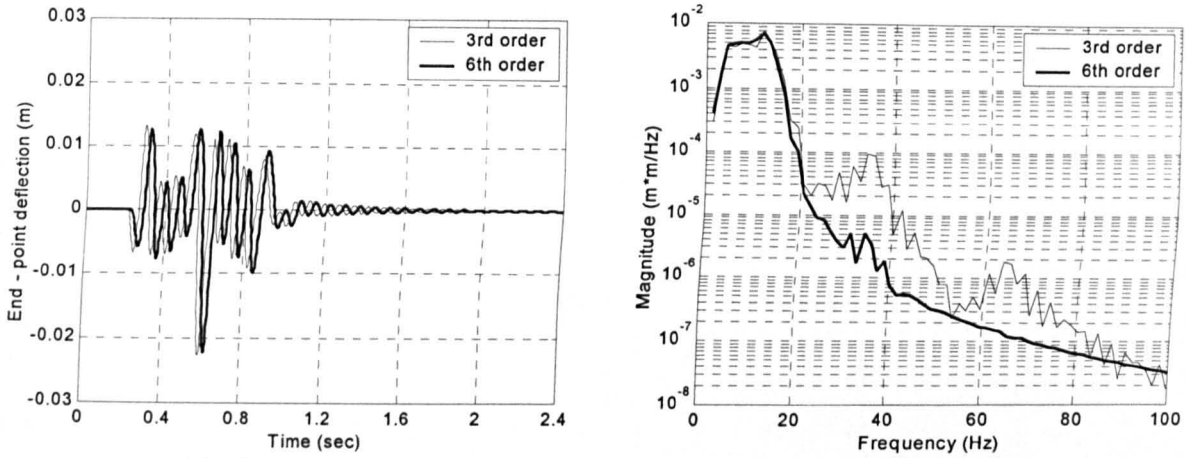

(a) Time domain. (b) PSD.

Figure 5.26: Simulated end-point deflection response of the manipulator to the low-pass filtered inputs with erroneous natural frequencies.

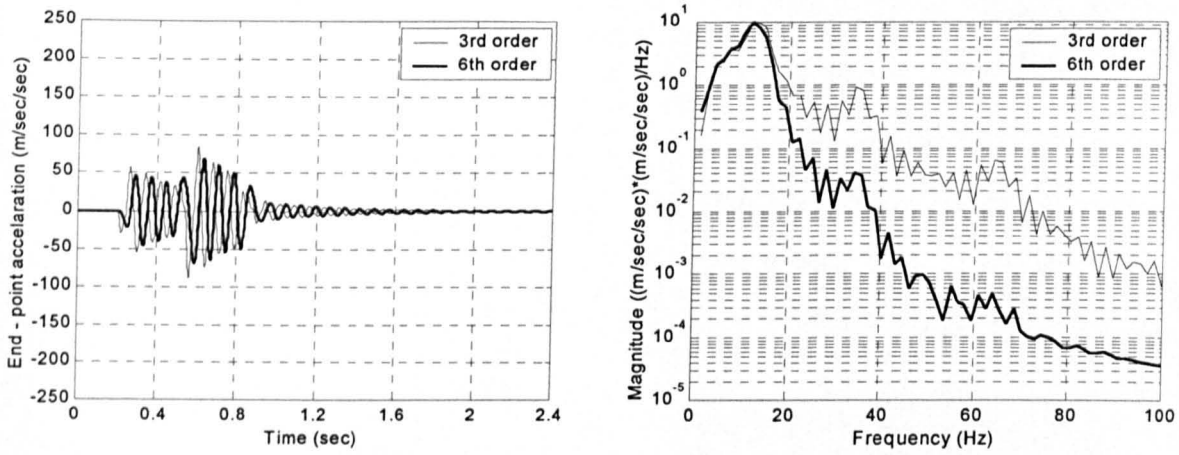

(a) Time domain. (b) PSD.

Figure 5.27: Simulated end-point acceleration response of the manipulator to the low-pass filtered inputs with erroneous natural frequencies.

Similarly, responses of the manipulator incorporating a payload of 40 grams to the sixth-order low-pass filtered input with exact and erroneous natural frequencies are shown in Figures 5.28 – 5.31. It is noted that considerable reduction in the system vibration was achieved using the low-pass filtered input with exact natural frequencies. However, the levels of vibration at the hub-angle, hub-velocity, end-point deflection and end-point acceleration were higher as compared to the system without payload. Moreover, significant improvement was not achieved using the filtered inputs with erroneous natural frequencies. In this case, the system vibrations were higher.

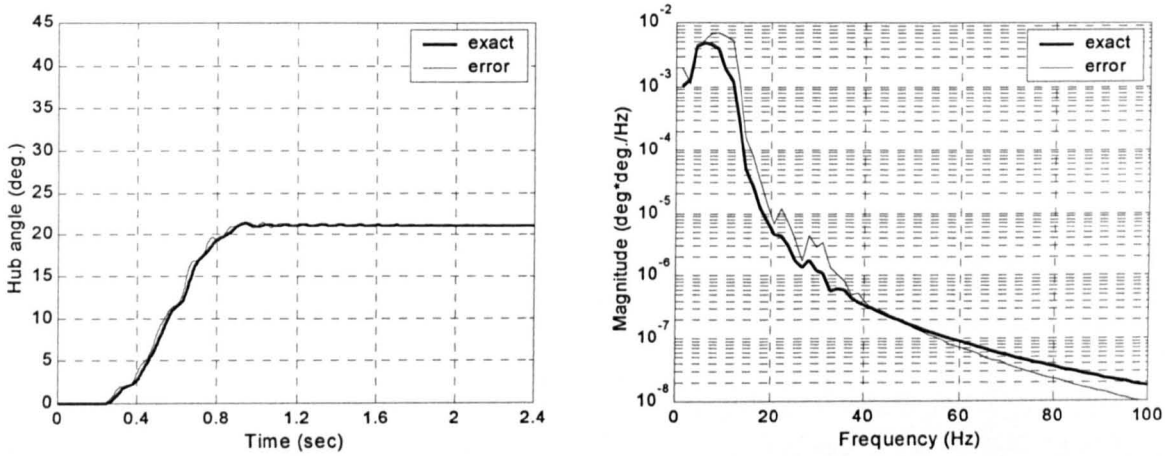

(a) Time domain. (b) PSD.

Figure 5.28: Simulated hub-angle response of the manipulator using the low-pass filtered inputs with exact and erroneous natural frequencies (with payload).

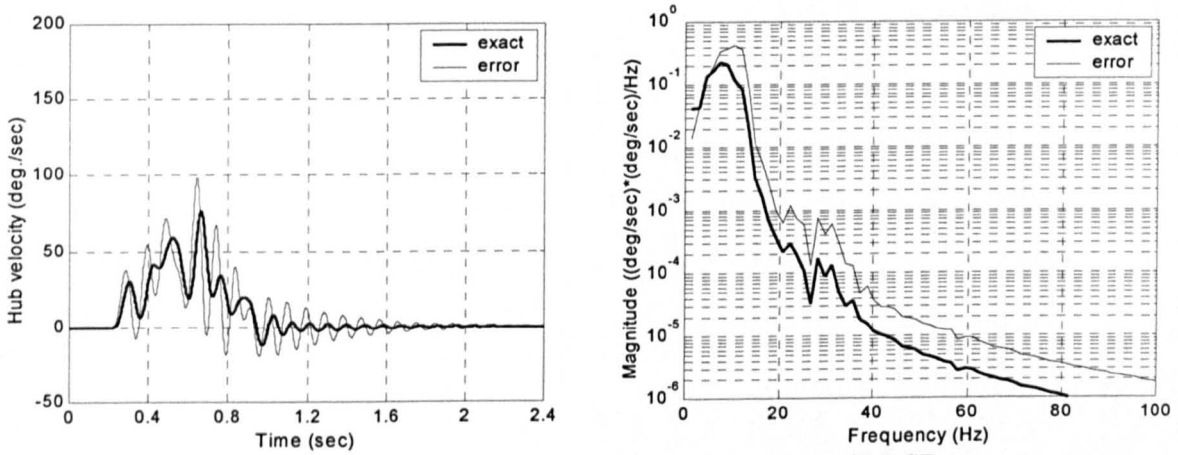

(a) Time domain. (b) PSD.

Figure 5.29: Simulated hub-velocity response of the manipulator using the low-pass filtered inputs with exact and erroneous natural frequencies (with payload).

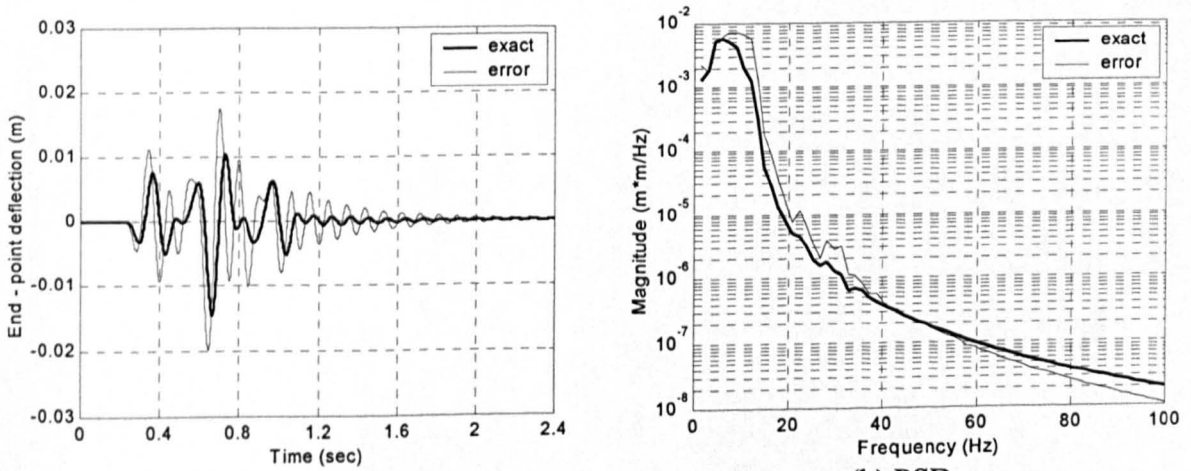

(a) Time domain. (b) PSD.

Figure 5.30: Simulated end-point deflection response of the manipulator using the low-pass filtered inputs with exact and erroneous natural frequencies (with payload).

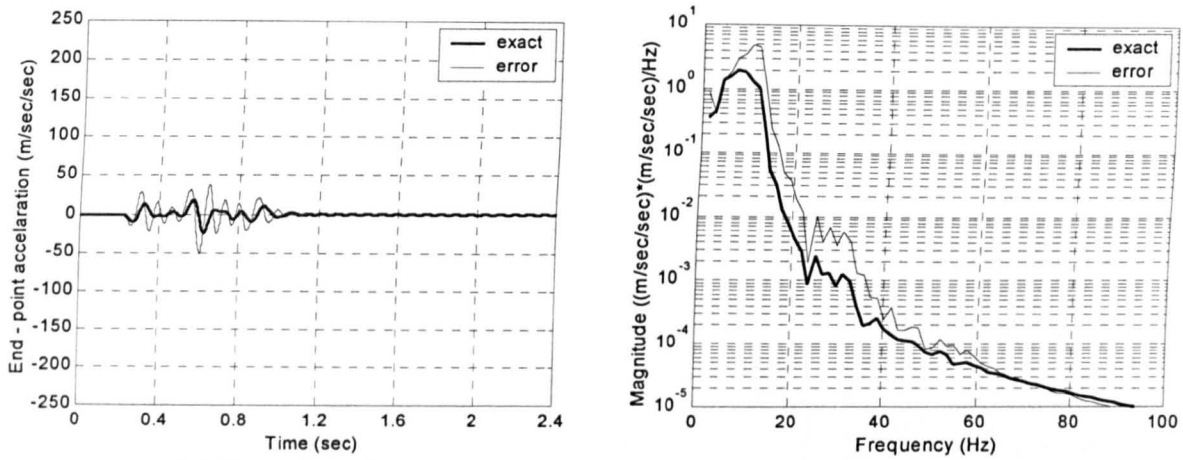

(a) Time domain. (b) PSD.

Figure 5.31: Simulated end-point acceleration response of the manipulator using the low-pass filtered inputs with exact and erroneous natural frequencies (with payload).

5.4.3. Band-stop Filtered Inputs

The simulated responses of the flexible manipulator system without payload to the third and sixth order Butterworth band-stop filtered inputs are shown in Figures 5.32 – 5.35. It is noted that considerable amount of vibration reduction at the first three vibration modes was achieved with the band-stop filtered inputs in comparison to the unshaped input. It is noted that with a higher filter order, improvement in reduction of vibration was not significant. The settling times of the hub-angle response were obtained as 0.812 sec and 0.830 sec with third and sixth order filters respectively.

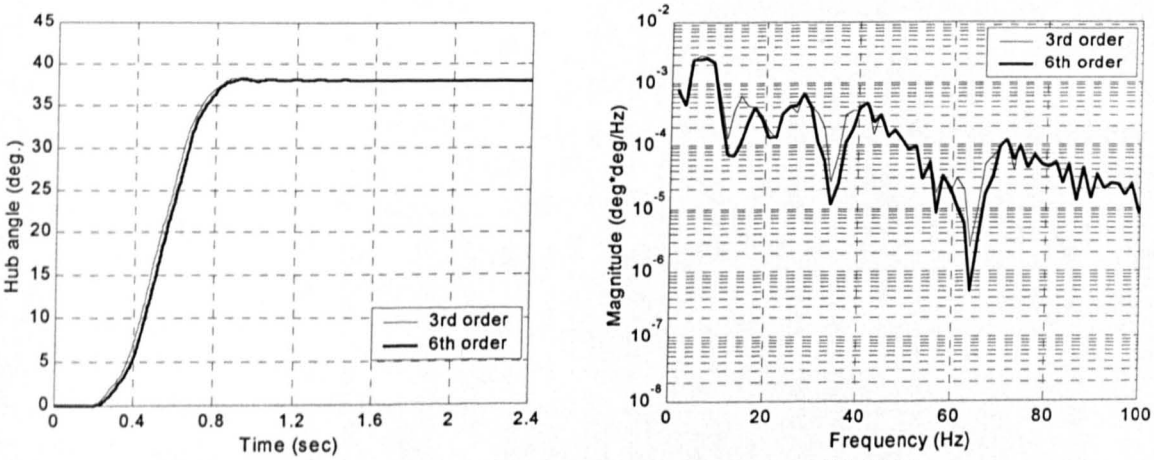

(a) Time domain. (b) PSD.

Figure 5.32: Simulated hub-angle response of the manipulator to the band-stop filtered inputs with exact natural frequencies.

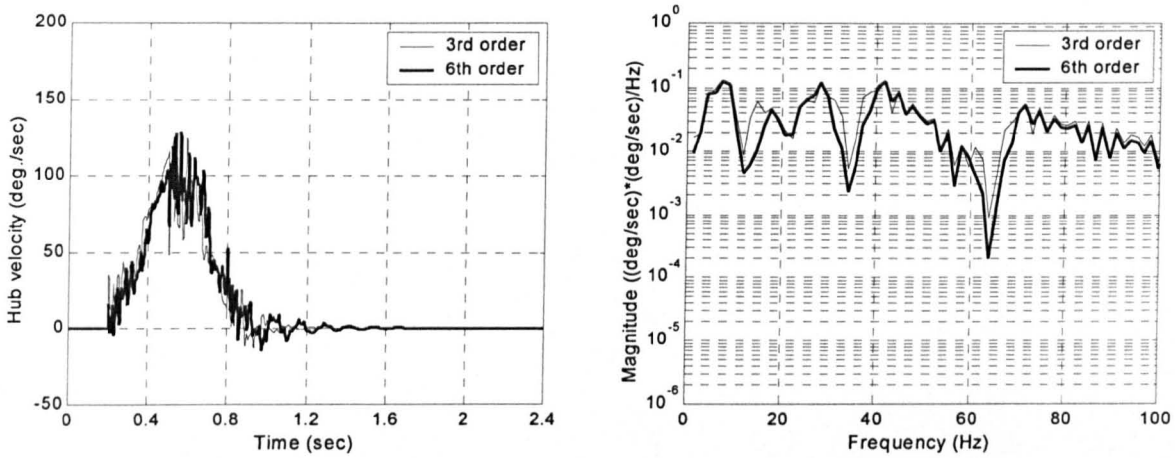

(a) Time domain. (b) PSD.

Figure 5.33: Simulated hub-velocity response of the manipulator to the band-stop filtered inputs with exact natural frequencies.

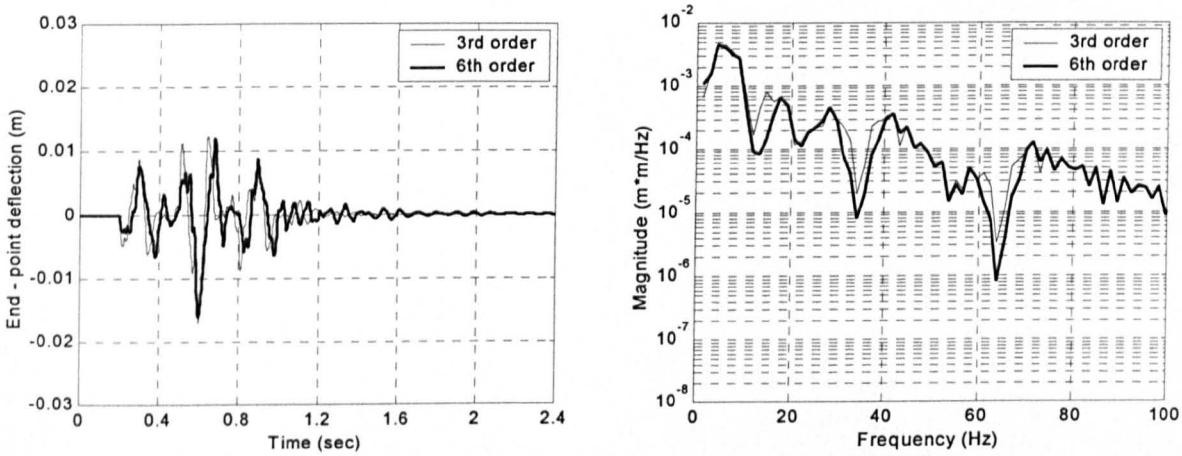

(a) Time domain. (b) PSD.

Figure 5.34: Simulated end-point deflection response of the manipulator to the band-stop filtered inputs with exact natural frequencies.

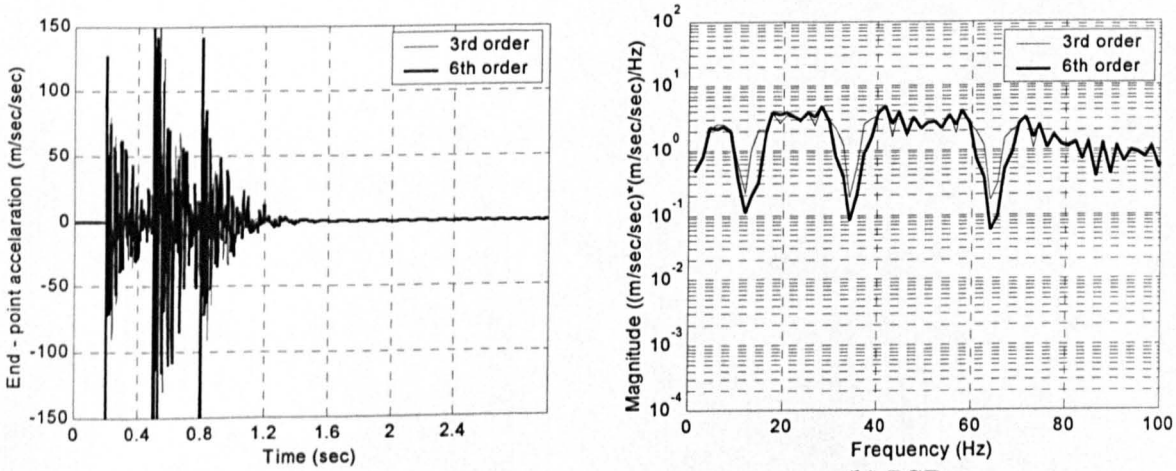

(a) Time domain. (b) PSD.

Figure 5.35: Simulated end-point acceleration response of the manipulator to the band-stop filtered inputs with exact natural frequencies.

Figures 5.36 – 5.39 show the system responses to the band-stop filtered inputs with erroneous natural frequencies. It is noted that the level of vibration of the system at resonance modes was not significantly affected as compared with the unshaped input case. Moreover, no reduction was achieved at the second and third vibration modes.

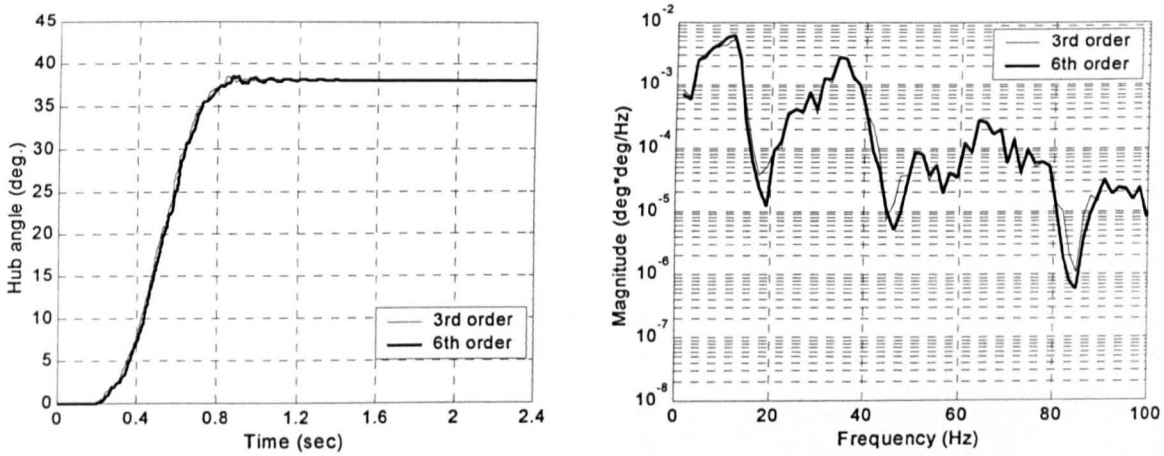

(a) Time domain. (b) PSD.

Figure 5.36: Simulated hub-angle response of the manipulator to the band-stop filtered inputs with erroneous natural frequencies.

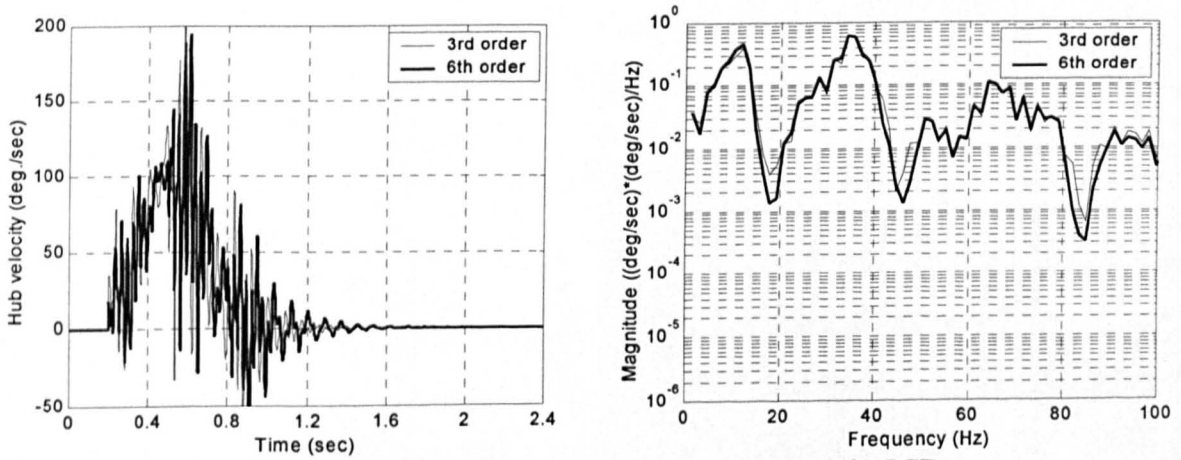

(a) Time domain. (b) PSD.

Figure 5.37: Simulated hub-velocity response of the manipulator to the band-stop filtered inputs with erroneous natural frequencies.

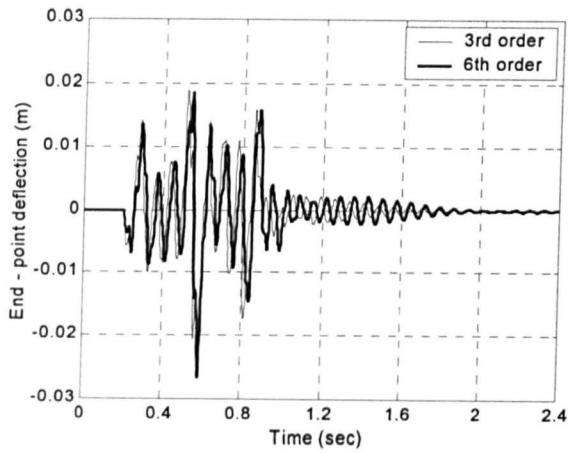

(a) Time domain.

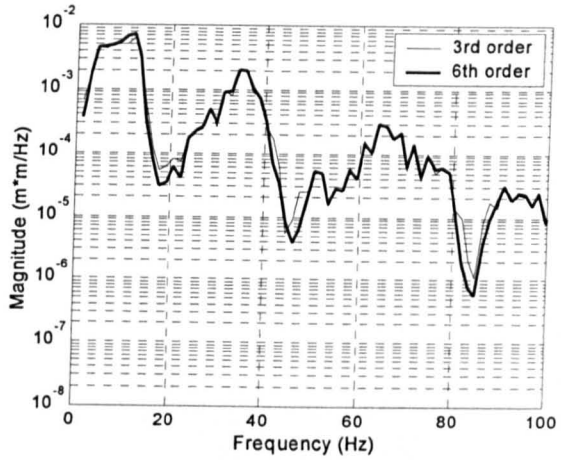

(b) PSD.

Figure 5.38: Simulated end-point deflection response of the manipulator to the band-stop filtered inputs with erroneous natural frequencies.

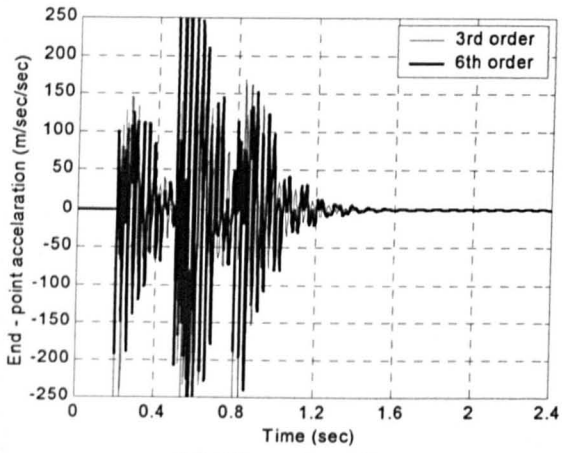

(a) Time domain.

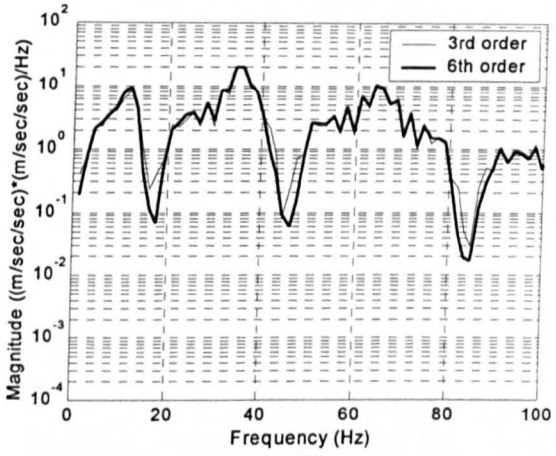

(b) PSD.

Figure 5.39: Simulated end-point acceleration response of the manipulator the band-stop filtered inputs with erroneous natural frequencies.

Figures 5.40 – 5.43 show responses of the manipulator incorporating a payload of 40 grams to the sixth-order band-stop filtered input with exact and erroneous natural frequencies. Similar to the low-pass filtered input, considerable reduction in the system vibration was achieved with exact natural frequencies. However, significant improvement was not achieved using the filtered inputs with erroneous natural frequencies. In this case, the system vibrations were higher.

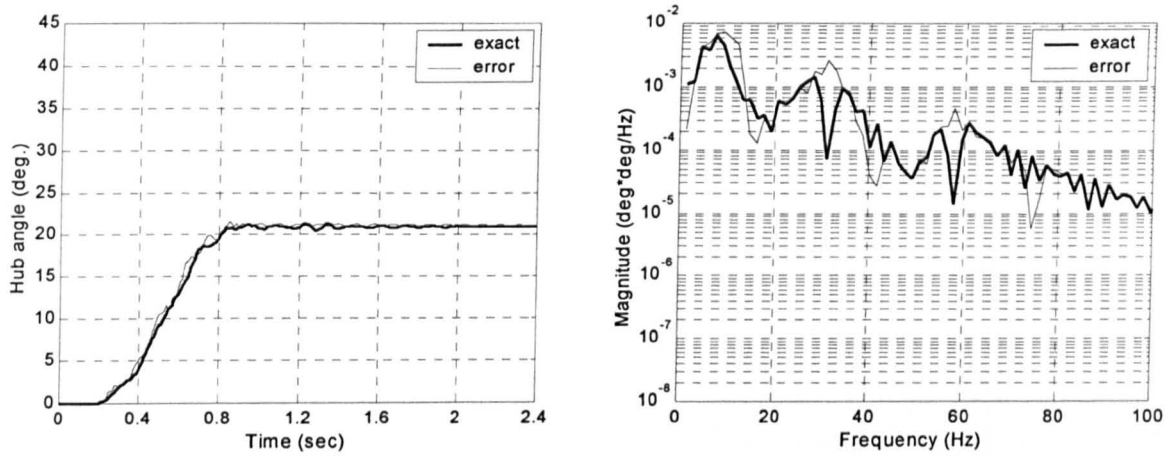

(a) Time domain. (b) PSD.

Figure 5.40: Simulated hub-angle response of the manipulator using the band-stop filtered inputs with exact and erroneous natural frequencies (with payload).

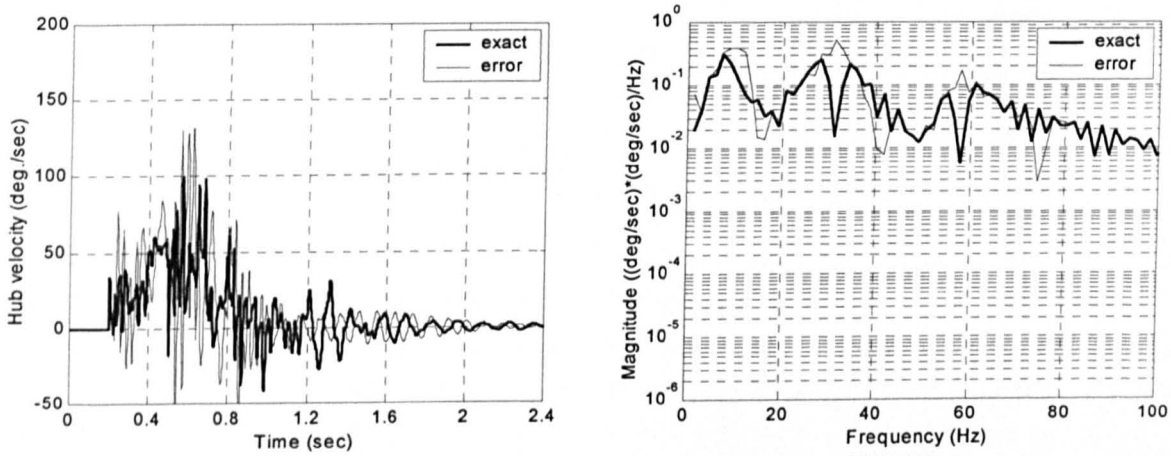

(a) Time domain. (b) PSD.

Figure 5.41: Simulated hub-velocity response of the manipulator using the band-stop filtered inputs with exact and erroneous natural frequencies (with payload).

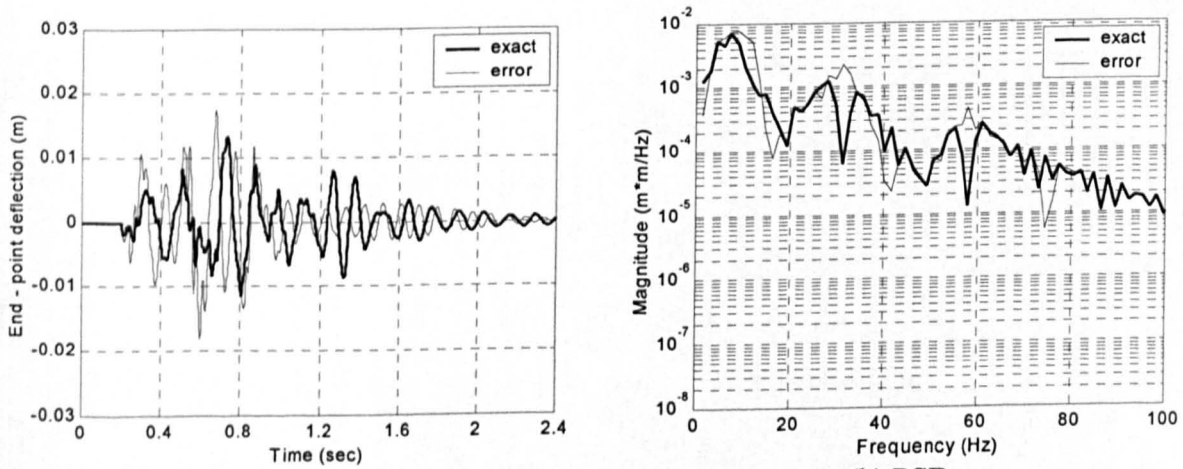

(a) Time domain. (b) PSD.

Figure 5.42: Simulated end-point deflection response of the manipulator using the band-stop filtered inputs with exact and erroneous natural frequencies (with payload).

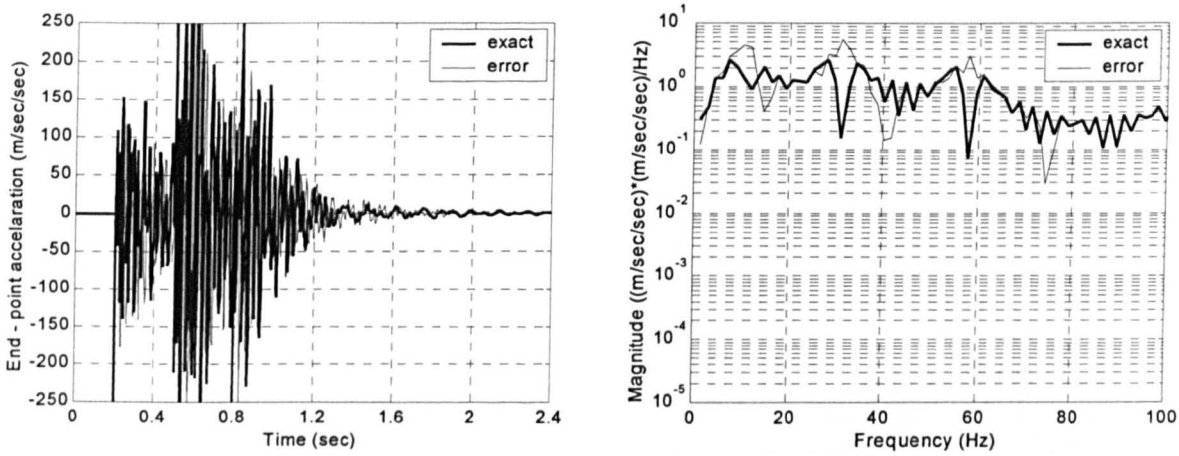

(a) Time domain. (b) PSD.

Figure 5.43: Simulated end-point acceleration response of the manipulator using the band-stop filtered inputs with exact and erroneous natural frequencies (with payload).

5.5. Experimental Results

In this section experimental results of the response of the flexible manipulator using the command shaping techniques are presented. Three system responses namely hub-angle, hub-velocity and end-point acceleration with the corresponding PSDs were measured.

5.5.1. Input Shaping

Figures 5.44 and 5.45 show the experimental responses of the flexible manipulator with the corresponding PSDs to the shaped input using two- and four-impulse sequences with exact and erroneous natural frequencies respectively. As in the case of simulation results, it is noted with exact frequencies that the magnitudes of vibration of the system, with the hub-angle, hub-velocity and end-point acceleration responses, have significantly been reduced at the natural frequencies. These can be observed by comparing the system responses to the unshaped input (Figures 3.18 – 3.20). With the four impulse-sequence, the oscillations in the end-point acceleration response were almost reduced to zero. By analysing the hub-angle response, it is noted that a much faster hub-angle response with less overshoot, as compared with response to the unshaped input, was achieved. The level of vibration reduction increases and the overshoot decreases with higher number of impulses at the expense of increase in the delay (settling times) in the response of the system. With error in natural frequencies, the level of reduction in the vibration of the manipulator is slightly less than the case without error. However, significant level of vibration reduction as compared with response to the unshaped input was achieved. It is noted that despite an increase in the time response

parameters, as compared with the case without error, significant reductions in the settling time and overshoot were achieved as compared with the response of the unshaped input.

Figure 5.46 shows the experimental response of the system incorporating a payload of 40 grams to the shaped inputs using a four-impulse sequence with exact and erroneous natural frequencies. It is revealed that input shaping can handle vibrations resulting from inclusion of payload in the system. In both cases, the magnitudes of vibration at the resonance modes of the system have significantly been reduced as compared with response to the unshaped input.

5.5.2. Low-pass Filtered Inputs

Figures 5.47 and 5.48 show the experimental responses of the flexible manipulator to the filtered torque using third and sixth order Butterworth low-pass filters with exact and erroneous natural frequencies respectively. With exact frequencies, it is noted from the responses that the system vibrations at the natural frequencies have been considerably reduced in comparison to the unshaped input. With erroneous frequencies, as evidenced in the magnitude of the time responses, relatively small reduction in the system vibration was achieved. It is noted by analysing the specifications of the hub-angle response with exact and erroneous frequencies, that significant reduction in the parameters was achieved as compared to the unshaped input. For the case of exact frequencies, the results show that the level of vibration reduction increases and the settling time and overshoot decrease with higher filter orders. For the case of error in the natural frequencies, it is noted that the settling time increased and higher overshoot than the response to the unshaped input was noted.

Experimental response of the system incorporating a payload to the sixth-order low-pass filtered input with exact and erroneous natural frequencies is shown in Figure 5.49. It is noted that considerable reduction in the system vibration was achieved using the filtered input with exact natural frequency. However, the levels of vibration at the hub-angle, hub-velocity and end-point acceleration were higher as compared to the system without payload. Moreover, significant improvement was not achieved using the filtered input with erroneous natural frequencies.

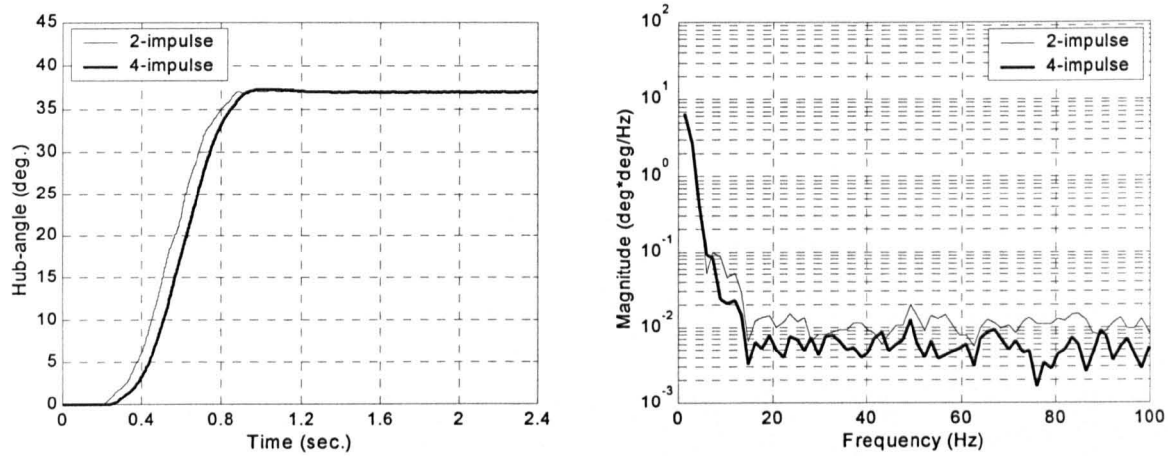

(a) Hub-angle.

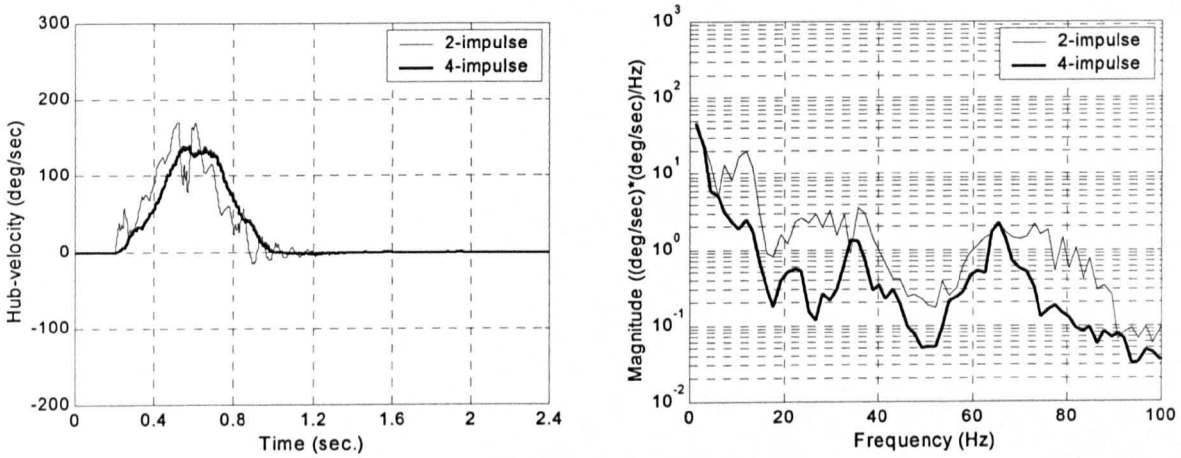

(b) Hub-velocity.

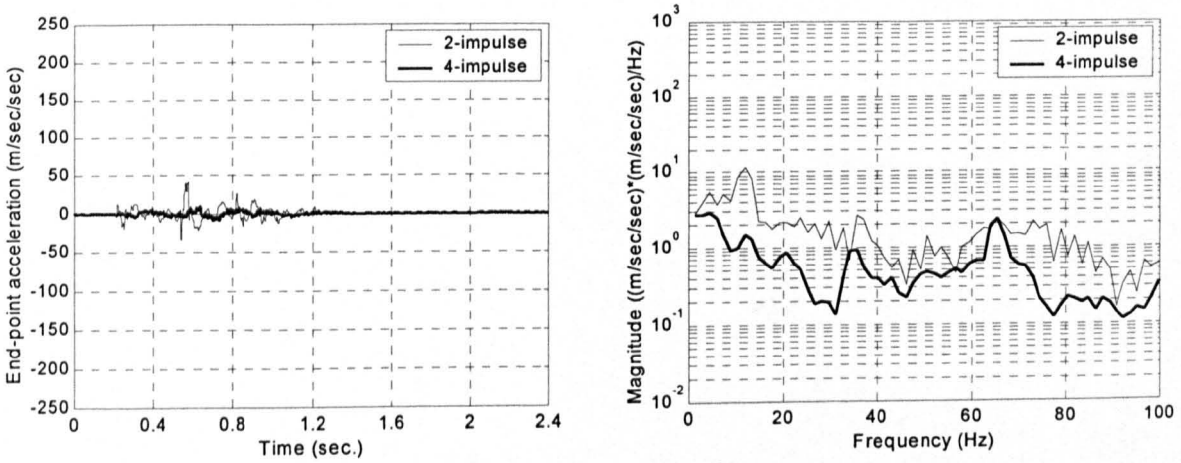

(c) End-point acceleration.

Figure 5.44: Response of the experimental rig to the shaped inputs with exact natural frequencies.

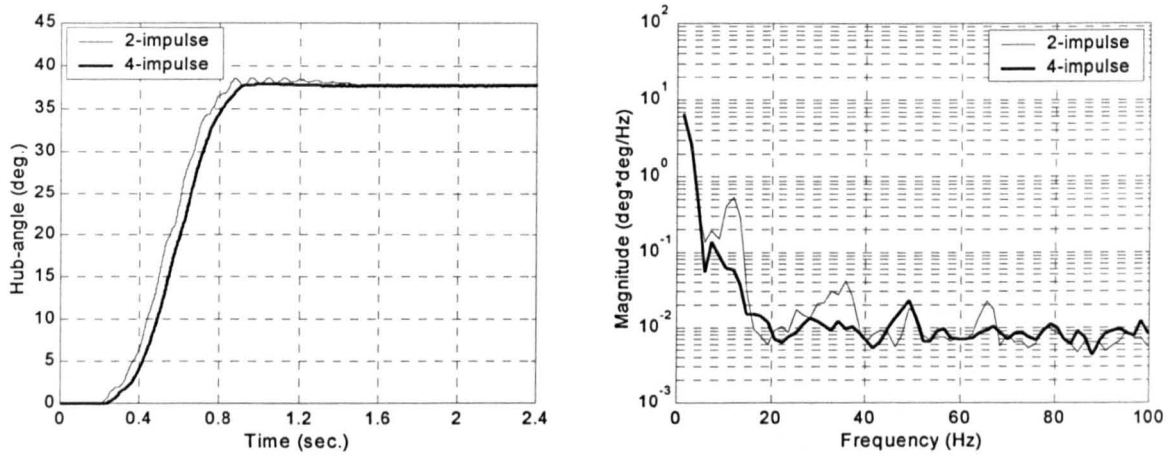

(a) Hub-angle.

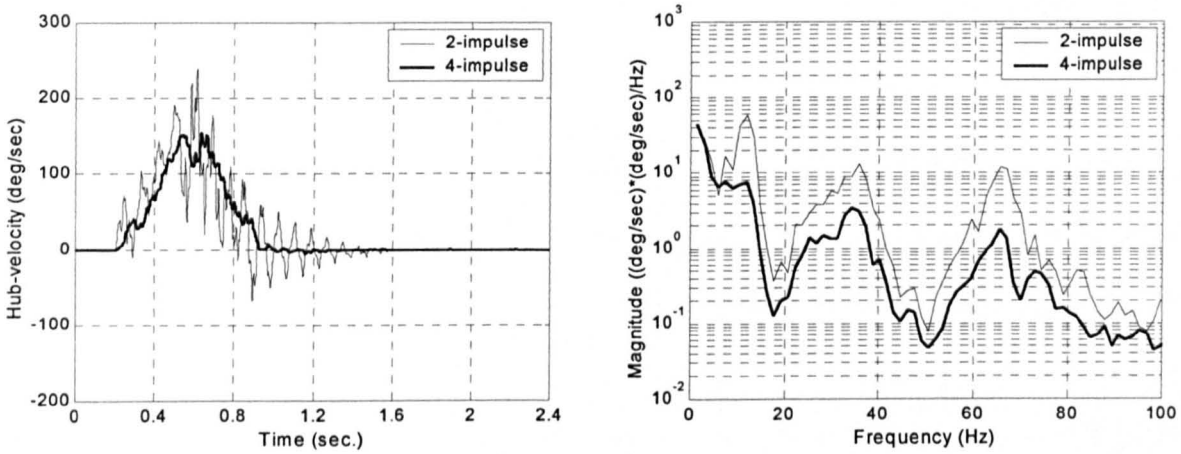

(b) Hub-velocity.

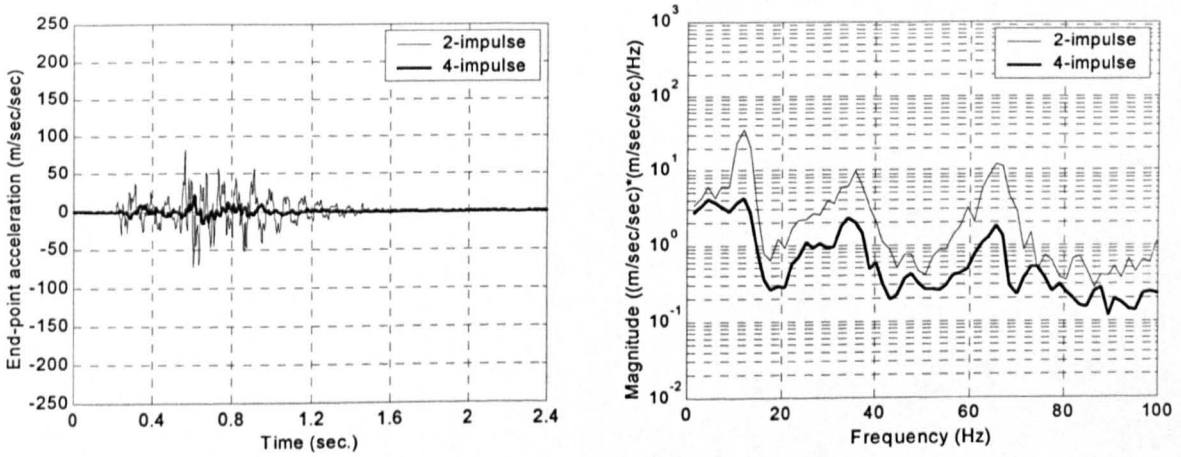

(c) End-point acceleration.

Figure 5.45: Response of the experimental rig to the shaped inputs with erroneous natural frequencies.

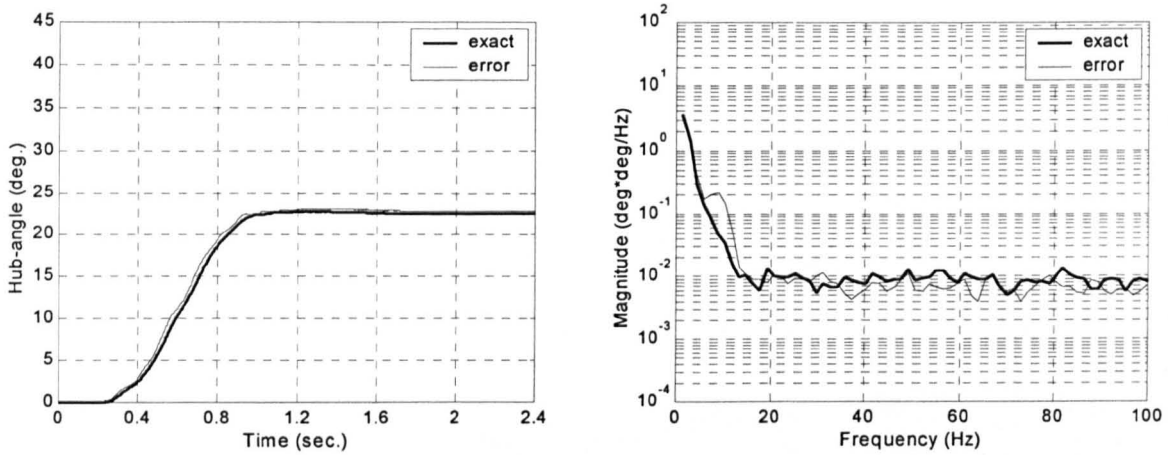

(a) Hub-angle.

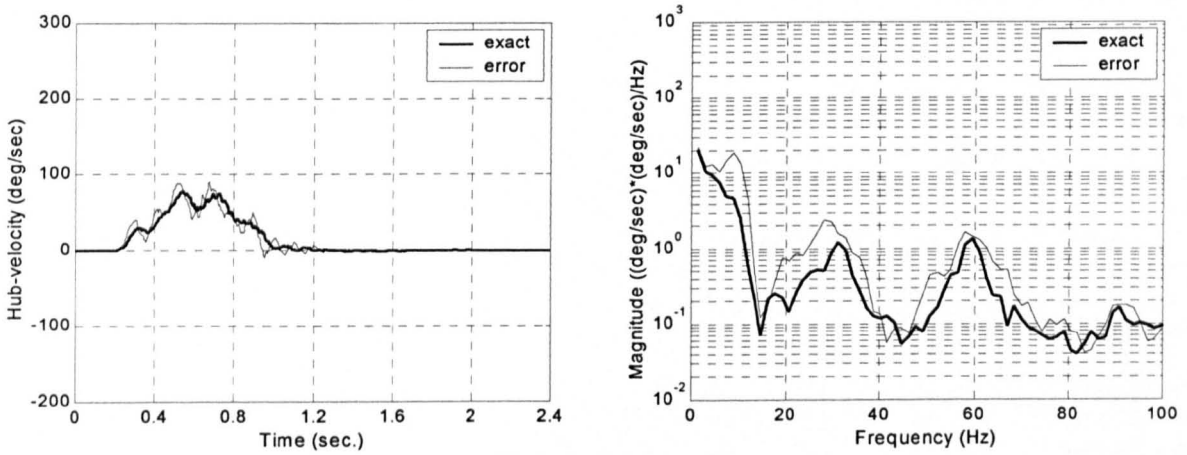

(b) Hub-velocity.

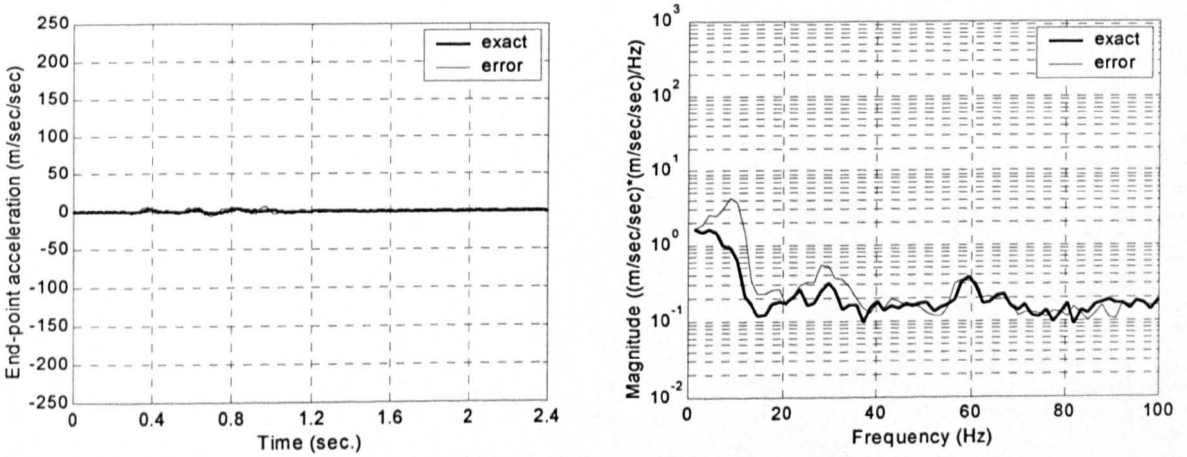

(c) End-point acceleration.

Figure 5.46: Response of the experimental rig using shaped inputs with exact and erroneous natural frequencies (with payload).

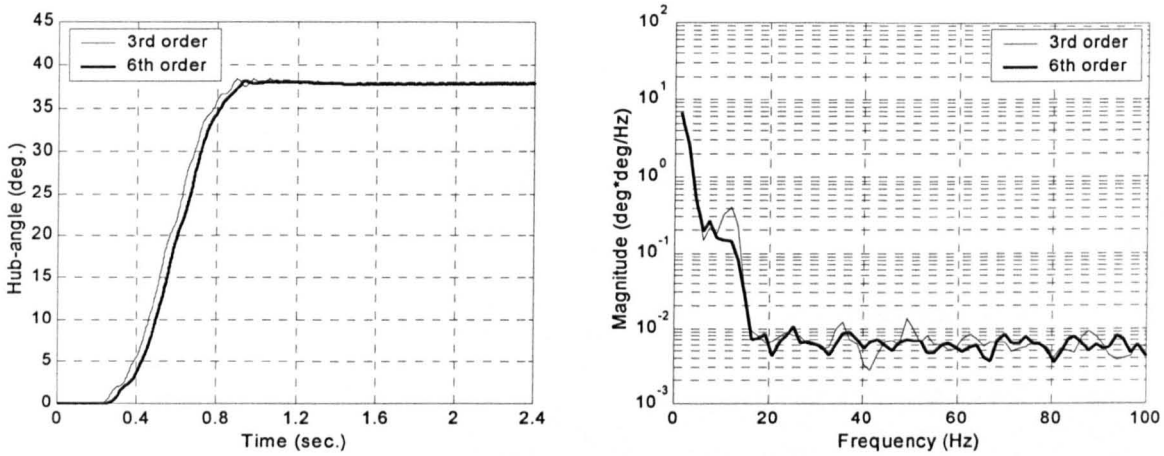

(a) Hub-angle.

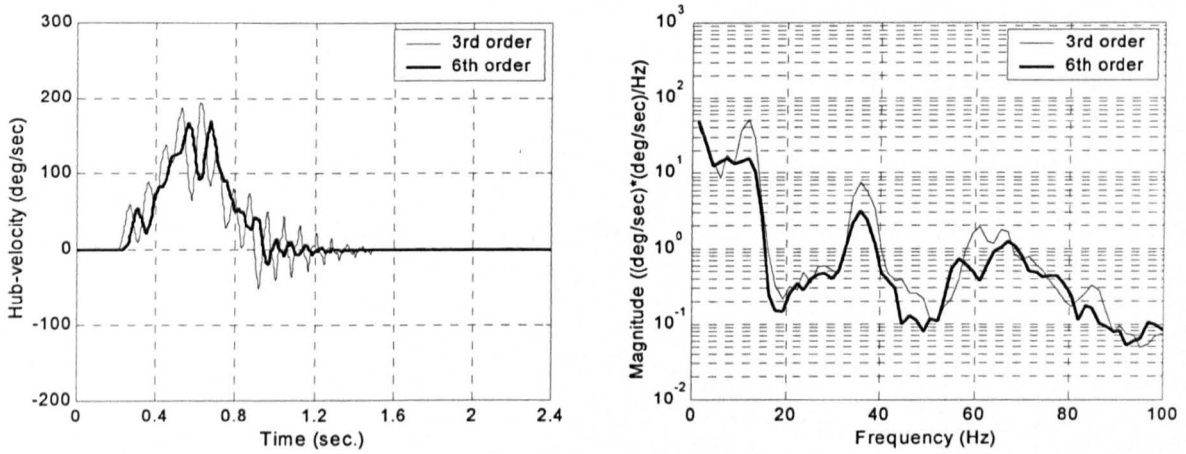

(b) Hub-velocity.

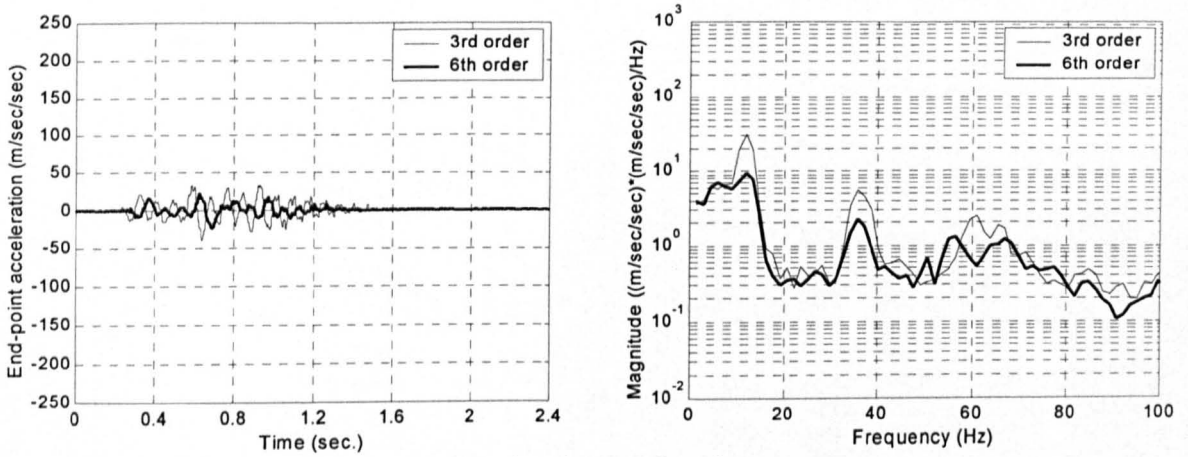

(c) End-point acceleration.

Figure 5.47: Response of the experimental rig to the low-pass filtered inputs with exact natural frequencies.

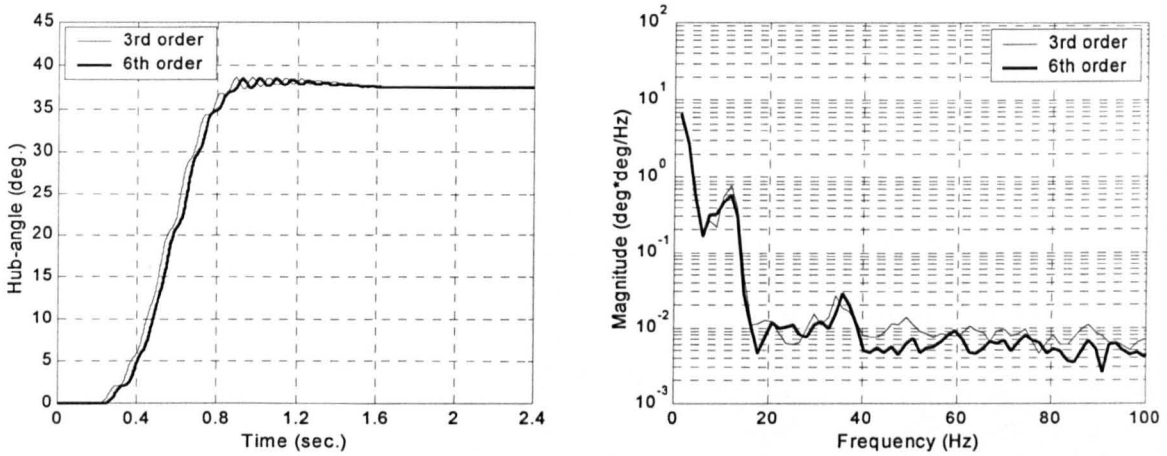

(a) Hub-angle.

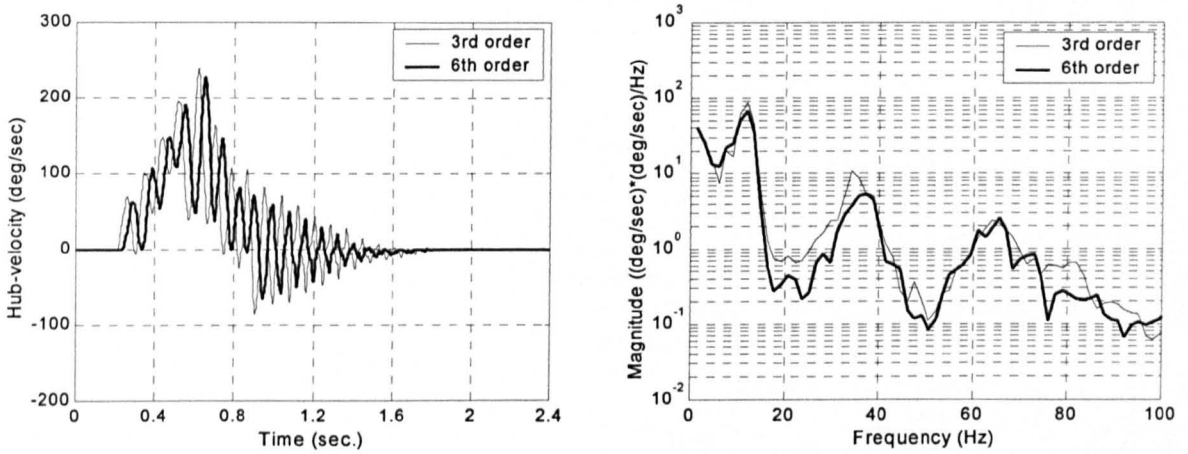

(b) Hub-velocity.

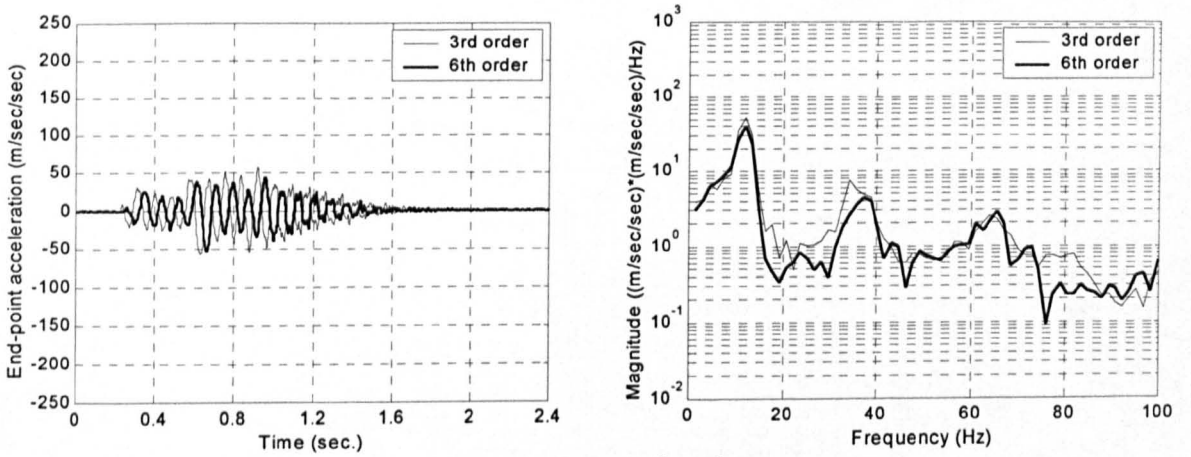

(c) End-point acceleration.

Figure 5.48: Response of the experimental rig to the low-pass filtered inputs with erroneous natural frequencies.

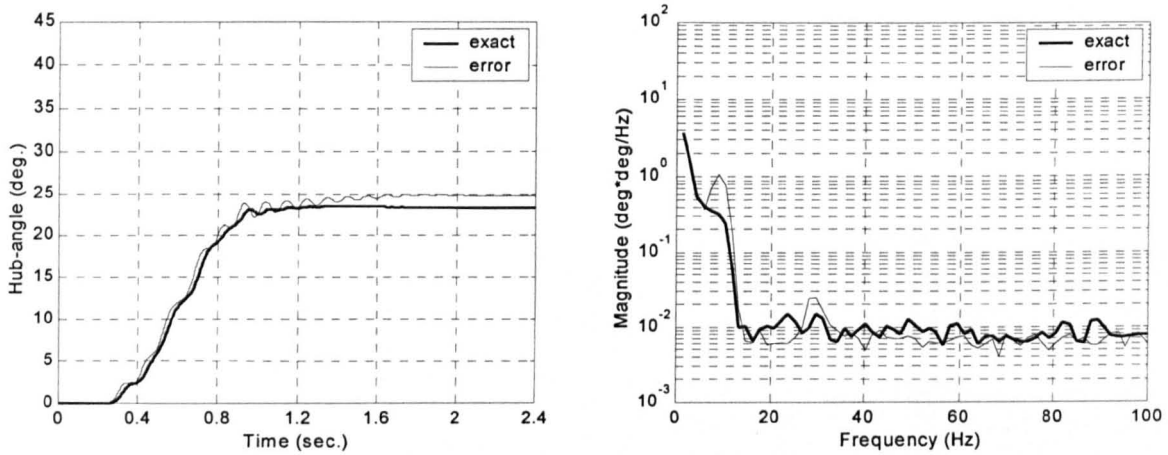

(a) Hub-angle.

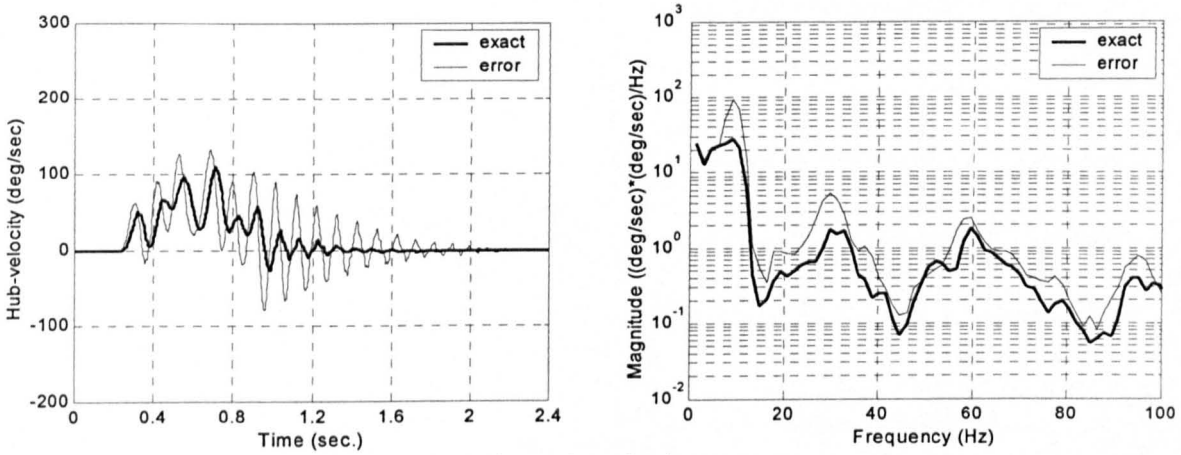

(b) Hub-velocity.

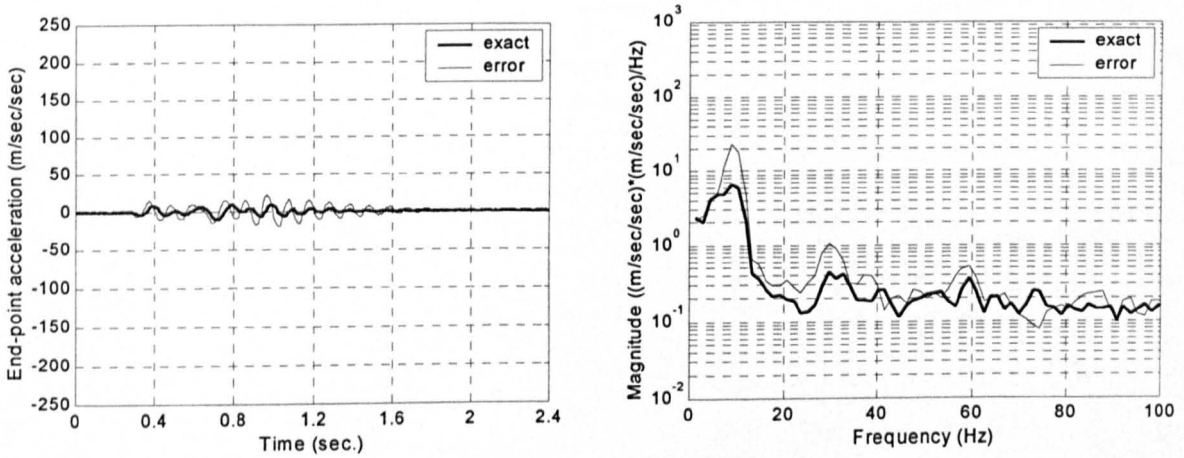

(c) End-point acceleration.

Figure 5.49: Response of the experimental rig using low-pass filtered inputs with exact and erroneous natural frequencies (with payload).

5.5.3. Band-stop Filtered Inputs

The flexible manipulator responses to the third and sixth order Butterworth band-stop filtered inputs with exact and erroneous natural frequencies are shown in Figure 5.50 and 5.51 respectively. For the former, it is noted that only small amounts of vibration reduction at the first three vibration modes were achieved in comparison with the response to the unshaped input. It is noted that significant reduction in settling time was achieved but with a relatively small reduction in the overshoot of the response. With a higher filter order, improvement in reduction of vibration was not significant and higher overshoot was achieved. This is due to the magnitude of the PSDs and higher oscillation in the filtered input as demonstrated in Figure 5.7. For the latter case, it is noted that the level of vibration of the system at the natural frequencies was not significantly affected as compared with the unshaped input case. Moreover, no improvement in the time-response was achieved as compared to the unshaped input.

Experimental response of the system incorporating a payload to the sixth-order band-stop filtered input with exact and erroneous natural frequencies is shown in Figure 5.52. It is noted that considerable reduction in the system vibration was achieved using the filtered inputs with exact natural frequency. However, the levels of vibration at the hub-angle, hub-velocity and end-point acceleration were higher as compared with those of the system without payload. Moreover, significant improvement was not achieved with the filtered input with erroneous natural frequencies. In this case, the system vibrations were higher.

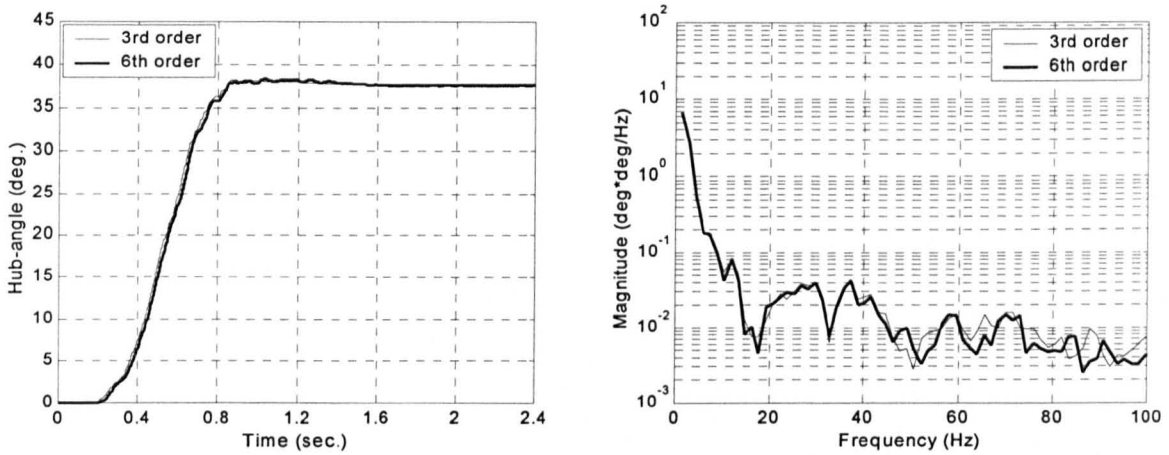

(a) Hub-angle.

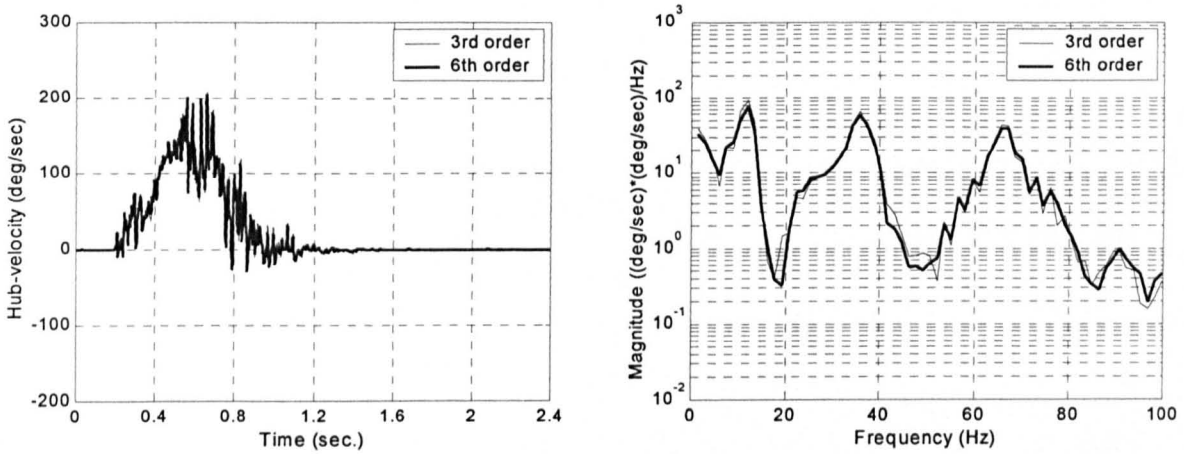

(b) Hub-velocity.

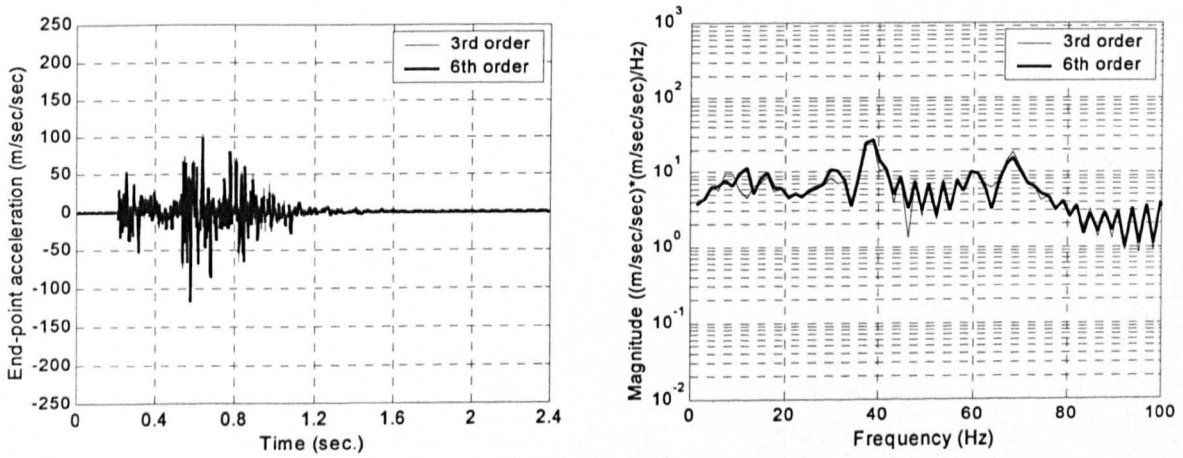

(c) End-point acceleration.

Figure 5.50: Response of the experimental rig to the band-stop filtered inputs with exact natural frequencies.

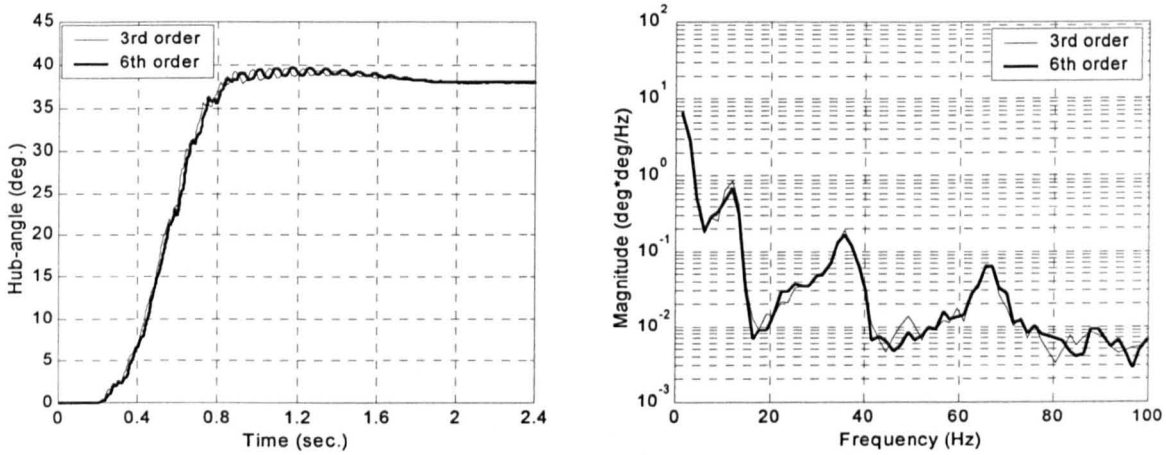

(a) Hub-angle.

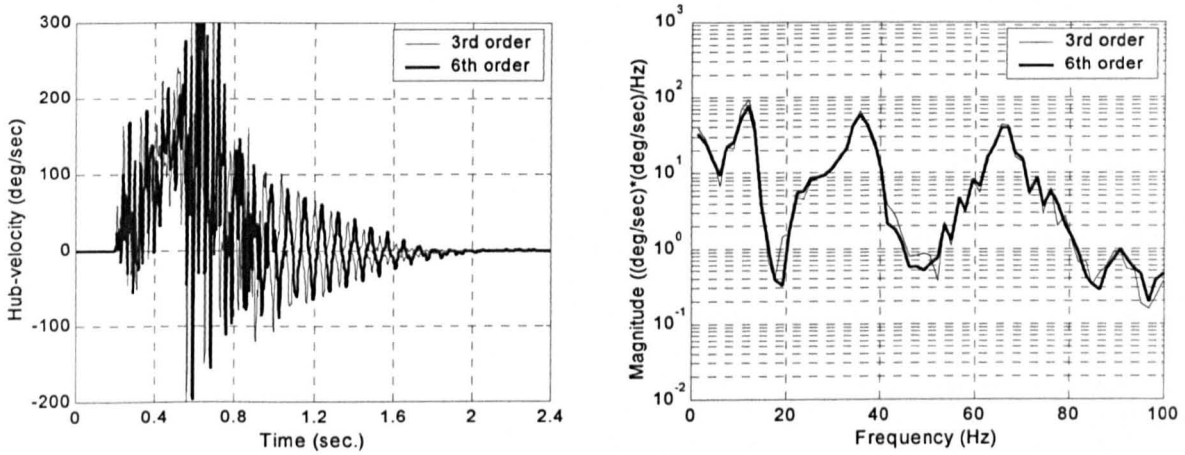

(b) Hub-velocity.

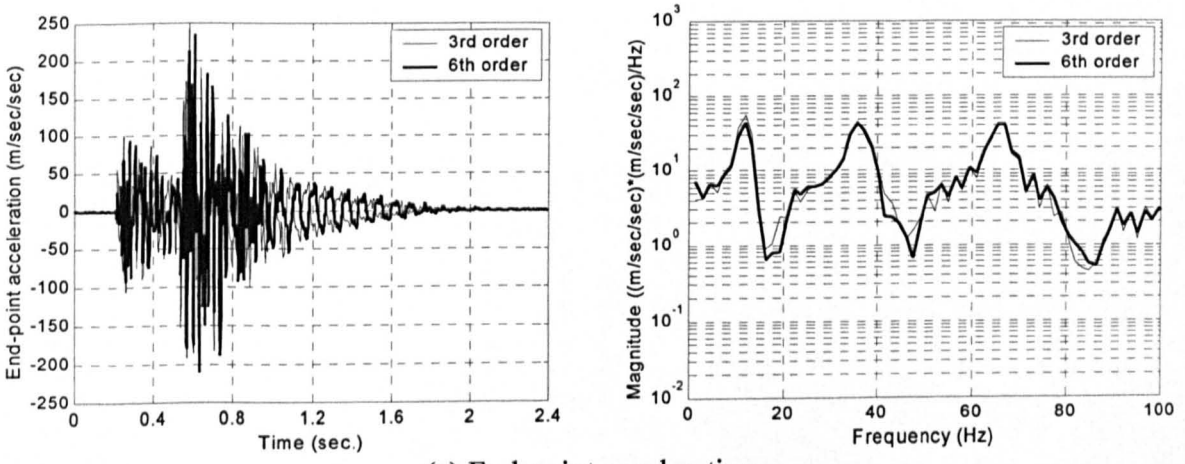

(c) End-point acceleration.

Figure 5.51: Response of the experimental rig to the band-stop filtered inputs with erroneous natural frequencies.

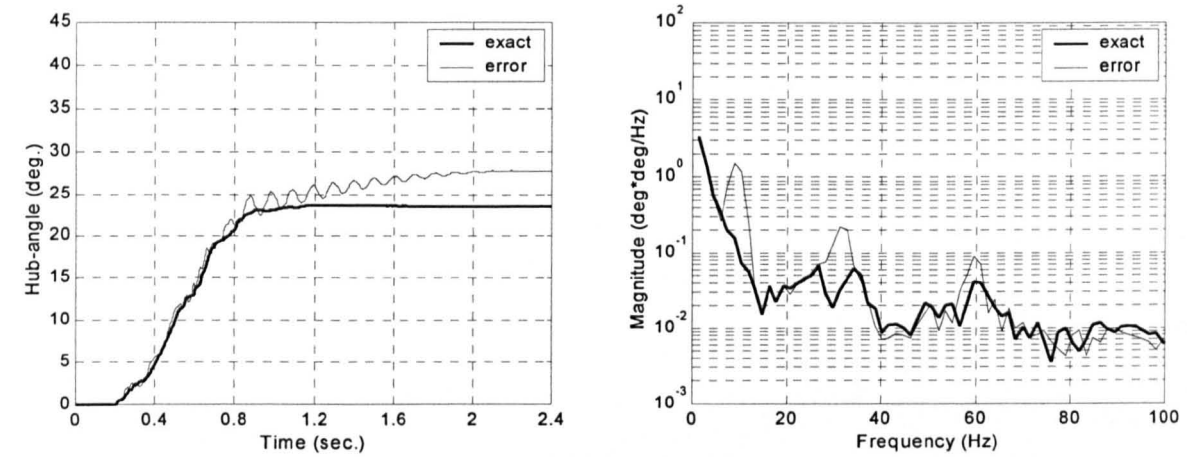

(a) Hub-angle.

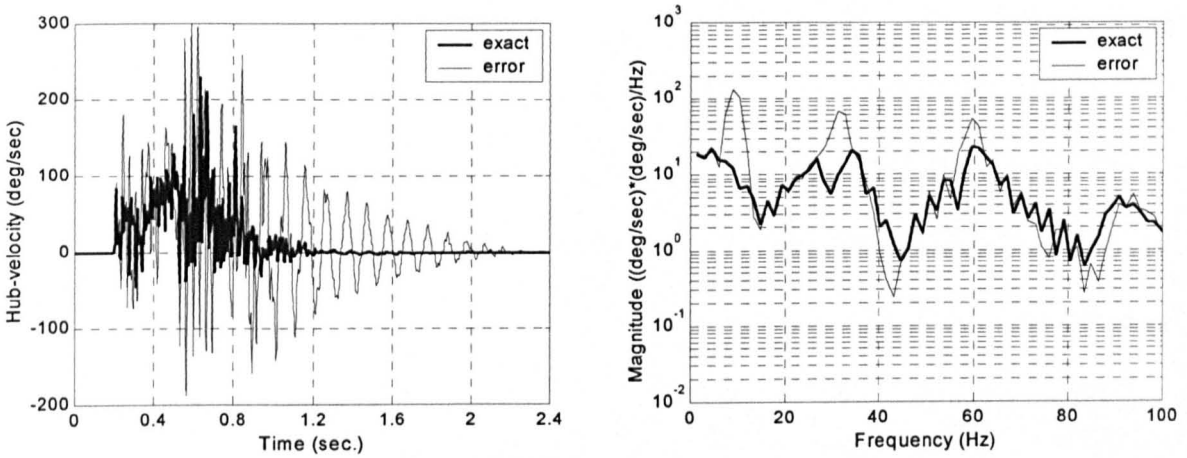

(b) Hub-velocity.

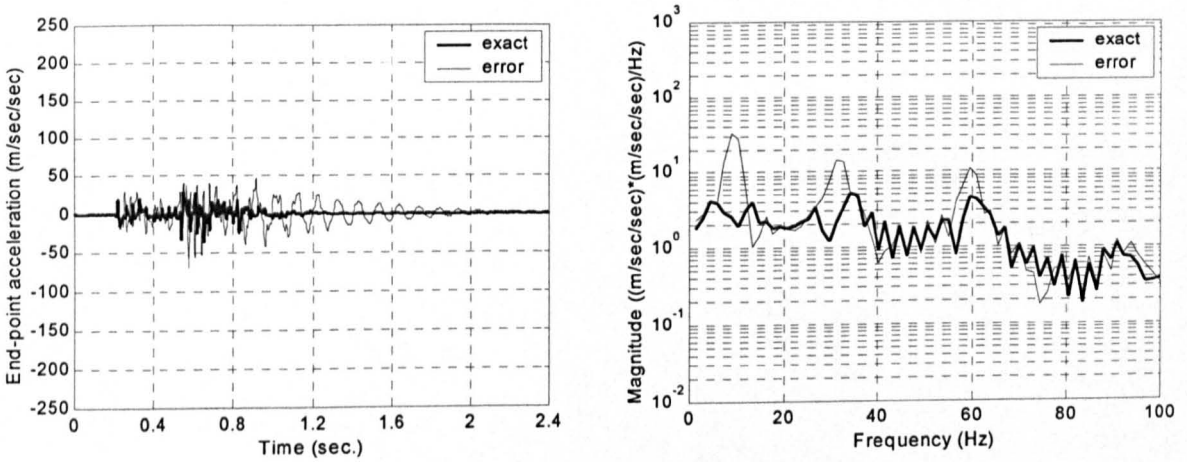

(c) End-point acceleration.

Figure 5.52: Response of the experimental rig using band-stop filtered inputs with exact and erroneous natural frequencies (with payload).

5.6. Comparative Performance Assessment

The level of vibration reduction achieved using the command shaping techniques with exact natural frequencies in comparison to the bang-bang torque input for simulation and experiment are summarised in Tables 5.2 and 5.3 respectively. In this study, the end-point deflection and end-point acceleration responses at the first three resonance modes are examined. A comparison of the simulated and experimental flexible manipulator responses and the level of reduction using the techniques reveals that the highest performance in reduction of vibration is achieved with the input shaping technique. This is further evidenced in Figures 5.53 and 5.54 that show the simulated level of vibration reduction with the end-point deflection and end-point acceleration responses at the resonance modes using input shaping with four-impulse sequence (IS), sixth-order low-pass filter (LP) and sixth order band-stop filter (BS) as compared with the unshaped input. Similarly, Figure 5.55 shows the experimental level of vibration reduction with the end-point acceleration achieved using the command shaping techniques.

It is noted that significant vibration reduction in the end-point deflection and acceleration responses was achieved using the command shaping techniques as compared with the unshaped bang-bang input. Within simulation exercises, the maximum end-point deflections were achieved as 4 mm, 15 mm and 17 mm with IS, LP and BS respectively. These demonstrated improvements between twofold and sevenfold as compared to the response with the unshaped input. Comparing the simulation results in Figures 5.11, 5.23 and 5.35, it is noted that input shaping technique provided the highest reduction in amplitude of end-point acceleration. Similar results are also noted with experiments by comparing Figures 5.44, 5.47 and 5.50. Moreover, the smoothest response was obtained with input shaping technique as shown by the oscillations in the hub-angle and hub-velocity responses. It is noted that better performance in vibration reduction of the system is achieved with the low-pass filtered input than the band-stop filtered input. This is mainly due to higher level of input energy reduction achieved with the low-pass filter, especially at the second and third vibration modes.

Table 5.2: Simulated level of vibration reduction using command shaping techniques with exact natural frequencies.

Techniques	Response	Number of impulses/filter order	Attenuation (dB)		
			Mode 1	Mode 2	Mode 3
Input shaping	End-point deflection	2	16.48	32.04	37.50
		4	50.46	82.50	83.52
	End-point acceleration	2	18.42	33.97	38.42
		4	45.46	87.96	107.96
Low-pass filter	End-point deflection	3	10.46	33.98	51.48
		6	16.48	66.02	73.98
	End-point acceleration	3	8.71	33.98	50.46
		6	15.56	67.96	100.92
Band-stop filter	End-point deflection	3	33.98	40.00	37.50
		6	40.92	47.98	50.46
	End-point acceleration	3	33.97	40.00	33.98
		6	43.52	47.96	44.44

Table 5.3: Experimental level of vibration reduction with end-point acceleration using command shaping techniques with exact natural frequencies.

Frequency	Number of impulses/filter order	Attenuation (dB)		
		Mode 1	Mode 2	Mode 3
Input shaping	2	18.06	27.96	23.52
	4	38.06	35.92	23.52
Low-pass filter	3	8.52	20.00	23.52
	6	20.00	27.96	29.54
Band-stop filter	3	21.06	17.08	12.64
	6	26.02	18.42	17.50

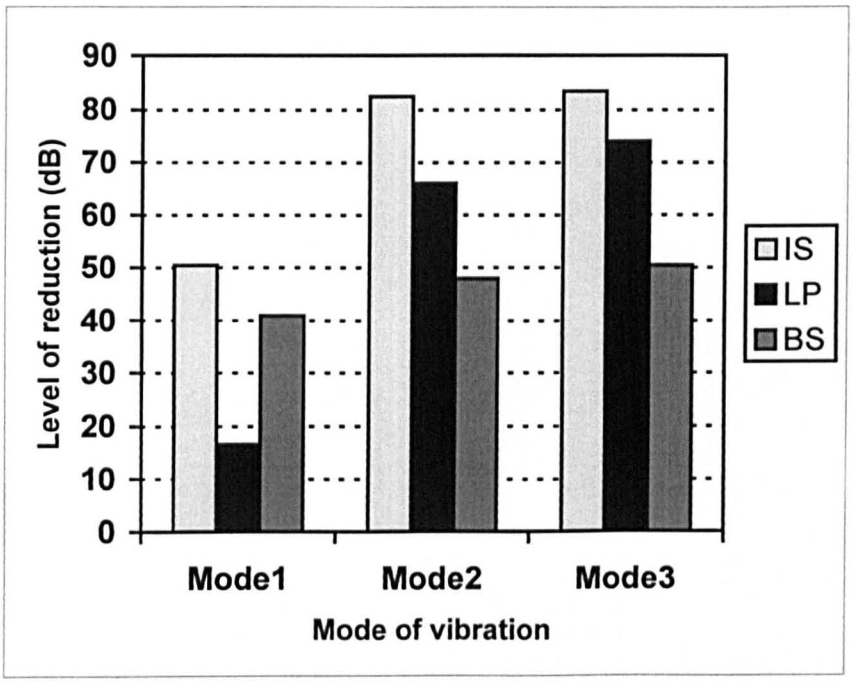

Figure 5.53: Simulated level of vibration reduction of the end-point deflection response using IS (input shaping), LP (low-pass filter) and BS (band-stop filter) with exact natural frequencies.

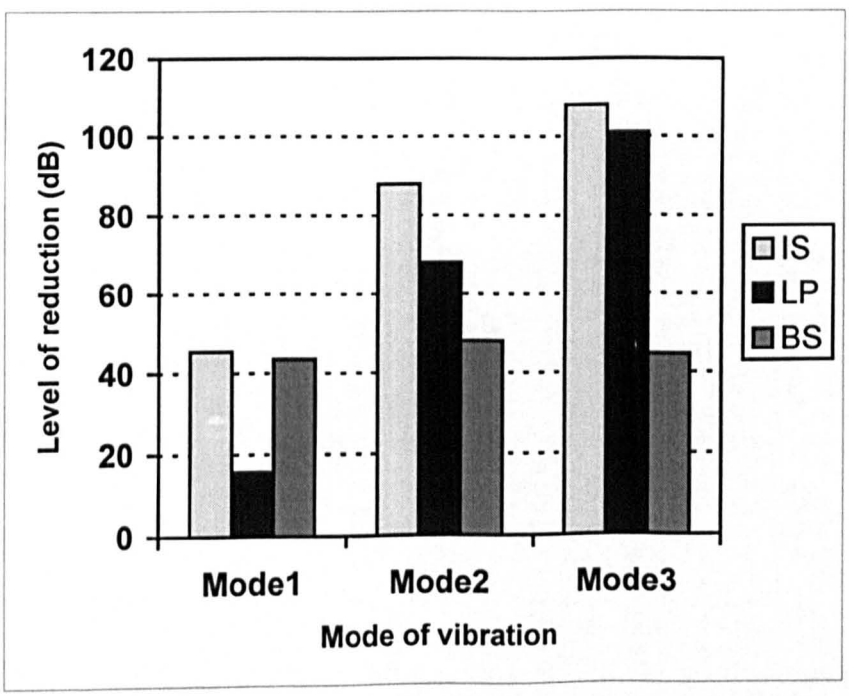

Figure 5.54: Simulated level of vibration reduction of the end-point acceleration response using IS (input shaping), LP (low-pass filter) and BS (band-stop filter) with exact natural frequencies.

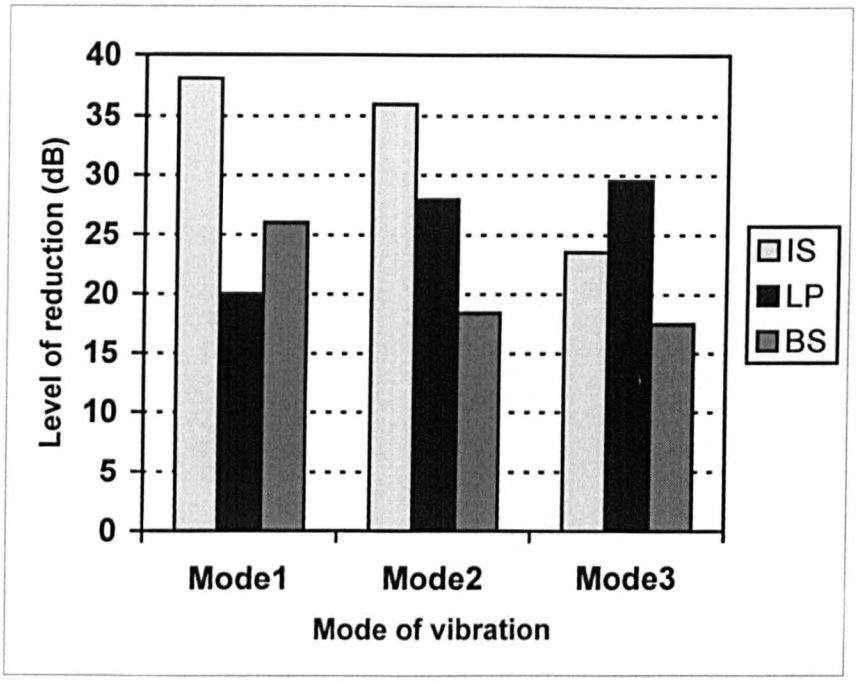

Figure 5.55: Experimental level of vibration reduction of the end-point acceleration response using IS (input shaping), LP (low-pass filter) and BS (band-stop filter) with exact natural frequencies.

Comparisons of the settling times of the simulated and experimental hub-angle responses using command shaping techniques are summarised in Table 5.4. It is noted that the differences in settling times among the techniques in both cases are negligibly small. As noted in the experimental results, significant reduction in the settling time was achieved with the command shaping techniques as compared with the unshaped input. Table 5.5 summarises the overshoot of the hub-angle response achieved using the command shaping techniques with exact and erroneous natural frequencies. With exact frequencies, it is revealed that the lowest overshoot was achieved using the input shaping technique with a four-impulse sequence.

Table 5.4: Settling times of the hub-angle response using command shaping techniques with exact natural frequencies.

Techniques	Number of impulses/filter order	Settling time (sec)	
		Simulation	Experiment
Bang-bang	-	0.788	1.555
Input shaping	2	0.820	0.844
	4	0.878	0.896
Low-pass filter	3	0.826	0.864
	6	0.858	0.894
Band-stop filter	3	0.812	0.834
	6	0.830	0.836

Table 5.5: Overshoot of the experimental hub-angle response using command shaping techniques with exact and erroneous natural frequencies.

Techniques	Number of impulses/filter order	Overshoot (%)	
		Exact	Erroneous
Bang-bang	-	2.6	2.6
Input shaping	2	0.82	2.39
	4	0.60	0.56
Low-pass filter	3	1.69	2.98
	6	0.98	2.83
Band-stop filter	3	1.27	3.91
	6	2.15	4.60

The level of vibration reduction achieved using the technique with erroneous natural frequencies in comparison to the bang-bang torque input for simulation and experimental investigations are summarised in Tables 5.6 and 5.7 respectively. A comparison of the system

responses and the level of vibration achieved using the command shaping techniques with erroneous natural frequencies reveals that the highest robustness to parameter uncertainty is achieved with the input shaping technique. It is noted with the simulation and experimental results, that the shaped input can successfully handle errors in the natural frequencies especially with higher number of impulses. In this case, significant reduction in system vibration was achieved using a four-impulse sequence as compared with other shaping techniques. This is further evidenced in Figures 5.56, 5.57 and 5.58 that show the simulated and experimental level of vibration reduction achieved at resonance modes at the end-point of the system. Using the filtered inputs, higher levels of vibration in the hub-angle, hub-velocity and end-point responses were observed. With simulation, the maximum end-point deflections of the manipulator were obtained as 7 mm, 22 mm and 26 mm using IS, LP and BS respectively. In this case, fourfold improvement was achieved with IS as compared to the unshaped input. Comparing the simulation results in Figures 5.15, 5.27 and 5.39 and the experimental results in Figures 5.45, 5.48 and 5.52, it is evidenced that the highest level of reduction in amplitude of end-point acceleration was achieved with input shaping. The settling times achieved with erroneous natural frequencies are summarised in Table 5.8. With the four-impulse sequence, the experimental settling time increased to 50% of the settling time of the unshaped input whereas settling times of 80-95% of the unshaped input were achieved using the filtering techniques. Moreover as shown in Table 5.5, the overshoot of the hub-angle response with input shaping was not affected with the error. On the other hand, higher overshoots than the unshaped input were obtained using low-pass and band-stop filtered inputs. It is noted that the input shaping technique is more robust, as significant reduction was achieved at the first mode of vibration, which is the most dominant mode. The band-stop filtered input did not handle the error well as only small amount of reduction of the system vibration was achieved. On the other hand, using the low-pass filter, a significant amount of attenuation of the system vibration was achieved at the second and third resonance modes.

Table 5.6: Simulated level of vibration reduction using the command shaping techniques with erroneous natural frequencies.

Techniques	Response	Number of impulses/filter order	Attenuation (dB)		
			Mode 1	Mode 2	Mode 3
Input shaping	End-point deflection	2	13.98	13.97	12.62
		4	30.45	26.02	43.52
	End-point acceleration	2	11.48	13.98	12.04
		4	31.48	26.02	43.10
Low-pass filter	End-point deflection	3	5.19	26.94	43.52
		6	6.02	53.98	66.02
	End-point acceleration	3	3.52	26.02	43.1
		6	6.62	51.48	90.46
Band-stop filter	End-point deflection	3	6.02	0	0
		6	6.02	0	0
	End-point acceleration	3	6.62	0	0
		6	6.62	0	0

Table 5.7: Experimental level of vibration reduction with end-point acceleration using command shaping techniques with erroneous natural frequencies.

Frequency	Number of impulses/filter order	Attenuation (dB)		
		Mode 1	Mode 2	Mode 3
Input shaping	2	8.52	15.92	9.54
	4	26.02	26.02	26.02
Low-pass filter	3	4.08	17.08	21.58
	6	8.52	21.94	23.52
Band-stop filter	3	2.50	0	0
	6	6.02	1.94	0

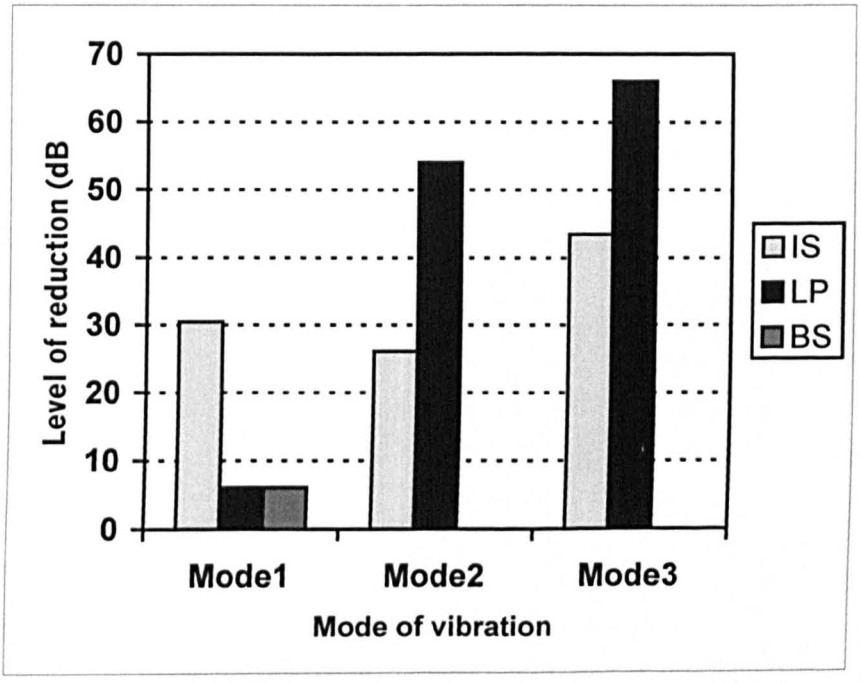

Figure 5.56: Simulated level of vibration reduction of the end-point deflection response using IS (input shaping), LP (low-pass filter) and BS (band-stop filter) with erroneous natural frequencies.

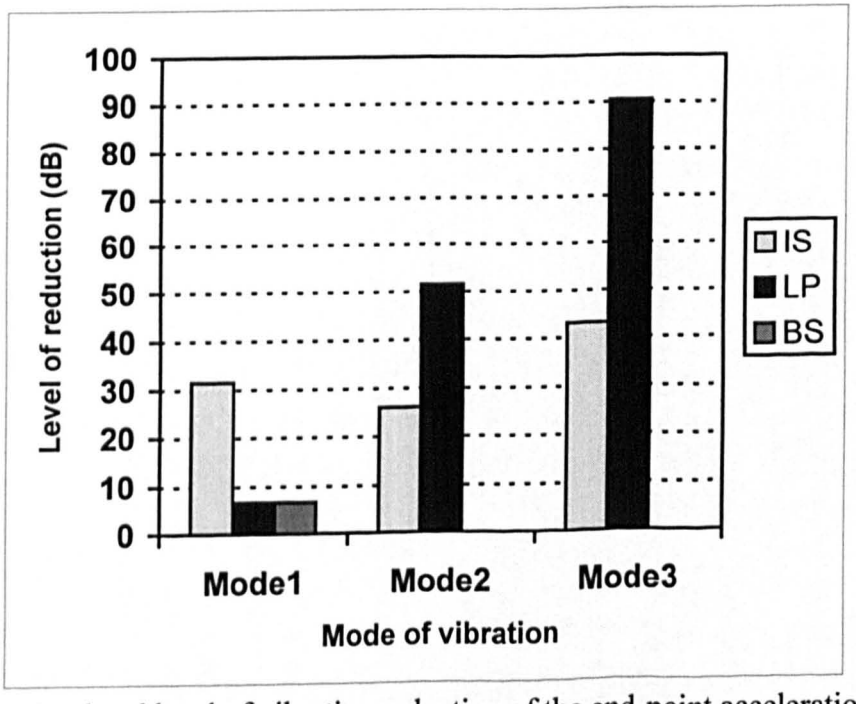

Figure 5.57: Simulated level of vibration reduction of the end-point acceleration response using IS (input shaping), LP (low-pass filter) and BS (band-stop filter) with erroneous natural frequencies.

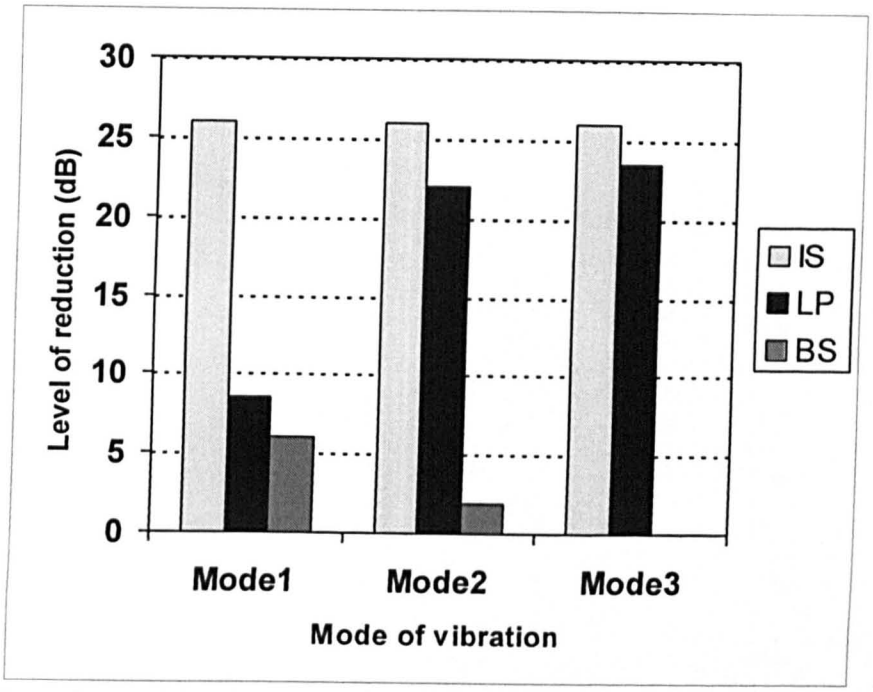

Figure 5.58: Experimental level of vibration reduction of the end-point acceleration response using IS (input shaping), LP (low-pass filter) and BS (band-stop filter) with erroneous natural frequencies.

Table 5.8: Settling times of the hub-angle response using four-impulse sequences, sixth-order low-pass and band-stop filters with erroneous frequencies.

Techniques	Settling time (sec)	
	Simulation	Experiment
Bang-bang	0.788	1.555
Input shaping	0.860	0.882
Low-pass filter	0.846	1.268
Band-stop filter	0.82	1.474

A comparison of the simulation and experimental results using the command shaping techniques reveals that input shaping can successfully handle vibrations in the presence of payload in the system. With exact and erroneous natural frequencies, vibrations in the hub-

angle, hub-velocity, end-point deflection and end-point acceleration were significantly suppressed. On the other hand, considerable reduction in vibration of the system was achieved using filtered inputs with exact frequencies. However, the filtered inputs are unable to suppress vibration in the presence of payload with error in natural frequencies. Figures 5.59 and 5.60 show the simulated level of vibration reduction of the system incorporating a payload with exact (IS1, LP1, BS1) and erroneous (IS2, LP2, BS2) frequencies at the end-point deflection and end-point acceleration responses respectively. Similarly, Figure 5.61 shows the experimental level of vibration reduction of the system at the end-point acceleration response with a payload. Similar to the case without payload, the input shaping technique provides the highest level of vibration reduction and robustness. The simulated and experimental settling times achieved using the shaping techniques for the manipulator incorporating a payload are shown in Figures 5.62 and 5.63 respectively. Using the shaped inputs with exact and erroneous natural frequencies, significant reduction in settling times was achieved. However, as shown with experimental results using the filtered inputs with erroneous natural frequencies, the settling time increased to 90%-100% of the unshaped input case. With input shaping, although the requirement to achieve the same steady-state hub-angle response level as the unshaped input was fulfilled, experimental results showed a steady-state error of 5 degrees in the hub-angle response. Further experimental investigations showed that with higher levels of vibration, the experimental rig moves to a higher angle. This might be due to the effects of payload rotary inertia. In this case, to ensure the same steady-state level as the unshaped input, a feedback controller is required. However, no steady-state error occurred in the simulation.

A comparison of the simulation and experimental results of the response of the system to the shaped and filtered inputs shows that a close agreement between the two was achieved. In both cases, input shaping was shown to result in the highest level of vibration reduction and robustness. Moreover, input shaping can successfully handle system vibrations with inclusion of payload. Hence the command shaping algorithms can be utilised for development and assessment of feedforward control techniques for vibration control of flexible manipulators.

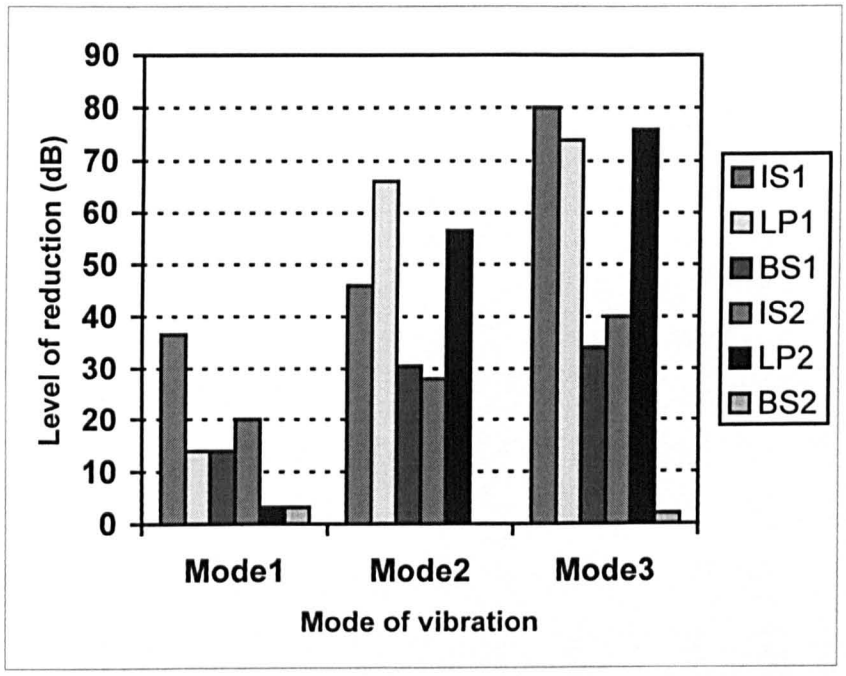

Figure 5.59: Simulated level of vibration reduction with the end-point deflection of the system incorporating a payload using IS1 (input shaping - exact), LP1 (low-pass filter – exact), BS1 (band-stop filter – exact), IS2 (input shaping – error), LP2 (low-pass filter – error) and BS2 (band-stop filter – error).

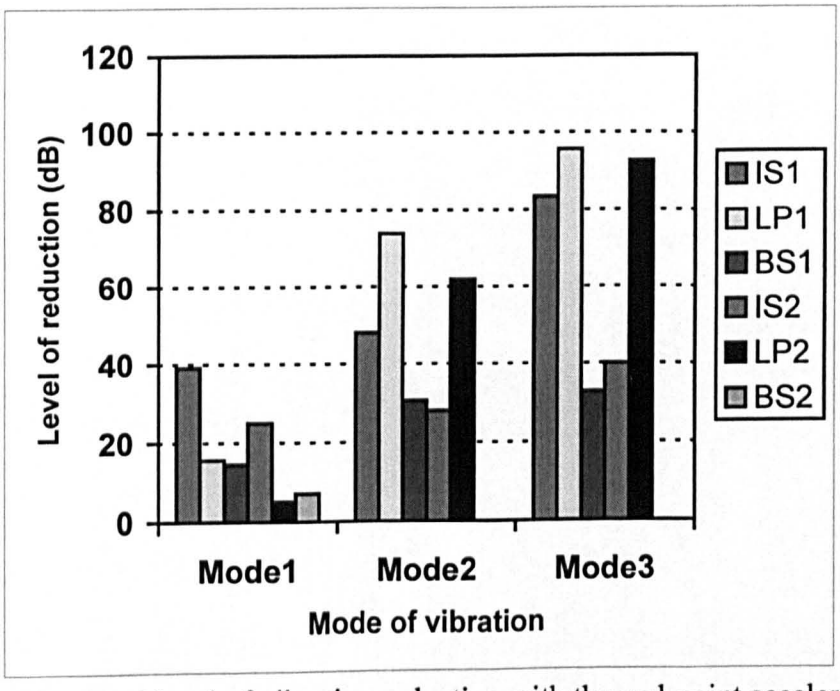

Figure 5.60: Simulated level of vibration reduction with the end-point acceleration of the system incorporating a payload using IS1 (input shaping - exact), LP1 (low-pass filter – exact), BS1 (band-stop filter – exact), IS2 (input shaping – error), LP2 (low-pass filter – error) and BS2 (band-stop filter – error).

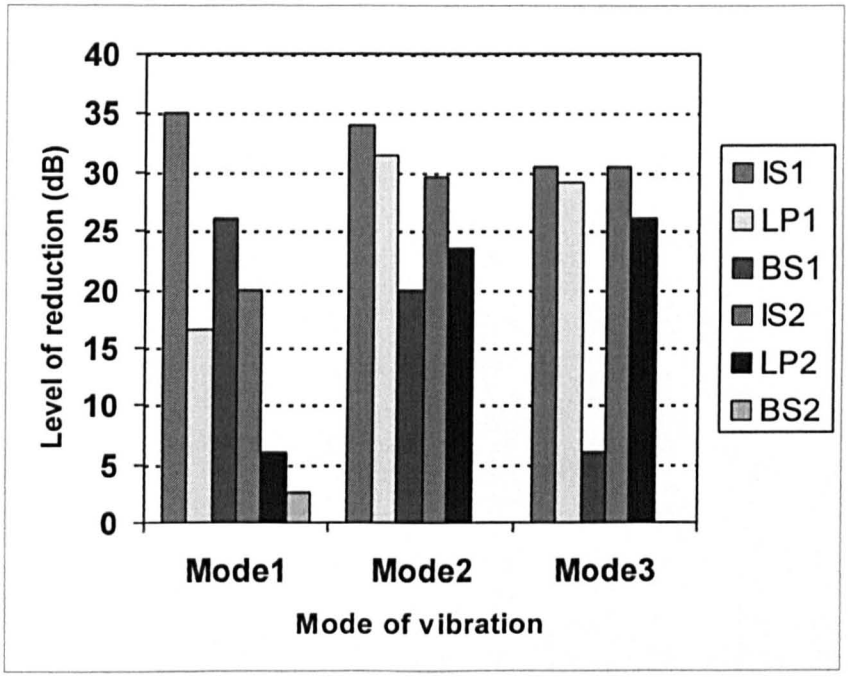

Figure 5.61: Experimental result of level of vibration reduction with the end-point acceleration response of the system incorporating a payload using IS1 (input shaping - exact), LP1 (low-pass filter – exact), BS1 (band-stop filter – exact), IS2 (input shaping – error), LP2 (low-pass filter – error) and BS2 (band-stop filter – error).

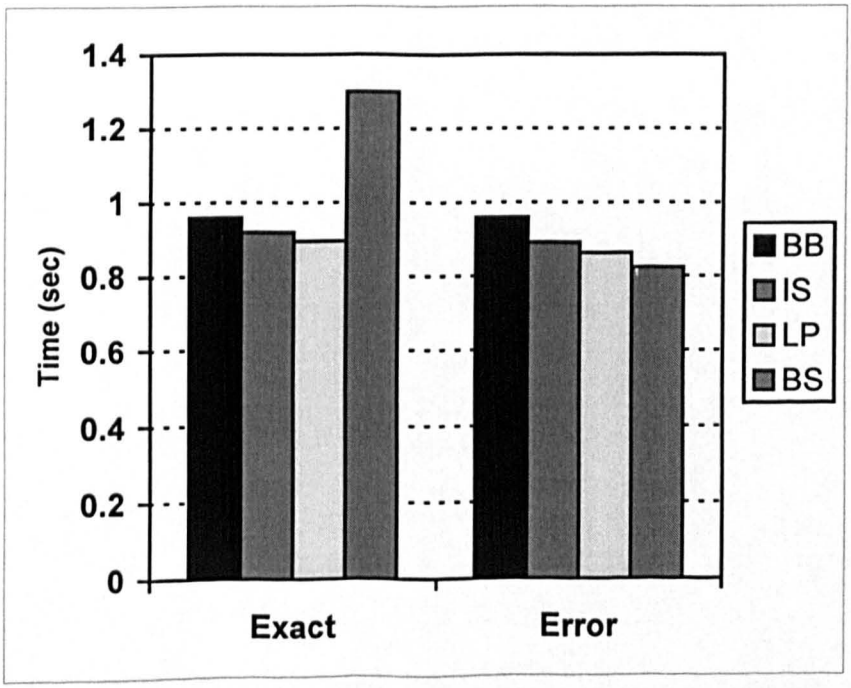

Figure 5.62: Simulated settling times of the hub-angle response of the system incorporating a payload using BB (bang-bang), IS (input shaping), LP (low-pass filter) and BS (band-stop filter).

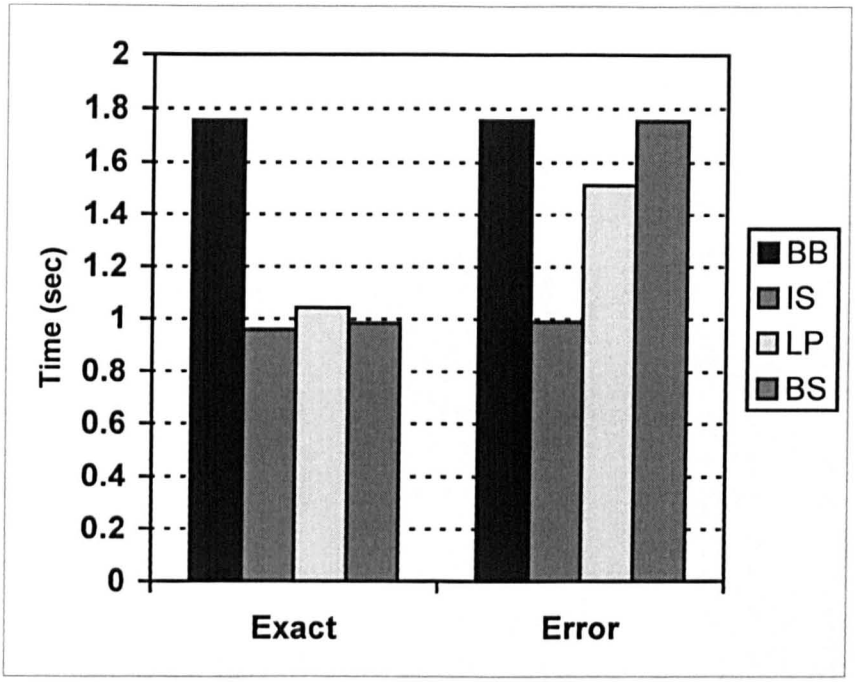

Figure 5.63: Experimental settling time of the hub-angle response of the system incorporating a payload using BB (bang-bang), IS (input shaping), LP (low-pass filter) and BS (band-stop filter).

To study the processing times of the input shaping and filtering techniques, the execution times to develop the inputs were calculated. Within the Matlab environment, the execution times for input shaping, low-pass filter and band-stop filter were obtained as 330 msec, 110 msec and 130 msec respectively. This shows that development of the low-pass filtered input requires the lowest processing time. The longest processing time required for the input shaping technique is due to the convolution that has to be performed in this process. This information is vital for consideration in designing and implementing such controllers in real-time.

5.7. Summary

Simulation and experimental investigations into the development of feedforward control strategies for vibration control of a flexible manipulator using input shaping, low-pass and band-stop filtered input techniques have been presented. The system response to the unshaped bang-bang torque input has been used to determine the parameters of the system for design and evaluation of the control strategies. Performances of the techniques have been evaluated in terms of level of vibration reduction, time response specifications, robustness

and processing times. The impact of using higher number of impulses and filter orders on the system performance has also been investigated. Significant reduction in the system vibration has been achieved with these control strategies. For the flexible manipulator and the specifications used in designing the input shapers and filters, the input shaping technique has been demonstrated to provide the best performance in vibration reduction and time response, especially in terms of robustness to errors. Moreover, vibration in the presence of payload in the system can successfully be suppressed using this technique. The low-pass filtered input has been shown to perform better than the band-stop filtered input. However, the processing time in developing an input shaping command is longer as compared to that required for the filtered inputs.

Chapter 6

Hybrid Control Schemes for Input Tracking and Vibration Control

6.1. Introduction

In the previous chapter, feedforward control strategies using command shaping techniques have been developed and investigated for vibration control of the flexible manipulator. Significant reduction in the vibration of the system has been demonstrated with these techniques. However, input tracking capabilities of the system are unsatisfactory especially in the presence of variations in the payload. In this case, the hub-angle response moves to different locations with various payloads. Moreover, the command shaping techniques are not robust to parameter changes and disturbances in the system. In order to overcome this problem, a controller that provides acceptable input tracking capability and low system vibration has to be developed.

An acceptable system performance with reduced vibration that accounts for system changes can be achieved by developing a hybrid control scheme that caters for rigid body motion and vibration of the system independently. This can be realised by utilising strategies consisting of either non-collocated control with collocated feedback controller or feedforward control with collocated feedback controller. In both cases, the former can be used for vibration suppression and the latter for input tracking of a flexible manipulator. Practically, a combination of the control techniques would position the end-point of the flexible manipulator from one point to another with reduced vibration. Both feedforward and feedback control structures have been utilised in the control of flexible manipulator systems. A hybrid collocated and non-collocated controller has previously been proposed for control of a flexible manipulator (Tokhi and Azad, 1996). The controller design utilises end-point acceleration feedback through a proportional-integral-derivative (PID) control scheme and a proportional-derivative (PD) configuration for control of rigid body motion. Experimental investigations have shown that the control structure gives a satisfactory system response with

significant vibration reduction as compared to the response with a collocated controller. A PD feedback control with a feedforward control to regulate the position of a flexible manipulator has been proposed by Shchuka and Goldenberg (1989). Simulation results have shown that although the pole-zero cancellation property of the feedforward control speeds up the system response, it increases overshoot and oscillation. A control law partitioning scheme which uses end-point sensing device has been reported by Rattan et al. (1990). The scheme uses end-point position signal in an outer loop controller to control the flexible modes, whereas the inner loop controls the rigid body motion independent of the flexible dynamics of the manipulator. Performance of the scheme has been demonstrated in both simulation and experimental trials incorporating the first two flexible modes. A combined feedforward and feedback method in which the end-point position is sensed by an accelerometer and fed back to the motor controller, operating as a velocity servo, has been proposed for the control of a flexible manipulator system (Wells and Schueller, 1990). This method uses a single mass-spring-damper system to represent the manipulator and thus the technique is not suitable for high speed operation.

This chapter presents investigations into the development of hybrid control schemes for input tracking and end-point vibration suppression of a flexible manipulator system. In these investigations, the FE simulation environment of the flexible manipulator presented in Chapter 3 is utilised for development and evaluation of performance of the control strategies. Hybrid control schemes based on feedforward with collocated feedback controllers and non-collocated with collocated feedback controllers are investigated. Initially, a fixed joint-based collocated PD controller utilising hub-angle and hub-velocity feedback is developed for control of rigid body motion. This is then extended to incorporate non-collocated and feedforward controllers for vibration suppression of the manipulator. For non-collocated control, end-point deflection feedback through a PID control configuration is developed whereas the input shaping technique is utilised in the feedforward scheme. As the PD controller can only provide optimum response for a certain loading condition, a collocated adaptive control is then proposed for rigid body motion control. Further, a hybrid control scheme based on a combined collocated adaptive control and feedforward controller is developed for input tracking and vibration suppression of the system. Simulation results of the response of the manipulator with the controllers are presented in time and frequency domains. The performances of the hybrid control schemes are assessed in terms of input tracking and level of vibration reduction in comparison with the response without vibration

control. To examine the robustness of the controllers, the control schemes are simulated with different loading conditions.

6.2. Hybrid PD Control Schemes

In this section, a collocated PD control is designed for control of rigid body motion of the flexible manipulator system. Then a non-collocated PID control and feedforward control based on input shaping are incorporated into the closed-loop system for vibration suppression of the system. The FE model with ten elements is utilised. This is acceptable, as the results with ten elements presented in Chapter 3 demonstrated a reasonably well representation of the flexible manipulator. Moreover, results of the response of the flexible manipulator with the PD controller and hybrid schemes are presented. Lastly, comparative assessment of the performance of both hybrid control schemes is studied.

6.2.1. Collocated PD Control

To demonstrate the performance of the hybrid control schemes, a PD feedback of collocated sensor signals is adopted for control of rigid body motion of the manipulator. A block diagram of the PD controller is shown in Figure 6.1, where K_p and K_v are the proportional and derivative gains respectively, θ represents hub-angle, $\dot{\theta}$ represents hub-velocity and r is the reference hub-angle. This control scheme has previously been tested on the experimental rig (Tokhi and Azad, 1996). Essentially, the task of this controller is to position the flexible arm to the specified angle of demand. The hub-angle and hub-velocity signals are fed back and used to control the hub-angle of the manipulator.

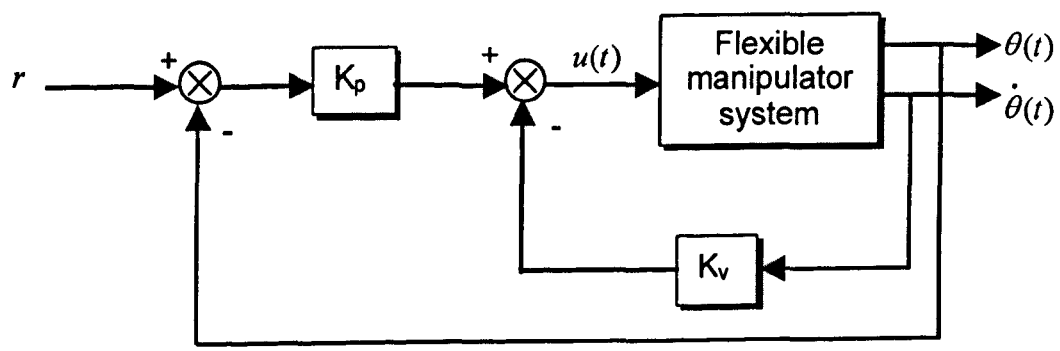

Figure 6.1: The collocated PD control structure.

The control signal $U(s)$ in Figure 6.1 can thus be obtained as

$$U(s) = K_p\{R(s) - \theta(s)\} - K_v\dot{\theta} \tag{6.1}$$

where s is the Laplace variable. Hence the closed-loop transfer function is obtained as

$$\frac{\theta(s)}{R(s)} = \frac{K_p G_2(s)}{1 + K_v(s + \frac{K_p}{K_v})G_2(s)} \tag{6.2}$$

where $G_2(s)$ is the open-loop transfer function from the input torque to the hub-angle given by

$$G_2(s) = C(sI_d - A)^{-1}B \tag{6.3}$$

A and B are the state-space matrices introduced in Chapter 3 and $C = [1 \quad 0 \quad ..... \quad 0]$. With ten elements, the sizes of matrices A, B and C are 42×42, 42×1 and 1×42 respectively. Thus, the closed-loop poles of the system are given by the characteristic equation as

$$1 + K_v(s + Z)G_2(s) = 0 \tag{6.4}$$

where $Z = K_p/K_v$ represents the compensator zero which determines the control performance of the closed-loop system. In this study, the root locus approach is utilised to design the PD controller. Analyses of the root locus plot of the system shows that dominant poles with maximum negative real parts could be achieved with $Z \approx 2$ and by setting K_p between 0 and 1.2 (Azad, 1994).

6.2.2. Hybrid Collocated PD and Non-collocated Control

A hybrid collocated and non-collocated control scheme for control of rigid body motion and vibration suppression of the system is presented in this section. The use of a non-collocated control system, where the end-point of the manipulator is controlled by measuring its position can be applied to improve the overall performance, as more reliable output measurement is

obtained. The control structure comprises two feedback loops: (1) The hub-angle and hub-velocity as inputs to a collocated control law for rigid body motion control. (2) The end-point deflection as input to a separate non-collocated control law for vibration control. These two loops are then summed together to give a torque input to the system. A block diagram of the control structure is shown in Figure 6.2 (Tokhi and Azad, 1996). r_α represents end-point deflection reference input, which is set to zero as the control objective is to have zero vibration during movement of the manipulator.

For rigid body motion control, the PD control strategy developed in the previous section is adopted whereas for the vibration control loop, the end-point deflection feedback through a PID control scheme is utilised. For the two control loops to work well they have to be decoupled from one another. This can be achieved by using a high-pass filter in the non-collocated control loop as shown in Figure 6.2.

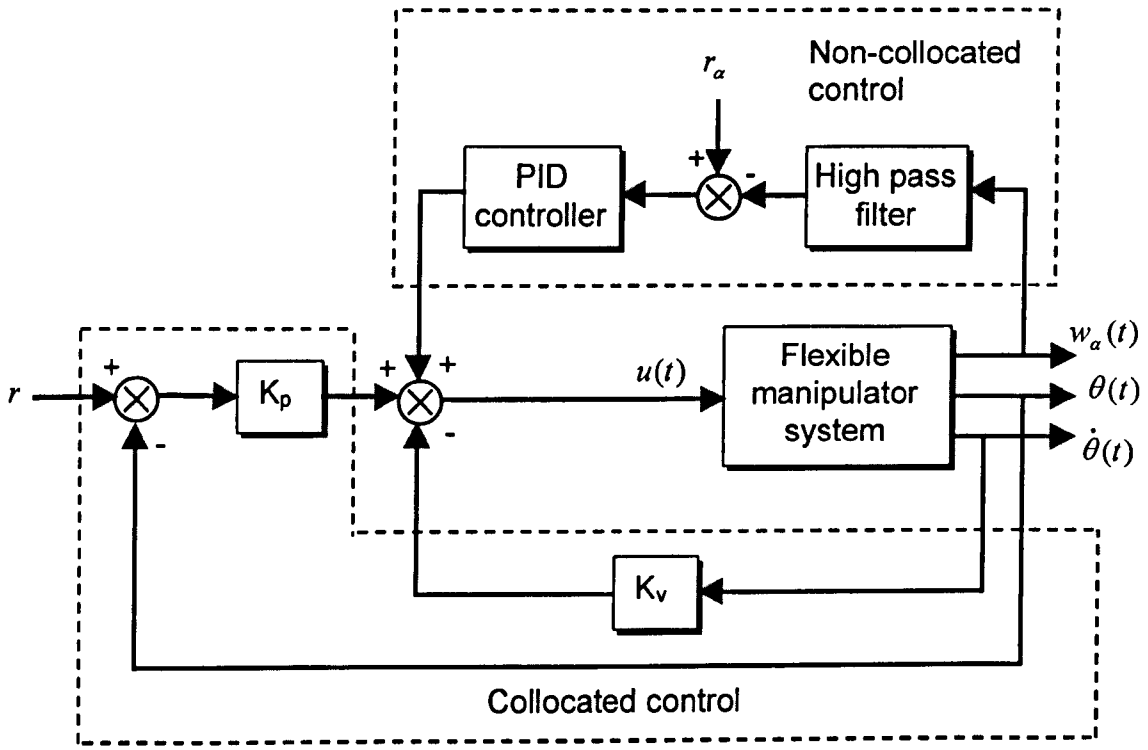

Figure 6.2: The collocated PD and non-collocated PID control structure.

6.2.3. Hybrid Collocated PD and Feedforward Control

A hybrid control structure for control of rigid body motion and vibration suppression of the flexible manipulator based on a collocated PD and feedforward control is proposed in this section. In this study, the feedforward control scheme is developed using an input shaping

technique with a four-impulse sequence. Basic theory and formulation of the input shaping technique was provided in Chapter 5. Simulation and experimental studies with the flexible manipulator showed that significant vibration reduction and robustness is achieved using a four-impulse sequence. It was demonstrated that the input shaping technique can handle up to 30% error tolerance in the vibration frequencies of the system. A block diagram of the hybrid control structure is shown in Figure 6.3.

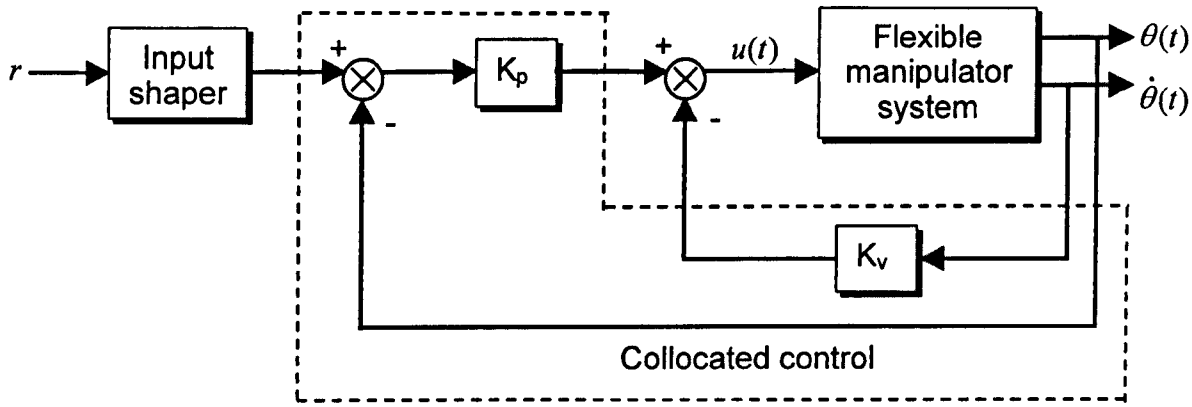

Figure 6.3: The collocated PD and feedforward control structure.

6.2.4. Implementation and Results

The proposed control schemes are implemented and tested within the simulation environment of the flexible manipulator and the corresponding results are presented in this section. The manipulator is required to follow a trajectory within the range of ± 80 degrees as shown in Figure 6.4. Four system responses namely the hub-angle, hub-velocity, end-point deflection and end-point acceleration are observed. To investigate the vibration of the system in the frequency domain, PSDs of the responses at the end-point are obtained. The performances of the hybrid controllers are assessed in terms of input tracking and vibration suppression in comparison to PD control. To investigate the performance of the controller in handling different loading conditions, the closed-loop control systems were simulated without and with a payload of 50 grams.

6.2.4.1. Collocated PD Control

For this investigation, the values of K_p and K_v were deduced as 0.64 and 0.32 respectively, using the approach given in Tokhi and Azad (1996). The required torque input driving the

manipulator without payload with the collocated PD control is shown in Figure 6.5. The corresponding system response and PSD are shown in Figure 6.6. It is noted that the manipulator reaches the required position from +80 degrees to –80 degrees within two seconds with no significant overshoot. A smooth hub-velocity profile is observed with a maximum speed of 120 deg/sec, achieved within 0.6 sec. However, a noticeable amount of vibration occurs during movement of the manipulator. It is noted from the end-point deflection and end-point acceleration that the vibration of the system settles within 4 sec with maximum deflection and acceleration of ±10 mm and ±190 m/sec^2 respectively. Moreover, from the PSDs of the end-point responses, the vibrations at the end-point are dominated by the first three vibration modes which are obtained as 12 Hz, 35 Hz and 65 Hz. Similarly, Figures 6.7 and 6.8 show the resulting torque input and corresponding response of the manipulator with a payload of 50 grams with the collocated PD control. It is noted that the performance of the system is unsatisfactory as significant overshoot occurs during movement of the manipulator. Moreover, the torque input and hub-velocity profiles are not as smooth as the profiles without payload. It is noted that the magnitude of vibration at the end-point reduces as compared with the vibration without payload. However, it requires more than 4 sec to settle down. It is evidenced from the PSDs of the responses at end-point, that the vibration frequencies of the closed-loop system shift to lower frequencies with increasing payloads. These are obtained as 10 Hz, 31 Hz and 58 Hz. The closed-loop parameters with the PD control will subsequently be used to design and evaluate the performance of non-collocated and feedforward control schemes.

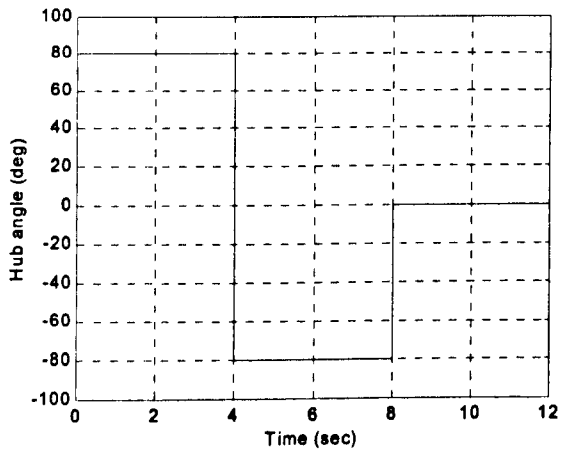

Figure 6.4: The reference hub-angle.

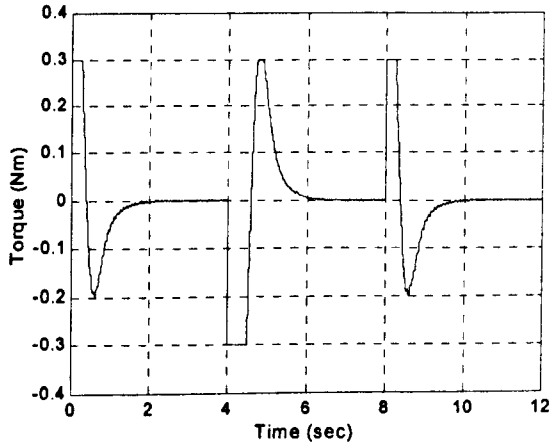

Figure 6.5: Torque input with the collocated PD control (0 gram).

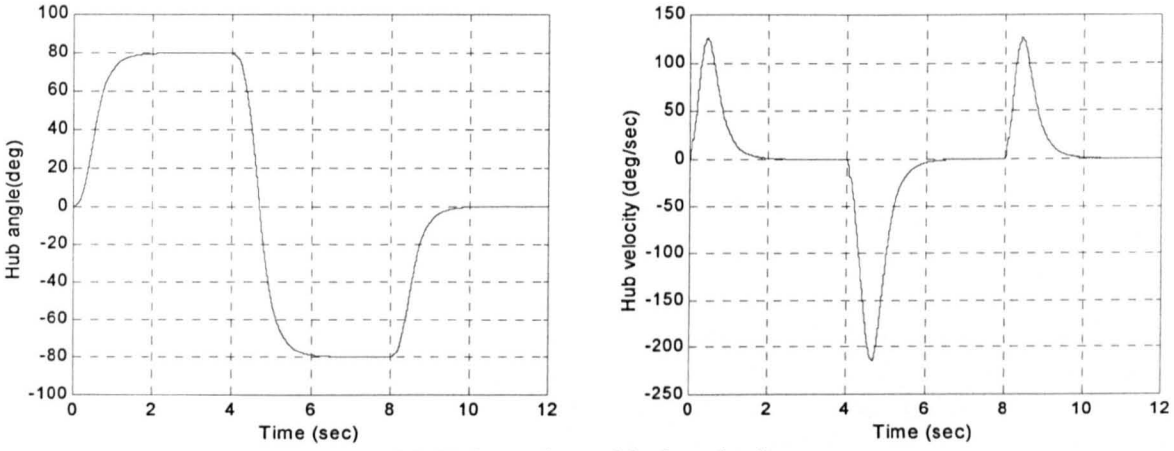

(a) Hub-angle and hub-velocity.

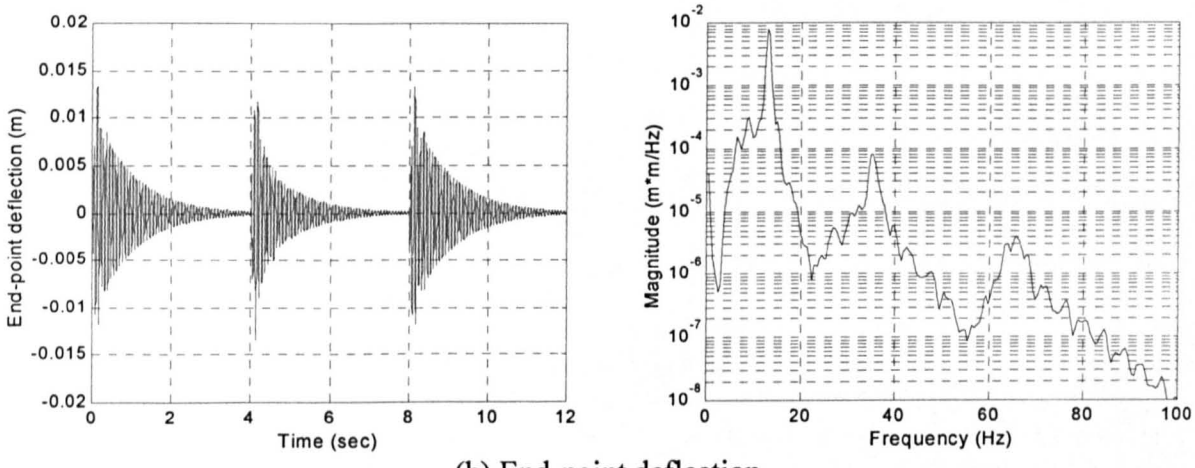

(b) End-point deflection.

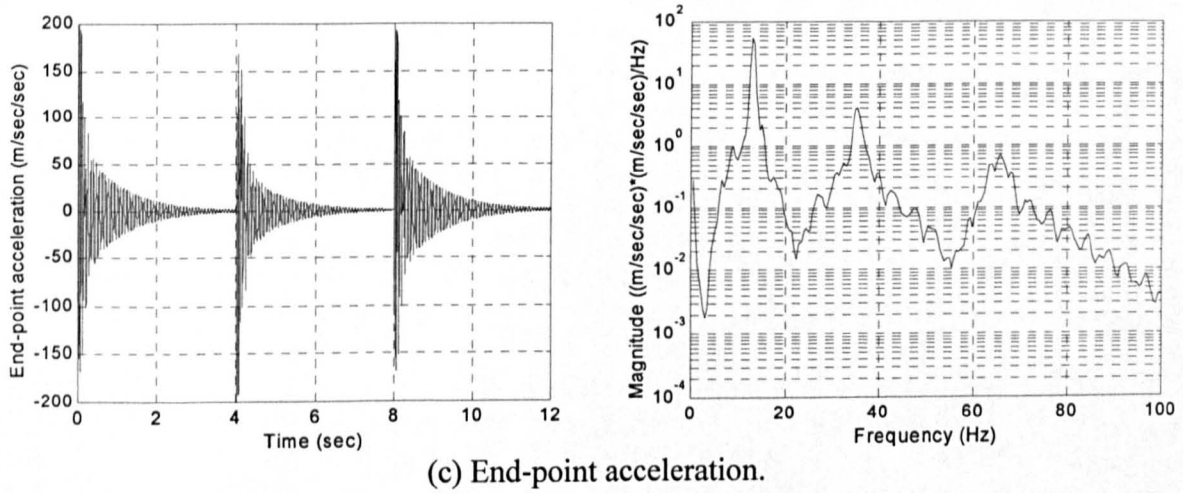

(c) End-point acceleration.

Figure 6.6: Response of the manipulator with the collocated PD control (0 gram).

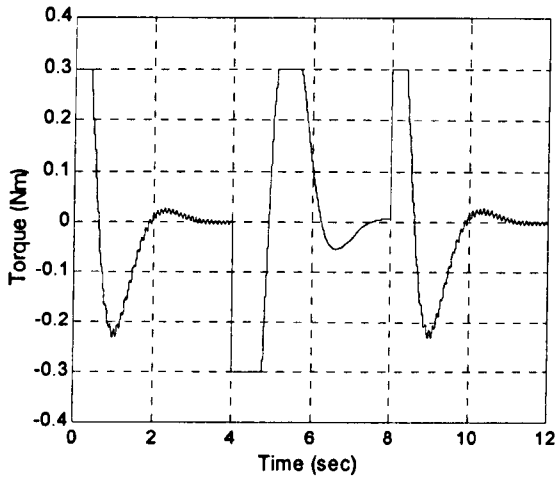

Figure 6.7: Torque input with the collocated PD control (50 grams).

6.2.4.2. Hybrid Control

In the collocated and non-collocated control scheme of PD-PID (PDPID), the PID controller parameters were tuned using the Ziegler-Nichols method, where the proportional gain K_p was initially tuned and the integral gain K_i and derivative gain K_d were then calculated (Warwick, 1989). Accordingly, the PID parameters K_p, K_i and K_d were deduced as 0.1, 70 and 0.01 respectively. To decouple the end-point measurement from the rigid body motion of the manipulator, a fourth-order IIR Butterworth high-pass filter was utilised. In this investigation, a high-pass filter with cut-off frequency of 5 Hz was designed as the first vibration mode of the system with a payload was obtained as 10 Hz.

In the case of hybrid collocated and feedforward control scheme (PDIS), an input shaper was designed based on the dynamic behaviour of the closed-loop system exhibited with the PD control. As demonstrated in the previous section, the natural frequencies of the manipulator were 12 Hz, 35 Hz and 65 Hz without payload and 10 Hz, 31 Hz and 58 Hz with 50 grams payload. As in Chapter 3, the damping ratios for the first three modes of the flexible manipulator were deduced as 0.026, 0.038 and 0.04 respectively. The magnitudes and time locations of the impulses were obtained by solving equation (5.8) for the first three modes. Similar to the analysis carried out in the previous chapter, for digital implementation of the input shaper, locations of the impulses were selected at the nearest sampling time. The developed input shaper was then used to pre-process the input reference shown in Figure 6.4.

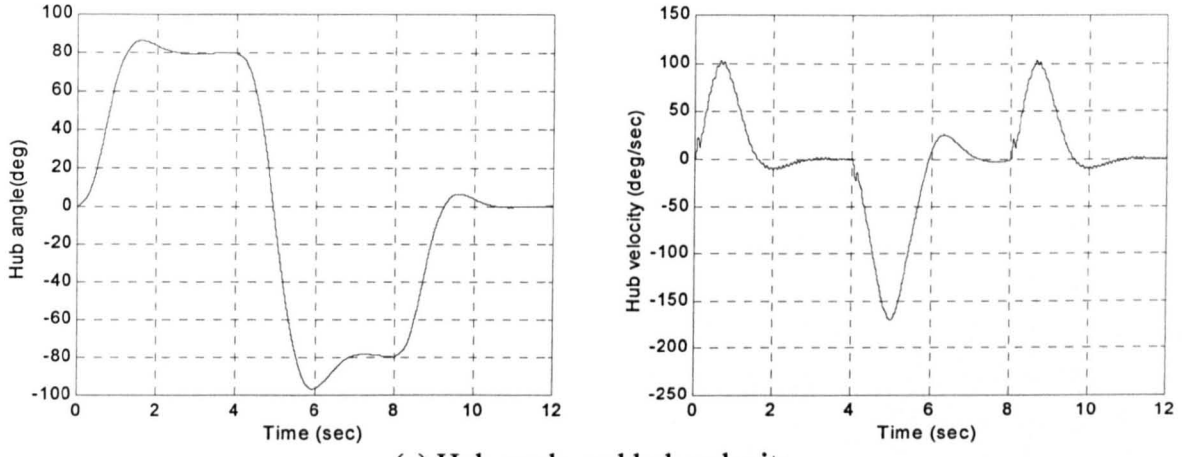

(a) Hub-angle and hub-velocity.

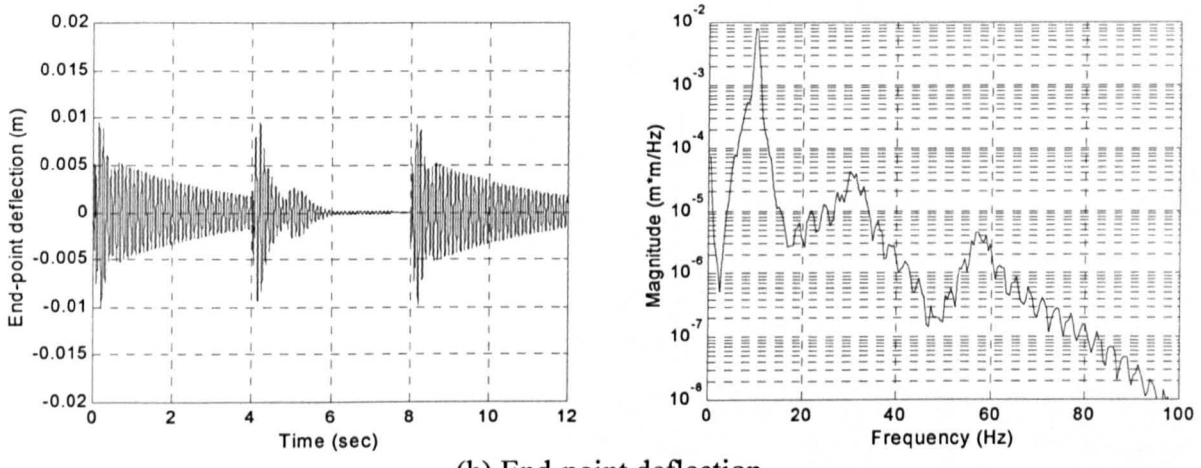

(b) End-point deflection.

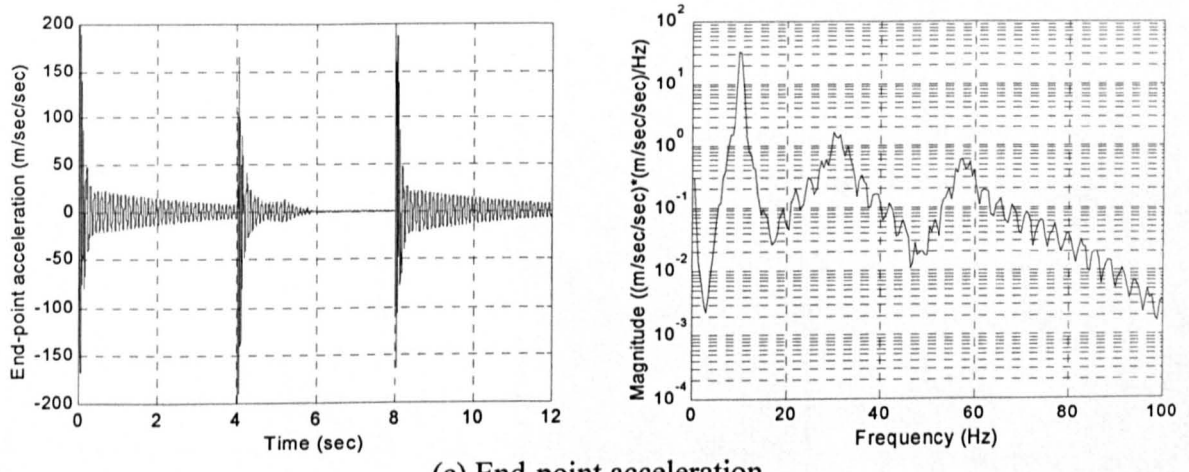

(c) End-point acceleration.

Figure 6.8: Response of the manipulator with the collocated PD control (50 grams).

Figure 6.9 shows the resulting torque input driving the manipulator without payload with PDPID and PDIS control. The corresponding responses and PSDs of the manipulator are shown in Figure 6.10. It is noted that the proposed hybrid controllers are capable of reducing the system vibration while maintaining the input tracking performance of the manipulator. The hub-angle and hub-velocity responses observed were similar to those with the PD controller. Moreover, as demonstrated in the hub-angle responses with PDPID and PDIS control, the minimum phase behaviour of the manipulator is unaffected. A significant amount of vibration reduction was achieved at the end-point of the manipulator with both control schemes. With PDPID control, the vibration of the end-point deflection and acceleration of the system settled within 2 sec, which is twofold improvement as compared to the PD control. With the PDIS control, the maximum deflection and acceleration at the end-point were ± 5 mm and ± 50 m/sec^2 respectively. Moreover, the vibration of the system settled within less than 2 sec, which are almost threefold improvement as compared to the PD control. This is also evidenced in the PSDs of the end-point deflection and acceleration that show lower magnitudes at the resonance modes.

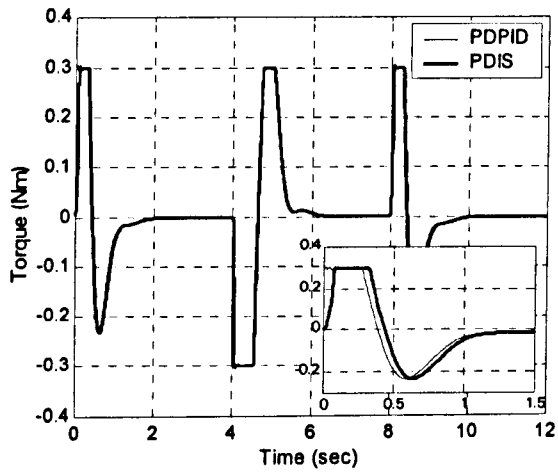

Figure 6.9: Torque inputs with PDPID and PDIS control (0 gram).

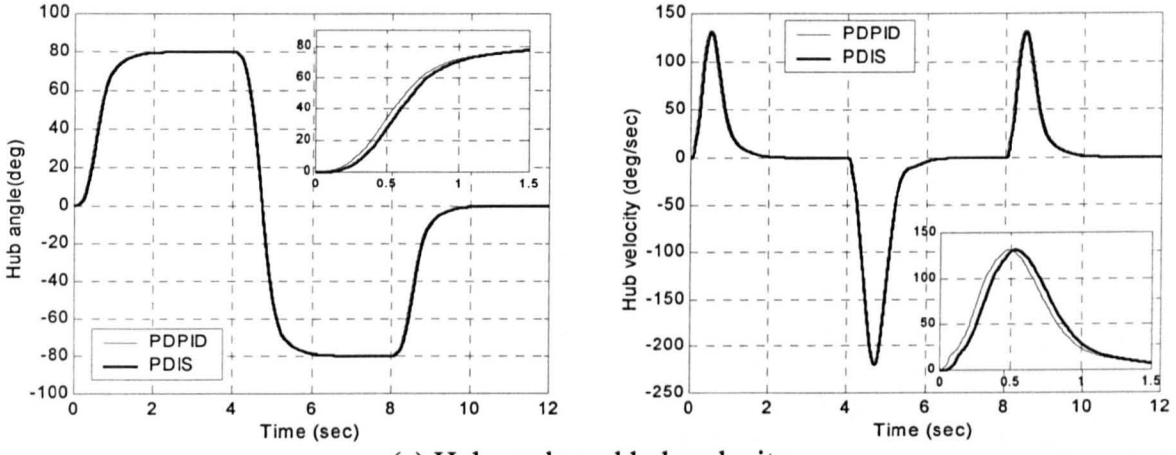

(a) Hub-angle and hub-velocity.

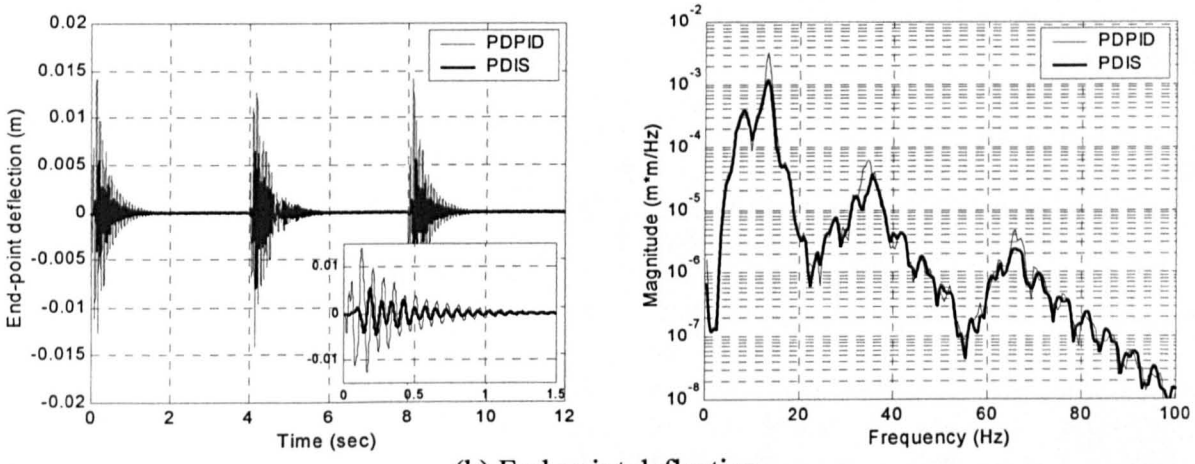

(b) End-point deflection.

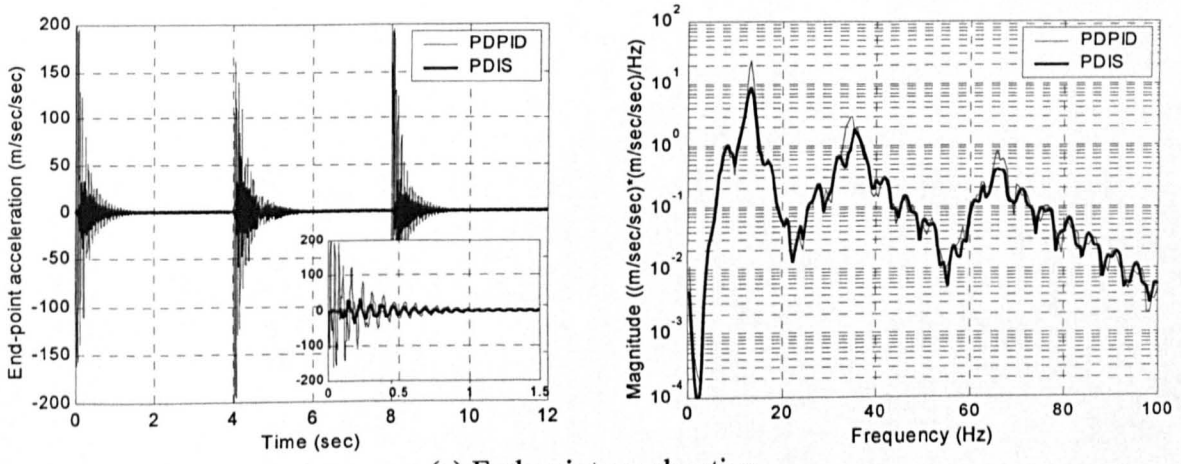

(c) End-point acceleration.

Figure 6.10: Response of the manipulator with PDPID and PDIS control (0 gram).

For the manipulator incorporating 50 grams payload, a similar trend of improvement is observed. Figures 6.11 and 6.12 show the resulting torque input and corresponding response of the manipulator with PDPID and PDIS control. It is noted that smoother velocity profiles are obtained with the hybrid controllers. The performance of the controller at input tracking control is maintained as the PD control. Moreover, the controllers are found to be able to handle vibration of the manipulator with payload as significant reduction in system vibration was observed. Furthermore, the closed-loop systems required only 2 sec to settle down.

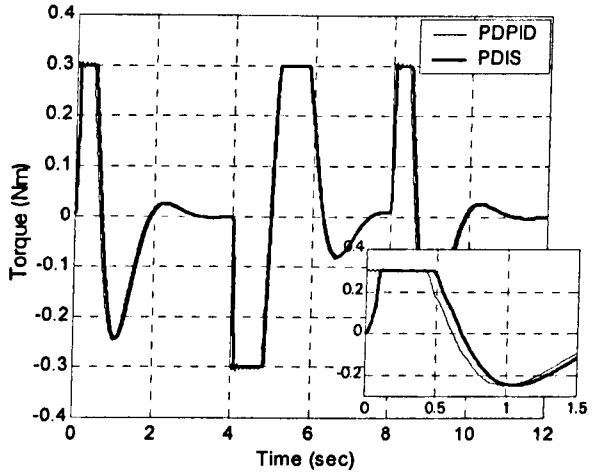

Figure 6.11: Torque inputs with PDPID and PDIS control (50 grams).

The simulation results show that the performance of PDIS control scheme is better than PDPID scheme in vibration suppression of the flexible manipulator. Almost twofold improvement in the vibration reduction with the end-point deflection and acceleration was observed with PDIS as compared to PDPID. This is further evidenced in Figures 6.13 and 6.14 that demonstrate the level of vibration reduction with the end-point deflection and acceleration responses at the resonance modes of the closed-loop system using the hybrid controllers as compared to the PD controller. It is noted that higher vibration reduction is achieved with PDIS at the first resonance mode, which is the most dominant mode. Moreover, implementation of PDIS is easier than PDPID as a large amount of design effort is required to determine the best PID parameters. Note that a properly tuned PID could produce better results. However, as demonstrated in the hub-angle response, slightly slower response was obtained using PDIS. The fixed PD controller gives optimum performance only for a certain loading condition of the flexible manipulator. To achieve better system performance

for various loading conditions, a control algorithm that can adaptively handle changes in system dynamics has to be designed.

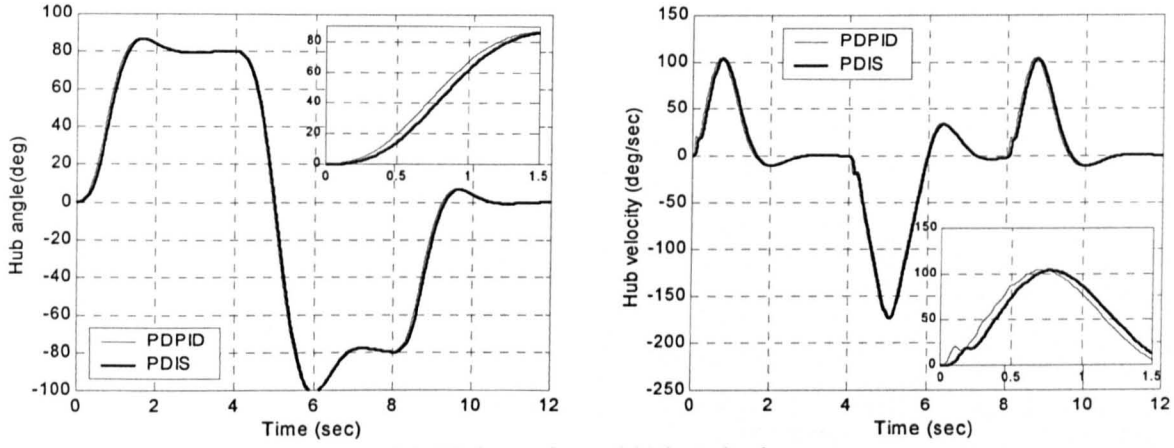

(a) Hub-angle and hub-velocity.

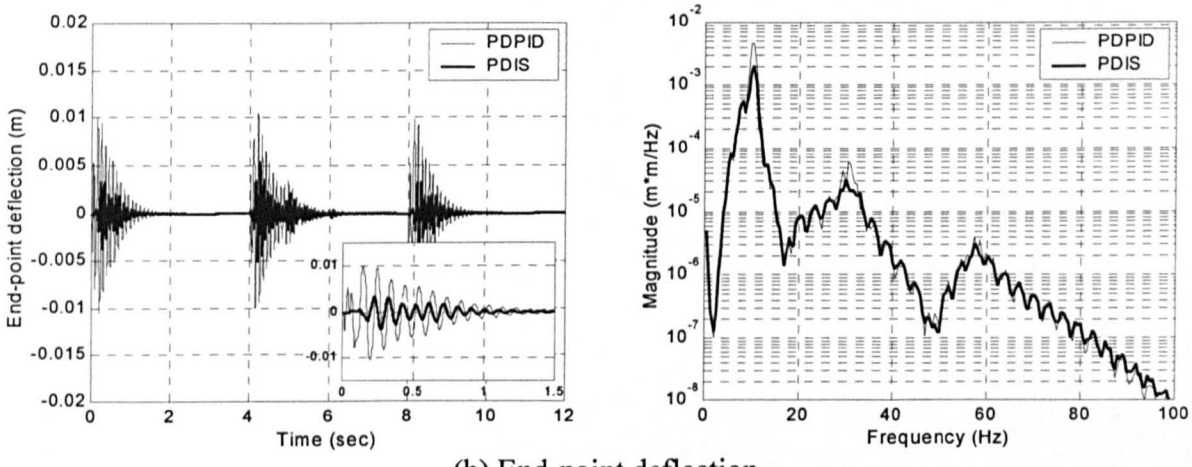

(b) End-point deflection.

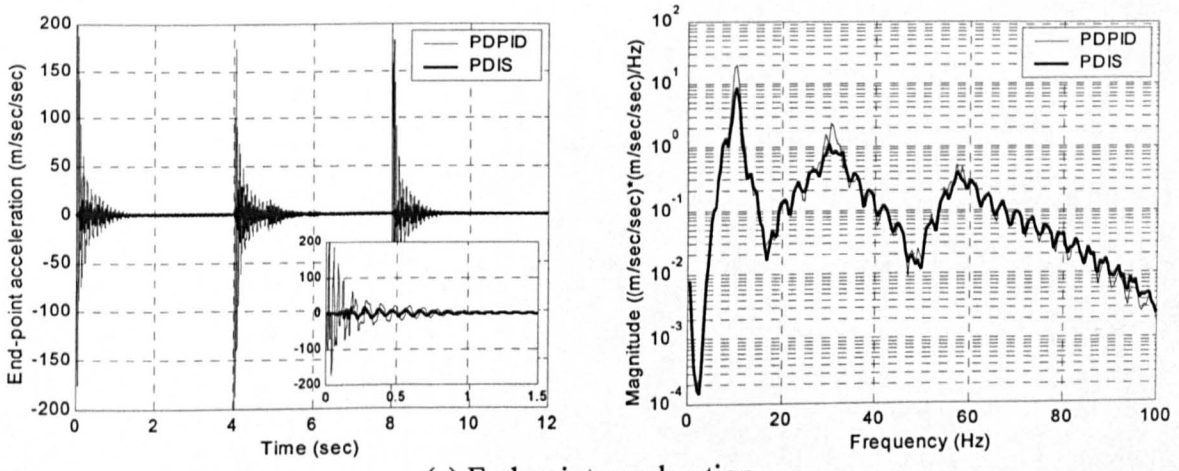

(c) End-point acceleration.

Figure 6.12: Response of the manipulator with PDPID and PDIS control (50 grams).

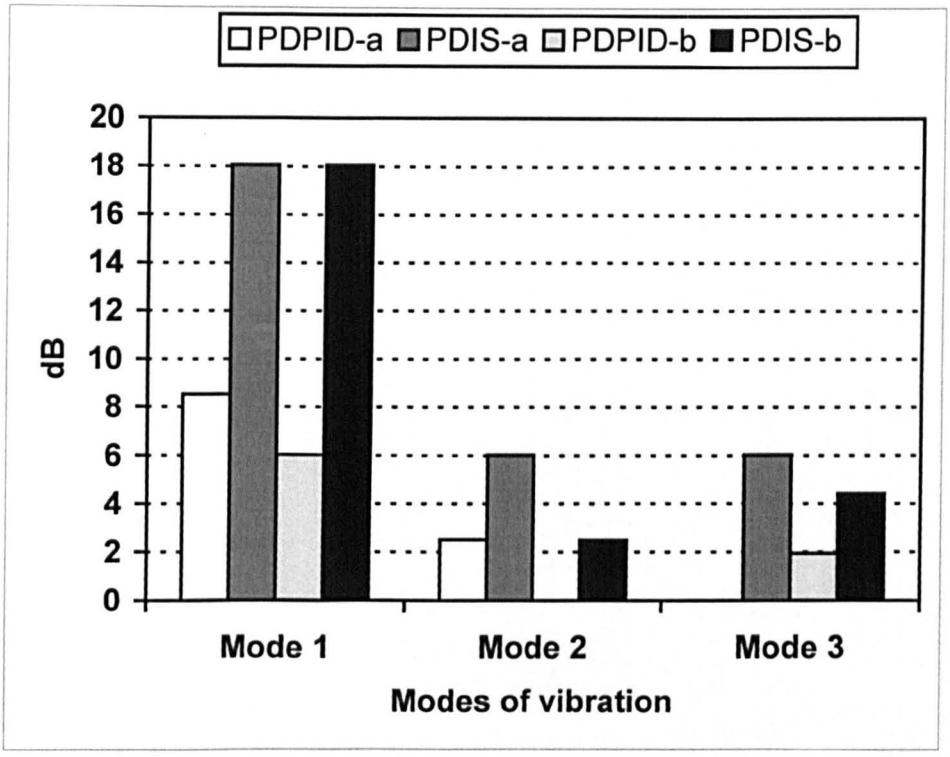

Figure 6.13: Level of vibration reduction using PDPID and PDIS control with the end-point deflection of the manipulator (a – 0 gram, b – 50 grams).

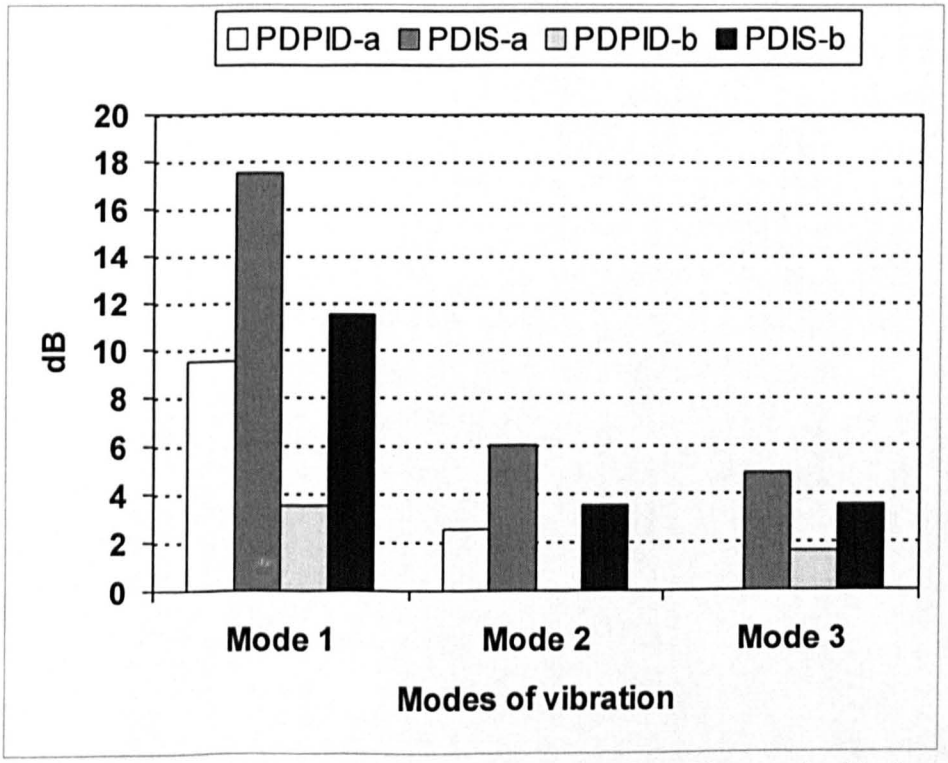

Figure 6.14: Level of vibration reduction using PDPID and PDIS control with the end-point acceleration of the manipulator (a – 0 gram, b – 50 grams).

6.3. A Hybrid Adaptive Control Scheme

To achieve acceptable uniform performance in the presence of payload variations, a hybrid control scheme utilising an adaptive control for rigid body motion control and input shaping for vibration suppression of the flexible manipulator is developed in this section. Initially, a collocated adaptive control is designed based on self-tuning pole assignment technique. Then a feedforward control based on input shaping is incorporated into the closed-loop system for control of vibration of the system. Simulation results of the response of the flexible manipulator with the adaptive control and the hybrid scheme are presented.

6.3.1. Collocated Adaptive Control

In this investigation, a pole assignment self-tuning control scheme is adopted in designing the adaptive control loop for rigid body motion control of the manipulator. Recursive least squares (RLS) estimator is utilised for identification of the corresponding parametric model of the system from torque input to the hub-angle output. The identified parameters of the system are then used to calculate the parameters of proportional and derivative gains of the PD controller. A block diagram of the collocated adaptive controller is shown in Figure 6.15, where r, θ, $\hat{K}_p$, $\hat{K}_v$ and τ_s are the desired hub-angle, actual hub-angle, proportional gain, derivative gain and sampling time respectively. The block diagram shows the layout of a pole assignment self-tuner in which an RLS estimator is combined with a pole assignment synthesis in order to continuously update the controller coefficients. Essentially, the task of this controller is to position the flexible arm to the specified angle of demand. The expectation is that the collocated adaptive controller could identify the changes in the characteristic of the flexible manipulator and thus, provide a better system response by feeding suitable control torque to the manipulator.

The control signal, $u(t)$ can thus be defined as

$$u(t) = \hat{K}_p r - \left[\hat{K}_p + \frac{\hat{K}_v}{\tau_s}(1 - z^{-1})\right]\theta(t) \tag{6.5}$$

where z is the time shift operator. In a general design setting where the underlying system may have complex dynamics, a number of rules of thumb exist which assist in the selection of the controller coefficients $\hat{K}_p$ and $\hat{K}_v$. In a synthesis situation, however, the requirements

on the underlying system are quite strict (Wellstead and Zarrop, 1991). In particular, in order to synthesise exactly the adaptive controller coefficients, the system to be controlled must be assumed to have a special structure of the form

$$\theta(z) = \frac{b_0 z^{-1}}{1 + a_1 z^{-1} + a_2 z^{-2}} u(z) \tag{6.6}$$

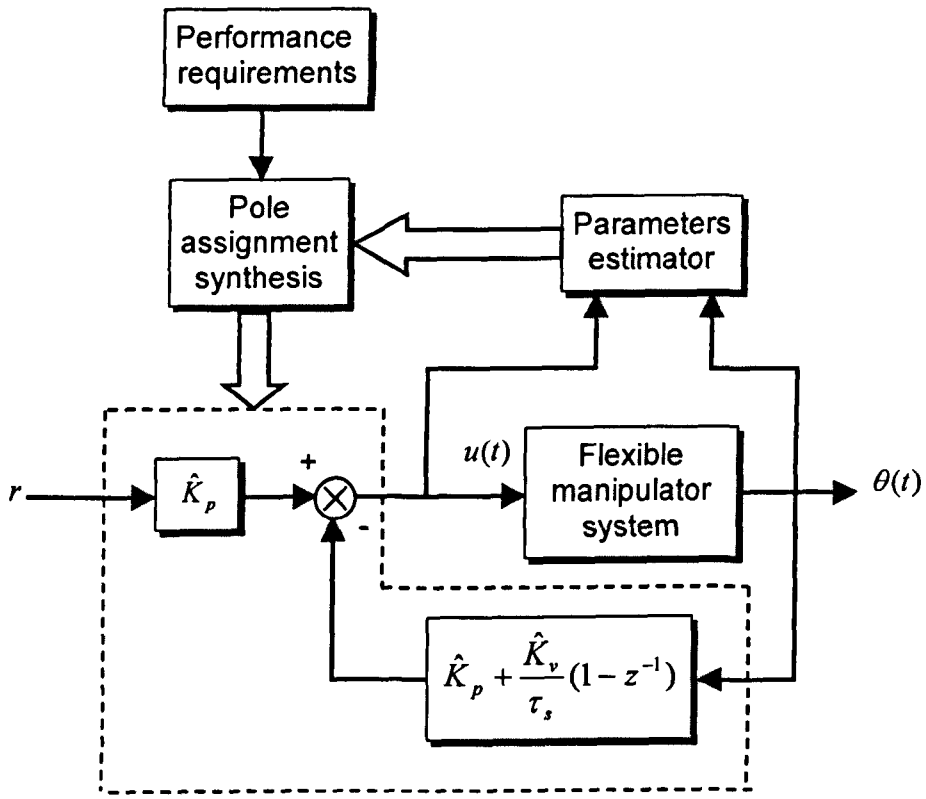

Figure 6.15: A block diagram of collocated adaptive control.

The restriction on the system model structure given in equation (6.6) is to ensure that only a unique set of controller coefficients arises from the design. The structure is reasonably valid for characterisation of rigid-body dynamic of the system for which the PD control loop is designed. By combining the system model in equation (6.6) and the controller equation in equation (6.5), a closed-loop system equation relating r and $\theta(t)$ can be obtained as

$$\frac{\theta}{r} = \frac{\hat{K}_p b_0 z^{-1}}{(1 + a_1 z^{-1} + a_2 z^{-2}) + [\hat{K}_v \tau_s^{-1}(1 - z^{-1}) + \hat{K}_p] b_0 z^{-1}} \tag{6.7}$$

Thus, the characteristic equation of the controlled system, which is the denominator of equation (6.7) can be written as

$$1+(a_1+\hat{K}_p b_0+\hat{K}_v \tau_s^{-1} b_0)z^{-1}+(a_2-\hat{K}_v \tau_s^{-1} b_o)z^{-2} \tag{6.8}$$

In designing the controller, a desired closed-loop characteristic equation, ψ-polynomial, is chosen in the form

$$\psi = 1+\psi_1 z^{-1}+\psi_2 z^{-2} \tag{6.9}$$

where

$$\psi_1 = -2e^{-\zeta\omega_n \tau_s}\cos(\tau\omega_n\sqrt{1-\zeta^2})$$

$$\psi_2 = e^{-2\zeta\omega_n \tau_s}$$

and ζ and ω_n represent the damping factor and natural frequency of the desired closed-loop second order transient response respectively. The controller coefficients $\hat{K}_p$ and $\hat{K}_v$ can be determined by equating the characteristic equation, equation (6.8), and the ψ- polynomial, equation (6.9). This yields

$$1+(a_1+\hat{K}_p b_0+\hat{K}_v \tau_s^{-1} b_0)z^{-1}+(a_2-\hat{K}_v \tau_s^{-1} b_o)z^{-2} = 1+\psi_1 z^{-1}+\psi_2 z^{-2} \tag{6.10}$$

By equating coefficients of like powers of z^{-1} in equation (6.10), the controller parameters can be obtained as

$$\hat{K}_p = \frac{\psi_1+\psi_2-a_1-a_2}{b_0} \tag{6.11}$$

$$\hat{K}_v = \frac{(a_2-\psi_2)\tau_s}{b_0} \tag{6.12}$$

Equations (6.11) and (6.12) constitute the controller design rules, realisation of which results in a pole assignment self-tuning control scheme, as shown in Figure 6.15.

As indicated, RLS estimator is utilised to estimate the system model as in equation (6.6). The system is excited with the square wave shown in Figure 6.16 for a period of 2.5 sec to move the flexible arm and allow the model parameters identified and converged to the correct set. The histories of the identified parameters of the system are shown in Figure 6.17. It is noted that the parameters converged after 2 sec. The last set of parameters are then used in obtaining suitable PD parameters in equations (6.11) and (6.12) for control of the flexible manipulator. The model would have to be updated in a similar manner if a change in the payload is envisaged. Thus, the method used is to initially identify the presence of payload and tune the required controller parameters accordingly.

6.3.2. Hybrid Collocated Adaptive and Feedforward Control

A hybrid control structure in which a collocated adaptive control is combined with a feedforward control scheme for rigid body motion control and vibration suppression of the flexible manipulator is designed in this section. The hybrid control structure with input shaping in the feedforward path was adopted here as this was shown in the previous section to provide better vibration reduction than the collocated and non-collocated PID controller. Moreover, results presented in the previous chapter have shown that significant vibration reduction for up to 30% error tolerance in the natural frequencies of the system can be achieved. With increasing payloads between 0 gram to 50 grams (Figures 6.6 and 6.8), the first natural frequency shifted to 16% lower than the frequency without payload. With a maximum payload (100 grams), it can be expected that the frequency shifts within the range of 30%. Thus, the technique can be utilised with adaptive control for input tracking and vibration suppression of the flexible manipulator with various payloads. A block diagram of the hybrid control scheme is shown in Figure 6.18. With the controller, the desired angle is shaped before feeding into the closed-loop system.

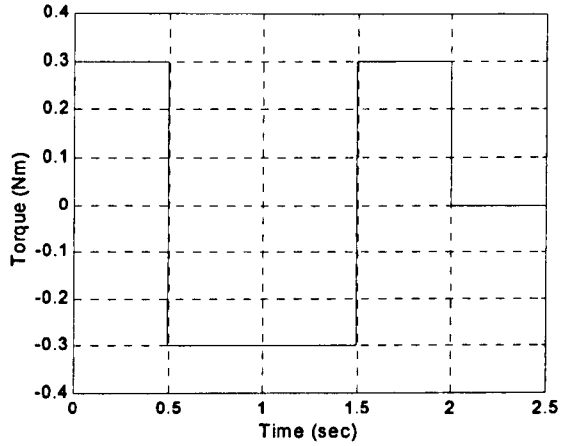

Figure 6.16: Input torque for system identification.

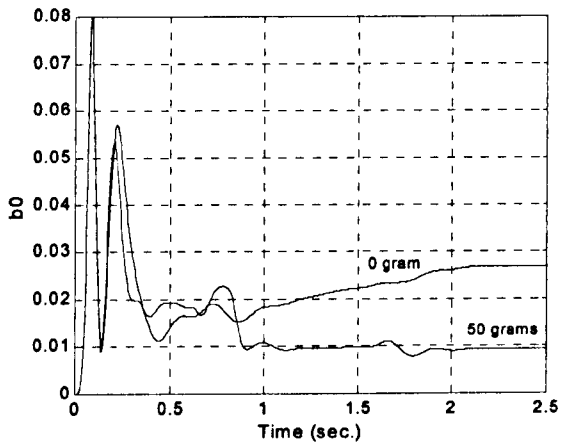

(a) b0.

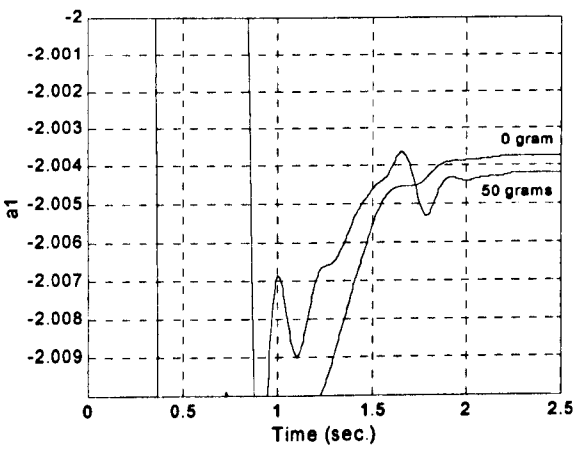

(b) a1.

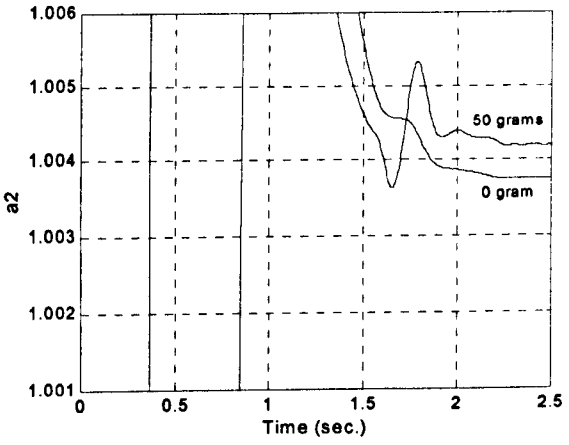

(c) a2.

Figure 6.17: Histories of the identified model parameters.

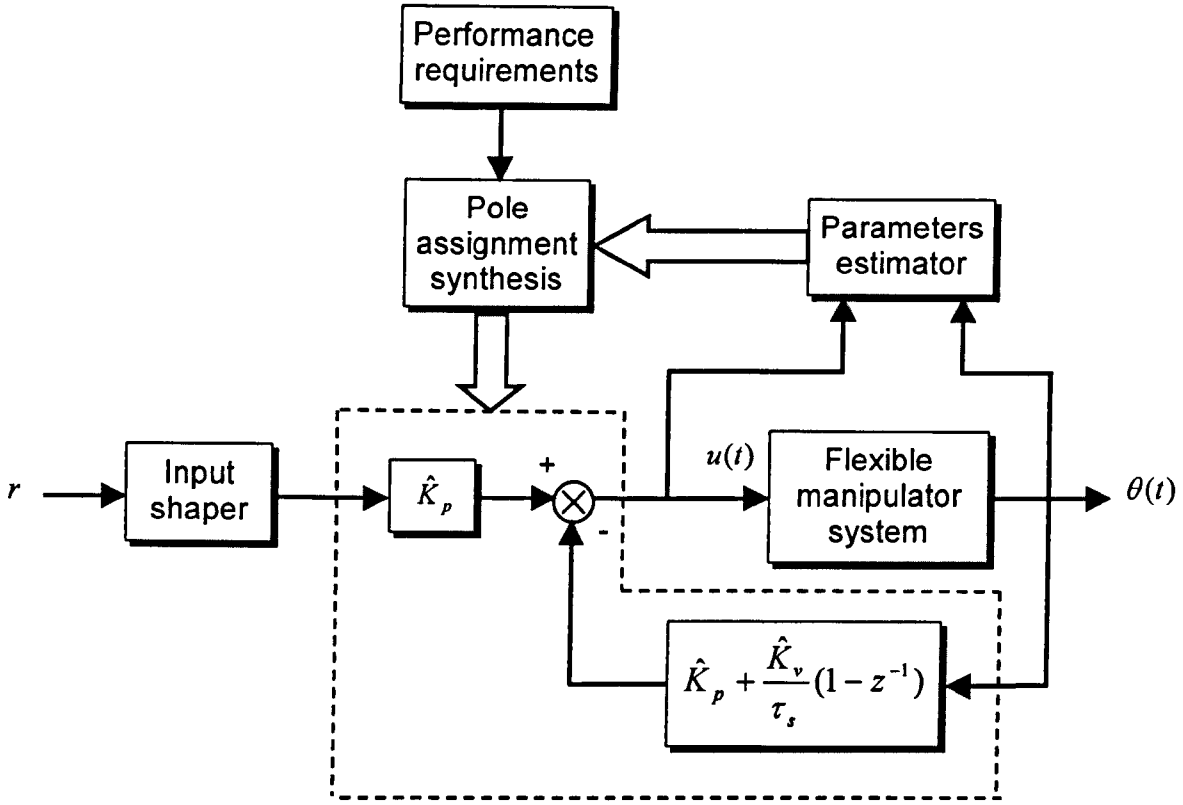

Figure 6.18: The hybrid control structure.

6.3.3. Implementation and Results

The hybrid adaptive and feedforward control scheme was implemented and tested within the simulation environment of the flexible manipulator and the corresponding results are presented in this section. The manipulator is to follow a desired trajectory within the range of ± 80 degrees as shown in Figure 6.19. Similarly, hub-angle, hub-velocity, end-point deflection and end-point acceleration responses of the system are observed with various payloads. Moreover, PSDs of the responses at the end-point are obtained. The performance of the hybrid controller is assessed in terms of input tracking and vibration suppression in comparison to the collocated adaptive control.

6.3.3.1. Collocated Adaptive Control

In this investigation, the ψ - polynomial in equation (6.9) was set such that the desired system has a critical damping, $\zeta = 1$ and natural frequency, $\omega_n = 2.5$ rad/sec with a sampling time of 2 msec. The natural frequency is chosen so that the adaptive control is able to position the manipulator while carrying different payloads. Figure 6.20 shows the required torque inputs

driving the manipulator with payloads of 0 gram and 50 grams using the collocated adaptive control. The corresponding hub-angle and hub-velocity responses of the manipulator with payloads of 0 gram and 50 grams are shown in Figures 6.21 and 6.22 respectively. It is noted that the manipulator reached the desired position between +80 degrees to –80 degrees with no significant overshoot in both cases. With the controller, a slower settling time was observed for the first desired angle, however, better settling times were achieved for subsequent angles. Moreover, as expected with a collocated system, the system responses exhibit minimum-phase behaviour. For the hub-velocities, smooth profiles were achieved with the collocated adaptive control. It is noted that the maximum levels of hub-velocities of the manipulator decrease with increasing payloads. These were obtained as 200 deg/sec and 125 deg/sec with payloads of 0 gram and 50 grams respectively.

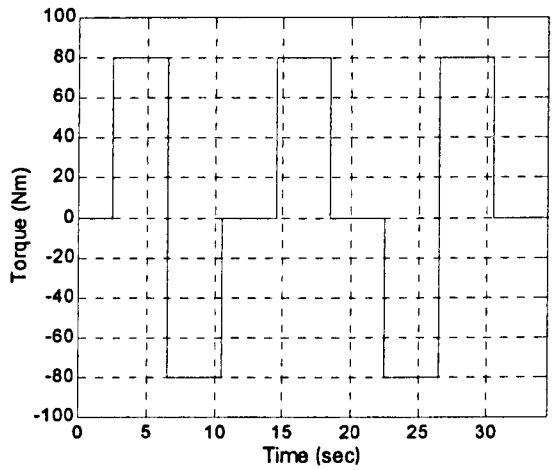

Figure 6.19: Reference input for hybrid adaptive and feedforward control.

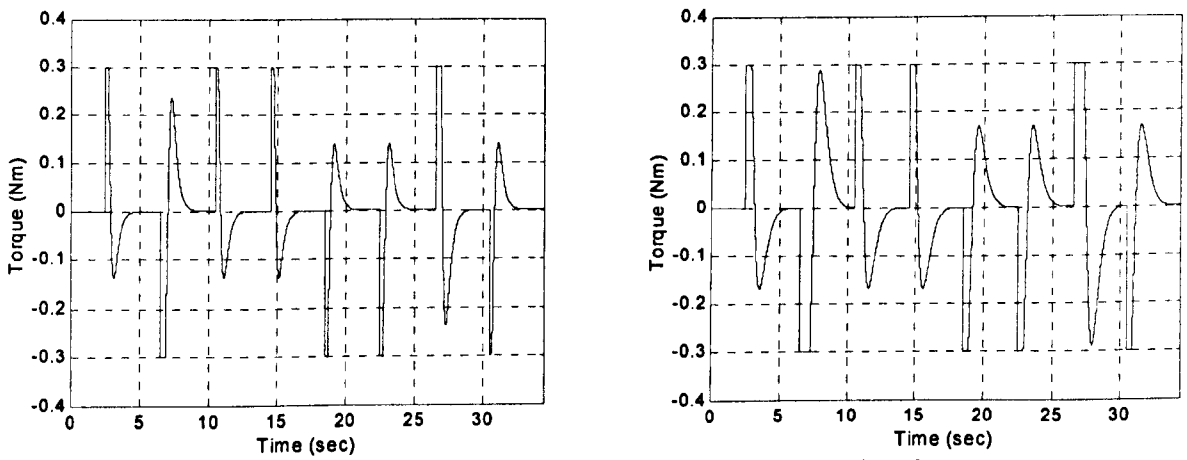

(a) 0 gram. (b) 50 grams.

Figure 6.20: Torque inputs with the adaptive control.

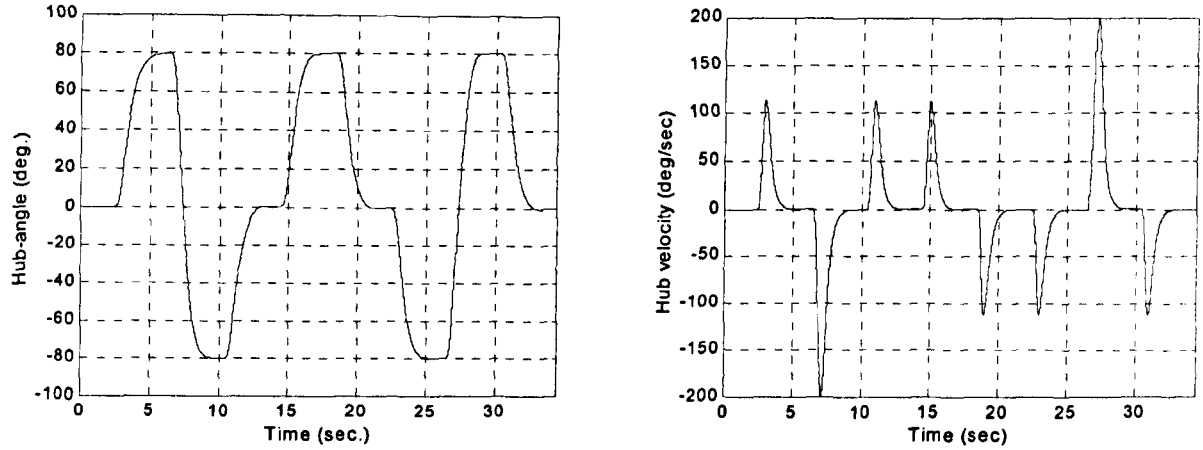

Figure 6.21: Hub-angle and hub-velocity responses of the manipulator with adaptive control (0 gram).

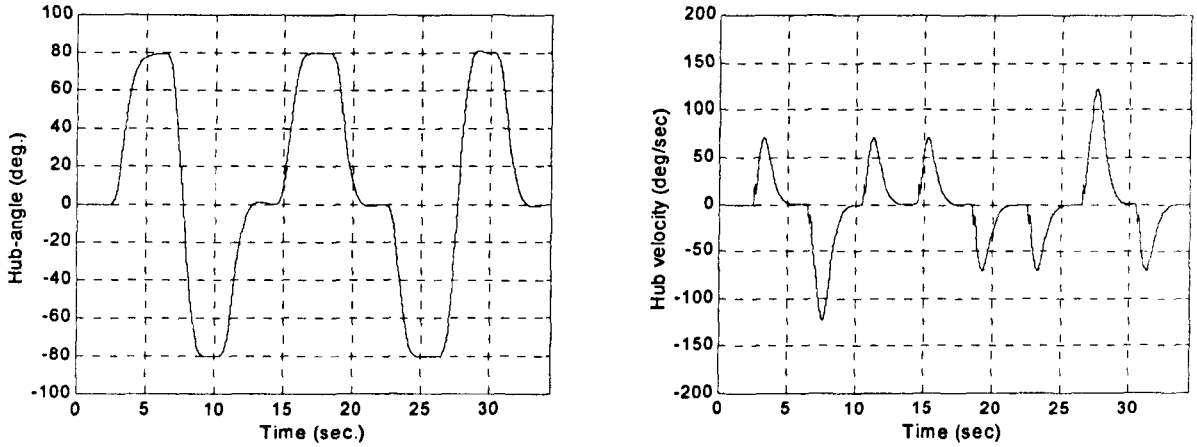

Figure 6.22: Hub-angle and hub-velocity responses of the manipulator with adaptive control (50 grams).

Figures 6.23 and 6.24 show the end-point deflection and end-point acceleration responses with the corresponding PSDs of the manipulator with payloads of 0 gram and 50 grams respectively. It is noted that a significant amount of vibration occurred at the end-point during movement of the manipulator. However, the magnitudes of oscillations reduce with increasing payloads. For the end-point deflection, the maximum levels were obtained as ±13 mm and ±8 mm for payloads of 0 gram and 50 grams respectively. On the other hand, maximum levels of the end-point acceleration were obtained as ±220 m/sec^2 and ±200 m/sec^2 respectively. It is also noted that the end-point responses reach their maximum level when the given torque to the flexible manipulator changes sharply. This is an important observation, which is useful in designing a suitable controller in minimising the vibration of the system. It is evidenced from the PSDs of the end-point deflection and acceleration that the vibration at

the end-point of the manipulator is dominated by the first three vibration modes. These are obtained as 12 Hz, 35 Hz and 65 Hz for 0 gram and 10 Hz, 31 Hz and 58 Hz for 50 grams payloads respectively. As noted, the natural frequencies shift to the lower frequencies with increasing payloads. It can be concluded that with the collocated adaptive control, a satisfactory performance in input tracking for various payloads is achieved. However, vibration at the end-point is unacceptable and can further be reduced. These results are considered as results without vibration control and will subsequently be used in designing and evaluating the performance of a hybrid adaptive controller for vibration suppression of the manipulator.

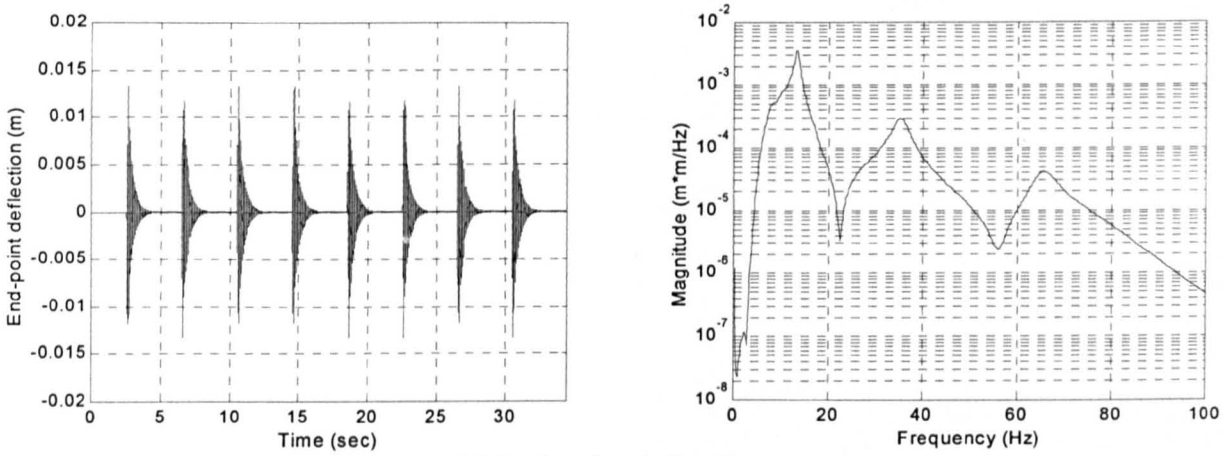

(a) End-point deflection.

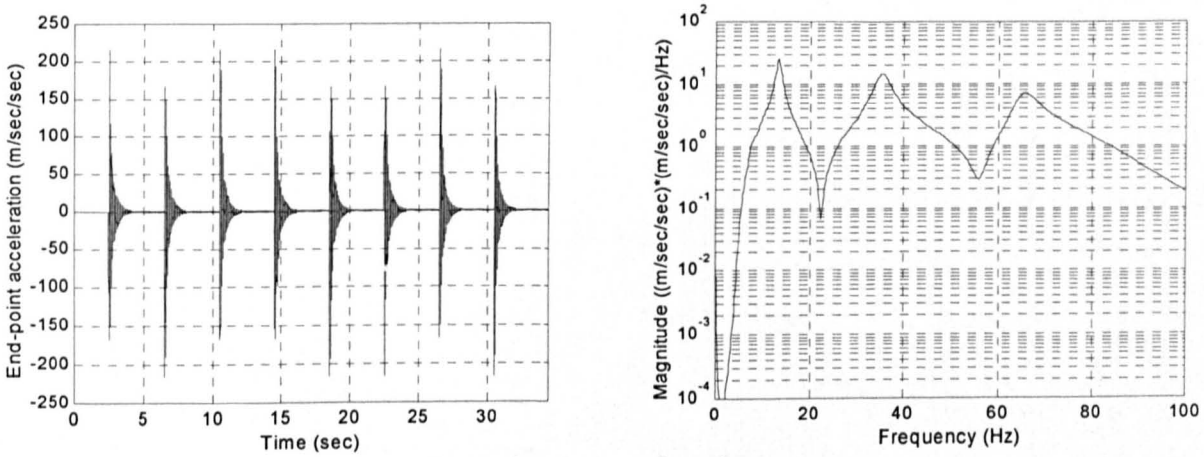

(b) End-point acceleration.

Figure 6.23: Response of the manipulator with adaptive control (0 gram).

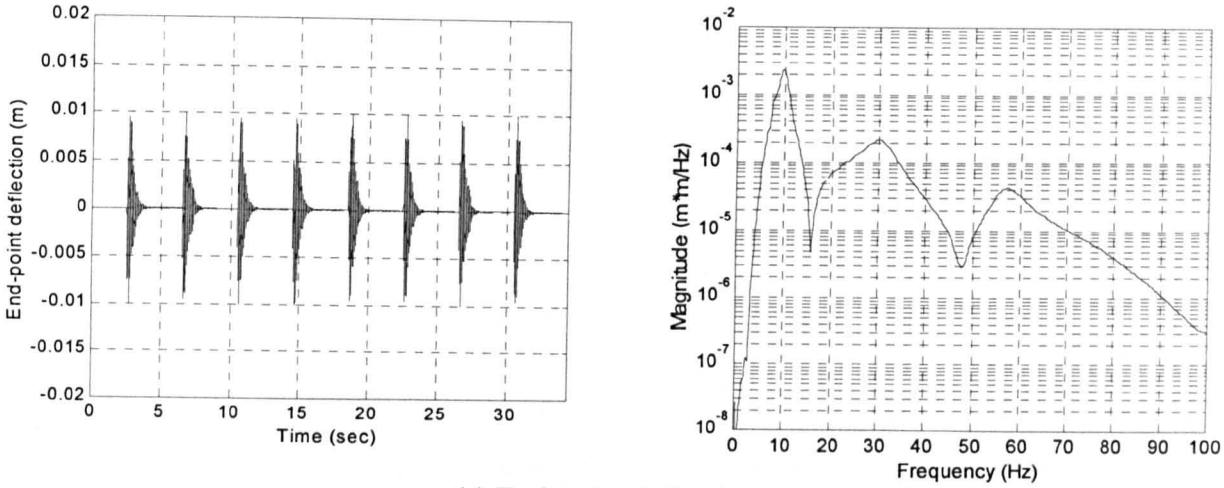

(a) End-point deflection.

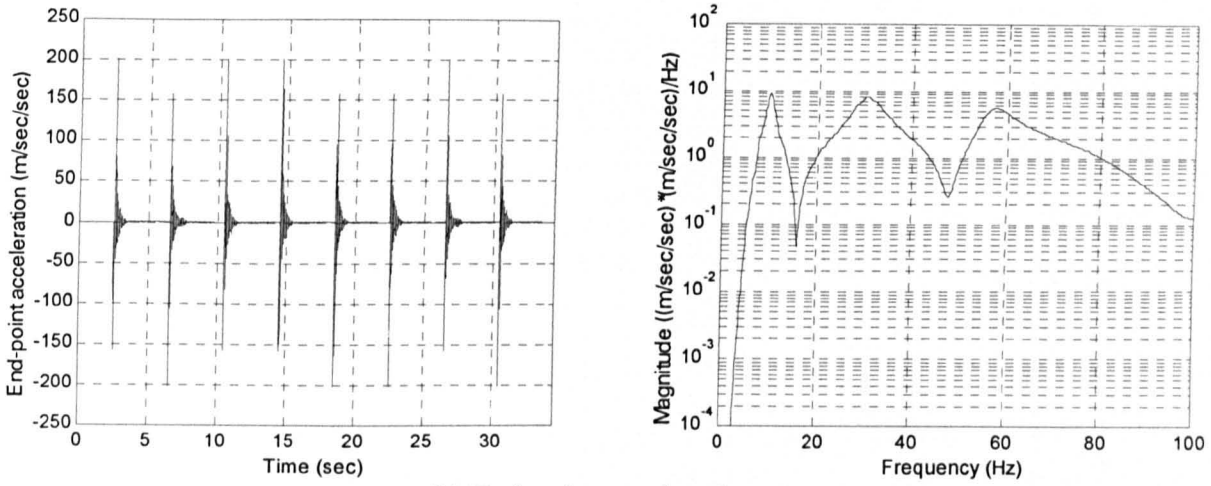

(b) End-point acceleration.

Figure 6.24: Response of the manipulator with adaptive control (50 grams).

6.3.3.2. Hybrid Control

In developing the feedforward control scheme for vibration suppression of the manipulator, an input shaper with a four-impulse sequence was designed based on the dynamic behaviour of the closed-loop system obtained using the collocated adaptive control. Since the input shaping technique is robust with up to 30% error tolerance in the natural frequencies and the natural frequencies of the closed-loop system incorporating payloads of 0 gram to 100 grams are within the range, significant vibration reduction can be achieved. In this investigation, the natural frequencies of the flexible manipulator without payload were utilised. The developed input shaper was then used to pre-process the input reference. The resulting shaped input is shown in Figure 6.25.

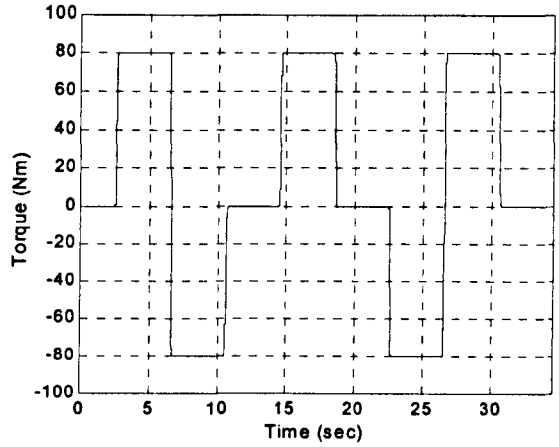

Figure 6.25: Shaped reference input.

Figure 6.26 shows the resulting torque inputs driving the manipulator with payloads of 0 gram and 50 grams with the hybrid controller. The corresponding hub-angle and hub-velocity responses of the manipulator with payloads of 0 gram and 50 grams are shown in Figures 6.27 and 6.28 respectively. It is noted that both responses are almost identical to the responses obtained using adaptive control. Figures 6.29 and 6.30 show the end-point deflection and end-point acceleration responses with the corresponding PSDs of the flexible manipulator with payloads of 0 gram and 50 grams respectively. It is noted that a significant amount of vibration reduction was achieved at the end-point of the manipulator. For the case without payload, the maximum levels of end-point deflection and acceleration were obtained as ±5 mm and ±30 m/sec^2 respectively. On the other hand, with 50 grams payload, the maximum levels were obtained as ±5 mm and ±25 m/sec^2 . These correspond to almost fourfold improvement in vibration reduction as compared to the results without feedforward control. This is also evidenced in the PSDs of the end-point responses that show lower magnitudes at all frequencies as compared to the adaptive control. Figures 6.31 and 6.32 demonstrate the level of vibration reduction achieved at the resonance modes using the hybrid control as compared to the adaptive control. For the first resonance mode, which is the most dominant mode, reductions of 12 dB and 5 dB were achieved for the manipulator with payloads of 0 gram and 50 grams respectively. Thus, the hybrid controller is capable of reducing the system vibration while maintaining the input tracking performance of the manipulator.

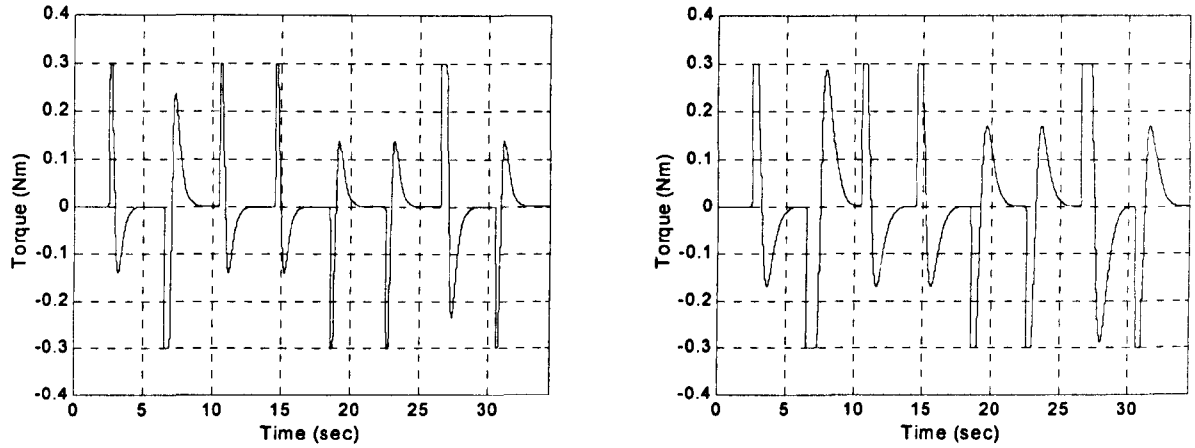

(a) 0 gram. (b) 50 grams.

Figure 6.26: Torque inputs with the hybrid control.

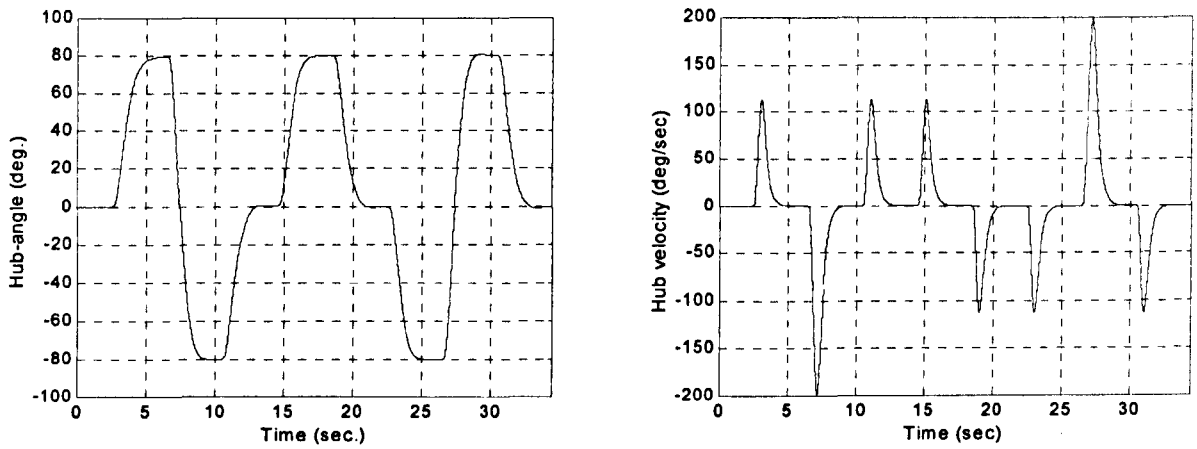

Figure 6.27: Hub-angle and hub-velocity responses of the manipulator with the hybrid control (0 gram).

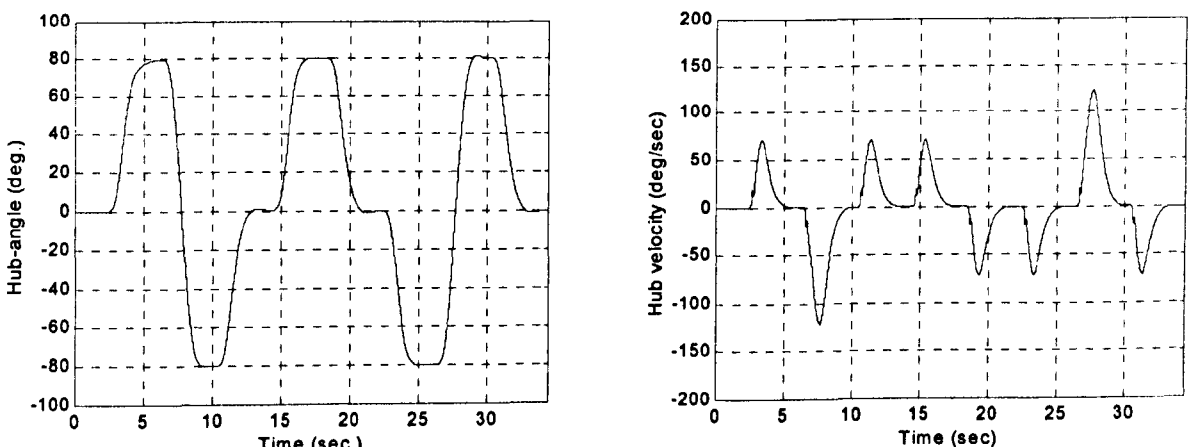

Figure 6.28: Hub-angle and hub-velocity responses of the manipulator with the hybrid control (50 grams).

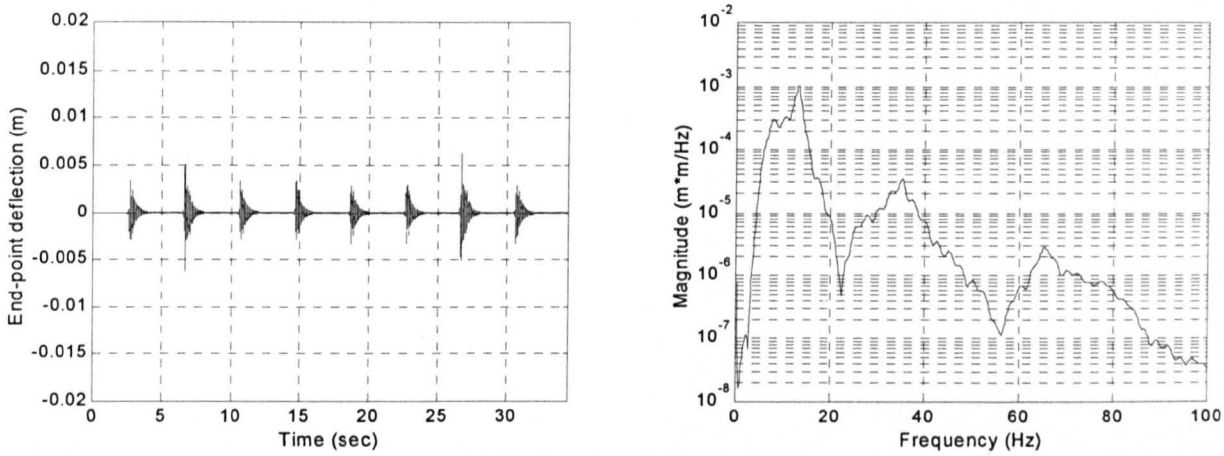

(a) End-point deflection.

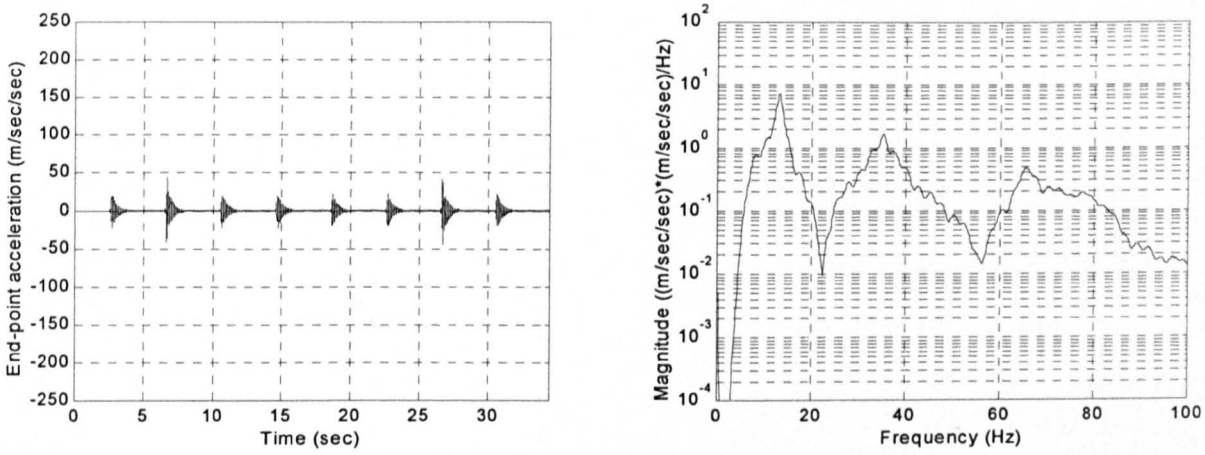

(b) End-point acceleration.

Figure 6.29: Response of the manipulator with the hybrid control (0 gram).

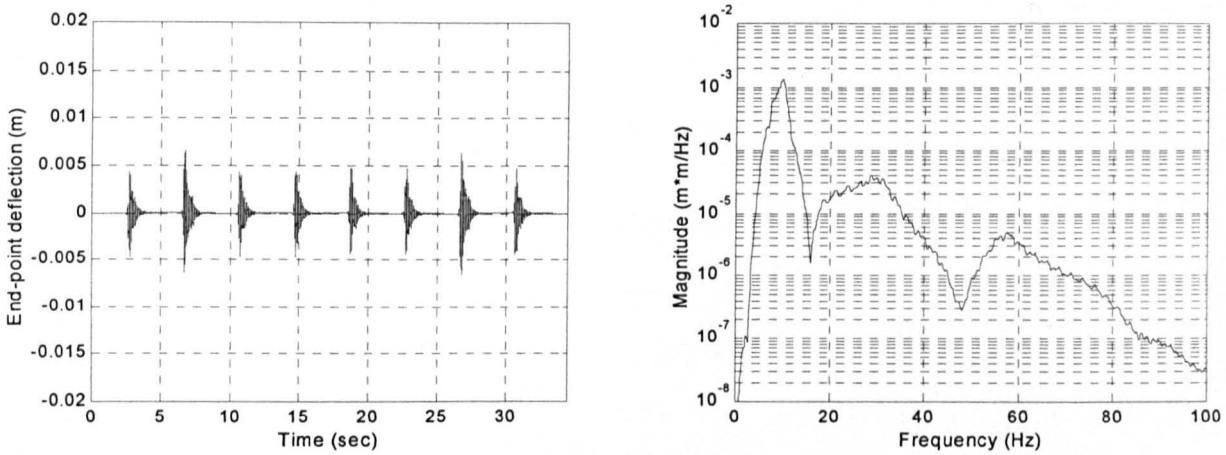

(a) End-point deflection.

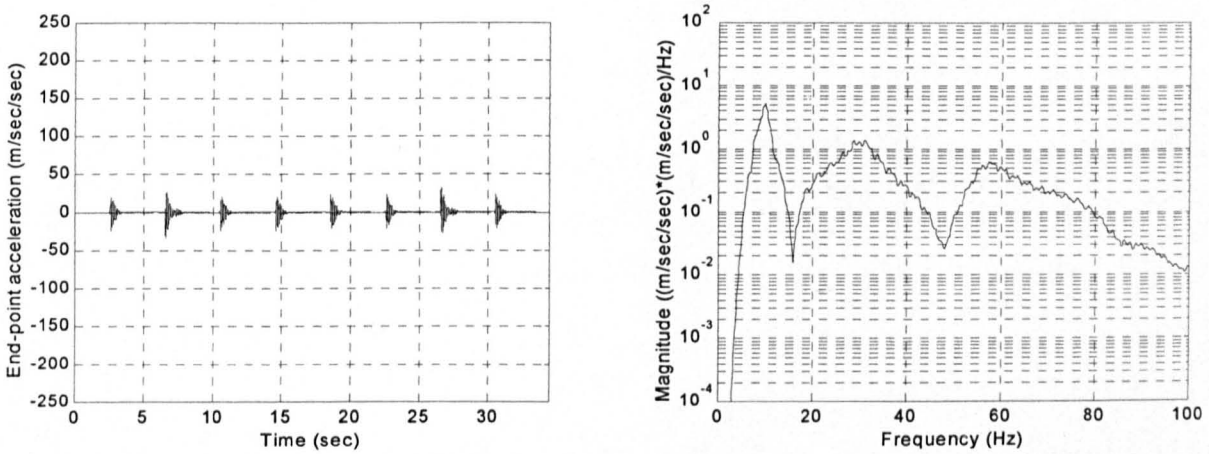

(b) End-point acceleration.

Figure 6.30: Response of the manipulator with the hybrid control (50 grams).

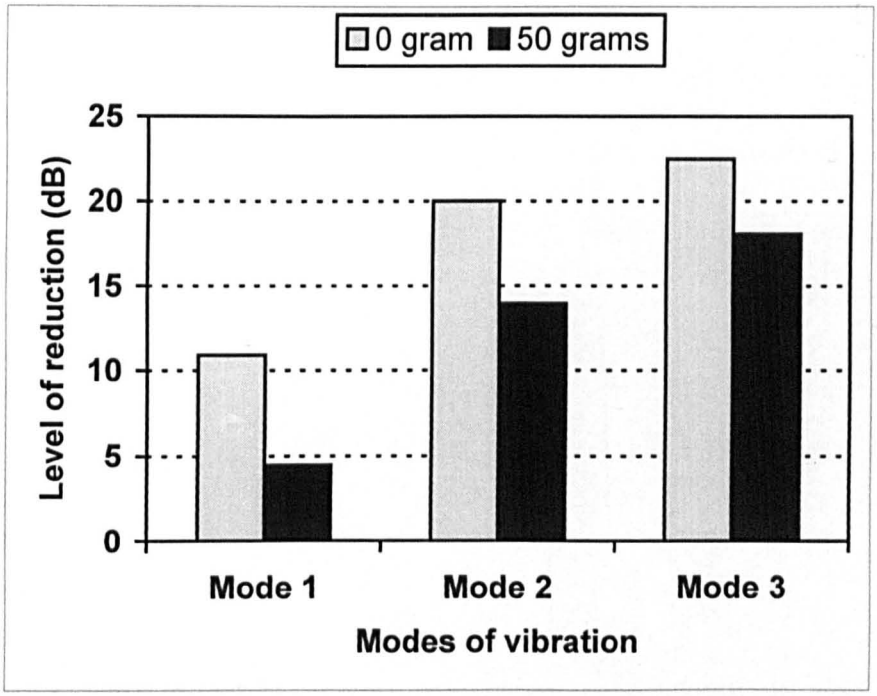

Figure 6.31: Level of vibration reduction with the end-point deflection using the hybrid control as compared to the adaptive control.

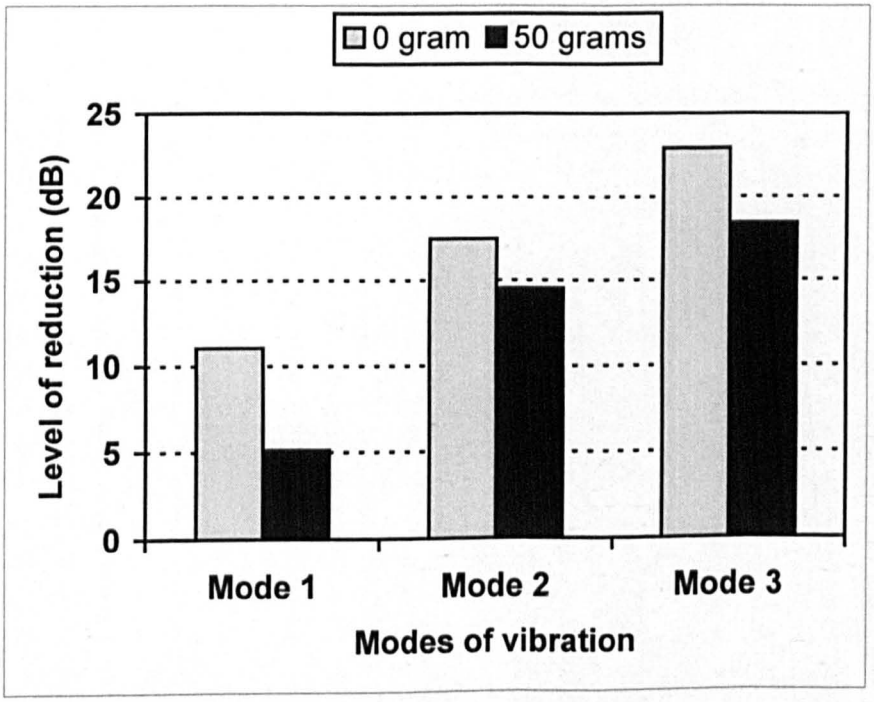

Figure 6.32: Level of vibration reduction with the end-point acceleration using hybrid control as compared to adaptive control.

6.4. Summary

The development of hybrid control schemes for input tracking and vibration suppression of a flexible manipulator has been presented. The hybrid control schemes have been developed based on collocated feedback controllers for rigid body motion control with non-collocated PID and feedforward control for vibration suppression of the system. The feedforward control scheme has been developed using an input shaping technique. For control of rigid body motion, a collocated PD control and adaptive control have been designed. The hybrid control schemes have been implemented and tested within simulation environment of the flexible manipulator without and with payload. The performances of the control schemes have been evaluated in terms of input tracking capability and vibration suppression of the flexible manipulator. A comparative assessment of the hybrid control schemes has shown that the PD control with input shaping (feedforward) performs better than the PD with non-collocated PID control in respect of vibration reduction at the end-point of the manipulator. However, the performance of input tracking control of the system with the PD controller is unsatisfactory for various payloads. With the hybrid control scheme based on a combined adaptive control and input shaping, acceptable performance in input tracking control and vibration suppression of the system has been achieved. Due to time constraints, the hybrid controllers could not be tested with the experimental rig, as the interface card broke down at this stage. However, as close results between simulation and experiments were obtained in Chapter 5, it is anticipated that the simulated results presented in this chapter will be confirmed by experimental investigations.

Chapter 7

Conclusion and Further Work

7.1. Conclusion

This thesis has presented investigations into dynamic modelling and control of a flexible manipulator system. Several modelling and control approaches have initially been discussed and the research direction has accordingly been identified. Simulation and experimental exercises with a single-link flexible manipulator with and without payload have been performed. Four system responses namely hub-angle, hub-velocity, end-point deflection and end-point acceleration have been obtained and presented in the time and frequency domains.

Dynamic modelling of the flexible manipulator has been investigated using the FE method with numerical and symbolic manipulation approaches. In the former, a dynamic model of the flexible manipulator incorporating structural damping, hub inertia and payload has been developed. Experiments have been performed on a laboratory-scale flexible manipulator and used for verification and assessment of the simulation results. The performance and accuracy of the simulation algorithm has been studied. Moreover, the effects of damping and payload on the dynamic behaviour of the manipulator have been addressed. A close agreement between the simulation and experimental results has been demonstrated in the time response and resonance frequencies of the system. However, slight differences in steady-state level of the simulated and experimental hub-angle responses of the system with payloads has been noted. It can be concluded that the developed FE model provides confidence in the accuracy of the model and can be utilised as a test and evaluation platform for development of control strategies for flexible manipulator systems.

The application of a symbolic manipulation approach for modelling and performance analysis of a flexible manipulator system has been examined. It has been demonstrated that the approach can be utilised in characterising the dynamic behaviour of the manipulator and to assess the system in different ways. The system transfer functions have been obtained in symbolic form and thus inter-relations between payload, hub inertia and system

characteristics have been explored. Simulation and experimental exercises have been presented demonstrating the performance of the symbolic approach in modelling and simulation of the flexible manipulator system.

Several feedforward and feedback control schemes for vibration suppression and input tracking control of flexible manipulator systems have been proposed and investigated in this research. Simulation and experimental investigations into the development of feedforward control strategies based on command shaping techniques for vibration suppression of a flexible manipulator have been presented. The command shaping techniques using input shaping, low-pass and band-stop filters have been considered. Performances of the techniques have been evaluated in terms of level of vibration reduction at the resonance modes, time response specifications of the hub-angle response, robustness to 30% error tolerance in the natural frequencies and processing times required in developing the shaped and filtered inputs. The impact of using higher number of impulses and filter orders on the system performance has also been investigated. Significant reduction in the system vibrations has been achieved with these control strategies. For the flexible manipulator and the specifications used in designing the input shapers and filters, the input shaping technique has been demonstrated to provide the best performance in vibration reduction and time response, especially in terms of robustness to errors. Moreover, system vibration in the presence of payload has successfully been suppressed using this technique. The low-pass filtered input has been shown to perform better than the band-stop filtered input. However, the processing time in developing an input shaping command is longer as compared to that required for the filtered input. It has been demonstrated that a close agreement between the simulation and experimental results of the response of the system to the command shaping techniques has been achieved. The command shaping techniques are not robust to parameter changes in the system. In this case, input tracking capabilities of the flexible manipulator has been shown to be unsatisfactory in the presence of payload. Thus, hybrid controllers that provide acceptable input tracking and low vibration of the system have been proposed.

The development of hybrid control schemes for input tracking and vibration suppression of a flexible manipulator has been presented. The hybrid control schemes have been developed based on collocated feedback controllers for rigid body motion control with non-collocated PID and feedforward control for vibration suppression of the system. The feedforward control scheme has been developed using an input shaping technique whereas for control of rigid body motion, a collocated PD control and collocated adaptive control have been examined. The hybrid control schemes have been implemented and tested within

simulation environment of the flexible manipulator with and without payload. The performances of the control schemes have been evaluated in terms of input tracking capability and vibration suppression of the flexible manipulator. It has been demonstrated that the hybrid schemes produce significant vibration reduction while maintaining the input tracking performance of the manipulator. It has been shown that the PD control with input shaping (feedforward) performs better than the PD with non-collocated PID control in respect of vibration reduction at the end-point of the manipulator. However, the performance of input tracking control of the system with the PD controller is unsatisfactory for various payloads. This has been addressed by the development of adaptive control scheme based on pole-assignment self-tuning control scheme for control of rigid body motion. The controller has been combined with input shaping and satisfactory performance in input tracking control and vibration suppression of the system with various payloads has been achieved.

7.2. Further Work

A number of investigations emanating from this research can be undertaken further. Some of those are identified below:

7.2.1. Development of an Accurate Dynamic Model

A more accurate dynamic model of the flexible manipulator with various payloads could be obtained by incorporating several effects such as gravity, payload rotary inertia and friction into the dynamic model of the system. The inclusion of these parameters could provide a closer representation of the actual system. The differences between simulation and experimental responses of the manipulator with payloads that were highlighted in Chapter 3 could be solved. Techniques in incorporating these effects into the existing FE simulation algorithm have to be identified. Alternatively, other numerical analysis techniques such as the boundary element method can be employed in characterising the dynamic behaviour of the manipulator.

7.2.2. The Application of Symbolic Manipulation Approach

This research has demonstrated that the symbolic manipulation approach provides an alternative technique in modelling and analysis of the flexible manipulator. The approach has shown several advantages over numerical approaches. Therefore, it is desirable to further utilise the symbolic approach for development of control strategies for flexible manipulator

systems. The controller could be designed in symbolic form and the performance analysis such as stability could be carried out. For flexible manipulators that use strain gauges for sensing signals for feedback control, computation can be carried out symbolically to determine the optimum location of the strain gauges that result in a satisfactory system response.

7.2.3. The Command Shaping Techniques

Input shaping has been shown to provide significant reduction in the vibration of a flexible manipulator. However, this has been achieved with a slight delay in the response of the system. Several extended input shaping techniques such as a negative input shaper could be investigated to obtain a faster system response. Moreover, other techniques in developing low-pass and band-stop filters such as Elliptic and Chebyshev could be employed and their performance in vibration suppression of the system be examined.

7.2.4. Hybrid Control Schemes

In this research, the hybrid control schemes were tested within the simulation environment of the flexible manipulator. It is desirable to realise the control schemes in practice and thus, the effectiveness of the proposed hybrid control schemes in real-time implementation could be investigated. In implementation of real-time adaptive control, a high performance and powerful processing unit is required especially for system identification. Several control techniques such as H-infinity and intelligent control could also be investigated in input tracking control of the flexible manipulator. The effects of combining these controllers with input shaping can be explored in input tracking control and vibration suppression of the system.

7.2.5. Development of a Two-link Flexible Manipulator

In practice, flexible manipulators with two-links are desirable as such manipulators have more degrees of freedom in movement. Modelling and control strategies could be developed within the framework presented in the thesis. Thus, the effectiveness of the developed modelling approach and control strategies can be examined. Modelling and control of a two-link manipulator will be more complicated and challenging. A laboratory-scale two-link flexible manipulator could be designed and constructed for verification of modelling and control approaches.

References

Alberts, T. E., Love, L. J., Bayo, E. and Moulin, H. (1990). Experiments with end-point control of a flexible link using the inverse dynamics approach and passive damping, *Proceedings of American Control Conference*, San Diego (USA), pp. 350-355.

Aoustin, Y., Chevallereau, C., Glumineau, A. and Moog, C.H. (1994). Experimental results for the end-effector control of a single flexible robotic arm, *IEEE Transactions on Control Systems Technology*, **2**(4), pp. 371-381.

Apkarian, P. and Adams, R. J. (1998). Advanced gain-scheduling techniques for uncertain systems, *IEEE Transactions on Control Systems Technology*, **6**(1), pp. 21-32.

Aspinwall, D. M. (1980). Acceleration profiles for minimising residual response, *Transactions of ASME: Journal of Dynamic Systems, Measurement and Control*, **102**(1), pp. 3-6.

Azad, A. K. M. (1994). *Analysis and design of control mechanism for flexible manipulator systems*, PhD. Thesis, Department of Automatic Control and Systems Engineering, The University of Sheffield, UK.

Balas, G. J. (1990). *Robust control of flexible structures: theory and experiments*, PhD. Thesis, Department of Aeronautical Engineering, California Institute Technology, Pasadena, USA.

Banavar, R. N. and Dominic, P. (1995). An LQG/H-infinity controller for a flexible manipulator, *IEEE Transactions on Control Systems Technology*, **3**(4), pp. 409-416.

Banks, S. (1990). *Signal processing, image processing and pattern recognition*, Prentice Hall International, London.

Bayo, E. (1988). Computed torque for the position control of open-loop flexible robots, *Proceedings of IEEE International Conference on Robotics and Automation*, Philadelphia (USA), pp. 316-321.

Book, W. J. (1984). Recursive lagrangian dynamics of flexible manipulator arms, *International Journal of Robotics Research*, **3**(3), pp. 87-101.

Book, W. J. (1990). Modeling, design, and control of flexible manipulator arms: a tutorial review, *Proceedings of the IEEE Conference on Decision and Control*, Honolulu (USA), pp. 500-506.

Book, W. J. and Majette, M. (1983). Controller design for flexile distributed parameter mechanical arm via combined state-space and frequency domain techniques, *Transactions of ASME: Journal of Dynamic Systems, Measurement and Control*, **105**(4), pp. 245-254.

Cannon, R. H. and Schmitz, E. (1984). Initial experiment on the end-point control of a flexible one-link robot, *International Journal of Robotics Research*, **3**(3), pp. 62-75.

Cetinkunt, S. and Ittop, B. (1992). Computer-automated symbolic modeling of dynamics of robotic manipulators with flexible links, *IEEE Transactions of Robotics and Automation*, **8**(1), pp. 94-105.

Chapnik, B. V., Heppler, G. R. and Aplevich, J. D. (1991). Modeling impact on a one-link flexible robotic arm, *IEEE Transactions on Robotics and Automation*, **7**, pp. 479-488.

Cheng, W. and Wen, J. T. (1993). A neural controller for the tracking control of flexible arms, *Proceedings of the IEW International Conference on Neural Networks*, pp. 749-754.

Cutforth, C. F. and Pao, L. Y. (1999). A modified method for multiple actuator input shaping, *Proceedings of American Control Conference*, San Diego (USA), pp. 66-70.

De Luca, A., Lucibello, P. and Nicolo, F. (1988). Automatic symbolic modelling and non-linear control of robots with flexible links, *Proceedings of IEE Seminar on Robotics and Control*, Oxford (UK), pp. 62-70.

De Luca, A. and Siciliano, B. (1991). Closed-form dynamic model of planar multilink lightweight robots, *IEEE Transactions on Systems, Man and Cybernetics*, **21**(4), pp. 826-839.

Donne, J. D. and Ozguner, U. (1994). Neural control of a flexible-link manipulator, *Proceedings IEEE International Conference on Neural Networks*, Orlando (USA), pp. 2327-2332.

Drapeau, V. and Wang, D. (1993). Verification of closed-loop shaped-input controller for a five-bar-linkage manipulator, *Proceedings of IEEE International Conference on Robotics and Automation*, Atlanta (USA), pp. 216-221.

Electrocraft Corporation. (1985). *DC motors speed control servo systems*, Electrocraft Corporation / Robbins & Mayers, Minnesota, USA.

Feliu, V., Rattan, K. S. and Brown, H. B. (1993). Control of flexible arms with friction in the joints, *IEEE Transactions on Robotics and Automation*, **9**(4), pp. 467-475.

Fung, E. H. K. and Cheung, F. C. K. (1995). A variable structure tracking controller for a flexible one-link robot, *Proceedings of IEEE International Conference on Systems, Man and Cybernetics*, Vancouver (Canada), pp. 4458-4463.

Garcia-Benitez, E., Yurkovich, S. and Passino, K. M. (1991). A fuzzy supervisor for flexible manipulator control, *Proceedings of IEEE International Symposium on Intelligent Control*, Virginia (USA), pp. 37-42.

Ge, S. S., Lee, T. H. and Tan, E. G. (1997). Adaptive neural network control of flexible link robots based on singular perturbation, *Proceedings of IEEE International Conference on Control Applications*, Hartford (USA), pp. 365-370.

Ge, S. S., Lee, T. H. and Zhu, G. (1996). Genetic algorithm tuning of Lyapunov-based controllers: an application to a single-link flexible robot system, *IEEE Transactions on Industrial Electronics*, **43**(5), pp. 567-574.

Gevarter, W. B. (1970). Basic relations for control of flexible vehicles, *AIAA Journal*, **8**(4), pp. 666-672.

Grimble. M. J. and Johnson, M. A. (1991). H-infinity robust control design - a tutorial review, *Computing and Control Engineering Journal*, **2**, pp. 275-282.

Gutierrez, L. B., Lewis, P. L. and Lowe, J. A. (1998). Implementation of a neural network tracking controller for a single flexible link: comparison with PD and PID controllers, *IEEE Transactions on Industrial Electronics*, **45**(3), pp. 307-318.

Harishima, F. and Ueshiba, T. (1986). Adaptive control of flexible arm using end-point position control sensing, *Proceedings of Japan-USA Symposium on Flexible Automation*, Osaka (Japan), pp. 225-229.

Hasting, G. G. and Book, W. J. (1986). Verification of a linear dynamic model for flexible robotic manipulators, *Proceedings of IEEE International Conference on Robotics and Automation*, San Francisco (USA), pp. 1024-1029.

Hasting, G. G. and Book, W. J. (1987). A linear dynamic model for flexible robot manipulators, *IEEE Control Systems Magazine*, **7**, pp. 61-64.

Hu, A. (1993). A survey of experiments for modelling verification and control of flexible robotic manipulators, *Proceedings of IEEE Regional Conference on Aerospace and Control Systems*, pp. 344-353.

Hughes, P. C. (1987). Space structure vibration modes: how many exist? Which are important, *IEEE Control Systems Magazine*, **7**, pp. 22-28.

Hung, J. Y. and Hung, J. C. (1993). Variable structure control: a survey, *IEEE Transactions on Industrial Electronics*, **40**(1), pp. 2-22.

Hyde, J. M. and Seering, W. P. (1991). Using input command pre-shaping to suppress multiple mode vibration, *Proceedings of IEEE International Conference on Robotics and Automation*, Sacramento (USA), pp. 2604-2609.

Ingole, A. R., Bandyopadhyay, B. and Gorez, R. (1994). Variable structure control application for flexible manipulators, *Proceedings of IEEE Conference on Control Applications*, Glasgow (Scotland), pp. 1311-1316.

Jackson, L. B. (1989). *Digital filters and signal processing*. Kluwer Academic Publishers, London.

Jain, S., Peng, P. -Y., Tzes, A. and Khorrami, F. (1994). Neural network designs with genetic learning for control of a single link flexible manipulator, *Proceedings of American Control Conference*, Maryland (USA), pp. 2570-2574.

Jamshidi, M., Akbarzadeh-T, M. and Vadiee, N. (1998). *Experimental test-beds for intelligent robot controllers based on soft-computing approaches with application to waste management*, Technical Report WERC 1207, New Mexico Waste-management Education and Research Consortium, USA.

Jayasuriya, S. and Choura, S. (1991). On the finite settling time and residual vibration control of flexible structures, *Journal of Sound and Vibration*, **148**(1), pp. 117-136.

Kapila, V., Tzes, A. and Yan, Q. (2000). Closed-loop input shaping for flexible structures using time-delay control, *Transactions of ASME: Journal of Dynamic Systems, Measurement and Control*, **122**, pp. 454-460.

Khorrami, F., Jain, S. and Tzes, A. (1994). Experiments on rigid body-based controllers with input preshaping for a two-link flexible manipulator, *IEEE Transactions on Robotics and Automation*, **10**(1), pp. 55-65.

Khorrami, F. and Ozguner, U. (1988). Perturbation methods in control of flexible link manipulators, *Proceedings of IEEE International Conference on Robotics and Automation*, Philadelphia (USA), pp. 310-315.

Kourmoulis, P. K. (1990). *Parallel processing in the simulation and control of flexible beam structures*, PhD. Thesis, Department of Automatic Control and Systems Engineering, The University of Sheffield, UK.

Kubica, E. and Wang, D. (1993). A fuzzy control strategy for a flexible link robot, *Proceedings of IEEE International Conference on Robotics and Automation*, Atlanta (USA), pp. 236-241.

Larcombe, P. J. and Brown, I. C. (1997). Computer algebra: a brief overview and application to dynamic modelling, *Computing and Control Engineering Journal*, **8**(2), pp. 53-57.

Lee, J. X., Vukovich, G. and Sasiadek, J. Z. (1994). Fuzzy control of a flexible link manipulator, *Proceedings of American Control Conference*, Maryland (USA), pp. 568-574.

Lin, J. and Lewis, F. L. (1994). A symbolic formulation of dynamic equations for a manipulator with rigid and flexible links, *International Journal of Robotics Research*, **13**(5), pp. 454-466.

Low, K. H. and Vidyasagar, M. (1988). A Lagragian formulation of dynamic model for flexible manipulator systems, *Transactions of ASME: Journal of Dynamic Systems, Measurement and Control*, **110**, pp. 175-181.

Mahmood, N. and Walcott, B. L. (1993). Neural network based adaptive control of a flexible link manipulator, *Proceedings of IEEE National Conference on Aerospace and Electronics*, Dayton (USA), pp. 851-857.

Meckl, P. H. and Seering, W. P. (1985). Minimizing residual vibration for point-to-point motion, *Transactions of ASME: Journal of Vibration, Acoustics, Stress and Reliability in Design*, **107**(4), pp. 38-46.

Meckl, P. H. and Seering, W. P. (1988). Controlling velocity-limited systems to reduce residual vibration, *Proceedings of IEEE International Conference on Robotics and Automation*, Philadelphia (USA), pp. 1428-1433.

Meckl, P. H. and Seering, W. P. (1990). Experimental evaluation of shaped inputs to reduce vibration of a cartesian robot, *Transactions of ASME: Journal of Dynamic Systems, Measurement and Control*, **112**(6), pp. 159-165.

Meirovitch, L. (1975). *Elements of vibration analysis*, McGraw-Hill Inc., New York.

Meldrum, D. R. and Balas, M. J. (1986). Application of model reference adaptive control of a flexible remote manipulator arm, *Proceedings of American Control Conference*, Seattle (USA), pp. 825-832.

Menq, C. H. and Chen, J. -S. (1988). Dynamic modeling and payload-adaptive control of a flexible manipulator, *Proceedings of IEEE International Conference on Robotics and Automation*, Philadelphia (USA), pp. 488-493.

Moallem, M., Khorasani, K. and Patel, R. V. (1998). Inversion-based sliding control of a flexible-link manipulator, *International Journal of Control*, **71**(3), pp. 477-490.

Morgan, R. G. and Ozguner, U. (1985). A decentralized variable structure control algorithm for robotic manipulators, *IEEE Transactions on Robotics and Automation*, **1**(1), pp. 57-65.

Moser, A. N. (1993). Designing controllers for flexible structures with H-infinity / μ - synthesis, *IEEE Control Systems Magazine*, **13**(2), pp. 79-89.

Moudgal, V. G., Passino, K. M. and Yurkovich, S. (1994). Rule-based control for a flexible-link robot, *IEEE Transactions on Control Systems Technology*, **2**(4), pp. 392-405.

Moulin, H. and Bayo, E. (1991). On the accuracy of end-point trajectory tracking for flexible arms by non-causal inverse dynamic solution, *Transactions of ASME: Journal of Dynamic Systems, Measurement and Control*, **113**, pp. 320-324.

Murphy, B. R. and Watanabe, I. (1992). Digital shaping filters for reducing machine vibration, *IEEE Transactions on Robotics and Automation*, **8**(2), pp. 285-289.

Nelson, W. L. and Mitra, D. (1986). Load estimation and load adaptive control of a flexible robot arm, *Proceedings. of IEEE International Conference on Robotics and Automation*, San Francisco (USA), pp. 206-211.

Nemir, D. C., Koivo, A. J. and Kashyap, R. L. (1988). Pseudolinks and self-tuning control of a non-rigid link mechanism, *IEEE Transactions*, SMC-**18**(1), pp. 40-48.

Newton, R. T. and Xu, Y. (1993). Neural network control of a space manipulator, *IEEE Control Systems Magazine*, **12**, pp. 14-22.

Nise, N. S. (1995). *Control systems engineering*, Addison-Wesley Publishing Company, California, USA.

Onsay, T. and Akay, A. (1991). Vibration reduction of a flexible arm by time optimal open-loop control, *Journal of Sound and Vibration*, **142**(2), pp. 283-300.

Pao, L. Y. (1996). Input shaping design for flexible systems with multiple actuators, *Proceedings of World Congress of the International Federation of Automatic Control (IFAC)*, San Francisco (USA), pp. 267-272.

Pao, L. Y. and Lau, M. A. (1999). Expected residual vibration of traditional and hybrid input shaping designs, *Journal of Guidance, Control and Dynamics*, **22**, pp. 162-165.

Piedboeuf, J. -C., Farooq, M., Bayoumi, M. M., Labinaz, G. and Argoun, M. B. (1993). Modelling and control of flexible manipulators - revisited, *Proceedings of 36th Midwest Symposium on Circuits and Systems*, Detroit (USA), pp. 1480-1483.

PMI Motion Technologies. (1988). *General application of printed motors*, PMI Motion Technologies, New York

Poerwanto, H. (1998). *Dynamic simulation and control of flexible manipulator systems*, PhD. Thesis, Department of Automatic Control and Systems Engineering, The University of Sheffield, UK.

Qian, W. T. and Ma, C. C. H. (1992). A new controller design for a flexible one-link manipulator, *IEEE Transactions on Automatic Control*, **37**, pp. 132-137.

Rao, S. S. (1989). *The finite element method in engineering*, Second Edition, Pergamon Press, New York.

Rappole, B. W., Singer, N. C. and Seering, W. P. (1994). Multiple-modes impulse shaping sequences for reducing residual vibrations, *23rd Biennial Mechanisms Conference*, Minneapolis (USA), pp. 11-16.

Rattan, K. S., Feliu, V. and Brown, H. B. (1990). Tip position control of flexible arms, *Proceedings of the IEEE Conference on Decision and Control*, Honolulu (USA), pp. 1803-1808.

Rijanto, E., Moran, A., Kurihara, T. and Hayase, M. (1996). Robust tracking control of flexible arms using inverse dynamics method, *Proceedings of 4th International Workshop on Advanced Motion Control*, Tsukuba (Japan), pp. 669-674.

Ross, C. T. F. (1996). *Finite element techniques in structural mechanics*, Albion Publishing Limited, West Sussex.

Rovner, D. M. (1987). *Experiments in adaptive control of a very flexible one-link manipulator*, PhD. Thesis, Department of Aeronautics and Astronautics, Stanford University, USA.

Rovner, D. M. and Cannon, R. H. (1987). Experiments towards on-line identification and control of a very flexible one-link manipulator, *International Journal of Robotics Research*, 6(4), pp. 3-19.

Rovner, D. M. and Franklin, G. F. (1988). Experiments in load adaptive control of a very flexible one-link manipulator, *Automatica*, **24**(4), pp. 541-548.

Sakawa, Y., Matsuno, F. and Fukushima, S. (1985). Modelling and feedback control of a flexible arm, *Journal of Robotic Systems*, **2**(4), pp. 453-472.

Sangveraphunsiri, V. (1984). *The optimal control and design of a flexible manipulator*, PhD. Thesis, School of Mechanical Engineering, Georgia Institute of Technology, USA.

Shchuka, A. and Goldenberg, A. A. (1989). Tip control of a single-link flexible arm using feedforward technique, *Mechanical Machine Theory*, **24**, pp. 439-455.

Sharma, S. K. (2000). *Soft computing for modelling and control of dynamic systems with application to flexible manipulator*, PhD. Thesis, Department of Automatic Control and Systems Engineering, The University of Sheffield, UK.

Singer N. C. and Seering, W. P. (1990). Preshaping command inputs to reduce system vibration, *Transactions of ASME: Journal of Dynamic Systems, Measurement and Control*, **112**(1), pp. 76-82.

Singh, T. and Vidali, S. R. (1994). Robust time-optimal control: a frequency domain approach, *Journal of Guidance, Control and Dynamics*, **17**(2), pp. 346-353.

Singhose, W. E., Derezinski, S. J. and Singer, N. C. (1996). Extra-insensitive input shaper for controlling flexible spacecraft, *Journal of Guidance, Control and Dynamics*, **19**, pp. 385-391.

Singhose, W. E., Singer, N. C. and Seering, W. P. (1995). Comparison of command shaping methods for reducing residual vibration, *Proceedings of Third European Control Conference*, Rome (Italy), pp. 1126-1131.

Song, B. and Koivo, A. J. (1998). Neural networks model based control of a flexible link manipulator, *Proceedings of IEEE International Conference on Robotics and Automation*, Leuven (Belgium), pp. 812-817.

Sun, F., Sun, Z., Zhang, R. and Zhang, F. (1996). A multirate adaptive composite controller for flexible-link robots using neural networks, *Proceedings of IEEE International Conference on Systems, Man and Cybernetics,* Beijing (China), pp. 1036-1041.

Sundareshan, M. K. and Askew, C. (1994). Neural network-based payload adaptive variable structure control of a flexible manipulator arm, *Proceedings of IEEE International Conference on Neural Networks,* Orlando (USA), pp. 2616-2621.

Swigert, J. C. (1980). Shaped torque techniques, *Journal of Guidance and Control*, **3**(5), pp. 460-467.

Talebi, H. A., Khorasani, K. and Patel, R. V. (1998). Neural network based control schemes for flexible-link manipulators: simulations and experiments, *Neural Networks*, **11**, pp. 1357-1377.

Tokhi, M. O. and Azad, A. K. M. (1995). Real time finite difference simulation of a single-link flexible manipulator incorporating hub inertia and payload, *Proceedings of IMechE-I: Journal of Systems and Control Engineering*, **209**(1), pp. 21-33.

Tokhi, M. O. and Azad, A. K. M. (1996). Control of flexible manipulator systems, *Proceedings of IMechE-I: Journal of Systems and Control Engineering*, **210**, pp. 113-130.

Tokhi, M. O. and Azad, A.K.M. (1997). Design and development of an experimental flexible manipulator system, *Robotica*, **15**(3), pp. 283-292

Tokhi, M. O., Mohamed, Z. and Azad, A. K. M. (1997). Finite difference and finite element approaches to dynamic modelling of a flexible manipulator, *Proceedings of IMechE-I: Journal of Systems and Control Engineering*, **211**(2), pp. 145-156.

Tokhi, M. O. and Poerwanto, H. (1996). Control of vibration of flexible manipulators using filtered command inputs, *Proceedings of International Congress on Sound and Vibration*, St. Petersburg (Russia), pp. 1019-1026.

Tokhi, M. O., Poerwanto, H. and Azad, A. K. M. (1995). Dynamic simulation of flexible manipulator incorporating hub inertia, payload and damping, *Machine Vibration*, **4**, pp. 106-124.

Trautman, C. and Wang, D. (1995). Experimental H-infinity control of a single flexible link with a shoulder joint, *Proceedings of IEEE International Conference on Robotics and Automation*, Nagoya (Japan), pp. 1235-1241.

Tuttle, T. D. and Seering, W. (1994). A zero-placement technique for designing shaped inputs to suppress multiple-mode vibration, *Proceedings of American Control Conference*, Maryland (USA), pp. 2533-2537.

Tzes, A. and Kyriakides, K. (1993). Adaptive fuzzy-control for flexible-link manipulators: a hybrid frequency-time domain scheme, *Proceedings of IEEE International Conference on Fuzzy Systems,* San Francisco (USA), pp. 122-127.

Tzes, A. and Yurkovich, S. (1993). An adaptive input shaping control scheme for vibration suppression in slewing flexible structures, *IEEE Transactions on Control Systems Technology*, **1**(2), pp. 114-121

Tzes, A. P., Yurkovich, S. and Langer, F. D. (1988). A symbolic manipulation package for modeling of rigid and flexible manipulators, *Proceedings of IEEE International Conference on Systems Engineering*, Philadelphia (USA), pp. 1526-1531.

Tzes, A. P., Yurkovich, S. and Langer, F. D. (1989). A method for solution of the Euler-Bernoulli beam equation in flexible-link robotic systems, *Proceedings of IEEE International Conference on Robotics and Automation*, Scottsdale (USA), pp. 557-560.

Usoro, P. B., Nadira, R. and Mahil, S. S. (1986). A finite element/lagrange approach to modelling lightweight flexible manipulators, *Transactions of ASME: Journal of Dynamic Systems, Measurement and Control*, **108**, pp. 198-205.

Wang, D. and Vidyasagar, M. (1987). Control of a flexible beam for optimum response, *Proceedings of IEEE International Conference on Robotics and Automation*, Raleigh (USA), pp. 1567-1570.

Wang, D. and Vidyasagar, M. (1991). Transfer functions for a single flexible link, *International Journal of Robotics Research*, **10**(5), pp. 540-549.

Warwick, K. (1989). *Control systems: an introduction*, Prentice Hall, London.

Wells, R. L. and Schueller, J. K. (1990). Feedforward and feedback control of a flexible manipulator, *IEEE Control System Magazine*, **10**, pp. 9-15.

Wellstead, P. E. and Zarrop, M. B. (1991). *Self-tuning systems: control and signal processing*, John Wiley and Sons, West Sussex, UK.

Yamano, M., Konno, A. and Uchiyama, M. (2000). Experiments on capturing a floating object by two flexible manipulators, *Proceedings of IEEE International Conference on Robotics and Automation*, San Francisco (USA), pp. 482-487.

Yang, H., Krishnan, H. and Ang, M.H. (1998). Variable structure controller design for flexible-link robots under gravity, *Proceedings of IEEE Conference on Decision and Control*, Tampa (USA), pp. 1494-1499.

Yang, T. -C, Yang, J. C. S. and Kudva, P. (1992). Load-adaptive control of a single-link flexible manipulator Systems, *IEEE Transactions on Systems, Man and Cybernetics*, **22**(1), pp. 85-91.

Yazdanpanah, M. J., Khorasani, K. and Patel, R. V. (1998). Uncertainty compensation for a flexible-link manipulator using non-linear H-infinity control, *International Journal of Control*, **69**(6), pp. 753-771.

Young, K. –K. D. (1978). Controller design for manipulator using theory of variable structure systems, *IEEE Transactions on Automatic Control*, SMC-**8**(2), pp. 101-109.

Yuan, B. –S., Book, W. J. and Siciliano, B. (1989). Direct adaptive control of a one-link flexible arm with tracking, *Journal of Robotics Systems*, **6**(6), pp. 663-680.

Yurkovich, S. (1992). Flexibility effects on performance and control, *Robot Control*, IEEE Press, Part 8, pp. 321-323.

Zuo, K. and Wang, D. (1992). Closed-loop shaped-input control of a class of manipulators with a single flexible link, *Proceedings of IEEE International Conference on Robotics and Automation*, Nice (France), pp. 782-787.